Université de Montréal

# Décodage des mécanismes cérébraux de la prise de décision chez l'humain

par

Thomas Thiery

Département de Psychologie Faculté des Arts et Sciences

Thèse présentée en vue de l'obtention du grade de Philosophiæ Doctor (Ph.D.) en Psychologie, option Sciences Cognitives et Neuropsychologie

Septembre 2021

Université de Montréal

Unité académique : Psychologie, Faculté des Arts et Sciences

---

*Ce mémoire (ou cette thèse) intitulé(e)*

**Décodage des mécanismes cérébraux de la prise de décision chez l'humain**

*Présenté par*

**Thomas Thiery**

*A été évalué(e) par un jury composé des personnes suivantes*

**Floris van Vugt**

Président-rapporteur

**Karim Jerbi**
Directeur de recherche

**Pierre Rainville**
Codirecteur (1er s'il y a lieu)

**Guillaume Dumas**
Membre du jury

**Emmanuel Procyk**
Examinateur externe

# Résumé

Choisir entre plusieurs actions possibles afin d'interagir avec son environnement constitue l'un des piliers fondamentaux du comportement chez l'animal, y compris l'humain, à travers l'évolution. Pour comprendre comment le cerveau détecte, distingue et catégorise l'information qui parvient à nos sens pour prendre une décision informée, plusieurs théories ont émergé dans le domaine des neurosciences cognitives. L'objectif de cette thèse est d'identifier les mécanismes neuronaux à l'origine de la prise de décision chez l'humain afin d'étoffer les connaissances théoriques existantes sur la manière dont notre cerveau parvient à délibérer, puis choisir entre plusieurs alternatives. Afin d'y parvenir, nous avons combiné l'utilisation de techniques électrophysiologiques et d'analyses d'apprentissage machine avancées pour analyser l'activité cérébrale pendant la réalisation de tâches décisionnelles. Dans le premier article, nous avons utilisé l'électroencéphalogramme (EEG) intracrânien pour enregistrer l'activité neuronale de patients épileptiques alors qu'ils devaient choisir librement entre deux actions de valeur égale (droite ou gauche). Nous avons ainsi pu montrer qu'une augmentation soutenue de l'activité neuronale haute fréquence dans un réseau de régions cérébrales frontales et pariétales permettaient de caractériser le processus de délibération lors d'un choix libre chez l'humain. Pour aller plus loin, nous avons ensuite identifié les mécanismes cérébraux à l'origine des choix pris dans des situations plus écologiques où l'évidence sensorielle fluctue dynamiquement au cours du temps. Dans cette deuxième tâche les participants sont libres de répondre à n'importe quel moment pour essayer d'optimiser leur taux de succès en implémentant des règles qui permettent d'ajuster le compromis entre vitesse et précision. En mesurant l'activité MEG de ces participants pendant qu'ils réalisaient une tâche de décision dynamique, nous avons utilisé une technique de réduction de dimensionalité (ACP, Analyse en Composantes Principales) afin d'identifier et de caractériser les composantes spatiales, temporelles et spectrales de l'activité neuronale sous-tendant les processus principaux de la prise de décision. Nous avons montré (1) le rôle d'un réseau de régions sensorimotrices et visuelles dans ***l'encodage de l'évidence sensorielle*** lors du processus de délibération entre plusieurs alternatives, ainsi que (2) que ***l'engagement dans un choix donné*** est reflété par les oscillations alpha (9-13 Hz) dans du cortex cingulaire postérieur et des régions visuelles (3) que ***l'exécution du mouvement*** permettant d'exprimer ce choix est sous-tendu par les oscillations

beta (16-24 Hz) au sein des régions motrices et prémotrices et enfin (4) ***un ajustement du compromis entre vitesse/précision****, caractérisé par* l'activité haute fréquence dans les aires sous-corticales comprenant les ganglions de la base, le noyaux caudé, le cervelet et le thalamus . Dans leur ensemble, les résultats de cette thèse ont permis d'identifier et de caractériser les composantes spatiales, temporelles et fréquentielles de l'activité neuronale à l'origine de la prise de décision entre plusieurs actions chez l'humain.

**Mots-clés :** Prise de décision, électrophysiologie, oscillations cérébrales, EEG intracrânien, MEG, apprentissage machine

# Abstract

Choosing between potential actions to interact with the environment is one of the fundamental pillars of behavior in animals, including humans. To understand how the brain detects, discriminates, and categorizes information from the senses to make an informed decision, a class of theories have emerged in the field of cognitive neuroscience. The goal of this thesis is to identify neural mechanisms underlying decision-making in humans to extend theoretical accounts on how the brain can deliberate and chose among multiple alternatives. To do so, we combined electrophysiological recordings and machine learning to analyze brain activity from participants performing decision-making tasks. In the first article, we used intracranial EEG to record neuronal activity from epileptic patients while they had to freely choose between two actions of equal value (right or left saccades). We found a sustained increase in high frequency neuronal activity in a network of frontoparietal areas specific to the deliberation process during free choice in humans. We then set out to identify neuronal mechanisms subserving decisions between actions in conditions approaching ecological situations, in which sensory evidence can dynamically change over time, and participants are free to decide at any time to try and optimize successes per unit time by implementing speed accuracy tradeoff policies. By measuring MEG activity from participants performing such dynamic decision-making task and using a dimensionality reduction technique (PCA, Principal Component Analysis), we revealed and characterized the spatial, temporal, and spectral components of neural activity underlying the key processes contributing to decision-making. We showed that alpha (9-13 Hz) and beta (16-24 Hz) principal components (PCs) are involved in ***tracking sensory information while participants were deliberating between two options*** in the sensorimotor, visual, and posterior cingulate cortex. We also highlighted the role of alpha PCs in ***committing*** to a particular choice, while beta PCs were associated with ***motor execution*** once the decision was made. Finally, high frequency PCs (> 16 Hz) in subcortical areas including the cerebellum, pallidum, caudate nucleus and the thalamus indexed the implementation and adjustments of ***speed accuracy tradeoff policies*** when participants to try to optimize successes per unit time. Overall, results from this thesis successfully characterized the spatial, temporal, and spectral components of neuronal activity involved in deciding between actions in humans.



**Keywords:** Decision-making, electrophysiology, neuronal oscillations, intracranial EEG, MEG, machine-learning

# Table des matières

# Liste des figures

**Chapitre 1 : Introduction générale**



**Chapitre 5 : Discussion générale**

# Liste des sigles et des abréviations

AIP : *Anterior IntraParietal,* ou intrapariétale antérieur

BOLD : *Blood-Oxygen-Level Dependent*

CPP : *CentroParietal Positivity,* ou positivité centropariétale

DA : *Decoding Accuracy,* ou précision de décodage

DDM : *Diffusion Drift Model,* ou modèle de diffusion

dlPFC : *dorsolateral Prefrontal Cortex*, ou cortex préfrontal dorsolatéral

DR : *Delayed Response,* réponse après délai

DT : *Decision Time,* temps de décision

EEG : *Electroencephalography*, ou électroencéphalographie

EOG : *Electrooculogram*, ou électroocculogramme

ERP : *Event-Related Potential*, ou potentiel évoqué

ERF : *Event-Related Field*, ou champ évoqué

FEF : *Frontal Eye Fields*, ou champs oculaires frontaux

fMRI : *function Magnetic Resonance Imaging*

fT : femtoTesla

HG : *High Gamma,* ou haut gamma

iEEG : *intracranial Electroencephalography,* ou électroencéphalogramme intracrânien

IPS : *IntraParietal Sulcul,* ou sulcul intrapariétal

IRMf : Imagerie par Résonance Magnétique fonctionnelle

KPMA : Kinématogramme de Points en Mouvement Aléatoire

LDA : *Linear Discriminant Analysis*

LFP : *Local Field Potential,* ou potentiel de champ local

LIP : *Lateral IntraParietal*, ou intrapariétale latérale

LLCs : *Leading Loading Coefficients*

MEG : *Magnetoencephalography*, ou magnétoencéphalographie

MFG : *Middle Frontal Gyrus,* ou gyrus frontal médian

MNI : *Montreal Neurological Institute*

ML : *Machine Learning,* ou apprentissage machine

MT *: Medial Temporal,* ou temporale médiane

PC : *Principal Component,* ou composante principale

PCC : *Posterior Cingulate Cortex,* ou cortex cingulaire antérieur

ROI : *Region of Interest*, ou région d'intérêt

RT : *Reaction Time,* ou temps de réaction

SAT : *Speed versus Accuracy Trade-off*, ou compromise vitesse versus précision

sEEG : *stereotactic Electroencephalography,* ou électroencéphalographie stéréotactique

SEF : *Supplementary Eye Fields,* ou champs oculaires supplémentaires

SFG : *Superior Frontal Gyrus,* ou gyrus frontal supérieur

SMA : *Supplementary Motor Area,* ou aire supplémentaire mortice

SP : *Success Probability,* ou probabilité de succès

UGM : *Urgency-Gating Model,* ou modèle d'urgence

# Remerciements

Je tiens à remercier toutes les personnes qui m'ont accompagné pendant cette belle aventure. Mon expérience de thèse a été synonyme de découvertes, de liberté et d'autonomie. J'ai eu la chance de satisfaire ma curiosité, d'être passionné par des sujets dans des domaines allant de la philosophie aux neurosciences, en passant par l'intelligence artificielle. J'ai pu me rendre compte que plus on en apprend, plus on sait qu'on ne sait rien et que le domaine des connaissances est infini. J'ai surtout pu faire des rencontres magnifiques, et si certaines d'entre elles resteront gravées comme des souvenirs impérissables, je sais que d'autres continueront à m'accompagner pendant le reste de ma vie. J'aimerais commencer par remercier ma mère, qui a eu le courage de toujours me soutenir dans ce que j'entreprenais sans pression ni jugement, et qui m'a donné la confiance de me décider à m'engager dans un doctorat en neurosciences avec le même enthousiasme que lorsque je voulais devenir journaliste ou écrivain. Je veux ensuite remercier mes amis, et surtout ceux que j'ai rencontré à Montréal, avec qui j'ai partagé les moments les plus fous, les plus forts et les plus drôles, à chaque fois que l'occasion se présentait (donc très souvent). Merci Nico, Gonzague, Hadrien, Vincent, Anne Ju et tous les autres pour votre bonne humeur et votre joie de vivre, pour les soirées, les pique-niques, les chalets, la coloc, les débats. Merci à ma meilleure amie, à ma plus belle rencontre, merci Anne-Lise d'être devenue la personne qui partage et illumine ma vie. Merci à tous les membres du CoCo Lab, à ceux qui sont devenus des amis bien plus que des collègues, qui m'ont donné envie d'aller les rejoindre tous les jours à l'Université, pour les pauses déjeuners qui s'éternisent, les babyfoots et les conférences, les soirées CoCo lab, merci Arthur, Victor, Tarek, Vaness, Yann, Loubna, Étienne et Golnoush. Enfin, merci à celui sans qui rien de tout ça n'aurait été possible, merci Karim pour m'avoir permis de faire partie de l'équipe incroyable que tu as su composer, d'avoir réussi à insuffler cette cohésion de groupe et cet esprit d'équipe au CoCo Lab, d'avoir su m'accompagner pendant les moments importants, de m'avoir laissé cette liberté dans mon travail, d'avoir su m'ouvrir toutes ces opportunités, ces discussions, ces collaborations. Merci pour ces voyages, et ces conférences mémorables, en Corée ou en Italie. Enfin, merci à Pierre pour sa bienveillance, ses encouragements et ses précieux conseils, merci d'avoir toujours supporté mes choix de recherche et d'avoir toujours été là aux moments clés. Pour finir, cette thèse n'aurait été possible sans le soutien financier d'IVADO, du Fonds de Recherche du Québec Nature et Technologies (FRQNT) et Santé (FRQS), et de NeuroUQAM.

# Chapitre 1

# Introduction générale

### 1.1.1 Présentation de la thèse

Chaque jour, du matin au soir, des myriades de décisions sont prises par chacun d'entre nous. La première phrase de l'introduction de cette thèse, d'une banalité déconcertante, recèle pourtant des richesses et des contradictions insoupçonnées. Depuis plus d'un siècle, d'éminents psychologues, économistes et plus récemment neuroscientifiques ont contribué au développement de théories devenues classiques permettant de mieux comprendre les mécanismes mentaux, comportementaux et cérébraux à l'origine de nos choix. Pourtant, le terme même de prise de décision peut faire allusion à des phénomènes très différents. Le lecteur conviendra qu'un processus abstrait, comme faire le choix d'acheter une maison ou établir une stratégie lors d'une partie d'échecs, est manifestement différent d'une action concrète comme freiner ou d'accélérer au moment où l'on aperçoit un feu orange sur la route.

L'histoire des philosophies successives a encouragé les penseurs, puis les chercheurs, à se concentrer particulièrement sur les décisions abstraites et économiques. En effet, l'influence des courants de pensée considérant (1) les phénomènes mentaux et cognitifs comme appartenant à un esprit coupé du corps, et (2) l'humain comme un être économique rationnel ont eu des répercussions importantes sur la psychologie et ont conduit à une perspective « cognitiviste » de la pensée et donc de la prise de décision. Selon les prémisses du cognitivisme, le fait de prendre une décision est caractérisé un processus abstrait et sériel, indépendant de la perception et de l'action (Fodor, 1983 ; Pylyshyn, 1984), conformément à l'exemple du joueur d'échecs qui délibère avant de déplacer l'un de ses pions. Cependant, il existe une vision alternative, ancrée dans une tradition écologique et évolutionniste, qui postule que la prise de décision ne peut être considérée comme un processus entièrement abstrait. Au contraire, nos choix seraient ancrés dans l'environnement, incarnés dans un corps, et interdépendants de la perception et de l'action. En effet, la majorité des organismes vivants évoluent dans un environnement dynamique et sont confrontés à un monde dans lequel des multitudes d'« affordances » (c.-à-d. des possibilités d'action, Gibson, 1979) guident des décisions qui sont en lien direct avec l'exécution d'actions manifestes. Du point de vue de l'évolution, tous les animaux sont amenés à faire des choix entre plusieurs actions possibles, que les décisions soient très simples, chez des organismes primitifs comme les vers plats (Gruber et Ewer, 1962), ou plus complexes, comme la recherche de nourriture chez les primates et le freinage de dernière minute au

feu orange chez l'être humain.

Depuis quelques dizaines d'années, l'étude de la prise de décision a bénéficié de l'émergence des neurosciences cognitives computationnelles, à la frontière entre la psychologie comportementale, les mathématiques et les neurosciences. Aujourd'hui, les théories classiques de la prise de la décision s'inscrivent principalement dans une discipline appelée neuroéconomie. En alliant théories économiques comportementales, modèles computationnels et enregistrements neurophysiologiques chez le singe et chez l'humain, des avancées considérables ont été accomplies pour caractériser les mécanismes cérébraux et comportementaux sous-tendant les décisions abstraites, économiques et statiques (c.-à-d., l'information sensorielle reste stable au cours du temps). En outre, de nouvelles théories alternatives, que nous appellerons théories dynamiques dans le cadre de cette thèse, ont émergé au cours des dernières années. En plus de mettre en évidence les limites des modèles neuroéconomiques existants, les théories dynamiques proposent une nouvelle conception de la prise de décision. Celles-ci postulent notamment que les décisions abstraites seraient en fait régies par des principes similaires à ceux qui gouvernent les décisions prises par nos ancêtres au cours de l'évolution (Gold et Shadlen, 2007).

Dans le cadre de cette thèse, nous mettrons en évidence la pertinence des théories dynamiques pour étudier la prise de décision en nous intéressant aux mécanismes cérébraux à l'origine des choix entre plusieurs actions possibles chez l'humain. Nous verrons quels sont les mécanismes qui permettent au cerveau de coder l'information sensorielle, de délibérer entre plusieurs alternatives, puis de s'engager dans un choix et d'effectuer la commande motrice qui y correspond. Nous passerons en revue l'état de la littérature sur les théories classiques et dynamiques de la prise de décision aujourd'hui, en décrivant pour chacune d'entre elles les modèles computationnels ainsi que leurs signatures électrophysiologiques chez le primate et chez l'humain.

### 1.1.2 Théories classiques de la prise de décision

Aujourd'hui, la vision prédominante dans le domaine des neurosciences cognitives postule que les comportements complexes comme nos prises de décision pourraient être expliqués par des

mécanismes cérébraux sous-tendant des processus abstraits, indépendants, et organisés de manière sérielle : la *perception*, la *cognition* et l'*action*. Cette vision est ancrée dans les théories traditionnelles psychologiques et économiques qui ont vu le jour à partir de la moitié du XX$^{e}$ siècle. Au cours de cette période, le ***cognitivisme*** prend son essor dans le domaine de la psychologie, et s'inspire de la métaphore d'un cerveau fonctionnant selon les mêmes principes qu'un ordinateur. Le cortex est considéré comme un organisme passif, qui pourrait recevoir des données du monde extérieur (*perception*), traiter l'information contenue dans ces données (*cognition*), puis émettre des signaux de sortie (*action*) en fonction de la tâche donnée (Albright et 46 al., 2000 ; Fodor, 1983 ; Gazzaniga, 2000 ; Johnson-Laird, 1988 ; Keele, 1968 ; Marr, 1982 ; Miller et coll., 1960 ; Pylyshyn, 1984). Pour adeptes du cognitivisme, le rôle de la perception s'articule avant tout autour de mécanismes chargés de recueillir les informations sensorielles pour construire, puis mettre à jour une représentation interne stable et unifiée du monde qui nous entoure (Marr, 1982 ; Riesenhuber et Poggio, 2002). Cette représentation interne, conceptualisée sous forme de code symbolique du monde extérieur, sert d'input aux processus cognitifs qui doivent manipuler ces symboles selon certaines règles, afin de porter des jugements éclairés sur les comportements à adopter en fonction des situations (Johnson-Laird, 1988 ; Newell et Simon, 1972 ; Shafir et coll., 1995). Une fois que les processus cognitifs ont « décidé » que faire, ceux-ci préparent un programme moteur, qui est transmis au système moteur afin que celui-ci l'interprète et génère le mouvement musculaire souhaité (Keele, 1968 ; Miller, 1960). Au même moment, le domaine de l'économie connaît un renouveau et un essor sans précédent, en conceptualisant les processus à l'origine des choix rationnels pris par l'homo economicus (Persky, 1995) sous forme de modèles mathématiques(Kahneman & Tversky, 1990). C'est ainsi que la ***théorie économique de l'utilité espérée***, introduite par de VonNeumann et Morgenstern en 1944, formalise la manière dont les êtres humains sont censés se comporter lorsqu'ils doivent faire des choix dans des situations qui comportent un risque. Selon les auteurs, l'humain en tant qu'agent décisionnel a la capacité d'intégrer les facteurs pertinents qui vont lui permettre de prendre la meilleure décision possible dans une seule et même variable, indépendante de tout paramètre contextuel. Cette variable décisionnelle reflète la valeur subjective de chacune des offres qui sont proposées à l'agent décisionnel (p. ex., gains attendus, risques), permettant ainsi de sélectionner l'offre qui a la plus grande valeur, puis d'élaborer un plan d'action pour l'appréhender, en accord avec le modèle

cognitiviste. Malgré la popularité de la théorie de l'utilité espérée, plusieurs travaux expérimentaux ont montré que les êtres humains ne se comportent pas de manière totalement rationnelle, et que leurs décisions ne sont pas toujours optimales. Par exemple, le modèle de la rationalité limitée (c.-à-d., « bounded rationality ») montre de façon convaincante que la capacité rationnelle de décision des individus peut être altérée par un ensemble de contraintes comme le manque d'information, le manque de temps ou des biais cognitifs (Simon, 1943, 1947). Pour autant, l'idée qu'une seule et même variable puisse intégrer les facteurs décisionnels pertinents reste dominante, et va influencer la manière de conceptualiser, et de modéliser le traitement de l'information lorsque nous sommes confrontés à des situations dans lesquelles nous devons faire des choix, et ce jusqu'à aujourd'hui.

#### 1.1.2.1 Les modèles computationnels

L'influence des théories psychologiques, économiques et mathématiques du siècle dernier a été primordiale pour permettre l'émergence des neurosciences cognitives computationnelles telles que nous les connaissons aujourd'hui. La convergence de ces disciplines a conduit au développement de modèles computationnels quantitatifs permettant de formaliser la manière dont se comportent les êtres humains lorsqu'ils se trouvent dans des situations de décision. En particulier, une classe de modèles, dits d'intégration limitée ou encore d'échantillonnage séquentiel, a été introduite afin de proposer une explication des mécanismes qui permettent de traiter l'information qui vient du monde extérieur lorsque nous devons prendre une décision, et que nous délibérons entre plusieurs alternatives possibles pour choisir la meilleure d'entre elles (c.-à-d. ce qui correspond à l'offre avec la plus grande valeur subjective selon la théorie de l'utilité espérée). À l'origine, les modèles d'intégration ont été conçus pour décrire cette période de délibération entre plusieurs options comme un processus itératif se déroulant au sein d'un système purement cognitif (Busemeyer & Townsend, 1993 ; Ratclif, 1978), conformément aux préceptes du cognitivisme. Prendre une décision simple, par exemple choisir entre deux options impliquerait un échantillonnage séquentiel de l'information sensorielle provenant du monde extérieur, et son intégration au cours du temps jusqu'à ce que la quantité d'information intégrée en faveur d'une option ou d'une autre soit suffisante pour atteindre un certain seuil, appelé seuil de décision. Lorsque le seuil de décision est atteint, cela signifie que la décision est prise par le système cognitif : l'une des alternatives a été sélectionnée, et la préparation d'un programme moteur est enclenchée, afin que l'action correspondant à la décision prise par le

système cognitif puisse être exécutée (Ratcliff, 1978 ; Mazurek et al., 2003). Un des paramètres importants des modèles d'intégration concerne évidemment la vitesse à laquelle l'évidence sensorielle est intégrée au cours du temps (notons que le terme « évidence » est utilisé délibérément dans cette thèse selon un sens similaire au terme anglais « evidence » pour signifier l'information sensorielle pertinente pour guider la décision et l'action). Les modèles d'intégration postulent que c'est la qualité, la « force » de l'information sensorielle en faveur d'une option ou d'une autre qui va faire varier ce paramètre, alors que le seuil de décision dépend plutôt de facteurs motivationnels, comme les gains potentiels et les risques encourus (Reddi and Carpenter, 2000).

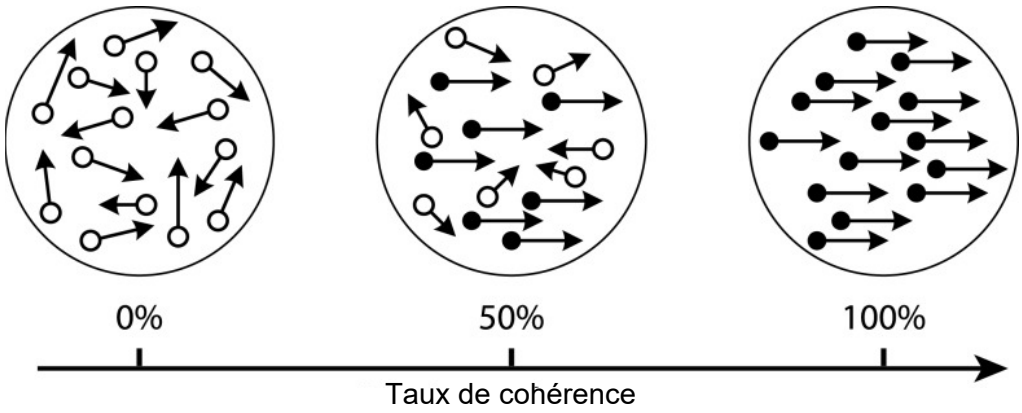


**Figure 1. Le stimulus utilisé dans une tâche de kinématogramme de points aléatoires (KPMA)** est constitué de deux ensembles de points : une partie de points qui bougent de manière aléatoire et une partie de points qui bouge de manière cohérente dans la même direction. La répartition des points entre ces deux ensembles est déterminée par le pourcentage de points qui bougent dans la même direction, que l'on appelle taux de cohérence et qui peut aller de 0 % (totalement aléatoire) à 100 % (tous les points bougent dans la même direction) (Newsome et al. 1989). La tâche du sujet est de regarder le KPMA et de décider de la direction du mouvement cohérent, puis de signifier sa décision, la plupart du temps par un mouvement de saccade des yeux ou un mouvement de bras dans la même direction que la direction de mouvement des points.

Au fil des années, plusieurs variations de ces modèles d'intégration se sont développées, et de nombreuses études ont pu démontrer leur capacité à prédire la distribution des temps de réaction, ou encore la fréquence des erreurs commises dans de nombreuses tâches de prise de décision perceptives (c.-à-d. lors de tâches dites perceptives, les participants doivent prendre des décisions en

fonction d'information sensorielle provenant du monde extérieur). Cela a notamment été possible grâce à l'utilisation de stimuli psychophysiques comme le kinématogramme de points en mouvement aléatoire (KPMA, voir Figure 1) dans le cadre de tâches décisionnelles. Grâce à la possibilité de contrôler précisément les propriétés des stimuli présentés aux participants, ces tâches de décision perceptives sont devenues le standard expérimental pour étudier la prise de décision et corroborer les prédictions des modèles d'intégration (Britten et coll., 1992 ; 1993 ; Gold & Shadlen, 2000 ; Roitman & Shadlen, 2002 ; Mazurek et autres, 2003 ; Ditterich et autres, 2003 ; 2006b ; Ratcliff & Smith, 2004 ; Huk & Shadlen, 2005 ; Palmer, Huk & Shadlen, 2005 ; Bogacz et autres, 2006 ; Kiani et autres, 2008 ; Drugowitsch et autres, 2012). La tâche du KPMA par exemple est particulièrement bien adaptée pour étudier le processus de délibération entre plusieurs options en fonction de l'évidence sensorielle donnée par le stimulus présenté. En effet, l'ajustement du taux de cohérence du stimulus KPMA, soit la proportion des points qui bougent dans la même direction (alors que le reste des points bouge aléatoirement) permet de manipuler la qualité de l'évidence sensorielle et d'évaluer son impact sur les temps de réaction ou la fréquence d'erreurs commises. Selon les modèles d'intégration, l'augmentation du taux de cohérence aurait un impact direct sur la fréquence à laquelle l'évidence sensorielle s'accumule jusqu'au seuil de décision, ce qui mènerait à un choix plus rapide (c.-à-d. exprimé par un temps de réaction plus court). La confirmation de la pertinence des modèles d'intégration à travers de nombreuses études comportementales a constitué une étape importante pour la compréhension des processus décisionnels. Malgré tout, il restait difficile de départager les différentes variations des modèles d'intégration, puisque leurs prédictions étaient similaires en dépit de différences dans l'ajustement de leurs paramètres respectifs.

Afin d'y remédier, des chercheurs ont plus récemment proposé que le moyen le plus judicieux pour départager la pertinence des différents modèles d'intégration soit d'évaluer la plausibilité biologique de leurs mécanismes computationnels respectifs (Ratcliff & McKoon, 1995 ; Gold & Shadlen, 2002 ; Churchland et coll., 2008). Ainsi, un modèle d'intégration convaincant devrait être en mesure de caractériser le comportement, mais aussi les signatures neuronales sous-tendant plusieurs facteurs décisionnels importants définis par le modèle, comme ***(1)*** le traitement et ***(2)*** l'intégration de l'évidence sensorielle, ou encore ***(3)*** l'implémentation de seuils de décision. Après plusieurs améliorations successives, c'est le modèle de diffusion (voir Figure 2), introduit par Ratcliff en 1978,

qui s'est imposé, devenant ainsi le modèle neurocomputationnel dominant dans le domaine de la prise de décision. En effet, nous allons voir que le modèle de diffusion permet non seulement d'expliquer le comportement, mais aussi la dynamique des variables neuronales impliquées lors de décisions entre plusieurs actions, au sein du système sensorimoteur (Gold & Shadlen, 2007). Celui-ci peut être formalisé par l'équation suivante :

$$x(t) = Z + \int_0^t E(\tau)d\tau$$

où $x(t)$ représente la variable neuronale de décision, soit une estimation interne de l'accumulation d'évidence sensorielle $E(\tau)$ au cours du temps $\tau$. Dans la tâche KPMA, cette évidence sensorielle est caractérisée par la différence entre l'évidence en faveur de l'option gauche et l'évidence en faveur de l'option droite. En d'autres termes, $E(\tau) = E_{gauche}(\tau) - E_{droite}(\tau)$. L'évidence sensorielle est intégrée au cours du temps, et ce plus ou moins rapidement, en fonction de la force (ou la qualité) de l'information sensorielle du stimulus, représentée par le taux de dérive $d$. Enfin, à chaque nouvel essai, le point de départ de la variable $x$ au temps 0, soit $x(0)$, est déterminé en fonction du biais a priori $Z$. Un exemple de biais serait de considérer la probabilité que les points du stimulus KPMA aillent vers la droite ou vers la gauche. Si dans 80% des essais, les points bougent vers la droite, le biais Z représentera une estimation a priori de cette probabilité. Dans le modèle de diffusion, la décision est prise lorsque la variable neuronale $x(t)$ dépasse un seuil de décision (S). Ce seuil de décision peut être positif $+S$, ce qui déclenche la sélection de l'option $gauche$. Au contraire, si la variable $x(t)$ baisse au cours du temps pour le seuil négatif $-S$, cela déclenche la sélection de l'option $droite$. Ainsi, la formalisation mathématique des paramètres qui caractérisent la variable neuronale de décision et son évolution au cours du temps lors de décisions perceptives a poussé les chercheurs a effectué des enregistrements du cerveau, pour vérifier la plausibilité du modèle de diffusion au niveau neurobiologique.

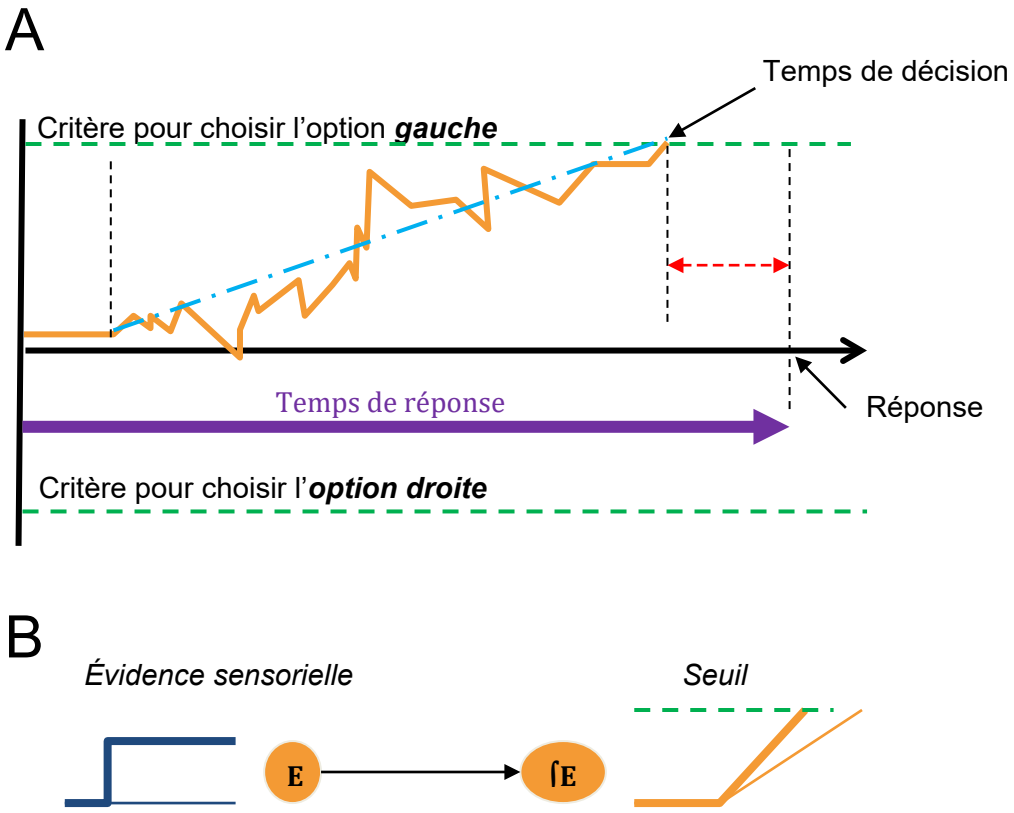


**Figure 2. Le modèle de diffusion. A.** Le point de départ de la variable neuronale de décision (ligne continue orange) est défini en fonction de biais a priori, puis évolue au cours du temps sous l'influence de l'évidence sensorielle E. La force de l'évidence sensorielle (c.-à-d. le taux de cohérence du KPMA) détermine le taux de dérive représenté par la ligne bleue en pointillés. Lorsque la variable de décision atteint un seuil déterminé par la précision désirée (lignes vertes en pointillés), la décision est prise et après un certain délai moteur (double flèche rouge), la réponse motrice est déclenchée. **B.** Illustration de l'intégration de l'évidence sensorielle ∫E en fonction de sa force, et de son influence sur le taux dérive, qui détermine la vitesse à laquelle la variable neuronale atteint le seuil de décision.

### 1.1.3 Les signatures électrophysiologiques

***Chez le primate non humain***

Dans un premier temps, les chercheurs dans le domaine des neurosciences cognitives se sont principalement intéressés aux signatures électrophysiologiques de la prise de décision chez le singe. Dans cette partie, nous allons voir que le développement de techniques d'enregistrement électrophysiologique du signal cérébral à l'échelle du neurone (c.-à-d., *single unit recording,* ou

enregistrement unitaire) combiné à la capacité des singes d'apprendre des tâches de décision relativement complexes a permis d'identifier avec précision certaines signatures neuronales associées aux processus décisionnels définis par le modèle de diffusion.

D'abord, les chercheurs ont tenté d'identifier les régions cérébrales permettant de recueillir, et de traiter l'information sensorielle fournie par le stimulus, ce qui constitue l'évidence sensorielle en faveur d'une option ou d'une autre dans le cadre du modèle de diffusion (noté $E(\tau)$ dans l'équation 1). En procédant à des enregistrements électrophysiologiques lorsque des singes effectuaient la tâche KPMA, de nombreuses études ont pu mettre en évidence le rôle crucial des neurones de l'aire médiotemporale (MT), une aire visuelle connue pour sa contribution importante dans la perception du mouvement (Born et Bradley, 2005). En effet, l'activité des neurones MT sensibles à la direction des mouvements était linéairement corrélée au taux de cohérence du stimulus KPMA, qui indexe la force de l'information sensorielle dans le cadre du modèle de diffusion. L'activité des neurones MT a donc été identifiée comme étant une signature neuronale de l'évidence sensorielle, pouvant être utilisée pour prédire l'exactitude des décisions prises lors de tâches de décision perceptives (Newsome et coll., 1989 ; Britten et coll., 1992 ; Britten et coll., 1993 ; Britten et coll., 1996 ; Shadlen et coll., 1996). Pour aller encore plus loin, certaines études ont aussi montré qu'en inactivant (pharmacologiquement ou par microsimulation électrique) l'activité des neurones de l'aire MT, les chercheurs ont pu directement manipuler les réponses comportementales des singes lors de tâches décisionnelles. Ces études ont donc permis de confirmer le rôle causal de l'aire MT dans le traitement de l'évidence sensorielle visuelle, en montrant que l'altération de son activité impactait les temps de réaction, ou la fréquence d'erreurs commises, conformément aux prédictions du modèle de diffusion (Ratcliff et Smith, 2004 ; Bogacz et al., 2006 ; Balci et coll., 2011). Enfin, un questionnement légitime consistait à se demander si ces résultats pouvaient être observés lors de tâches décisionnelles faisant intervenir d'autres modalités sensorielles comme l'audition, le toucher, ou encore l'olfaction. Plusieurs études ont en effet montré une activité de codage de l'information sensorielle similaire à celle générée par les neurones de l'aire MT, mais dans les aires sensorielles auditives (Sally et Kelly, 1988 ; Kaiser et coll., 2007 ; Yang et coll., 2008; Jaramillo & Zador, 2011; Bizley et coll., 2013; Znamenskiy & Zador, 2013), somato-sensorielles (Salinas et coll., 2000 ; Romo et Salinas, 2003 ; Houweling et Brecht, 2008 ; Hernández et coll., 2010), et olfactives (Uchida & Mainen, 2003 ; Uchida et al., 2006). Dans leur

ensemble, ces travaux démontrent donc l'importance cruciale de l'activité des neurones situés dans les aires sensorielles, qui ont pour rôle de recueillir et de traiter l'information sensorielle afin d'informer et de guider les processus décisionnels vers une des alternatives possibles. Ensuite, les chercheurs se sont concentré les signatures neuronales représentant l'intégration de l'évidence sensorielle à proprement parler. En effet, nous avons vu que les neurones des régions sensorielles, comme l'aire MT pour les tâches de décisions visuelles, étaient responsables de coder, de suivre l'information sensorielle fournie par le stimulus à un instant *t. P*ar exemple, les neurones MT codent la direction du mouvement des points vers la droite ou vers la gauche, lors de la présentation d'un stimulus KPMA. En revanche, le modèle de diffusion postule également l'existence d'un mécanisme qui permettrait d'intégrer cette évidence sensorielle au cours du temps, afin que celle-ci puisse s'accumuler jusqu'à atteindre un seuil de décision. Selon un large éventail de recherches neurophysiologiques, l'accumulation d'évidence sensorielle au cours du temps serait pour sa part reflétée par l'activité neuronale des régions motrices de haut niveau lors de tâches décisionnelles. Dans un premier temps, certains chercheurs ont montré à plusieurs reprises l'activité des neurones situés dans le colliculus supérieur - une région motrice permettant de diriger le regard en produisant des mouvements oculomoteurs - était significativement corrélée à la probabilité, mais aussi à la latence d'une réponse comportementale qui s'ensuit lorsque celle-ci est une saccade oculaire (Dorris et Munoz, 1998 ; Dorris et al., 2000 ; Basso et Wurtz, 1998 ; Everling et coll., 1999). En d'autres termes, plus l'activité du colliculus augmente, plus la probabilité que le singe effectue une saccade pour choisir une option est importante, ce qui correspond à ce que l'on pourrait attendre d'une activité neuronale qui indexe l'accumulation d'évidence sensorielle jusqu'à un certain point. Lors de tâches KPMA, plusieurs études ont également mis en évidence le fait que l'activité des neurones qui codent pour la direction du mouvement dans les champs oculaires frontaux (FEF) et dans les aires intrapariétales latérales (LIP) augmente en fonction du taux de cohérence, mais aussi en fonction du temps de visualisation du stimulus KPMA, comme on peut l'observer sur la Figure 3 (Gold & Shadlen, 2000 ; Roitman & Shadlen, 2002 ; Ding & Gold, 2012), contrairement à l'activité des neurones de l'aire MT qui codent uniquement pour la direction du mouvement. Ces observations sont en accord avec les postulats du modèle de diffusion, et viennent corroborer le rôle fondamental qu'ont les aires motrices de haut niveau dans le processus de délibération lors de tâches de prise de décision entre plusieurs

actions. Ce rôle a été confirmé dans des taches de décision motrice sans indice perceptif (i.e. auto-généré) qui montrent un recrutement progressif de l'activité des neurones codant pour la direction choisie pendant la période de décision et de préparation du mouvement (Dorris & Glimcher, 2004 ; Platt & Glimcher, 1999 ; Sugrue & coll., 2004 ; Yang & Shadlen, 2007).

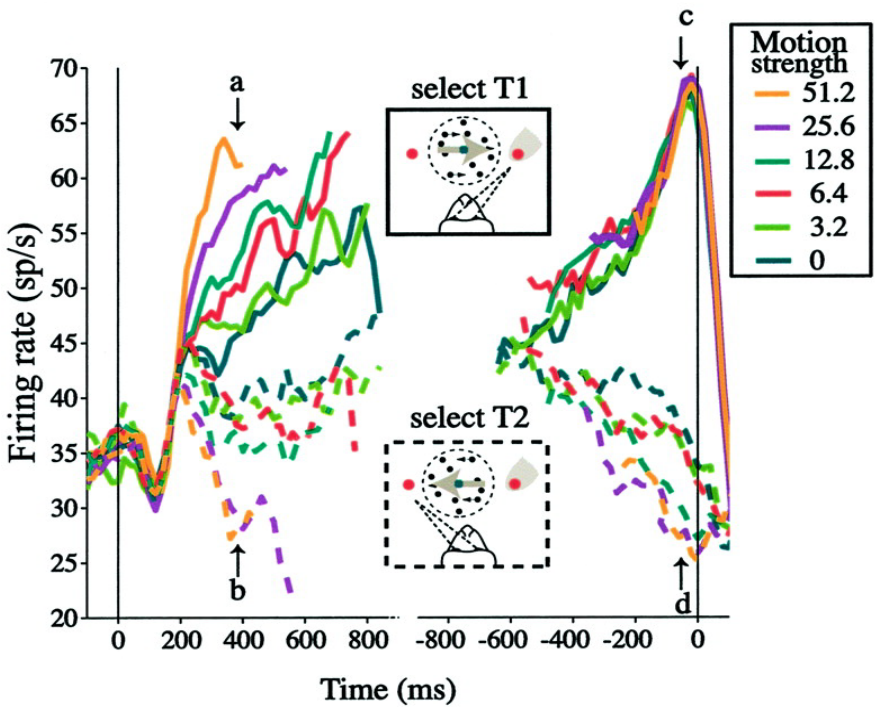


**Figure 3. Accumulation d'évidence et seuils décisionnels dans l'aire intrapariétale latérale chez le singe.** Réponses des neurones du LIP lors d'une tâche KPMA, de Roitman & Shadlen (2002). À gauche, l'activité neuronale est alignée sur la présentation du stimulus. La fréquence d'accumulation de l'activité neuronale est déterminée par la force de l'évidence sensorielle du stimulus KPMA (c.-à-d. le taux de cohérence). À droite, l'activité neuronale est alignée sur le moment d'exécution de la saccade, et montre que la saccade est déclenchée lorsque l'activité neuronale du LIP atteint un certain seuil (c et d).

Par ailleurs, le modèle de diffusion postule l'existence d'un seuil de décision, qui serait établi à un niveau fixe en fonction de la précision désirée et que l'activité neuronale devrait franchir pour s'engager dans une décision et engendrer la réponse comportementale associée. À ce jour, la démonstration la plus claire des mécanismes neuronaux jouant ce rôle de seuil provient d'une étude de Roitman & Shadlen en 2002 (voir Figure 3). Ces derniers ont enregistré l'activité de neurones dans l'aire LIP chez le singe lors d'une tâche KPMA. En alignant l'activité neuronale sur le moment estimé du

début de la décision, ils ont montré que la transition de l'accumulation d'évidence sensorielle vers l'action semblait se produire au moment où l'activité neuronale du LIP atteignait effectivement un certain seuil, indépendamment du taux de cohérence du stimulus. De plus, aucune différence n'a été observée entre les essais corrects et incorrects, ce qui suggère que les neurones du LIP ne reflètent pas la direction objective du mouvement du stimulus, mais indiquent plutôt la croyance subjective des singes et une estimation interne de l'évidence sensorielle qui leur permet de prendre leur décision (Roitman et Shadlen, 2002 ; Yang et Shadlen, 2007). Une série d'étude est venue corroborer et approfondir ces résultats, en montrant l'existence de seuils absolus au niveau de l'activité neuronale, dont le franchissement prédit à la fois la nature du choix final (droite ou gauche par exemple) et le moment auquel le sujet rapporte avoir pris sa décision (Ratcliff, Cherian & Segraves, 2003 ; Mazurek et al., 2003 ; Kiani et coll., 2008 ; Ding et Gold, 2012). Cela correspond aux prédictions du modèle de diffusion, puisque pour rappel, celui-ci définit l'évidence sensorielle comme étant la différence entre l'évidence en faveur de l'option gauche et l'évidence en faveur de l'option droite ($E(\tau) = E_{gauche}(\tau) - E_{droite}(\tau)$, voir équation 1), et qui devrait franchir un des deux seuils de décisions, soit $+S$ ce qui déclenche la sélection de l'option $gauche$ ou $-S$ qui déclenche la sélection de l'option $droite$. Ces résultats ont donc renforcé l'idée que l'activité neuronale des régions motrices de haut niveau, et particulièrement l'aire LIP, peut être interprétée comme une variable neuronale d'accumulation d'évidence vers un seuil fixe, indépendamment du taux de cohérence et du temps de décision. Enfin, les variations des temps de décision observés lors des tâches de décision perceptives ne seraient pas attribuables à des changements de la valeur des seuils au cours du temps (ceux-ci seraient constants au sein d'un même essai), mais bien aux variations liées à la force de l'évidence sensorielle, reflétée au niveau de l'activité neuronale (Roitman et Shadlen, 2002 ; Mazurek et al., 2003 ; Kiani et coll., 2008).

Enfin, en parallèle et en complément des recherches concentrées exclusivement sur les signatures neuronales sous-tendant les paramètres du modèle de diffusion, d'autres chercheurs ont tenté de comprendre ce qui caractérisait le fait de prendre une décision librement (réponse autodéterminée), c'est à dire de choisir entre deux options qui ont la même valeur sans être influencé par quelconque indices sensoriels extérieurs. Pour y répondre, une tâche classique dite « motrice différée » (« delayed motor task ») a été développée. Celle-ci consiste à présenter un indice visuel

indiquant de planifier un mouvement moteur vers l'une des alternatives présentées (gauche ou droite par exemple), puis de l'exécuter après un certain délai, après l'apparition d'un deuxième indice visuel (signal GO). La direction du mouvement moteur pouvant être déterminée librement (condition de décision autodéterminée) ou guidée par le premier indice visuel (condition de décision/planification guidée), il était possible pour les chercheurs de caractériser les processus neuronaux propres sous-tendant le fait même de choisir librement entre plusieurs options données. Les recherches effectuées chez le singe ont montré que la planification guidée d'une saccade implique les mêmes régions que lors de mouvements oculaires, soit les régions FEF et LIP, ainsi qu'une activité soutenue de l'activité neuronale dans les aires frontales, représentant le maintien en mémoire de travail de l'information données par l'indice visuel lors de la période de délai(Constantinidis et al., 2018; Lundqvist et al., 2018; Stokes, 2015). D'autre part, plusieurs études chez le primate non-humain ont mis en évidence le fait que les processus de décision libre étaient représentés au sein d'un réseau cérébral frontopariétal dépendant de la modalité utilisée pour le mouvement moteur (Christopoulos et al., 2018; Cisek & Kalaska, 2005; Klaes et al., 2011; Mochizuki & Funahashi, 2016; Pesaran et al., 2008; Procyk & Goldman-Rakic, 2006; Shima et al., 1991; Suriya-Arunroj & Gail, 2019; Watanabe et al., 2006; Wilke et al., 2012), mais les dynamiques temporelles de l'activité neuronale pendant la décision est encore mal compris. Ces recherches chez l'animal continuent d'être déterminantes pour essayer de dissocier les réponses neuronales correspondant aux processus clefs qui interviennent lors de la prise de décision, notamment en distinguant la préparation motrice du traitement d'un stimulus sensoriel, ou de bien de la délibération entre plusieurs options en tant que telle.

***Chez l'humain***

À partir des travaux de recherches fondateurs effectués chez le singe, les chercheurs ont dirigé des recherches chez l'humain, dans le but de pallier certaines limites inhérentes aux études chez le singe et d'approfondir les connaissances dans le domaine de la prise de décision. En effet, les enregistrements électrophysiologiques chez le singe permettent de mesurer l'activité neuronale avec une résolution spatiale (à l'échelle du neurone) et temporelle (ms) remarquables, mais au sein d'une ou de quelques régions cérébrales seulement. Vu les défis techniques que ces méthodes présentent, très peu d'études ont étudié les dynamiques cérébrales sous-tendant les décisions à travers plusieurs régions corticales simultanément (Hernández et coll., 2010 ; Siegel et al., 2015 ; Yates et coll., 2017 ;

Pinto et coll., 219). De plus, les singes ne sont capables d'effectuer des tâches de prises de décision, même simples, qu'au bout d'innombrables heures d'entraînement, ce qui limite la faisabilité de certaines études.

Chez l'humain, l'utilisation de méthodes d'imagerie cérébrale comme l'électroencéphalographie (EEG) et la magnétoencéphalographie (MEG) permettent de mesure l'activité électrique et magnétique générée par des populations de neurones à l'échelle du cerveau tout entier, sans se restreindre à une région en particulier et en conservant une très bonne résolution temporelle (à l'échelle de la milliseconde). Cette différence est cruciale, puisqu'elle permet non seulement de mesurer l'activité cérébrale au sein d'une même région, mais aussi la communication et la transmission d'informations entre plusieurs aires cérébrales, grâce aux méthodes de connectivité fonctionnelle et effective (Varela et coll., 2001). Le développement de méthodes d'analyse du signal EEG et MEG (voir encadré) a donc permis de capturer les dynamiques cérébrales du cerveau entier chez l'humain, sans avoir besoin de choisir une région a priori et avec des participants capables d'effectuer un large éventail de comportements cognitifs complexes sans surentraînement.

## LES MÉTHODES D'ANALYSE DU SIGNAL EEG ET MEG

L'activité électrique (enregistrées par l'EEG) et magnétique (enregistrée par la MEG) sont des mesures directes des fluctuations d'activité au sein de populations de neurones dans le cerveau, grâce à des capteurs/électrodes situés à l'extérieur de la boîte crânienne. Les signaux EEG et MEG sont issus de la sommation temporelle et spatiale des potentiels électriques post-synaptiques (PPS) générés par les neurones pyramidaux du cortex cérébral, qui ont une orientation parallèle particulièrement favorable à ce qu'on puisse les mesurer. L'EEG va directement mesurer ces signaux électriques émis par les neurones dans le cerveau, alors que la MEG va mesurer les champs magnétiques générés par les PPS. Les champs magnétiques sont moins sensibles aux déformations liées au fait de traverser les tissus et le crâne, ce qui permet une meilleure localisation des sources spatiales du signal enregistré par les capteurs de la MEG. Il est important de retenir qu'il faut qu'au moins 1 million de neurones s'activent simultanément pour pouvoir le capter grâce à l'EEG (environ 100 µV) ou à la MEG (mesuré en femtotesla (fT)).

***1. Les potentiels évoqués (ERP).*** Une pratique commune lors de la passation de paradigmes expérimentaux dans le domaine des neurosciences cognitives consiste à répéter de nombreuses fois la présentation de la tâche d'intérêt, afin d'avoir une meilleure estimation statistique des différences qui existent entre plusieurs conditions, et de maximiser le ratio signal/bruit de l'activité cérébrale enregistrée. L'analyse des potentiels reliés aux évènements consiste simplement à moyenner l'activité électrique enregistrée à travers les essais, afin d'obtenir une onde représentative de l'activité générée par l'apparition d'un stimulus ou par un comportement (Luck, 2014). Au fil des années, certaines propriétés de ces ondes moyennées ont été identifiées et caractérisées de manière systématique. Par exemple, l'apparition d'un stimulus visuel produit un signal caractéristique, avec une augmentation de l'activité électrique moyennée environ 100 ms après l'apparition du stimulus dans les aires visuelles. Cet ERP est nommé P100 (onde positive apparaissant atour de 100 ms), et est généralement suivi d'une baisse d'activité autour de 135 ms, appelée N135. Au total, des dizaines d'ERP ont été répertoriés, correspondant à des phénomènes sensoriels et cognitifs variés, à travers plusieurs modalités sensorielles. Il est important de noter que les mêmes analyses peuvent être effectuées avec le signal MEG, avec la différence que les ondes moyennées à travers les essais proviennent des champs magnétiques, et sont donc dénommées champs reliés aux évènements (ERF, event-related field).

***2. Les oscillations cérébrales.*** Une autre méthode d'analyse populaire pour caractériser les propriétés du signal EEG ou MEG consiste à décomposer le signal enregistré à travers plusieurs bandes de fréquence. Cette méthode, utilisée dès les premières années de l'invention de l'EEG par Hans Berger en 1929, part du principe que l'activité de populations entières de neurones qui se synchronisent et se désynchronisent (c.-à-d., oscillent) de manière rythmique et que ces oscillations jouent un rôle crucial dans de nombreux processus cognitifs et perceptifs (Varela, 2001). Au fil du temps, les chercheurs ont pu identifier et caractériser le rôle fonctionnel de ces oscillations, allant des basses fréquences, souvent associées au sommeil (delta, [2 – 4 Hz], Dang-Vu et al., 2008) et aux processus sous-tendant la mémoire et la navigation spatiale (theta, [4 – 8 Hz], Herweg et al., 2020), aux oscillations de plus hautes fréquences impliquées entre autres dans les processus attentionnels (alpha, [8 – 12] Hz, Foxe et Snyder, 2011), moteurs (beta, [15 – 30] Hz, Engel et Fries, 2010 ; Jenkinson et Brown, 2011), ou encore décisionnels (gamma, [30 – 100 Hz], Thiery et coll., 2020). Enfin, il est important de noter que la décomposition du signal en oscillations dans plusieurs bandes de fréquences s'applique aussi bien au signal EEG qu'au signal MEG. Cette technique peut être utilisée pour caractériser aussi bien l'activité locale, au sein même d'une région cérébrale, que l'activité globale au sein de régions cérébrales distantes, ou la synchronisation d'activité entre plusieurs régions cérébrales formant un réseau, qui sont enregistrées simultanément lors de l'utilisation de la MEG et de l'EEG.

Dans le domaine des neurosciences de la prise de décision, les chercheurs ont d'abord effectué une série d'études EEG ayant pour but d'identifier des signatures neuronales sous-tendant les variables des modèles de diffusion chez l'humain lors de tâches de décision perceptives classiques (p. ex. la tâche KPMA), sans sélectionner de régions a priori, et en enregistrant l'activité de tout le cortex en simultané. Dans la littérature existante, un potentiel relié aux évènements (ERP, voir encadré) classique, appelé « P300 » ou « P3 » (ERP positif autour de 300 ms) a été spécifiquement identifié comme étant lié au fait de prendre des décisions. En effet le P300 n'est évoqué que lorsque des évènements liés à la tâche requièrent de prendre des décisions (Sutton et al., 1965; Hillyard et al., 1971; Rohrbaugh et al., 1974), augmente significativement lorsqu'un stimulus est détecté comparé à un stimulus non détecté (Hillyard et al., 1971; Parasuraman and Beatty, 1980), et varie en fonction de variables comportementales comme les temps de réaction (Ritter et al., 1972; Kutas et al., 1977; McCarthy and Donchin, 1981). Pourtant, même si ces caractéristiques semblent en accord avec les postulats des modèles d'intégration, aucune de ces études n'avait explicitement testé les propriétés fondamentales des variables de décision, comme l'accumulation d'évidence sensorielle ou les seuils de décisions. C'est dans ce contexte qu'une série d'études a été menée en utilisant des paradigmes expérimentaux classiques de décisions perceptives comme la tâche KMPA lors d'enregistrement du signal EEG chez l'humain (Kelly et O'Connell, 2015). Ces études ont mené à l'identification d'un nouveau ERP, que les chercheurs ont nommé « CPP » (centro-parietal positivity), au niveau des électrodes EEG situés au-dessus des aires centrales pariétales (voir Figure 4). L'une des caractéristiques principales du CPP est son accumulation graduelle au cours de la visualisation d'un stimulus KPMA (e O'Connell et coll., 2012 ; Kelly and O'Connell, 2013). La fréquence de cette accumulation, conformément aux prédictions du modèle de diffusion, était proportionnelle à la force de l'évidence sensorielle déterminée (c.-à-d., taux de cohérence du stimulus KPMA), et invariante à la direction du mouvement des points (O'Connell et al., 2012a ; Kelly and O'Connell, 2013). De plus, des études subséquentes ont pu montrer que le CPP était observé indépendamment de la modalité sensorielle (visuelle ou auditive), de la modalité de réponse (appui bouton ou saccade oculaire), ou encore de l'aspect du stimulus. Ces observations ont conduit les auteurs à considérer le CPP comme une signature neuronale supramodale et abstraite de l'accumulation d'évidence sensorielle lors de prises de décisions entre plusieurs actions, et comme une preuve additionnelle en faveur des modèles

classiques d'intégration (Gold and Shadlen, 2007). D'autre part, le rôle des oscillations cérébrales (voir encadré) lors de décisions perceptives s'est confirmé, notamment grâce à certaines études EEG (Wyart et coll. 2012) et MEG (Donner et coll., 2009 ; Wilming et coll., 2020) récentes. En effet, lors de tâches KPMA, les oscillations de basse fréquence dans les aires sensorielles ont la charge de collecter et de traiter l'évidence sensorielle momentanée (< 20 Hz), alors que l'augmentation de l'amplitude des oscillations de haute fréquence (bêta et gamma [20-100 Hz]) correspond au processus d'accumulation d'évidence au sein des aires motrices de haut niveau, selon la modalité de réponse utilisée (Wyart et coll. 2012 ; Donner et coll., 2009 ; Wilming et coll., 2020)

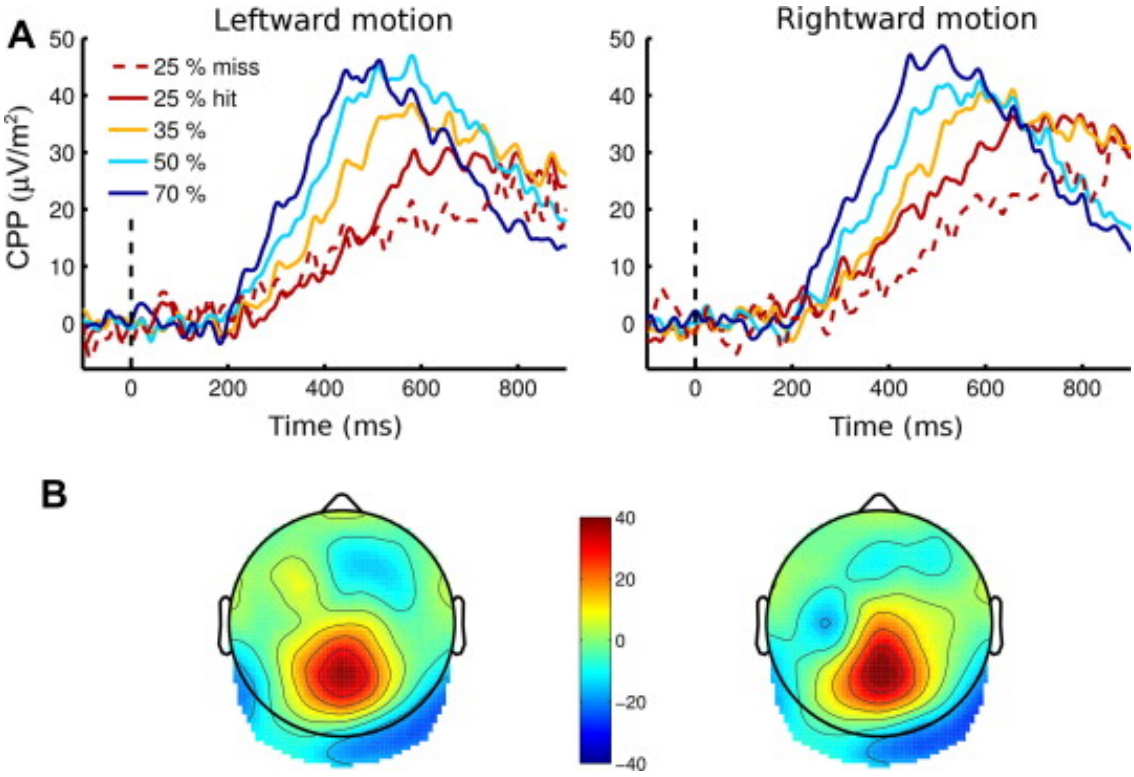


**Figure 4. A. Le potentiel évoqué CPP**, mesuré en EEG chez l'humain lors d'une tâche KPMA par Kelly et O'Connel (2013). L'accumulation du CPP est proportionnelle à la force de l'évidence sensorielle (taux de cohérence) et invariante à la direction du mouvement des points du stimulus KPMA (gauche ou droite). **B.** Topographies du CPP entre -150 et -50ms avant le mouvement de réponse. Les topographies sont identiques pour les deux directions de mouvement, et le pic d'activité est localisé au niveau des électrodes centropariétales.

Pour conclure, nous avons vu que des signaux neurophysiologiques qui présentent une dynamique cohérente avec une accumulation d'évidence sensorielle lors de la planification d'actions liées à des prises de décisions ont été observés chez plusieurs espèces (Hanes et al., 1996 ; Roitman & Shadlen, 2002 ; Gold and Shadlen, 2007 ; Hanks & Summerfield, 2017). La découverte de ces signatures neuronales vient renforcer les postulats des modèles d'intégration, en particulier celles du modèle de diffusion, mais nous allons voir que cela a également mis en lumière les limites de ces modèles, des tâches comportementales utilisées, et même des concepts fondamentaux qui définissent la prise de décision. Dans la partie suivante de cette introduction, nous verrons qu'un courant de pensée alternatif s'est construit sur les limites de l'approche classique de la prise de décision, en proposant une conception s'articulant autour de l'aspect dynamique de l'environnement dans lequel nous prenons des décisions lors de situations écologiques.

## 1.2 Théories dynamiques de la prise de décision

La combinaison d'approches neuroscientifiques et computationnelles pour étudier les processus cognitifs, en s'ancrant dans les théories traditionnelles cognitives et économiques de la fin du XX$^{e}$ siècle, ont permis des progrès considérables dans la compréhension des mécanismes qui sous-tendent la prise de décision. Néanmoins, l'arrivée des études sur le cerveau a aussi permis de questionner certains des postulats prédominants des théories cognitives et économiques classiques. Au niveau conceptuel, l'idée même qu'il existerait des systèmes perceptifs, cognitifs, et moteurs entièrement indépendants et fonctionnant de manière sérielle est peu probable. En effet, de nombreuses études montrent que les représentations neuronales (internes) du monde que nous percevons sont fortement influencées par la pertinence comportementale de l'information perçue par nos sens (Coe et al., 2002 ; Dorris et Glimcher, 2004 ; Gold et Shadlen, 2000 ; Platt et Glimcher, 1997 ; Schall & Bichot, 1998 ; Shadlen et Newsome, 2001 ; Treue, 2001 ; Yang et Shadlen, 2007). La perception et la cognition ne pourraient donc pas être considérées comme deux étapes de traitement entièrement indépendantes, puisque l'information sensorielle pertinente serait elle-même sélectionnée par des processus attentionnels endogènes (Boynton, 2005 ; Moran & Desimone, 1985) afin de permettre des

réponses comportementales adaptées (Pestilli et coll., 2011). Dans cette perspective, la perception devient un processus actif de la part du sujet et vient s'opposer à une conception passive d'un cerveau à l'image de l'ordinateur, dont le rôle serait de recevoir des inputs. La même critique peut également s'appliquer à la distinction entre la sélection parmi plusieurs actions et la planification d'un mouvement moteur. Selon les cognitivistes, la sélection d'une alternative doit précéder l'élaboration d'un plan moteur, (Tversky & Kahneman, 1981), ces deux fonctions étant réalisées par des corrélats neurophysiologiques distincts, sans aucun chevauchement temporel (Keele, 1968 ; Miller, 1960). Pour les décisions économiques et abstraites, on peut imaginer que cette hypothèse intuitive ait été soutenue par les théories économiques de l'époque. Pourtant, il est difficile d'imaginer que d'autres types de décisions, plus fréquentes lorsqu'on évolue dans un environnement naturel et dynamique, puissent s'effectuer selon le même schéma. En effet, les animaux et les humains n'ont que très rarement le luxe de délibérer indéfiniment, et de collecter la totalité des informations afin d'acquérir une connaissance complète de l'environnement dans lequel ils se trouvent avant de prendre une décision. La plupart du temps, ils sont amenés à prendre des décisions sur ce qu'il faut faire (sélection de l'action) et comment le faire (spécification de l'action) dans l'instant, en construisant des représentations d'actions possibles, ou affordances (Gibson), mêmes si les informations sont partielles ou trompeuses. Lorsqu'un animal est en train d'essayer d'échapper à un prédateur, ou que Zinedine Zidane se dirige vers le but, mais que deux défenseurs adverses foncent vers lui, le temps joue un rôle crucial, et les décisions qui s'ensuivent ne peuvent être envisagées comme séquentielles ou abstraites.

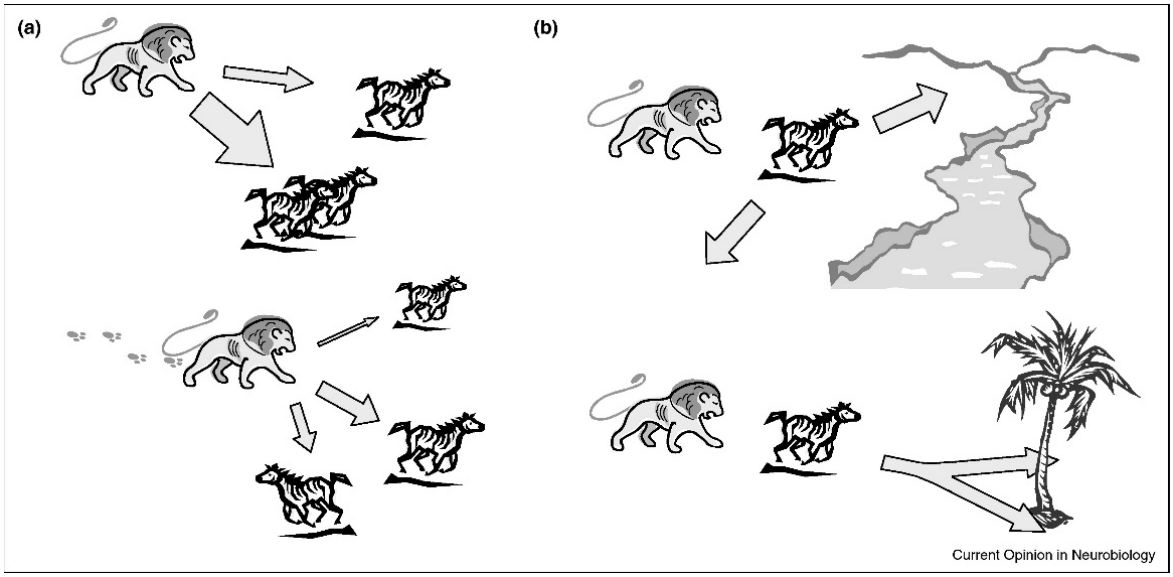


**Figure 5. Schéma de scénarios de prise de décision lors de comportements naturels. A.** L'environnement dans lequel évolue le lien fournit des informations par rapport aux métriques spatiales, et aux valeurs relatives au fait de poursuivre certaines actions (flèches, la valeur est indiquée par la largeur de la flèche). Lors de situations naturelles, l'information est constamment en train de changer, et ce qui était autrefois une seule action peut d'un seul coup se séparer en deux (en bas). B. Lorsque le zèbre fait face à deux options pour s'échapper (en haut), celui-ci doit prendre une décision tout ou rien, alors que quand les deux chemins pour s'échapper sont proches l'un de l'autre, celui peut mélanger les options au début, puis tendre vers l'une ou l'autre au fur et à mesure qu'il s'approche de l'obstacle (adapté de Cisek, 2012).

À partir de ce constat, des théories alternatives se sont développées, en s'ancrant dans une perspective évolutionniste et écologique et en proposant que les décisions entre plusieurs actions naissent d'une ***interaction dynamique*** entre la perception et l'action, plutôt que de cloisonner le processus de décision dans le stade abstrait que serait la cognition (Cisek, 2012). Selon « l'hypothèse de la compétition d'affordances », les décisions sont prises par un consensus distribué, dans lequel les coûts et les paramètres spatiaux de l'action sont directement pris en considération. De plus, au lieu d'envisager qu'une seule et même variable abstraite puisse prendre en compte la totalité des paramètres pertinents avant de faire un choix, le processus décisionnel est envisagé comme étant le résultat d'une compétition entre de multiples représentations internes générées par les possibilités d'actions présentes dans l'environnement. En se basant sur la littérature existante, l'hypothèse de la compétition d'affordances fait les propositions suivantes : ***(1)*** les actions potentielles pourraient être

représentées et pré-activées simultanément dans une zone corticale donnée. Cela a été indirectement montré par des données neurophysiologiques qui suggèrent que les neurones dans les régions motrices correspondant aux bras ou aux yeux (en fonction de la modalité choisie pour exprimer la réponse comportementale) pouvaient simultanément représenter deux actions potentielles, jusqu'à ce qu'un choix soit fait. À ce moment, l'activité correspondante à l'option non choisie serait supprimée, alors que l'activité liée à l'option choisie serait amplifiée (Baumann et coll., 2009 ; Cisek et Kalaska, 2005 ; Glimcher, 2003 ; McPeek et Keller, 2002 ; Scherberger et Andersen, 2007). **(2)** Le processus de compétition entre les alternatives possibles se déroule dans les mêmes régions cérébrales que celles qui spécifient les actions (Cisek, 2006, 2007a). Cette suggestion est en accord avec le mécanisme d'attention sélective, qui postule que le processus de sélection se déroule au sein même des régions cérébrales sensorielles, dont le rôle est de traiter les percepts (Boynton, 2005 ; Desimone et Duncan, 1995 ; Treue, 2001). Les neurones sélectifs à l'orientation des stimuli, ou à un mouvement donné dans les régions impliquées dans la perception inhiberaient les neurones codant pour des représentations ou actions alternatives, ce qui aurait comme effet de créer une compétition directe entre les percepts ou actions potentiels. **(3)** La prise de décision, loin d'être un processus cognitif abstrait et isolé, influencerait directement l'activité du système sensorimoteur (Gold et Shadlen, 2000, Platt et Glimcher, 1999, Salinas et Romo, 1998, Wallis et Miller, 2003). Lorsque les animaux sont confrontés à de multiples options de réponse, le cerveau les représenterait en parallèle au sein des régions sensorimotrices (Baumann et coll., 2009, Cisek et Kalaska, 2005, McPeek et al., 2003), et ces représentations seraient modulées par les différentes variables décisionnelles (Basso et Wurtz, 1998, Dorris et Glimcher, 2004, Pastor-Bernier et Cisek, 2011, Roitman et Shadlen, 2002, Yang et Shadlen, 2007). Par exemple, les informations permettant de décider entre plusieurs actions manuelles influencent l'activité neuronale des régions prémotrices et pariétales (Hernández et coll., 2010, Klaes et al., 2011, Pastor-Bernier et Cisek, 2011), modulent l'excitabilité corticospinale (Klein-Flügge et Bestmann, 2012, Michelet et coll., 2010), et peuvent même provoquer certains réflexes (Selen et coll., 2012). Cependant, pour déterminer si les régions motrices reflètent simplement les informations provenant de régions « décisionnelles » en amont ou si le système sensorimoteur joue un rôle actif dans la délibération, l'activité neuronale doit être examinée avant l'engagement dans un choix donné, lors de tâches de décision dynamiques. Dans partie suivante, nous verrons que cette

nouvelle conception de la prise de décision a poussé les chercheurs dans le domaine des neurosciences cognitives à concevoir de nouveaux paradigmes expérimentaux dans lesquels l'information sensorielle évolue dynamiquement, et que cela a motivé l'élaboration de nouveaux modèles computationnels, et de nouvelles interprétations sur les mécanismes cérébraux à l'origine de nos prises de décision.

#### 1.2.1.1 Les modèles computationnels

Inspirés par les théories cognitives classiques, les modèles computationnels les plus populaires dans le domaine de la prise de décision se sont principalement concentrés sur des décisions nécessitant une délibération minutieuse et portant sur des informations qui restent stables au cours du temps. En effet, l'achat d'une maison par exemple, est une décision abstraite qui nécessite de collecter les informations pertinentes, et de prendre le temps de réfléchir à la meilleure option possible. Les décisions perceptives ont donc généralement été étudiées à l'aide de stimuli dont le contenu informationnel est constant au cours du temps, comme lors de la tâche KPMA (Britten et coll., 1992, Romo et al., 2004), ce qui a conduit à l'élaboration des modèles considérant que l'évidence sensorielle était intégrée jusqu'à un seuil (Gold et Shadlen, 2007, Ratcliff, 1978). Cependant, si le cerveau des vertébrés a évolué pour guider les comportements dans un monde dynamique, et que l'on considère que les décisions sont prises sur le vif à partir d'options qui changent continuellement au cours du temps, alors il devient nécessaire de tester la pertinence des modèles classiques d'intégration sur des décisions dynamiques. C'est avec cet objectif que Cisek et ses collaborateurs (2009) ont élaboré une tâche expérimentale de prise de décision, la « tâche des jetons » (c.-à-d., « tokens task »), dans laquelle l'évidence sensorielle en faveur ou contre un choix donné (gauche ou droite par exemple) varie dynamiquement au cours du temps, au sein d'un même essai (voir Figure 5).

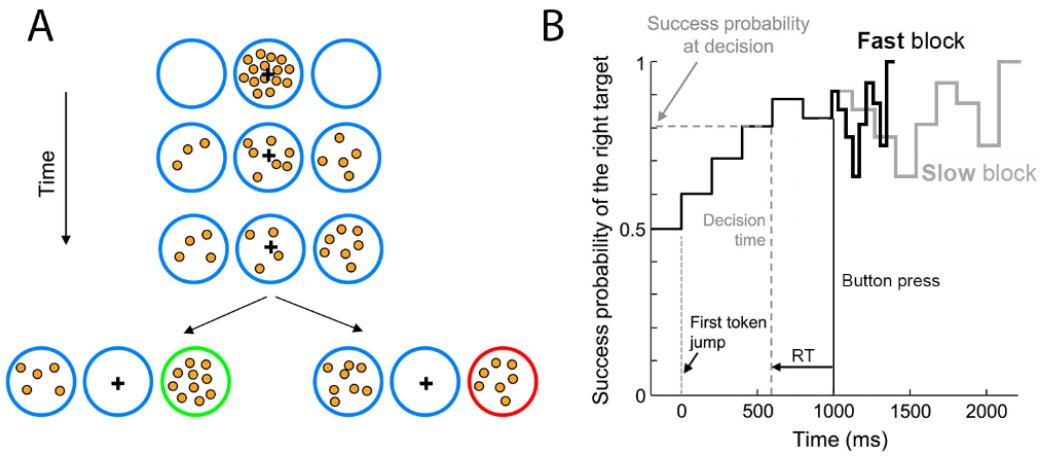


**Figure 6. La tâche des jetons. A.** L'objectif était de deviner laquelle des deux cibles périphériques (gauche ou droite) allait recevoir la majorité des 15 jetons, qui sautent du cercle central à l'une des deux cibles toutes les 200 ms. Les sujets pouvaient répondre à n'importe quel moment dans le temps, leur objectif était d'obtenir le plus de bonnes réponses possibles, le plus rapidement possible. Dans l'illustration, chaque ligne représente une étape au sein d'un même essai. **B. Évolution de la** probabilité de succès au cours d'un essai dans lequel la cible droite a été choisie. La ligne noire indique la probabilité de succès avant que la cible ne soit choisie, lorsque les jetons sautent toutes les 200ms. Après avoir choisi une cible, les jetons restants (dans le cercle central) sautent toutes les 150ms (blocs « lents », ligne grise) ou toutes les 50ms (blocs « rapides », ligne noire) vers l'une des deux cibles. Le design expérimental de cette tâche permettait donc d'introduire un compromis vitesse/précision qui était le suivant : attendre que tous les jetons aient sauté (décisions « prudentes »), ou répondre rapidement en essayant de deviner à l'avance (décisions hâtives), ce qui fait gagner du temps, mais augmente le risque de faire le mauvais choix.

L'un des éléments fondamentaux de la tâche des jetons est l'implémentation d'un compromis entre vitesse et précision (c.-à-d., speed-accuracy trade-off). En effet, lors de situations écologiques, il est souvent crucial de faire le choix le plus juste possible, mais aussi le plus rapidement possible, afin d'optimiser non pas chaque décision indépendamment, mais plutôt la fréquence de succès résultant des choix que nous faisons. Dans la tâche des jetons, les sujets sont libres de répondre à n'importe quel moment, et étant donné que l'évidence sensorielle varie au cours du temps, ils sont confrontés au dilemme suivant : s'ils choisissent de répondre trop rapidement, ils prennent le risque de ne pas avoir collecté assez d'évidence sensorielle, et de faire le mauvais choix. Au contraire, si les sujets

attendent de collecter la totalité de l'évidence sensorielle à chaque essai, ils perdent un temps considérable (i.e. coût), et la fréquence de succès sera significativement diminuée (le nombre de réponse correcte peut aussi diminuer si la durée de la tâche est limitée). Après avoir essayé de modéliser le comportement (temps de réaction, fréquence des erreurs commises) grâce au modèle de diffusion (Cisek et coll., 2009), les auteurs en sont arrivés à la conclusion suivante. Le modèle de diffusion, et de manière plus globale les modèles d'intégration, ne permettent pas de prédire avec justesse le comportement des humains lorsque l'évidence sensorielle évolue dynamiquement au cours du temps. Une des causes de cet échec est le postulat de l'existence d'un seuil fixe et constant des modèles d'intégration. En effet, un animal ou un être humain évoluant dans un environnement dynamique dans lequel il est crucial de prendre des décisions sur le champs ne peut pas se permettre d'avoir un seuil fixe, qui implique une accumulation d'évidence sensorielle toujours aussi importante pour l'atteindre, sans prendre en compte le temps qui passe et les conséquences potentielles de l'inaction (i.e. coût). Imaginez par exemple que vous êtes au volant de votre voiture, que vous partez en vacances et que vous arrivez à un croisement. Vous n'êtes pas sûr de la route qu'il faut emprunter, malgré les multiples évidences sensorielles fournies par les panneaux de circulation, le GPS, votre copilote qui regarde une carte… Dans ce cas de figure, même si vous n'êtes pas sûr de la route à emprunter et que l'évidence sensorielle est incomplète, il va falloir faire le choix de tourner à droite ou à gauche. Si l'évidence sensorielle devait atteindre un seuil fixe et constant, vous devriez attendre d'avoir toutes les informations nécessaires pour prendre la bonne décision, mais le temps que vous soyez complètement sûr, vous aurez probablement eu un accident. L'autre problème fondamental des modèles d'intégration classiques concerne la manière d'accumuler l'évidence sensorielle au cours du temps. Dans la plupart des tâches utilisées pour étudier la prise de décision, comme la tâche KPMA, l'information nouvelle n'apparaît qu'au début de chaque essai et n'évolue pas au cours du temps (p. ex., le taux de cohérence ne va pas évoluer au sein d'un même essai). Pourtant, nous avons vu que les chercheurs ont bien observé une augmentation prolongée de l'activité neuronale, et des temps de réaction corrélés à l'évidence sensorielle donnée par le stimulus (p. ex., le taux de cohérence du stimulus KPMA). Ceux-ci expliquaient ces résultats par le fait qu'à chaque moment du temps, l'information présente dans le stimulus est intégrée jusqu'à atteindre un certain seuil. Mais pourquoi le cerveau intégrerait-il de l'information redondante ? La logique voudrait que seule l'information

nouvelle, et donc utile pour la prise de décision soit intégrée. C'est ce que propose Cisek dans l'élaboration d'un nouveau modèle computationnel de la prise de décision : le modèle d'urgence (i.e., the urgency-gating model, voir Figure 7). Celui-ci répond aux deux critiques principales adressées aux modèles d'intégration, et propose que l'augmentation de l'activité neuronale, observée dans les études classiques de la prise de décision, provienne plutôt de la combinaison entre l'intégration d'évidence sensorielle uniquement lorsque celle-ci est nouvelle, et un signal d'urgence qui implémente un compromis vitesse/précision, mathématiquement équivalent à un seuil qui diminue au cours du temps.

Le modèle peut être formulé ainsi :

$$x_i(t) = g \cdot E_i(t) \cdot u(t)$$

L'activité neuronale $x_i(t)$ est donc le produit ***(1)*** d'un signal d'urgence $u(t)$, indépendant de l'évidence sensorielle provenant du stimulus et dont le but est de « pousser » à agir, et ***(2)*** de l'évidence sensorielle $E_i(t)$, filtrée par un filtre passe-bas et qui intègre uniquement l'information nouvelle. Celle-ci est obtenue via l'analyse perceptive afin d'identifier l'alternative la plus avantageuse.

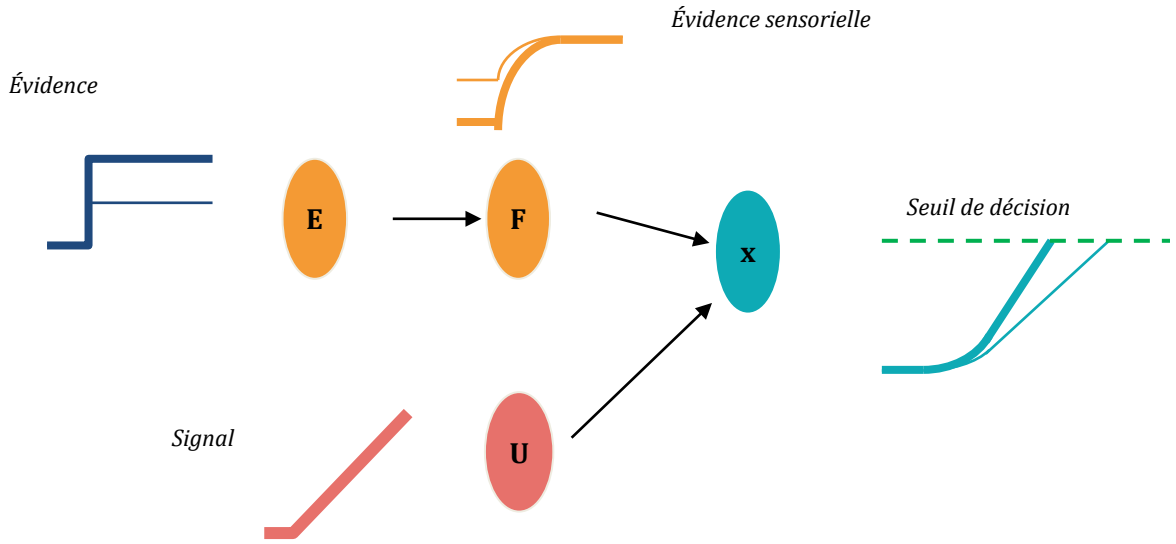


**Figure 7. Le modèle d'urgence**. L'activité neuronale *x* est le résultat de l'intégration de l'évidence sensorielle (E) filtrée par un filtre passe-bas F (en orange) uniquement lorsque celle-ci est nouvelle, et un signal d'urgence U qui augmente linéairement au cours du temps et pousse à agir (en rouge). Lorsque l'activité neuronale atteint un seuil (lignes vertes en pointillés) déterminé par la précision désirée, la décision est prise, et après un certain délai moteur (double flèche rouge), la réponse motrice est déclenchée.

Selon cette perspective, ce qui détermine le moment de l'action n'est donc plus la fin de processus décisionnels abstraits, suivis d'une préparation, puis d'une exécution motrice. Ce serait plutôt la force de l'évidence sensorielle en faveur d'une alternative donnée, combinée à un signal moteur lié à l'urgence de faire un choix, qui ensemble permettraient de transformer les décisions en actions. L'idée que le seuil de décision ne serait pas fixe, mais pourrait décroître au cours du temps à cause d'un signal d'urgence grandissant qui pousserait l'activité neuronale à s'engager dans un choix a été considérée par plusieurs chercheurs, qui ont utilisé aussi bien des tâches classiques que dynamiques (Churchland et al. 2008 ; Cisek et coll. 2009, 2016).

En effet, lorsque les participants pouvaient répondre à n'importe quel moment, et que le fait même de délibérer plus longuement avait un coût puisqu'une pression temporelle (implicite ou explicite) était introduite dans les instructions ou dans le design expérimental, l'utilisation signal d'urgence était nécessaire pour modéliser les réponses comportementales (Drugowitsch et coll., 2012 ; Frazier et Yu, 2008, Thura et al., 2012 ; Carland et coll., 2016). En se basant sur ces résultats, les chercheurs ont ensuite voulu évaluer la pertinence des prédictions du modèle d'urgence au-delà du comportement,

en se tournant vers des études neurophysiologiques afin de cartographier les variables décisionnelles du modèle au niveau cérébral.

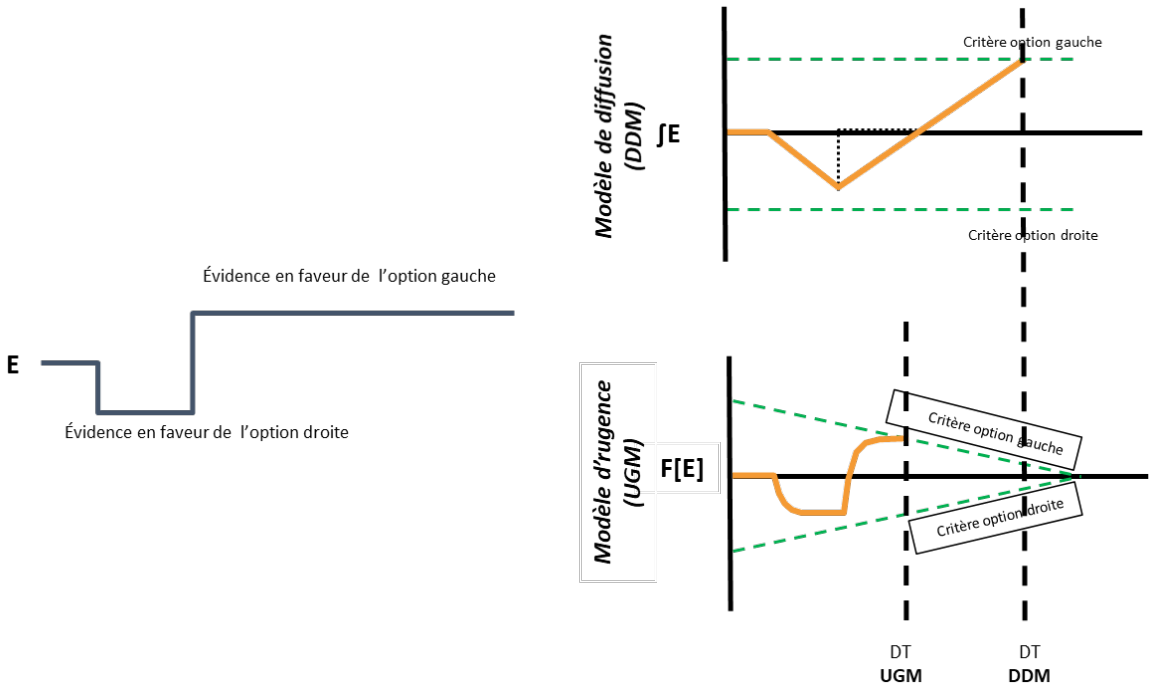


**Figure 8. Schéma comparatif entre le modèle de diffusion (DDM) et le modèle d'urgence (UGM) lorsque l'évidence sensorielle change au cours du temps.** Modélisation de l'évidence sensorielle *E* qui change de direction, en se dirigeant dans un premier temps vers l'option droite, puis vers l'option gauche. Selon le modèle de diffusion, l'évidence sensorielle est intégrée (∫E) au cours du temps alors que pour le modèle d'urgence, l'évidence est filtrée (passe-bas), intégrée uniquement lorsqu'il y a de l'information nouvelle (comme un changement en faveur de l'une des deux options), et combinée à un signal d'urgence illustré ici par des seuils de décision convergents (équivalent mathématique). Ce schéma illustre le fait que le modèle d'urgence est plus dynamique et s'adapte plus rapidement aux changements d'évidence sensorielle, ce qui résulte en un temps de décision (DT) plus rapide, donc plus réactif.

### 1.2.1.2 Les signatures électrophysiologiques

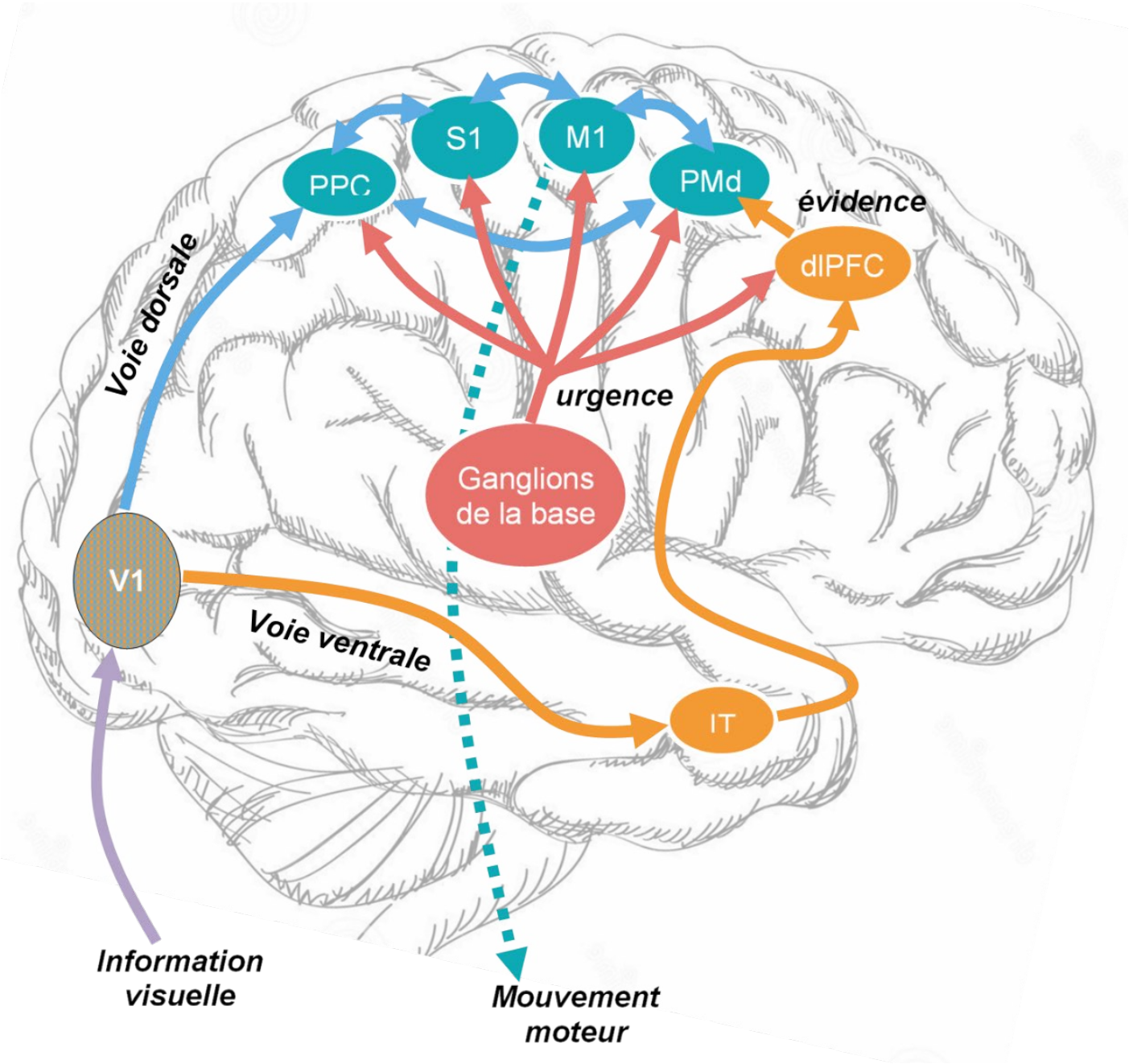


**Figure 9.** Cartographie des aires cérébrales sous-tendant les variables décisionnelles du modèle d'urgence. L'information visuelle parcourt la voie ventrale en passant par le cortex temporal inférieur, avant d'atteindre le cortex dorsolatéral préfrontal (dlPFC), chargé de suivre (« track ») l'évidence sensorielle. En parallèle, un signal d'urgence est généré par les ganglions de la base. Celui-ci augmente linéairement au cours du temps, son rôle étant de pousser à l'action. L'évidence sensorielle et le signal d'urgence sont envoyés aux aires sensorimotrices M1, PMd, S1 et PPC, au sein desquelles la compétition entre les différentes actions potentielles a lieu, jusqu'à ce que cette compétition soit résolue, ce qui se traduit par l'engagement dans un choix et la production d'un mouvement moteur.

Au cours des dernières années, Cisek et ses collaborateurs ont mené plusieurs études neurophysiologiques chez le singe pendant qu'ils effectuaient la tâche de décision dynamique des jetons (Figure 6), dans le but de tester les prédictions du modèle d'urgence (Thura & Cisek, 2010; 2014 ; 2016). Grâce à ces travaux de recherche, les auteurs ont pu mettre en évidence le rôle de différentes régions cérébrales dans les processus décisionnels lorsque l'évidence sensorielle change dynamiquement au cours du temps, au sein d'un même essai. Les neurones du cortex dorsolatéral préfrontal (dlPFC) sont en mesure de recueillir et de « suivre » l'évidence sensorielle au cours du temps (Thura & Cisek, 2010). En effet, une corrélation significative a été observée entre l'activité des neurones du dlPFC et la probabilité de succès $p_i(t)$ associée à la distribution des jetons (nombre de jetons ayant sauté dans la cible droite, dans la cible gauche, et nombre de jetons restants au centre) au cours du temps. L'activité des neurones du dlPFC n'était pas modulée ni par le fait de s'engager dans une décision ni par l'exécution du mouvement moteur (dans cette étude, un mouvement du bras) pour atteindre la cible choisie. Toujours selon le modèle d'urgence, l'augmentation d'activité neuronale au cours du temps ne serait donc pas liée à l'intégration de l'évidence sensorielle, mais à la combinaison d'un signal chargé de suivre l'évidence sensorielle (dlPFC) et d'un signal d'urgence, qui permettrait de « pousser » à l'action en fonction du compromis vitesse/précision. Toujours en utilisant la tâche des jetons, les auteurs ont montré qu'un signal neuronal d'urgence pouvait être observé dans le globus pallidus interne et externe, et que celui-ci permettait de contrôler le compromis vitesse/précision à adopter lors de prises de décision dynamiques, afin d'optimiser la fréquence de récompense (Thura et coll., 2012 ; Thura & Cisek, 2016). En d'autres termes, un signal neuronal d'urgence plus faible était généré par les ganglions de la base lorsque la situation nécessitait de délibérer plus longuement, afin de retarder le moment de l'engagement dans un choix. Au contraire, une activité neuronale plus forte engendrait des réponses plus rapides. Ces résultats sont en accord avec l'hypothèse selon laquelle les ganglions de la base motivent la génération de mouvements volontaires (Pasquereau et coll., 2007), et influencent la vigueur du mouvement (Dudman and Krakauer, 2016 ; Turner and Desmurget, 2010). Il est aussi important de noter que d'autres études expérimentales utilisant des tâches différentes de celle des jetons ont montré l'existence d'un signal d'urgence, indépendant de l'évidence sensorielle, dans l'aire LIP (Churchland et coll., 2008 ; Hanks et al.,2014) ainsi que dans les aires motrices et prémotrices (Thura et Cisek, 2014). Une hypothèse

plausible, formulée par les articles de Cisek, serait que ce signal d'urgence soit généré par les ganglions de la base, et transmis à de nombreuses régions cérébrales impliquées dans la prise de décision, comprenant les régions sensorimotrices.

Enfin, le modèle d'urgence postule l'existence d'une région cérébrale qui pourrait combiner (1) le flux continu d'informations relatives à l'évidence sensorielle provenant du dlPFC et (2) le signal d'urgence généré par les ganglions de la base, afin qu'une compétition s'établisse entre les différentes actions possibles. En 2014, Thura et Cisek montrent que ce sont les régions motrices (M1) et prémotrices (PMd) qui jouent ce rôle particulièrement important en reflétant à la fois l'évidence sensorielle, le signal d'urgence, et l'engagement dans un choix précédent l'exécution du mouvement moteur approprié. Pour résumer, ces résultats viennent non seulement corroborer les postulats du modèle d'urgence, mais aussi l'hypothèse de la compétition d'affordances, selon laquelle de multiples actions potentielles sont spécifiées simultanément et entrent en compétition au sein du système sensorimoteur (Cisek, 2007). Cette compétition est influencée par un flux continu d'informations sensorielles (Coles et coll., 1985, Kim et Shadlen, 1999), combiné à un signal d'urgence qui crée progressivement des tensions entre les alternatives possibles, jusqu'à ce que l'une d'elles devienne suffisamment forte pour supprimer l'autre. Ce moment, qui correspond à la résolution de cette compétition entre actions au sein du système moteur, correspond à l'engagement volontaire dans un choix d'action donné.

À travers cette introduction, nous avons pu voir qu'une alternative aux théories classiques de la prise de décision a émergé au cours des dernières années. Le postulat qu'un signal d'urgence serait nécessaire lors de décisions proches de celles que nous prenons dans un environnement naturel a été confirmé par plusieurs études comportementales à travers plusieurs espèces, et par de récentes études neurophysiologiques chez le singe. Mais plusieurs questions subsistent : comment peut-on confirmer que les régions cérébrales choisies chez le singe (dlPFC, ganglions de la base, cortex sensorimoteur par exemple) sont les seules à être impliquées dans les variables décisionnelles lors de situations dynamiques ? Quelles sont les interactions entre ces différentes régions ? Les mécanismes neuronaux sont-ils similaires ou différents de ceux observés chez le singe lorsque des participants humains prennent des décisions dynamiques ? À notre connaissance, aucune étude à ce jour n'a exploré les corrélats neuronaux sous-tendant la prise de décision dynamique chez l'humain.

Cependant, quelques études ont été menées en imagerie par résonnance magnétique fonctionnelle (IRMf), et ont utilisé des tâches classiques avec ou sans pression de temps pour révéler l'existence de ce qui s'apparente à un signal d'urgence chez l'humain. Lorsqu'une pression de temps était présente, l'activité cérébrale était plus forte dans les aires frontales, incluant le dlPFC (van Veen et coll., 2008), pariétales et dans le striatum (Forstmann et coll., 2008 ; Ivanoff et al., 2008). Les auteurs suggèrent que l'activité de base (c.-à-d., baseline activity) des neurones qui ont la charge d'intégrer l'évidence sensorielle au cours du temps serait plus élevée, et pousserait les participants à agir plus vite. Une autre étude, menée par Murphy et ses collaborateurs (2016) en EEG, a mis en évidence l'augmentation des oscillations alpha (8-14 Hz) au niveau des électrodes se situant au-dessus des régions motrices lorsqu'une contrainte de temps était imposée, durant la période qui précédait la réponse des participants. Enfin, plus récemment, la même équipe de chercheur a montré que la variable de décision était encodé dans les régions corticales impliquées dans la planification d'actions motrices, et que les oscillations neuronales dans la bande de fréquence alpha au sein des régions du cortex visuel reflètent l'évolution de la variable de décision, et son accumulation au cours du temps (Murphy et al., 2021). L'ensemble des résultats de ces études vient confirmer que chez l'humain, une modification de l'activité neuronale dans certaines régions corticales (frontales, pariétales) et sous-corticales (striatum, ganglions de la base) sous-tend l'existence de contraintes temporelles lors de la prise de décision.

Dans cette introduction, nous avons pu faire un état de la littérature sur l'évolution des concepts, des expériences et des résultats accumulés au fil des ans autour des neurosciences de la prise de décision. Dans la partie suivante, nous introduirons les objectifs généraux de cette ainsi que les articles qui la composent.

.

# Chapitre 2

# Objectifs généraux et présentation de articles

La présente thèse comporte deux articles principaux, présentés dans cette section. Nous avons également inclus en annexe un 3e article, effectué pendant la même période et partiellement relié au travail principal présenté dans cette thèse au niveau des méthodes utilisées. L'auteur de cette thèse est le premier auteur de tous ces articles. Les deux articles principaux de cette thèse portent sur les corrélats électrophysiologiques de la prise décision entre plusieurs actions chez l'humain. En ce sens, les objectifs généraux de cette thèse consistent à identifier les signatures neuronales électrophysiologiques à l'origine des processus qui permettent de délibérer entre plusieurs actions possibles et de façon dynamique avant de s'engager dans un choix en particulier.

### 2.1.1 Premier article

Dans le premier article de cette thèse, nous utilisons pour la première fois une mesure directe de l'activité neuronale chez l'humain grâce à l'EEG intracrânien, permettant ainsi de décoder les corrélats neuronaux qui sont spécifiques au processus de délibération lors de décisions volontaires grâce à l'utilisation d'algorithmes d'apprentissage machine. Le résultat principal de cette étude est l'observation d'une augmentation soutenue dans le temps de l'activité neuronale de haute fréquence (60-140 Hz) dans les aires frontales et pariétales lors d'un choix libre et volontaire. Cette augmentation soutenue était spécifique au choix libre puisque (1) dans la condition contrôle impliquant un choix indicé (« cued »), aucune augmentation de l'activité haute fréquence n'était observée lors de la phase de planification, et (2) lorsque les participants devaient planifier un mouvement sur la base d'instructions données par un indice visuel, une augmentation de l'activité haute fréquence était également observée, mais celle-ci n'était pas soutenue à travers le temps. Ces résultats mettent en évidence l'importance de la dynamique temporelle de l'activité neuronale lors du processus de délibération entre deux actions lors d'un choix libre et volontaire. Cet article a été écrit par Thomas Thiery (TT), Anne-Lise Saive (ALS), Étienne Combrisson (EC), Arthur Dehgan (AD), Julien Bastin (JB), Philippe Kahane (PK), Alain Berthoz (AB), Jean-Philippe Lachaux (JPL) et Karim Jerbi (KJ). AB, PK, JPL et KJ ont conçu l'expérience, KJ a programmé la tâche et s'est occupé de la collecte de données en collaboration avec AB, JB, PK, JPL et AB. TT, ALS, EC et AG ont analysé les données, TT a écrit le premier jet du manuscrit, ALS et KJ ont révisé le manuscrit. Cet article a été publié dans le journal PloS Biology (doi : https://doi.org/10.1371/journal.pbio.3000864).

### 2.1.2 Deuxième article

Dans le deuxième article de cette thèse, nous avons enregistré pour la première fois l'activité cérébrale de participants humains lors d'une tâche de prise de décision dynamique (c.-à-d., la tâche des jetons). L'objectif principal du deuxième article était donc d'analyser les caractéristiques fondamentales du processus décisionnel lors de situations dynamiques de prise de décision, soit la délibération entre plusieurs actions, l'engagement dans un choix, l'exécution du mouvement moteur permettant d'exprimer ce choix, et enfin l'implémentation d'un compromis entre vitesse et précision afin d'optimiser son taux de succès. Pour ce faire, nous avons extrait les oscillations cérébrales du signal MEG (voir encadré), dans les bandes de fréquences suivantes : thêta (5-8 Hz), alpha (9-13 Hz), bêta (16-24 Hz), gamma (30-60 Hz) et haut gamma (60–100 Hz). Nous avons ensuite utilisé une technique de réduction de dimensionnalité, l'analyse en composantes principales (PCA), pour identifier les composantes principales des oscillations de l'activité cérébrale, correspondant à chacun des processus fondamentaux intervenant lors de prise de décision dynamique. Nous avons montré que certaines composantes des oscillations alpha et bêta dans les régions visuelles et sensorimotrices permettaient de coder les changements de l'évidence sensorielle provoqués par les sauts successifs de jetons lors de la délibération. D'autre part, nous avons mis en évidence le rôle des oscillations alpha dans l'engagement dans un choix donné, et le rôle des oscillations bêta dans la préparation et l'exécution du mouvement moteur permettant d'exprimer son choix (appui bouton avec l'index gauche ou droit). Enfin, nous avons montré que l'activité cérébrale dans les hautes fréquences dans les régions sous-corticales était modulée en fonction du compromis vitesse/précision adopté par les participants.

Cet article a été écrit par Thomas Thiery (TT), Pierre Rainville (PR), Paul Cisek (PC) et Karim Jerbi (KJ). PC a conçu l'expérience, et PC, TT, PR et KJ l'ont adapté pour qu'elle soit compatible chez l'humain en MEG. TT et PC ont programmé la tâche, et TT s'est occupé de la collecte de données. TT a analysé les données, et a écrit le premier jet du manuscrit. PR, PC et KJ ont révisé le manuscrit. Cet article a été soumis au journal Nature Neuroscience, et une version est disponible sur un serveur de prépublications.

# Chapitre 3

# Article 1

# Decoding the neural dynamics of free choice in humans

Thomas Thiery[1], Anne-Lise Saive[1], Etienne Combrisson[1,2], Arthur Dehgan[1],
Julien Bastin[3], Philippe Kahane[3], Alain Berthoz[4], Jean-Philippe Lachaux[2], Karim Jerbi[1]

[1] Université de Montréal, QC, Canada

[2] Centre de Recherche en Neurosciences de Lyon (CRNL), Lyon, France

[3] Grenoble Institut des Neurosciences, Grenoble, France

[4] Collège de France, Paris, France

Corresponding author: Thomas Thiery Email: thomas.thiery@umontreal.ca

Address: Department of Psychology, University of Montreal, C.P. 6128 succ. Centre- Ville, Montréal, QC, H3C 3J7, Canada

## 3.1 Abstract

How do we choose a particular action among equally valid alternatives? Nonhuman primate findings have shown that decision-making implicates modulations in unit firing rates and local field potentials (LFPs) across frontal and parietal cortices. Yet the electrophysiological brain mechanisms that underlie free choice in humans remain ill defined. Here, we address this question using rare intracerebral electroencephalography (EEG) recordings in surgical epilepsy patients performing a delayed oculomotor decision task. We find that the temporal dynamics of high-gamma (HG, 60–140 Hz) neural activity in distinct frontal and parietal brain areas robustly discriminate free choice from instructed saccade planning at the level of single trials. Classification analysis was applied to the LFP signals to isolate decision-related activity from sensory and motor planning processes. Compared with instructed saccades, free-choice trials exhibited delayed and longer-lasting HG activity during the delay period. The temporal dynamics of the decision-specific sustained HG activity indexed the unfolding of a deliberation process, rather than memory maintenance. Taken together, these findings provide the first direct electrophysiological evidence in humans for the role of sustained high-frequency neural activation in frontoparietal cortex in mediating the intrinsically driven process of freely choosing among competing behavioral alternatives.

**Keywords**

Decision-making; Free choice; Oculomotor; Intracerebral EEG; Neuronal oscillations; Machine learning; Gamma band; Saccades; Stereotactic-EEG

## 3.2 Introduction

Deciding where to look to explore the visual world, i.e. picking one out of many alternative targets is a crucial aspect of our daily interactions with the environment. Exploring the neural mechanisms underlying eye movement control provides a promising approach for learning about sensorimotor and cognitive aspects of voluntary action selection and planning (Sweeney et al., 2007). Studies in non-human primates have extensively described the temporal dynamics of spiking activity and local field potentials (LFPs) in frontoparietal areas when animals perform delayed oculomotor response tasks. Planning an instructed saccade involves the same effector specific circuits that execute eye movements, namely the frontal eye fields (FEF), (Coe et al., 2002; Schall & Bichot, 1998) and the lateral intraparietal area (LIP), (Dorris & Glimcher, 2004; Gold & Shadlen, 2007; Platt & Glimcher, 1999; Sugrue et al., 2004; Yang & Shadlen, 2007), as well as a characteristic sustained neuronal activity in frontal areas, representing information about stimuli maintained in working memory during the delay period (Constantinidis et al., 2018; Lundqvist et al., 2018; Stokes, 2015). On the other hand, while monkey studies have demonstrated that free choice decision processes (e.g, choosing between two equal reward options) appear to be represented in an effector specific frontoparietal network (Christopoulos et al., 2018; Cisek & Kalaska, 2005; Klaes et al., 2011; Mochizuki & Funahashi, 2016; Pesaran et al., 2008; Procyk & Goldman-Rakic, 2006; Shima et al., 1991; Suriya-Arunroj & Gail, 2019; Watanabe et al., 2006; Wilke et al., 2012), the temporal dynamics of the neural correlates of free choice decisions compared to those underlying instructed planning are poorly understood.

In humans, behavioral and neural signatures of voluntary, free choice have been studied extensively (see reference (Haggard, 2019) for review). Converging evidence from neuroimaging studies suggests that the neural processes which mediate saccade decisions, planning and execution arise across large-scale brain networks that involve parietal, frontal, and motor cortices (Anderson et al., 2012; Kagan et al., 2010; McDowell et al., 2008; Sweeney et al., 2007). A parietal oculomotor field (PEF), located in the posterior part of the parietal cortex (which is thought to correspond to LIP in monkeys) (Berman et al., 1999), seems to be principally implicated in triggering reflex saccades. By contrast, the FEF is thought to play a central role in preparation of the saccades by coding both the motor preparation and the intention to make a saccade (Bastin et al., 2012; Blanke & Seeck, 2003;

Connolly et al., 2002; Olk et al., 2006; Petit et al., 1997; Pierrot-Deseilligny et al., 2002; Tobler & Müri, 2002). Lastly, functional magnetic resonance imaging (fMRI) studies have shown that internally driven decisions were associated with greater activation of a neural system involving premotor (and particularly the caudal pre Supplementary Motor area, preSMA) and prefrontal areas such as the medial and dorsolateral prefrontal cortex (Ariani et al., 2015; Nachev et al., 2005, 2008; Zapparoli et al., 2018). In a study by Rowe and colleagues, the authors showed that the prefrontal cortex was involved in both response selection and maintenance within working memory during a ''free-selection'' task (Rowe et al., 2000). Importantly, two fMRI studies using the same delayed saccade task used in this article have specifically shown that voluntary saccades were preceded by activation in the dorsolateral prefrontal cortex (DLPFC) and in the frontal eye fields, suggesting the involvement of these areas in the process of choosing where to look when facing two possible visual targets (Khonsari et al., 2007a; Milea et al., 2007a). However, fMRI can unfortunately not resolve the precise temporal dynamics of activity in these brain areas, neither can it probe the role of rhythmic brain activity. To address these questions, electrophysiological investigations are required.

Non-invasive electrophysiological studies have demonstrated the involvement of high-frequency neuronal oscillations in several areas ("eye or oculomotor fields") of the cerebral cortex during saccade planning and execution using techniques such as MEG and EEG (Carl et al., 2016; Moon et al., 2007; Van Der Werf et al., 2009; Werf et al., 2008, 2010). Of note, two MEG studies showed increased medial frontal gamma power during the response competition in delayed motor tasks (Carl et al., 2016; Grent-'t-Jong et al., 2014), and one EEG study found differences in the P300 event-related component during action selection when comparing free choice and instructed planning (Fleming et al., 2009). Despite being extremely insightful, non-invasive techniques have several limitations in terms of signal quality, spatial resolution and sensitivity to artefacts. Fortunately, it is possible in some rare cases to access invasive electrophysiological recordings in humans (e.g. surgical epilepsy patients) and thus probe task-based changes via direct LFP recordings. The latter reflect the synchronized postsynaptic potentials of local populations of neurons (Frost & Pöppel, 1976; Mitzdorf, 1985) and allow for direct comparisons between invasive recordings of population-level activity in human and non-human primates. A handful of studies have benefited from direct recordings of neural activity

(e.g. in human FEF and DLPFC) to probe neural activation in the frontal eye fields during saccade execution (peri-saccade activity) in humans using intracranial EEG (J.-P. Lachaux et al., 2006; Sakamoto et al., 1991; Yamamoto et al., 2004). Importantly, Lachaux and colleagues (J.-P. Lachaux et al., 2006) found that the preparation and the generation of saccades were subserved by focal and transient increases in high gamma (HG) activity (above 60 Hz) in the FEF. Yet, to our knowledge, no study has so far investigated the neural correlates of oculomotor decisions (i.e. free choice saccades) using direct intracranial recordings in humans.

Taken together, previous findings from oculomotor and decision-making studies in human and non-human primates provide converging evidence for the central role of high-frequency LFP components in eye movement selection and execution. Although, some evidence from non-invasive studies partly support these observations in humans, direct electrophysiological measurements are necessary to bridge the gap between human and non-human primate literature on oculomotor decision-making. In the present study, we probe for the first time the temporal, spectral and spatial characteristics of human cortical networks engaged in the selection, planning and execution of saccades with unprecedented resolution thanks to multi-site intracerebral EEG (iEEG) recordings. In particular, we set out to test the predictions that (i) the temporal dynamics of delay-period LFP would differ between *instructed* and *self-chosen* saccade trials, and that (ii) the most prominent differences will be visible in high-frequency LFP components in key frontal and parietal areas.

In brief, we found that the intrinsically driven process of selecting among competing behavioral alternatives during free-choice decisions is associated with sustained increases of broadband high gamma (HG) (60-140 Hz) activity in distinct frontal and parietal areas that might reflect the process of deliberation between competing alternatives. By contrast, instructed saccade trials were associated with short-lived transient HG increases. The unique intracerebral recordings reported here provide important insights into the spatio-temporal characteristics of the neural patterns underlying free choice and help bridge the gap with previous animal electrophysiology and non-invasive studies in humans.

## 3.3 Results

Six participants (4 females, mean age 30.3 ± 9.6, see Material and Methods and Fig 1B, C) performed a delayed saccade task (Fig 1A) while electrophysiological data were recorded from multi-lead EEG depth electrodes. In each trial, participants were instructed to perform horizontal saccades toward one of two targets, but only after a variable delay period. The information about saccade direction was indicated by a visually presented central cue (Cue 1), followed by a saccade execution Go signal (Cue 2). The task consisted of three interleaved experimental conditions (Fig 1A): In the ***Free*** condition, a diamond at Cue 1 prompted the participants to freely choose the direction of the forthcoming saccade. In the ***Instructed*** condition, an arrow pointing left or right indicated to the participants the direction of the saccade they were to prepare. After a variable delay (3.5-7.75 seconds) during which the participants prepared the adequate saccade while fixating the central fixation point, a GO signal (Cue 2) prompted the participants to immediately execute the saccade. In the ***Control*** condition, participants were presented with a square at Cue 1, indicating that they would need to wait for the GO signal (Cue 2) to find out the required saccade direction and execute it immediately. Behavioral saccade onset latency data were collected, and spectral power features were extracted from the iEEG data across multiple time windows and all electrode sites. Power features were computed in five standard frequency bands: theta (θ) [4–8 Hz], alpha (α) [8–15 Hz], beta (β) [16–30 Hz], low-gamma (low γ) [30–60] and high gamma (high γ, HG) [60-140 Hz]. A supervised machine learning framework was implemented to decode (through space, time and frequency) the experimental conditions (free, instructed and control), and thereby identify the most discriminant neural patterns that distinguish between free-choice and instructed actions during saccade planning and execution (see Material and Methods for details).

**Behavioral results**

We computed the mean reaction times (RTs, i.e., saccade onset latency, see Material and Methods) for each experimental condition across all participants, and found that mean RTs were significantly longer for the ***Control*** condition (mean RT = 466 ± 66ms) condition compared to both ***Free*** (mean RT = 334 ± 36ms; $t_{(6)} = 2.75$, $p = 0.0403$) and ***Instructed*** (mean RT = 321 ± 33ms; $t_{(6)} = 2.68$, $p = 0.0435$) conditions (see Fig 1D). No significant differences were found between Free and Instructed conditions ($t_{(6)} = 1.31$, $p = 0.24$). These results were also observed at the single participant level in 5 out of 6 participants (see Material and Methods section). These results are consistent with the fact that the availability of saccade target information (whether self-generated or instructed) during the delay period allowed the participants to plan the upcoming saccades, and hence execute them faster upon the Go signal compared to the ***Control*** condition where no directional information was available during the delay period. Mean saccade duration, saccade speed, mean latency and the number of saccades executed per condition by each participant are reported in S2 Table.

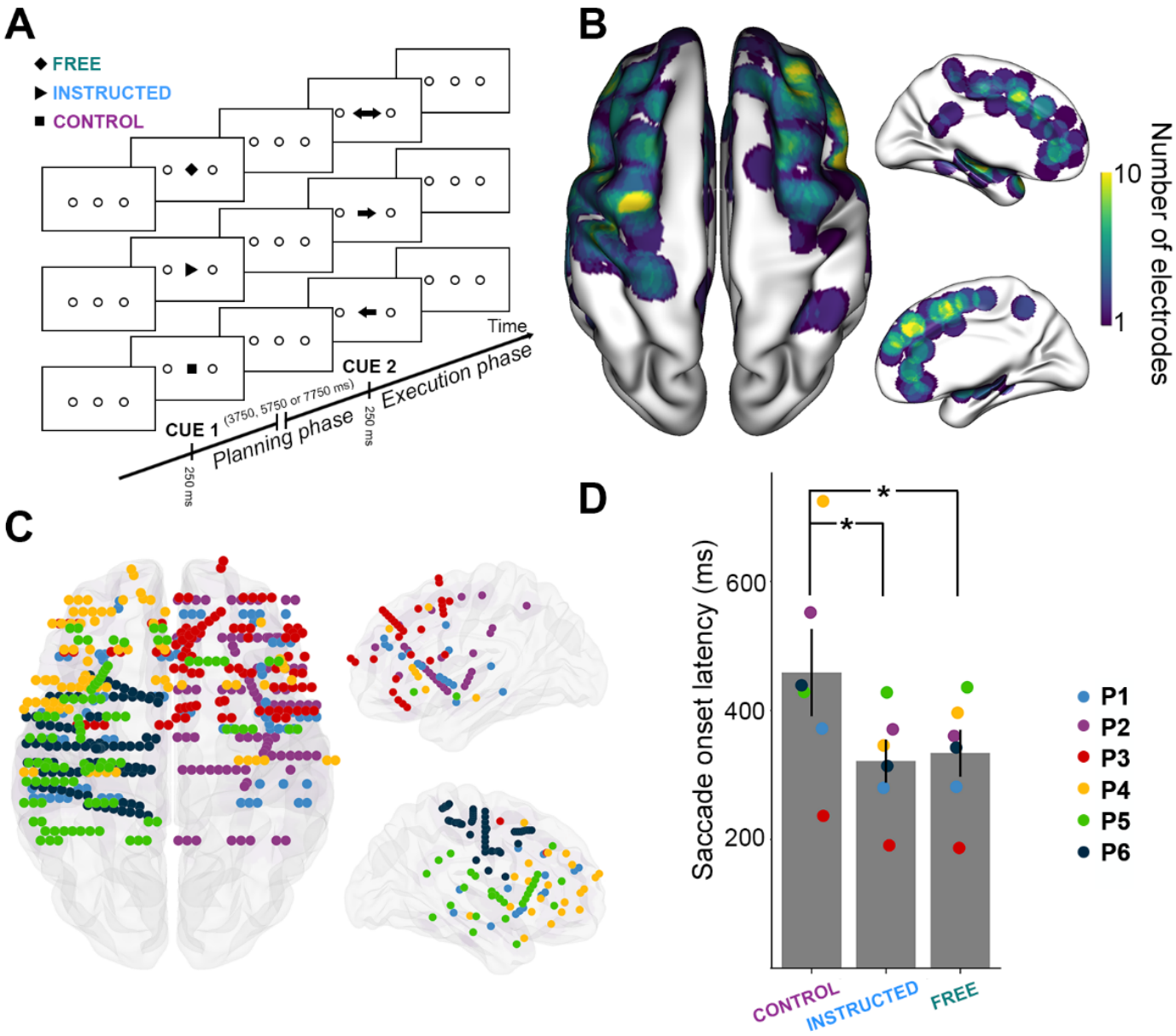


**Fig 1. Experimental design and distribution of intracranial electrode contacts across participants. A.** Experimental design of the delayed motor task. For each trial, participants were instructed to perform horizontal saccades toward one of two targets after a delay of 3750 ms, 5750 ms or 7750 ms, depending on a visually presented central cue appearing briefly for 250 ms. **B.** Top, left and right views of the number of recording sites that contribute to each vertex (i.e. spatial density) projected on a standard 3D MNI brain. Electrodes contribute to a location when they are within 10 mm of a given site on the brain surface. In all brain images, right side of the image is the right side of the brain. **C.** Top, left and right view of the depth-electrode recording sites, projected on a standard 3D MNI brain. Each color represents a participant. Left: Rostral is up, Right: medial views. **D.** Barplot of mean reaction times for the three conditions across all participants (***Control***, ***Instructed***, ***Free***). Each triangle represents the mean reaction times for one participant. The data underlying this panel **D** can be found in S1 Data.

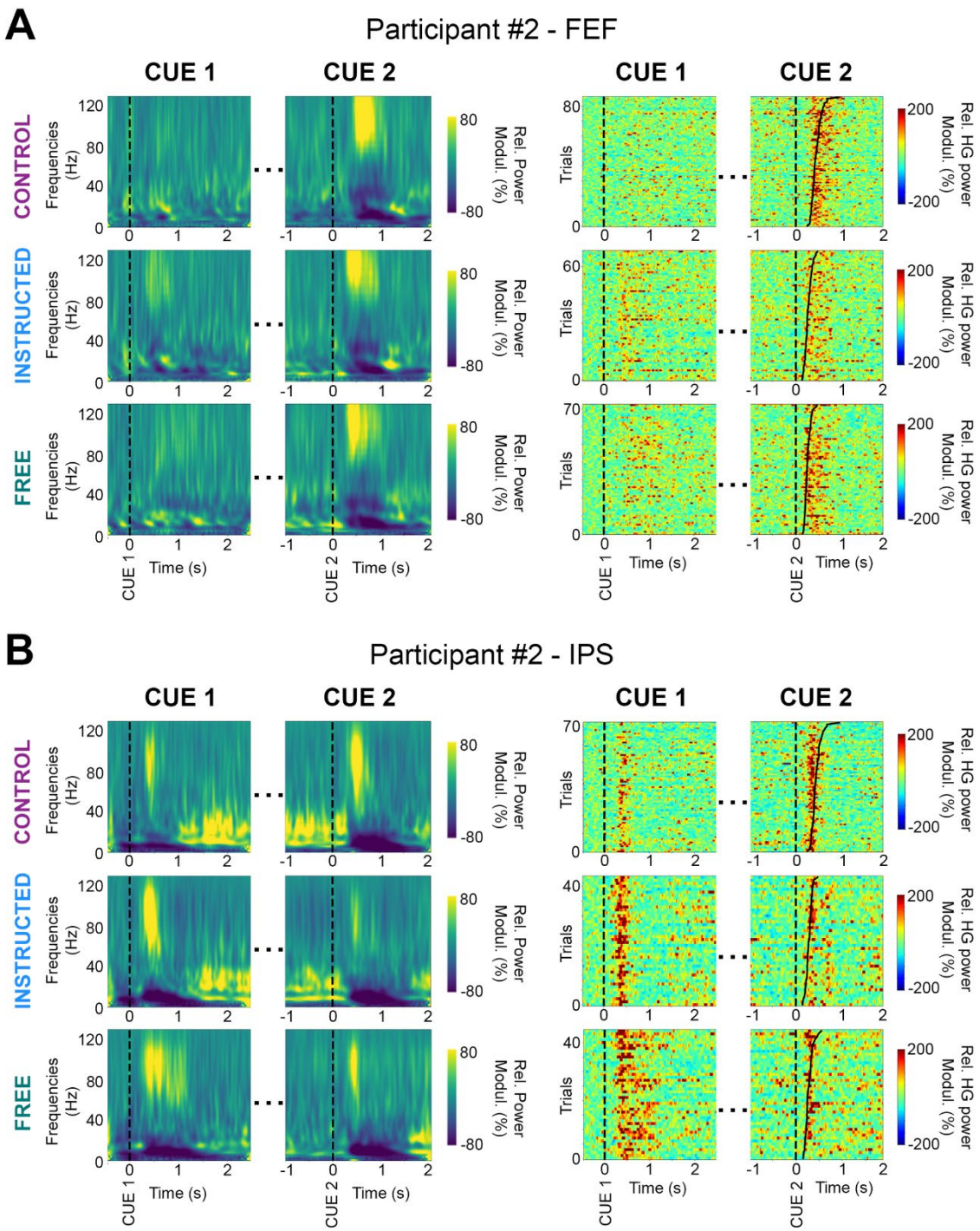


**Fig 2. Illustrative time-frequency maps and single-trial high gamma (HG) activity in FEF and IPS.** Time-frequency maps (left) and single-trial high gamma plots (right) from two recording sites in an illustrative participant (P2). Data are shown for the three experimental conditions (*Control*, *Instructed* and *Free*), during planning (Cue 1, stimulus onset) and execution (Cue 2, go signal). Trials in the single-trial gamma plots are sorted according to saccade onset latencies (IPS: intraparietal sulcus, FEF: Frontal Eye Field).

To assess modulations of the neural activity across the three delayed saccade trial types (i.e. ***Free,*** ***Instructed*** and ***Control***) over space, frequency and time, we computed time-frequency representations (locked either on stimulus onset, i.e. Cue 1, or saccade execution cue, i.e. Cue 2), as well as single-trial spectral amplitude envelopes in multiple frequency bands (theta (θ) [4–8 Hz], alpha (α) [8–15 Hz], beta (β) [16–30 Hz], low-gamma (low γ) [30–60] and high gamma (high γ, HG) [60-140 Hz]). Fig 2 illustrates these feature computations and the high quality of the intracranial data by showing time-frequency maps derived from electrodes in FEF and IPS in participant 2, as well as single-trial high-gamma activity, aligned to stimulus presentation and to saccade Go signal (ordered by saccade onset latencies). In addition, we used Linear Discriminant Analysis (LDA) to probe the ability of these spectral features to decode experimental conditions from single trial data. Importantly, we applied this machine learning framework individually to data from each recording site and in a time-resolved manner over the course of the task (see Material and Methods section for details).

**Decoding delay-period neural activity in free choice vs. instructed saccade trials**

To identify the neural patterns related to making autonomous choices, we first compared the delay-period neural responses observed during free choice saccade trials to those recorded during instructed saccade trials. This was conducted by applying LDA to classify ***Free*** vs ***Instructed*** saccade trials based on spectral amplitude estimated during the delay interval in all five frequency bands (Fig 3, see also S4 Fig). Panels A-C of Fig 3 show that, among all frequency bands, HG activity was the neural feature that provided the highest decoding accuracy and largest number of significantly decoding sites when classifying ***Free*** *vs* ***Instructed*** trials, during the delay period ([0 ; 3000ms] after Cue 1). The HG activity led to statistically significant classification in 61 sites (4 out of 6 participants) and yielded a maximum DA of 92.9 % and a mean DA of 79 % (Fig 3A-C). Interestingly, out of the two participants that did not yield any significantly decoding sites, P5 was the only participant that showed similar reaction times across the three conditions (see Figure 1D). This might reflect the fact that this participant did not make use of Cue 1 which would explain why HG activity could not significantly decode Free vs Instructed conditions during the delay period in this participant.

We then used a multi-feature classification approach (***Free*** vs ***Instructed*** trials) where observations across all electrode sites were now included simultaneously in the decoding feature space (repeated for each frequency band). We assessed the statistical significance of time-resolved decoding accuracy using permutation tests, corrected for multiple comparisons across participants, electrodes, frequencies and time points). As shown in Fig 3E, the multi-site decoding accuracy was highest for HG activity, reaching 86.8 %. Given that both single and multi-site classification results (Fig 3A-C,E) indicate that HG amplitude is the most prominent predictor of target class (***Free*** vs ***Instructed***), the next sections of the results focus on the characterization of the fine-grained temporal and spatial profiles of HG neural decoding.

Averaging the HG data across all trials from all significantly decoding sites illustrates the temporal dynamics of delay HG activity that distinguish between ***Free*** and ***Instructed*** saccade trials (Fig 3D). The associated time-resolved mean decoding accuracy is shown in Fig 3H. Because the analysis is based on averaging across all sites, panels D and H only provide a schematic representation of the temporal dynamics, without statistical assessment. Thus, we conducted standard paired t-tests to further quantify the difference in HG peak amplitudes and latencies between ***Instructed*** (mean peak HG amplitude = +39% ± 0.74 ; mean peak latency = 475ms ± 14) and ***Free*** (mean peak HG amplitude = +24% ± 1.18 ; mean peak latency = 812ms ± 97) conditions from all 61 significantly decoding sites (in 4 out of 6 participants). The results revealed significant differences (peak amplitude: $t_{(4)} = 8.34$, $p < 0.003$, Fig 3F ; peak latency : $t_{(4)} = 21$, $p < 0.0002$, Fig 3G) and were also confirmed in single-trial analyses performed individually in each of the 4 participants ($p < 0.05$, see Material and Methods). All the statistical results within and across participants are listed in S3 Table.

Additionally, Fig 3I-J represent HG decoding dynamics resolved across both space and time: In the early part of the delay period, significant decoding electrodes are associated with stronger HG power in the ***Instructed*** than in the ***Free*** condition. But over time, HG power then becomes higher for the ***Free*** saccade planning than for ***Instructed*** saccade planning during later stages of the delay period in fronto-parietal brain areas. More specifically, we show that all significant electrodes in the [0, 500ms] time-window after Cue 1 during the delay period are associated with higher HG activity in the Instructed condition (Fig 3 I-J, [0, 500ms]). On the other hand, as time goes by, significant electrodes begin to become more associated with higher HG activity in the ***Free*** compared to ***Instructed***

condition. From 1000 to 2000ms after Cue 1, we see that all significant electrodes are now associated with higher power in the ***Free*** condition (Fig 3I-J, [1000, 1500ms], [1500, 2000ms]). Additionally, we find that from 1500ms to 2000ms after Cue 1, the only electrodes that still significantly decode ***Free*** from ***Instructed*** conditions are located in frontal regions (Fig 3 I-J; [1500, 2000ms]). Interestingly, we also found sites for which HG activity was still significantly stronger in ***Free*** than ***Instructed***, at the end of the delay period, from -2000 to 0 ms before Cue 2 (Fig 3I-J). This suggests that some electrodes may display persistent activity lasting throughout the whole delay period and led to subsequent analyses described in more detail below.

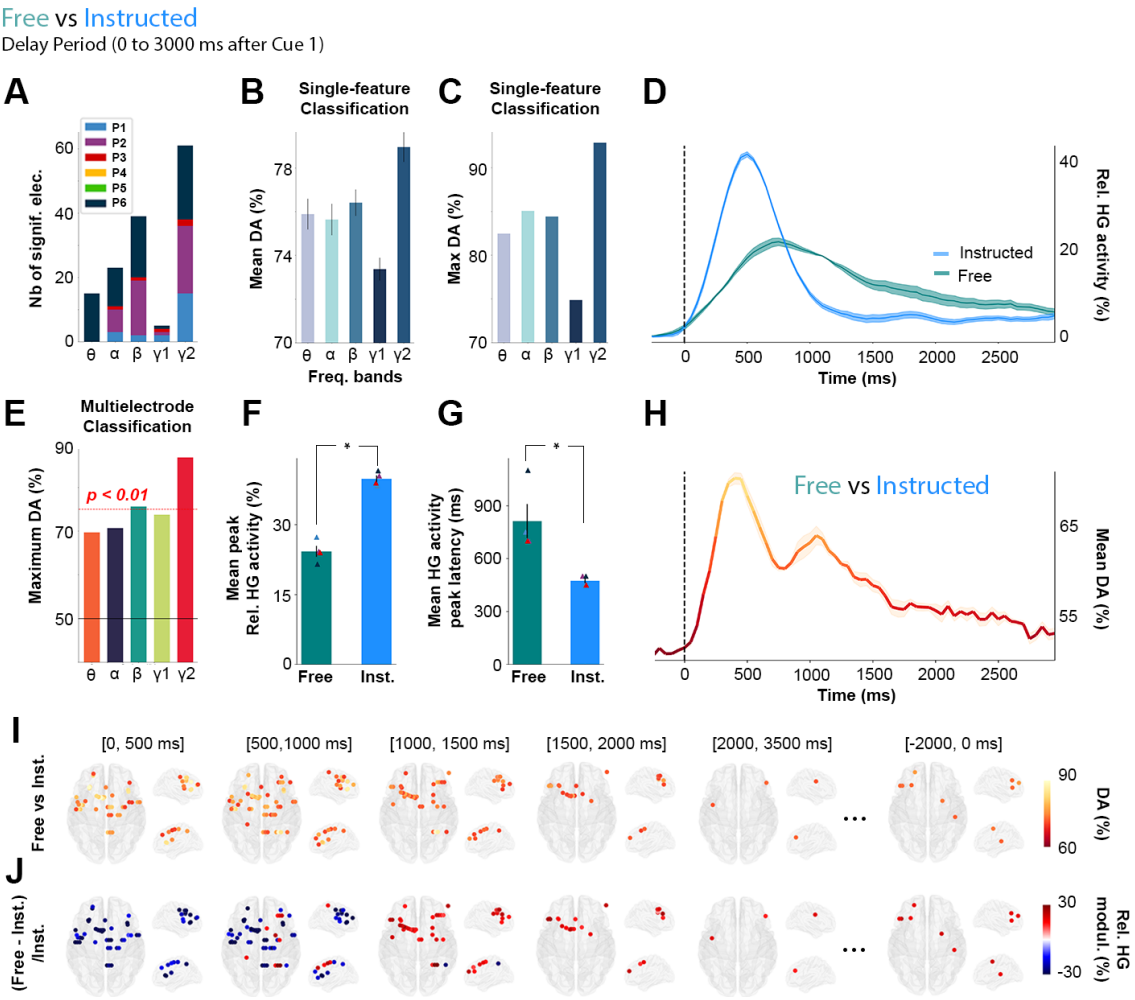


**Fig 3. Single-trial classification of *Free vs Instructed* trials based on delay-period HG activity. A.** Summary of all significant electrodes by participant across frequencies showing that the largest clusters were found in the HG frequency band. **B.** Mean and **C.** Maximum decoding accuracies across participants and significant electrodes for each frequency band for *Free vs Instructed* classification (error bars represent s.e.m.). **D**. Time course of baseline corrected (-500 to -100 ms) HG activity aligned on Cue 1, for all electrodes that significantly classify Free vs Instructed conditions and **H.** its associated mean decoding accuracy across significant electrodes. **E.** Maximum decoding accuracies across participants and significant electrodes for each frequency bands for Free vs Instructed multi-electrode classification. **F.** Relative mean HG peak activity (in %) and **G.** latency (in ms) for electrodes significantly decoding *Free* vs *Instructed* conditions during the delay period (from 0 to 3000ms after Cue 1). **I.** Decoding Free vs Instructed conditions with HG activity in 5 successive time windows during the delay period (0 to 500 ms; 500 to 1000 ms; 1000 to 1500 ms ; 1500 to 2000 ms ; 2000 to 3500 ms after Cue 1 and -2000 to 0 ms before Cue 2). Only sites with significant decoding accuracies are shown ($p < 0.01$, with max stats correction across electrodes, time, and frequency bands). **J**. Percent relative power change ([Free - Instructed]/Instructed) for all significant sites shown in panel I. The data underlying this Figure can be found in S1 Data.

In order to further characterize the temporal HG dynamics specific to ***Free*** and to ***Instructed*** saccades (beyond the strict difference between the two) while also taking into account low level stimulus-related processes, we replicated the same decoding framework as above but now with the goal of distinguishing each of the main two conditions from the ***Control*** condition (i.e. ***Instructed vs Control,*** and ***Free vs Control,*** see Fig 4). First, we found that over the first 3000ms after Cue1, there was an overlap of 56 electrodes between the electrodes that significantly classify ***Instructed*** vs ***Control*** trials as well as ***Free*** vs ***Control*** trials. In other words, 82.4 % of the sites that significantly discriminate ***Free*** vs ***Control*** conditions also significantly discriminate ***Instructed*** vs ***Control*** conditions (Fig 4A). Furthermore, we found that when participants freely chose the saccade direction, the delay HG activity lasted on average 618ms ± 57, while the instructed saccade condition displayed mean HG durations of only 368ms ± 60. The difference was statistically significant (length of time points above the significance threshold in ***Free*** vs ***Control*** compared to ***Instructed*** vs ***Control*** classifications, $t_{(4)}$ = 3.52, $p < 0.04$ across 4 participants and confirmed in intra-participant analysis in 1 individual with $p < 0.05$, see Fig 4B). We also found that HG activity during Instructed saccade planning (mean onset = 152ms ± 39) reached significant classification earlier than HG activity in the Free choice condition (mean onset = 465ms ± 49) when compared to the control (latency of first significant decoding accuracies in ***Free*** vs ***Control*** compared to those associated with ***Instructed*** vs ***Control*** classifications, $t_{(4)}$ = 7.09, $p < 0.006$ across 4 participants, see Fig 4C). This difference was confirmed with intra-participant analyses in 3 out of 4 participants with $p < 0.05$. Lastly, we show that decoding accuracy peaked significantly earlier in the ***Instructed*** condition (mean onset = 527ms ± 61) than in the ***Free*** condition (mean onset = 822ms ± 70) when compared to the Control condition (Peak decoding accuracy latencies in ***Free*** vs ***Control*** compared with ***Instructed*** vs ***Control*** classifications, $t_{(5)}$ = 3.39, $p < 0.03$ across 5 participants, confirmed with intra-participant analyses in 4 out of 5 participants with $p < 0.05$, see Fig 4D). All the statistical results within and across participants are listed in S3 Table.

**Probing HG delay temporal dynamics via temporal generalization**

In order to further characterize the fine temporal organization of information-processing during the delay period in the ***Instructed*** and ***Free*** choice conditions, we probed cross-temporal generalization (17,51) of decoding ***Instructed*** vs ***Control*** and ***Free*** vs ***Control*** conditions using HG activity (Fig 4I). In brief, temporal generalization consists in training a classifier with data from one time point $t_1$ and testing it on data from a different time point $t_2$. In principle, cross-temporal generalization indicates that the neural code identified at $t_1$ also occurs at $t_2$ (see Material and Methods). More specifically, we used temporal generalization to better characterize short-lived (transient) and longer lasting (sustained) HG activity processes underlying ***Free*** and ***Instructed*** planning. Our findings show that HG activity during instructed saccade planning yields a generalization pattern typical of transient coding (see the first column of Fig 4I), while free choice is characterized by a HG decoding process that is more sustained in time (second column of Fig 4I). Taken together, the observed cross-temporal decoding patterns and their accuracies are consistent with the view that decision-related discriminant HG activity during the delay period is more sustained and starts later in ***Free*** choice trials compared to ***Instructed*** saccade trials. In contrast, when no choice is involved, task-related information reflected in HG activity is more transient and most relevant shortly after stimulus onset. Importantly, the cross-temporal generalization results also highlight that although HG decoding in the ***Free*** choice is more sustained, it does not last systematically the entire duration of the delay period until the GO signal (Cue 2). This is consistent with our earlier observations in Fig 3I-J, that over the course of the delay period, less sites discriminate between free and instructed trials. This may suggest that while several sites display sustained HG activity for free choice saccade trials, only a few actually display persistent increases up until saccade execution. This important distinction is probed in the next section.

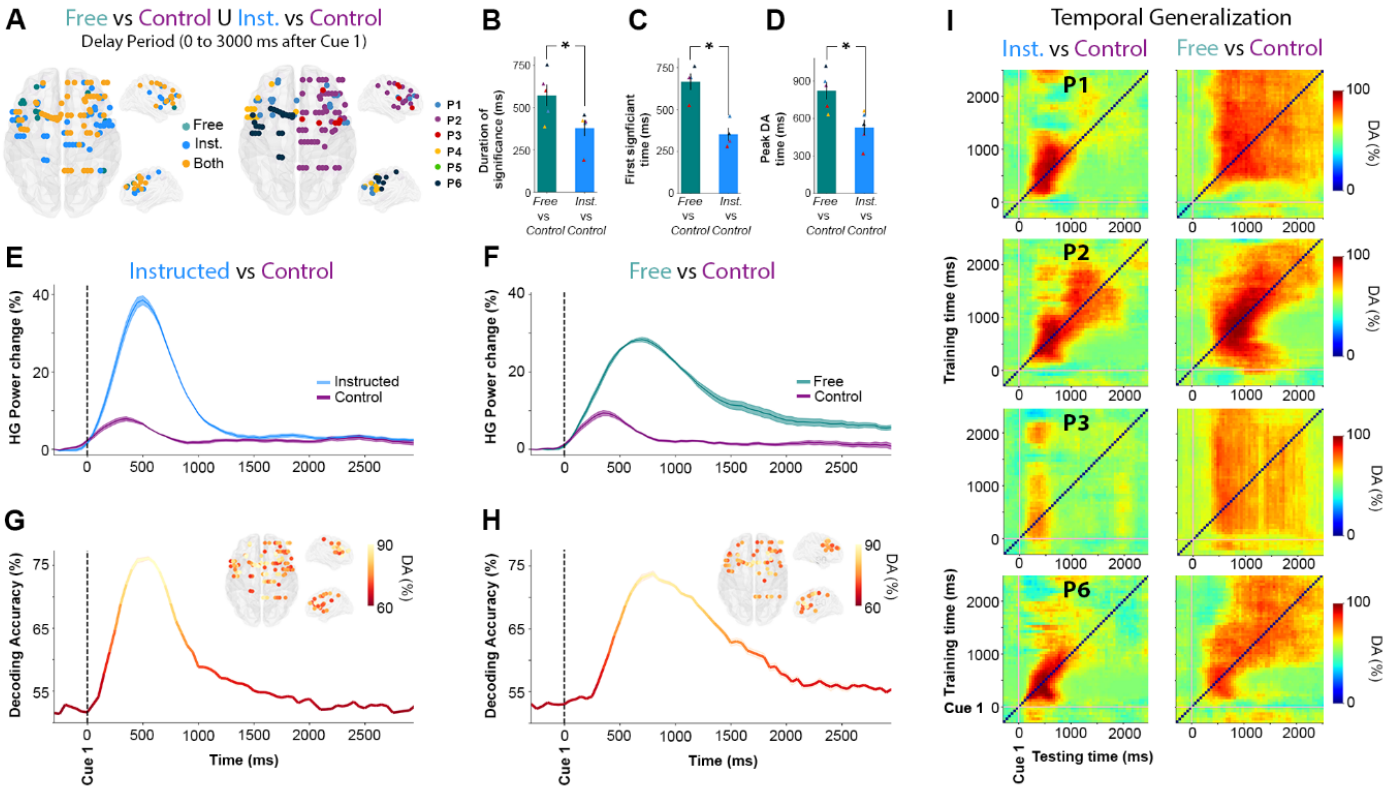


**Fig 4. Temporal dynamics of HG activity during Free and Instructed (vs Control) conditions during the delay period. A.** Location of electrode sites where HG activity discriminates *Free* vs *Control* and/or *Instructed* vs *Control* mapped on transparent 3D brain images for all participants (*p<0.01, corrected)*. Left: electrodes colored in green, blue and yellow respectively indicate sites that discriminate *Free* vs *Control* trials only, *Instructed* vs *Control* only, or both *Free* vs *Control* and *Instructed* vs *Control* during the delay period (0 to 3000 ms after Cue 1). Right: colors indicate different participants. **B.** Duration (length of time points) above the significance threshold **C**. Decoding onset (i.e**.** Latency of first significant decoding accuracies) **D.** Latency of the peak decoding accuracies (in ms) for sites significantly decode *Free* vs *Control* (in green) and *Instructed* vs *Control* (in blue) across participants. **E, F**. Time course of baseline corrected (-500 to -100 ms) HG activity aligned on Cue 1, for all electrodes that significantly classify *Instructed* vs *Control* (**E**) and *Free* vs *Control* (**F**) conditions, and **G, H.** Their associated mean decoding accuracy across significant electrodes in time, respectively. **I.** Temporal generalization of trial-type decoding using HG activity across significant sites derived from the previous analyses (***Free*** vs ***Control*** and ***Instructed*** vs ***Control***) during the delay period (0 to 3000ms after Cue 1) for 4 participants. Generalization matrices show decoding performance plotted as a function of training time (vertical axis) and testing time (horizontal axis). Decoding of ***Instructed*** vs ***Control*** (left column) trials illustrates the expected profile for transient coding, while decoding of ***Free*** vs ***Control*** (right column) trials leads to smoother and extended decoding patterns, typical of a single process that is sustained over time. The data underlying this Figure can be found in S1 Data.

**Spatial distribution of early vs late delay HG activity during free choice**

To specifically isolate the brain areas where HG increases index neural processing specific to free saccade decisions, we used a conjunction analysis (***Free*** > ***Control*** ∩ ***Free*** > ***Instructed***) applied to all electrode sites with significant classification of ***Free*** vs ***control*** and ***Free*** vs ***Instructed*** trials. Importantly, we conducted this conjunction analysis in two distinct time windows during the delay period: An EARLY window defined as the first 2000 ms after Cue1, and a LATE window from -2000 to 0 ms before Cue 2. Fig 5A depicts for both time windows the sites with significant decoding accuracies for all participants where the increase in HG activity was stronger during free choice compared both to control (***Free*** > ***Control***) and instructed (***Free*** > ***Instructed***) trials (see also S5 Fig for more details). Fig 5B combines the results for EARLY and LATE into a common representation (35 electrodes, 4 participants) indicating thereby for each free-choice specific site whether it showed HG increases only in the EARLY (0 to 2000 ms after Cue 1), only in LATE (-2000 to 0 ms before Cue 2) or in both EARLY and LATE intervals. We found that most free-choice specific sites exhibited enhanced HG activity only during the EARLY part of the delay period (29 electrodes, 3/4 participants) in a network of regions including SFG, MFG, SMA, IPS and FEF (see Fig 5C,D, first two rows for illustrative EARLY electrodes in IPS and SFG). However, for 5 sites (in 2/4 participants) located in SFG (2 electrodes), MFG (2 electrodes) and FEF (1 electrode), significant decoding accuracies were found both in the EARLY and LATE parts of the delay period, indicating HG activity spanning the entire duration of the delay period (see Fig 5C, D, last row for an illustrative EARLY+LATE electrode in SFG). The localization details of all 35 electrodes depicted in Fig 5B are provided in S4 Table. Note that, among all participants, the electrode site with maximum HG decoding accuracy for both ***Free*** vs ***Control*** (86.1 %) and ***Free*** vs ***Instructed*** (91.4 %) was located in the right intraparietal sulcus (IPS) (P2, electrode derivation *p9-p8*, see Fig 5, last row of C, D).

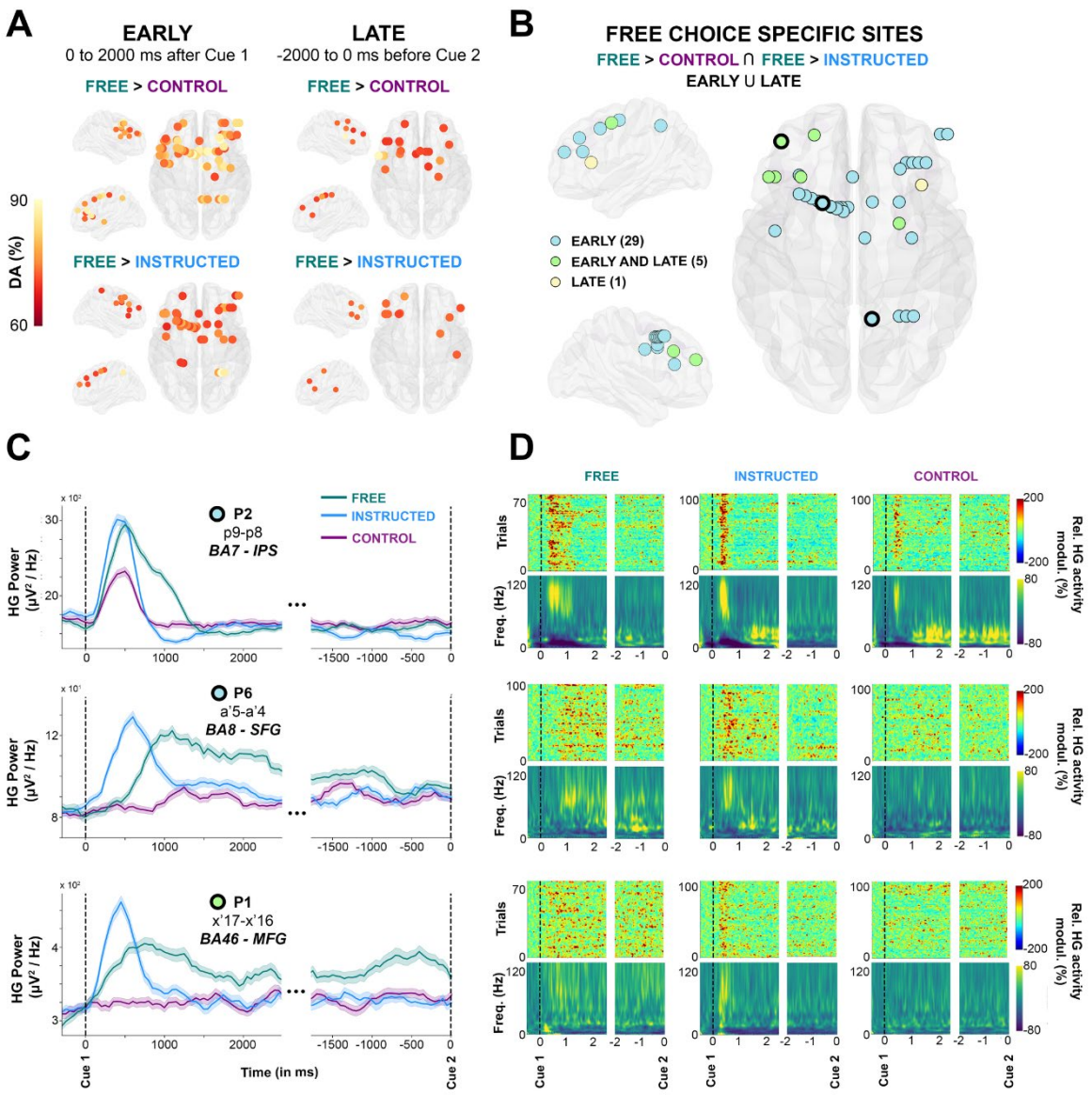


**Fig 5. Early and late free choice specific HG activity. A**, Electrode sites with significant decoding accuracies (*p<0.01, corrected*) for all participants mapped on transparent 3D brain images when HG activity is significantly stronger in the ***Free*** condition than in the ***Control*** condition (first row), and when HG activity is significantly stronger in the ***Free*** condition than in the ***Instructed*** condition (second row) during the delay period, from 0 to 2000 ms after Cue 1 (first column, EARLY) and from -2000 ms before Cue 2 (second column, LATE). **B.** Electrode sites where HG is higher in ***Free*** compared to ***Instructed*** and ***Control,*** determined by a conjunction analysis (***Free*** > ***Control*** ∪ ***Free*** > ***Instructed***). Free choice specific sites are colored in blue if significant decoding was observed in the EARLY part of the delay ; in yellow if significant decoding was found in the LATE part; and in green for sites that survived the conjunction analysis both in EARLY and LATE phases of the delay period. For three individual electrodes, we plotted HG activity over time (**C,** The data underlying this panel can be found in S1 Data), single-trial plots (**D,** upper row) and time-frequency-maps (**D**, lower row) for ***Free***, ***Instructed*** and ***Control*** conditions.

To further appreciate individual participant contributions to the global findings, we also analyzed all electrode sites that survived the conjunction analysis in Fig 5B, grouping the data either by ROI or delay period window (EARLY or LATE). The results (Fig 6) largely speak to the similarity of temporal HG dynamics across regions and conditions. Data from P2 indicate that the Control condition elicits HG responses in IPS but not in MFG, and that the strongest and longer-lasting HG responses in MFG comes from the Free choice trials (Fig 6A, B). This is consistent with an involvement of parietal regions –among other things- in low-level sensory processing, and a prominent role of frontal HG activity in deliberation. The distinction between merely "longer-lasting" HG activity (EARLY) and "persistent" HG activity throughout the delay period (EARLY and LATE) is shown in Fig 6C. We then conducted an analysis to evaluate trial history effects during the free choice condition. We used an unpaired t-test to evaluate statistical differences between n-1 conditional probabilities and random (history-free) probabilities for each participant, and found no obvious across-trial dependences in choice behavior during the Free condition for 5/6 subjects (see S1 Fig). For one participant (P2), we found a significant trial history effect that was driven by a tendency to alternate behavior (e.g., left, right, left, right…). Interestingly, this participant showed the same delayed and sustained HG free choice effects observed in the other participants, with the notable difference that the HG response was shorter-lived compared to other participants (Fig 6B). This result seems to be consistent with our interpretation that the sustained HG activity observed during the Free condition is indeed related to deliberation between competing alternatives in fronto-parietal brain areas. Specifically, this analysis suggests that the tendency of P2 to alternate between left and right saccade choices was associated with shorter deliberation during the delay (indexed by shorter sustained HG responses). Note that while significant, the observed alternating behavior in P2 was not systematic (see conditional probabilities reported in S1 Fig). Lastly, to verify whether our findings could not be confounded by spatial tuning effects in the delay period, we replicated the classification analyses separately for left and right saccade trials. However, no significantly spatially tuned delay period decoding was found in the ***Free, Instructed*** or ***Control*** conditions (see S6 Fig). More specifically, the three illustrative sites shown in Fig 5C-D did not show statistically significant differences when trials for left and right saccades were investigated separately (see S6B-D Fig). We also ruled out the possibility that our findings were confounded by

involuntary saccades made in response to the presentation of Cue 1 by contrasting mean EOG traces for left and right trials, and for ***Free*** and ***Instructed*** conditions (see Fig S3).

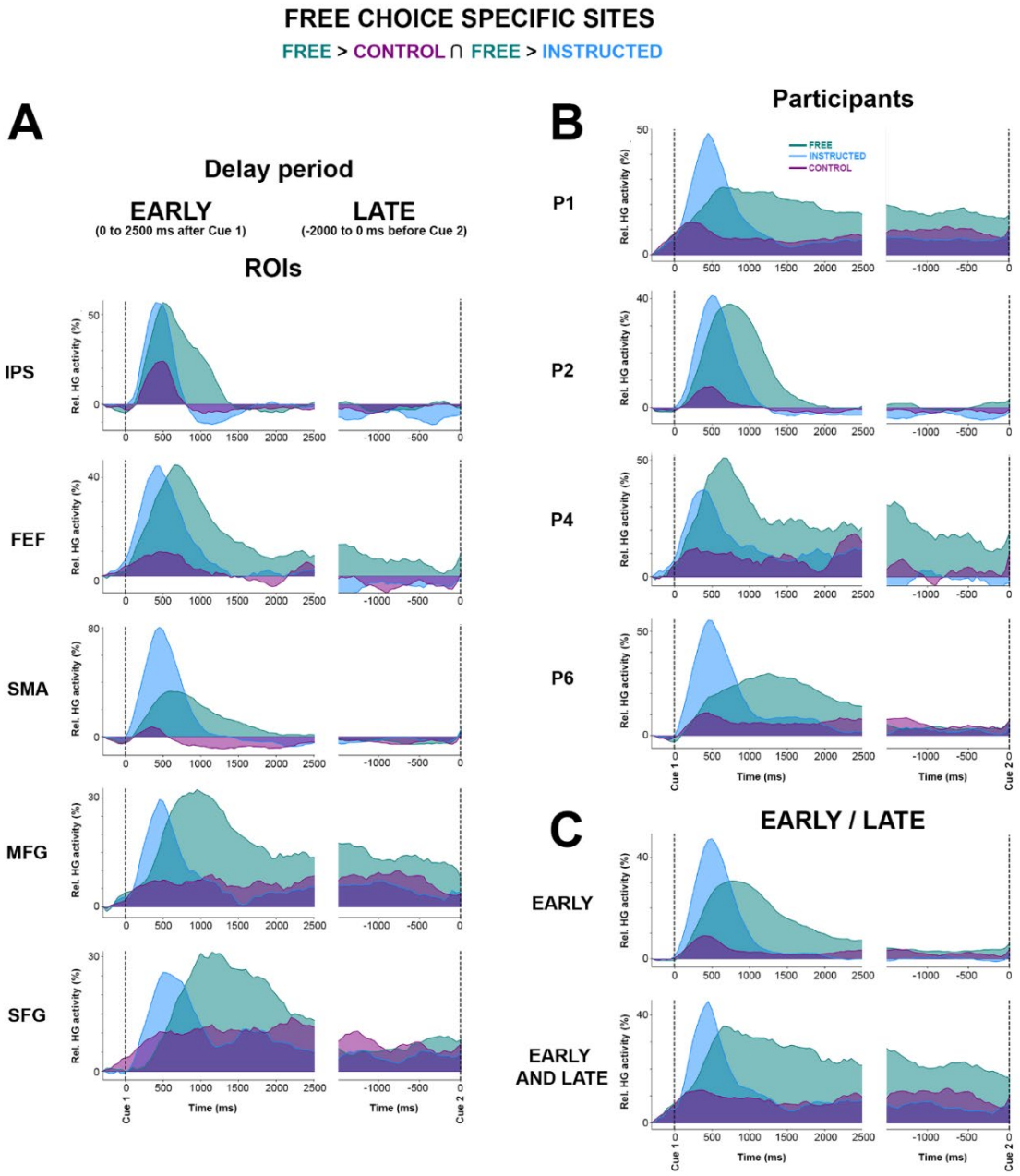


**Fig 6.** Mean HG activity time courses for free choice specific sites grouped here by (A) ROIs, (B) subjects and (C) EARLY / LATE. Mean time course of baseline corrected (-500 to -100ms) HG activity for Free, Instructed and Control conditions aligned on Cue 1 (first columnn) and Cue 2 (second columns) in electrodes that have enhanced HG in the free choice condition compared to both control ad instructed saccade conditions (i.e determined by a conjunction analysis (see Fig 5B). The data underlying this Figure can be found in S1 Data.

**Disentangling the correlates of oculomotor execution and oculomotor planning**

Previous reports using intracranial EEG in humans have shown that saccade execution in response to a go signal is associated with distributed increases in high gamma power (J.-P. Lachaux et al., 2006). Yet, it has been so far hard to determine whether such gamma activity reflects target selection, motor planning, actual oculomotor commands or a combination thereof. Analyzing the execution component (cue 2) of the delayed saccade paradigm in the present study provides an opportunity to address some of these questions. Therefore in the final analysis, we set out to compare HG responses induced by the Go signal in conditions where target selection already occurred in the delay period (i.e. ***Free*** and ***Instructed***) to the ***Control*** condition, in which participants were given no information on saccade target before the Go signal . To achieve this, we conducted a supervised classification analysis on ***Free***, ***Instructed*** and ***Control*** conditions as above, but this time using data collected during saccade execution (0 to 2000 ms after Cue 2). We found that, during saccade execution, the HG power modulations were similar whether the saccade was instructed or self-chosen (i.e. no significant classification between ***Free*** and ***Instructed***). However, HG activity associated with saccade execution in the ***Control*** condition was significantly different from both ***Free*** and ***Instructed*** saccades (Fig 7A). These results are consistent with the fact that no significant difference in reaction time (saccade onset latency) were found between ***Free*** and ***Instructed*** conditions, while mean reaction time across participants was significantly longer for the ***Control*** condition compared to both ***Free*** and ***Instructed*** trials (see Fig 1D).

Next, we examined the trial-by-trial relationship between saccade onset latency and neural activity specifically in areas that exhibit these significant HG differences between the ***Control*** condition and the ***Free*** and ***Instructed*** conditions. To this end, we first used a conjunction analysis to identify the sites of interest defined as sites for which significant classification was mediated by HG power in the Control condition being higher than in the other two conditions (Fig 7B). This identified 28 electrodes in parietal and frontal regions (2/6 participants at $p < 0.01$). Interestingly, in 43 % of these significant sites, the reverse pattern was true during the delay period: HG activity was significantly stronger in the ***Free*** and the ***Instructed*** conditions compared to the ***Control*** condition during the delay. Three representative examples of this task-specific HG pattern inversion between delay and execution

windows are shown in Fig 7C (first column). This suggests the involvement of these HG responses in action selection processes: When such processes are engaged during the delay period during ***Free*** and ***Instructed*** conditions, they do not need to be repeated during the execution period. By contrast, in the ***Control*** condition, no action selection processes were possible during the delay period (hence the weaker HG activity) but they were recruited at execution.

By plotting the mean time courses of HG power (Fig 7C), as well as mean time-frequency representations and single trial HG power plots, sorted according to RT (Fig 7D), it becomes clear that the temporal dynamics of HG power differ quite substantially depending on electrode location and trial type. In order to probe the various relationships between saccade onset and HG activity in these areas in a quantitative manner, we computed Pearson's rank correlation coefficients between saccade onset latency and HG onset latency across trials in each of the three experimental conditions (see Material and methods). Significant correlations were observed in a limited number of sites, and the results need to be interpreted with caution. This said, we observed three correlation patterns that we considered to be of interest: For some sites, the onset of HG activity after the Go signal did not correlate with saccade onset in any of the three conditions (pattern 1 / execution independent). Other sites exhibited correlations between HG onset and saccade onsets across all conditions (pattern 2 – oculomotor execution). Finally, in the third pattern, correlations between HG onset and saccade onset latencies were only observed in ***Control*** trials (pattern 3 / oculomotor planning). The recording sites that displayed these patterns came from distinct brain areas; We found evidence for pattern 1 (i.e. no correlation with saccade onsets in any condition) for the electrodes located in the intraparietal sulcus (IPS, 4 sites, 1 participant) (e.g. Fig 7C, D, first row and S7 Fig) (e.g. Electrode p9-p8; ***Control*** [p = 0.62, *r* =-0.06], ***Free*** [p = 0.69, *r* = - 0.06] and ***Instructed*** [p = 0.43, r =- 0.12]). Next, pattern 2 (i.e. saccade and HG onset latencies significantly correlated in all three conditions) was observed in SMA (1 out of 4 electrodes) (e.g. Fig 7C, D second row and S7 Fig; Electrode b3-b2; ***Control*** [p = 0.001, *r* =0.32], ***Free*** [p = 0.003, *r* =0.29] and ***Instructed*** [p = 0.041, *r* =0.2]). The fact that these correlations were present in the three conditions is consistent with the involvement of SMA in oculomotor execution. Thirdly, in the middle frontal gyri (1 out of 3 electrode), we observed the third pattern 3, namely that HG onsets were correlated with saccade onset latencies only in the ***Control*** condition (e.g. Fig 7C, D, last row and S7 Fig: Electrode m13-m12; ***Control*** [p = 0.04, *r* =0.26], ***Free*** [p = 0.13, *r* = 0.26] and ***Instructed*** [p =

0.67, $r$ = -0.07]). Despite being of interest, this observation is not surprising given that the relevant sites did not have significant HG response after cue 2 in the ***Free*** and ***instructed*** conditions (e.g. third row of Fig 7C, D). The detailed list of HG and saccade onset correlations across the three conditions are available in S5 Table.

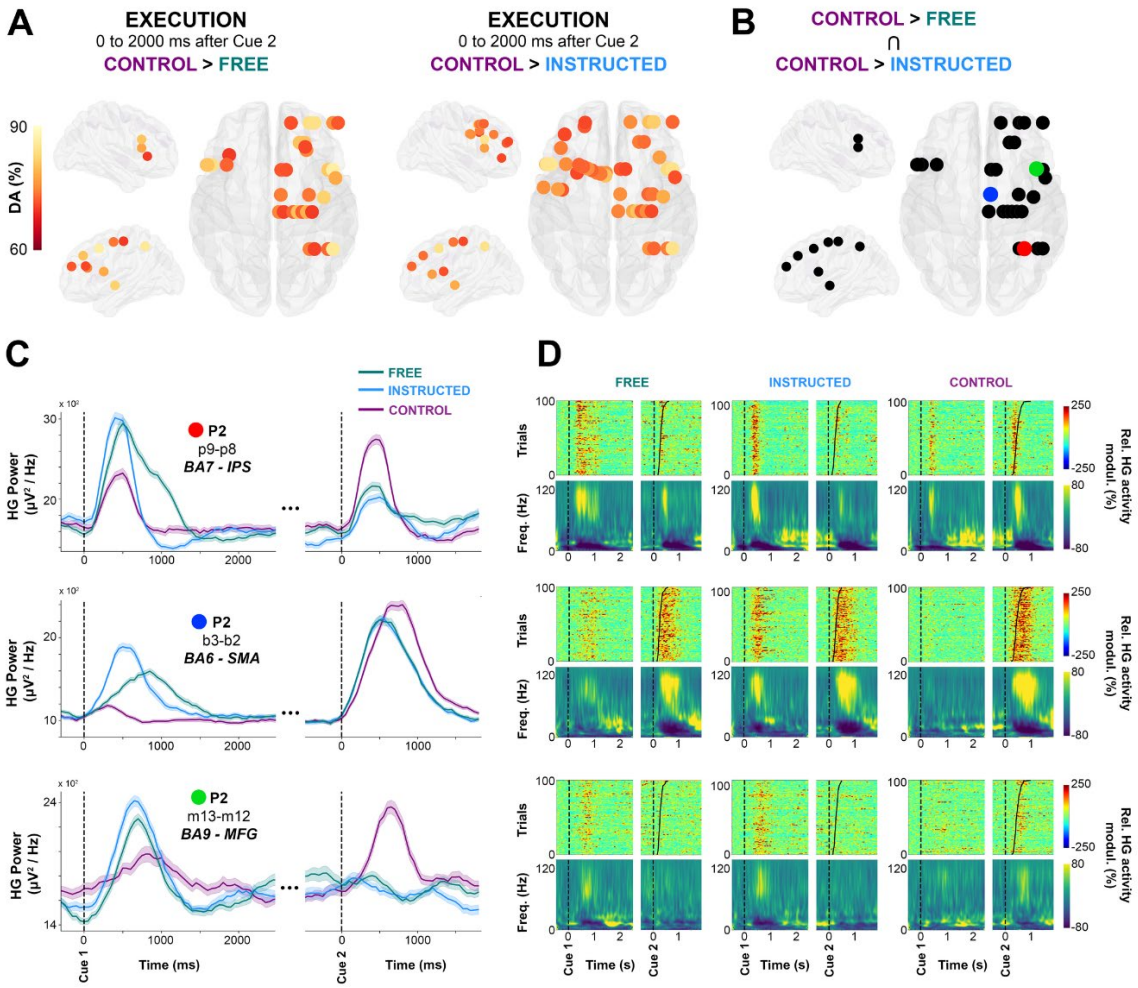


**Fig 7. Single-trial HG activity decoding during saccade execution. A.** electrodes with significant decoding accuracies (*p<0.01, corrected*) for all participants are mapped on transparent 3D brain images when HG activity is significantly stronger in the ***Control*** condition than in the ***Free*** condition (first row), and when HG activity is significantly stronger in the ***Control*** condition than in the ***Instructed*** condition (second row) in the interval from 0 to 2000 ms after Cue 2. **B.** using a conjunction analysis (***Control*** > ***Free*** ∩ ***Control*** > ***Instructed***), we show sites in which HG is stronger in the Control condition than in the ***Free*** and ***Instructed*** conditions. Colored sites correspond to three individual electrodes, for which we plotted HG activity over time (**C,** The data underlying this panel can be found in S1 Data), single-trial HG plots (sorted according to RTs) (**D,** upper row) and time-frequency-maps (**D**, lower row) for ***Free***, ***Instructed*** and ***Control*** conditions.

## 3.4 Discussion

The present paper provides, to the best of our knowledge, the first investigation of the neural dynamics underlying oculomotor decision-making in the human brain using intracranial EEG. Our results confirm the hypothesis that oculomotor decision processes (free choice saccades) in humans are associated with sustained enhances in the high frequency component of population-level neuronal activity across a parieto-frontal circuit. Single-trial classification allowed for a fine-grained investigation of the spatial, temporal and spectral properties of the neural dynamics underlying free choice saccades. In particular, compared to lower frequency components, broadband high frequency (60-140Hz) activity in parietal and frontal brain areas yielded the highest classification between free choice and instructed saccade trials. Importantly, while the brain regions associated with both conditions were largely shared, the temporal dynamics of the HG activity during the delay period were distinct. The free choice trials were associated with a delayed and more sustained induced HG response, while instructed saccade trials were characterized by an earlier transient HG response. Critically, the longer-lasting HG response in free choice trials did not systematically persist throughout the duration of the delay period. This stands in stark contrast to the well-established dynamics of persistent neural activity typically associated with working memory during delayed motor tasks. As will be discussed in more detail below, these findings expand previous non-invasive human studies and bridge the gap with animal investigations of free choice tasks.

**Broadband HG activity in fronto-parietal areas tracks free choice processes**

Compared to planning an instructed saccade, we found that freely deciding where to look is associated with a longer-lasting augmentation of broadband HG activity in the delay period. The enhanced HG activity induced in the free choice trials spans a decision circuit that consists primarily of frontal and parietal brain areas. The large frequency bandwidth of the observed HG responses reported here (60-140 Hz) distinguishes the present results from investigations of narrow-band

gamma oscillation. Broadband HG activity has been suggested to reflect a global enhancement of the local neuronal firing in the underlying cortical tissue, and has been occasionally described as a "spike bleedthrough" in the power spectrum of the LFP signals (Kucewicz et al., 2017a; Manning et al., 2009; R. Mukamel et al., 2005a; Nir et al., 2007; Ray et al., 2008; Ray & Maunsell, 2011). Consistent with previous work, the HG activity reported here most likely reflects the cumulative discharge of local neuronal networks in superficial cortical layers (Leszczynski & Schroeder, 2019; Manning et al., 2009; R. Mukamel et al., 2005a; Ray et al., 2008; Ray & Maunsell, 2011). Given previous reports showing tight correlations between neuronal firing and high frequency components of the LFP, it is tempting to consider the observed HG activity in our study to be a marker of local neural activation, or a correlate of neuronal firing. As such, the sustained HG activity specifically observed during the free choice trials probably indexes an extended active deliberation process.

**Sustained HG delay activity: Decision-making or working memory?**

Both the trial-by-trial classification framework, as well as standard trial-by-trial statistical tests, indicate that what we refer to as longer-lasting or sustained HG activity (in free choice trials) is not maintained up to saccade execution. In fact, in most of the probed parietal and frontal areas, the elevated HG activity ceases to be significant around 2000ms after Cue 1, irrespective of the total duration of the delay period (3750, 5750 or 7750ms). As revealed by our analysis contrasting EARLY versus LATE delay period activity, out of 34 sites that exhibited decision-specific HG enhancements within the first 2 seconds following stimulus onset, only 5 sites still showed significant HG increases in the last 2 seconds leading up to the Go cue. We argue that the sustained HG activity reported here differs from the more persistent patterns of neuronal responses reported in parietal and prefrontal areas in humans and monkeys performing working memory tasks, and which generally remain elevated until movement execution (e.g. 9–11,59). Rather than reflecting information maintenance or successive changes of mind, we believe that the extended HG activity -observed specifically in free choice trials- reflects the unfolding of internally driven action selection. This ongoing process of deliberation between competing alternatives extends over time until commitment to a saccade

choice. Importantly, cross-temporal generalization decoding confirmed that HG activity during free choice trials reflects a single, sustained process, rather than a dynamic coding phenomenon (Stokes, 2015). In other words, the off-diagonal cross-temporal decoding results argue against the view that the reported sustained HG activity actually is indicative of multiple, distinct successive processes (King & Dehaene, 2014). More generally, we propose that the sustained HG response reported here is related to an ongoing free choice process rather than to working memory. Indeed, participants had to maintain information about the direction of the upcoming saccade during the delay period whether it was self-determined (Free condition) or cued (Instructed condition). Therefore, working memory requirements are similar across both conditions and do not account for the observed increase in HG activity in free choice compared to instructed saccade trials. This is in line with the increasingly accepted view that persistent neuronal firing is a ubiquitous phenomenon observed broadly across many cortical and subcortical areas and that it reflects not only working memory maintenance, but also a variety of other cognitive processes, including decision making (Andersen & Buneo, 2002; Curtis & Connolly, 2008; Curtis & Lee, 2010; Meyer et al., 2007). In the light of the aforementioned findings and existing theories of action selection (Cisek & Kalaska, 2005; Costello et al., 2013; Coulthard et al., 2008; Cui & Andersen, 2007; Oliveira et al., 2010; Pastor-Bernier et al., 2012; Pastor-Bernier & Cisek, 2011; Shadlen & Newsome, 2001), we argue that the observed sustained HG activity in frontal and parietal areas during free saccade trials in the present task may reflect sustained neuronal firing that helps maintain enhanced competition between various potential movement plans with equal rewarding outcomes compared to a single movement plan in instructed saccades (cf. 76), until commitment to a particular choice. This interpretation is consistent with the involvement of the fronto-parietal network in implementing action selection (free choice) when maximally competing alternatives are present, both in humans (de Jong, 2011; Kable & Glimcher, 2009) and in monkeys (Gold & Shadlen, 2007; Pesaran et al., 2008).

**Relationship to previous delayed saccade tasks in humans**

The present study provides the first account of the neural dynamics underlying free choice saccades using invasive recordings in humans. While some of our findings provide critical confirmation of previous non-invasive research in this field, other observations extend or stand at odds with the non-invasive literature. First of all, an fMRI study based on the exact same paradigm used here, found that the free choice condition specifically activated DLPFC, alongside supplementary eye fields (SEF), FEF and IPS (Khonsari et al., 2007b; Milea et al., 2007b). This spatial correspondence between these BOLD responses and our iEEG HG activity in an identical task is expected and consistent with the view that broadband HG activity band modulations largely co-localize with BOLD variations in humans (Kayser et al., 2004; J.-P. Lachaux et al., 2007, 2012; Logothetis et al., 2001; R. Mukamel et al., 2005b; Niessing et al., 2005; Ojemann et al., 2013). In addition to corroborating BOLD localization results through electrophysiological evidence, our findings expand the fMRI account by incorporating the temporal and frequency dynamics in key parietal and frontal nodes of the decision circuit. Our findings are also consistent with an event-related fMRI study by Curtis et al. (Curtis & Connolly, 2008) where the authors found sustained BOLD responses in parietal and frontal areas during a delayed pro and anti-saccade task. Importantly, the deferred saccade task they used eliminated the memory maintenance component inherent in memory-guided saccade tasks by keeping the visual cue present throughout the preparation interval. Their interpretation of the parieto-frontal BOLD responses as reflecting spatial selection and preparation of saccades, rather than working memory, is in line with our interpretations. However, the fact that their task did not include a free choice saccade condition and the sluggish and delayed nature of the haemodynamic response (which peaks seconds after the neuronal response) limit direct comparisons between the temporal dynamics reported in their study using fMRI and the ones reported here using iEEG.

Investigating the electrophysiological correlates of oculomotor behavior with non-invasive methods is challenging because eye movements generate artefacts in EEG and MEG signals. However, by focusing on the delay activity preceding execution, a few MEG studies have reported compelling evidence for enhanced parieto-frontal gamma oscillations during saccade planning

Compared to guided saccades, autonomously choosing between competing alternatives has been shown with MEG to yield stronger sustained gamma increases that persist until movement execution (Carl et al., 2016). Our findings are, in part, consistent with these MEG results. However, a notable difference with the latter findings is that their delay period was fixed and short (1 s), while our delay period varied from 3,75 s to 7,75 s. This discrepancy probably explains why the gamma increase they report lasted the entire duration of the delay period, while we found that it drops around 2 to 2,5 s after stimulus onset. In fact, these important differences emphasize the importance of using long and variable delay periods to disentangle interpretations based on motor preparation or memory maintenance (Constantinidis et al., 2018; King & Dehaene, 2014; Kucewicz et al., 2017b; Lundqvist et al., 2018; Stokes, 2015) from processes directly involved in choosing between alternatives. Further differences between previous MEG investigations and the present results can be due to the differences in number of alternative saccade targets. Arguably, with only left or right saccade choices, our experimental design places less emphasis on memory maintenance during the delay, than tasks that involve for example 16 targets (Carl et al., 2016). Moreover, the absence of a pure sensory control condition in other studies may also be a limiting factor that we were able to overcome in this study. The Control condition used here allowed us to disentangle low-level stimulus processing from internally generated plans. Overall, compared to previous non-invasive human studies, the spatial and temporal resolution of iEEG and its high signal-to-noise ratio allowed for a fine-grained investigation of the temporal, spectral and spatial dynamics of the brain responses at play. Our ability to conduct these analyses up to frequencies of 140Hz and at the single-trial level is an important advantage when it comes to bridging the gap with animal research.

**Comparing saccade execution-related HG activity across conditions**

Comparisons of HG activity across trial types and correlation analyses between saccade onset and HG onset latencies revealed region-specific temporal patterns of activity during the execution period (Fig 7). We found an increase in HG activity specific to ***Control*** trials (i.e., the only condition during which participants did not plan a decision during the delay period) when compared to both ***Free*** and

***Instructed*** trials during the execution period. This finding implies the involvement of HG in oculomotor planning processes (including action selection and oculomotor preparation). Furthermore, we probed potential correlations between single-trial HG response onsets and saccade onsets. Significant correlations were scarce and the results, although interesting, need to be considered with caution; In all IPS sites, HG power onset did not correlate with saccade onset latency in any of the three experimental conditions. These analyses and the single-trial maps (sorted by RT) suggest that HG in IPS was not locked to oculomotor execution but was rather aligned to the Go stimulus onset. This is consistent the role of the intraparietal in preparing and redirecting movements and movement intentions (i.e., motor attention, see 91). By contrast, in SMA (BA6), a significant correlation between HG onset and saccade onsets was observed in all three conditions. This may reflect SMA involvement in eye movement execution (Schall, 1991), irrespective of whether target information was present prior to cue 2. Interestingly we also found evidence for correlations between HG onset and saccade onsets that only occurred for ***Control*** trials (i.e., when no action selection processes were engaged during the delay period), but neither for the ***Free*** nor ***Instructed*** trials. This occurred for instance in right MFG and thereby suggests that this area is involved in saccade execution only when the participants could not plan the direction of their saccades during the delay period. This view is consistent with previous findings in humans that suggest that the DLPFC is necessary for the executive control of saccades (Sendhilnathan et al., 2017).

**Limitations and open questions**

Participants in our study were neurosurgical patients with drug resistant epilepsy. To minimize the effect of epilepsy-related alterations and artefacts we followed strict data exclusion procedures in line with our previous intracranial EEG work (Bastin et al., 2017; Billeke et al., n.d.; Jerbi, Ossandón, et al., 2009; Ossandón et al., 2011). These consist primarily of systematic inspection of the data and exclusion of signals showing typical epileptic waveforms (e.g., epileptic spikes). In addition, we excluded data from any electrode subsequently identified by the clinical staff as being part of the resection area. Moreover, it should also be noted that the advantages of depth S-EEG recordings (incl.

high spatial and temporal resolution, high signal-to-noise ratio across a wide range of frequencies up to 140 Hz, 68), come at the cost of heterogenous spatial sampling among participants. This limitation is inherent to all iEEG studies. The electrode implantation across the six participants (see Fig 1B,C) yielded a reasonable coverage (a total of 778 intracerebral sites) of frontal and central areas, but the posterior parietal cortex was under-represented and none of our participants were implanted in the occipital cortex for instance. Furthermore, we and others have shown that unwanted eye movements can potentially lead to artefacts in iEEG due to saccadic spike potentials in extra-ocular muscles (Jerbi, Freyermuth, et al., 2009; Kovach et al., 2011). These eye-movement artefacts occur in SEEG electrodes especially in the high gamma-range and are most prominent in anterior and medial temporal lobe (81). The localization and time-course of HG activity reported in the present study suggest that it is not attributable to ocular artifacts. Moreover, we also verified that brain signals during the delay period were not affected by unwanted eye movements; Averaging EOG signals with respect to stimulus onset did not reveal any systematic EOG activity in left vs right instructed saccade trials. Lastly, based on non-human primate studies (Hwang & Andersen, 2012; Pesaran et al., 2008; Sendhilnathan et al., 2017), we expected to see differences between right and left saccades during the delay period. However, no differences were found when we trained an LDA algorithm to classify left and right saccades in Free and Instructed conditions (see S6 Fig). This means that the iEEG signals recorded in the present study do not seem to carry spatial information. This could in part be attributed to the fact that saccade directions were cued symbolically and foveally, or because of larger fields captured in bipolar sEEG recordings compared to electrophysiological recordings in macaques. It may also very well be possible that other signal features not considered in our analyses may be able to successfully predict saccade direction from delay period neural activity. Future analyses are needed to address such questions.

To conclude, the present study provides the first direct electrophysiological investigation of delayed eye movement decisions using depth recordings in humans. Compared to instructed saccades, we found free choice saccades to be associated with a more sustained HG activity in a parieto-frontal network. In a few prefrontal sites this HG enhancement persisted throughout the duration of the delay period, however, in most of the decision-related sites, HG activity modulations were present only in the early part of the delay period (i.e. first 2 seconds). We interpret the sustained HG activity as

reflecting deliberation processes lasting until commitment to a choice. These results bridge the gap between findings in human and non-human primates and expands our understanding of the brain's spatial, temporal and spectral dynamics underlying human decision making.

**Acknowledgments**

We wish to thank P. Cisek and A. Green for valuable discussions and comments.

**Author Contributions**

Conceptualization: K.J., A.B., P.K and J-P.L.; Data collection: K.J., J.B., and P.K.; Methodology: T.T, A-L.S., A.D., E.C., K.J. and J-P.L.; Formal Analysis: : T.T, A-L.S., A.D, E.C and K.J.; Writing – Original Draft: T.T and K.J; Writing – Review & Editing: : T.T, A-L.S., and K.J.; Supervision: K.J.; Funding Acquisition: K.J., J-P.L., A.B.

**Declaration of Interests**

The authors declare no competing interests.

## 3.5 Material and Methods

### Contact for Reagent and Resource Sharing

All requests for further information and resources should be directed to and will be fulfilled by the Lead Contact, Thomas Thiery (thomas.thiery@umontreal.ca).

### Ethics statement

All participants provided written informed consent, and the experimental procedures were approved by the local Ethical Committee (CPP Sud-Est V n° 09-CHU-12), which was carried out according to the Declaration of Helsinki.

### Experimental Model and Participant Details

Six patients with drug-resistant epilepsy participated in this study (6 females, mean age 30.3 ± 9.6). The participants were stereotactically implanted with multisite EEG depth electrodes at the Epilepsy Department of the Grenoble Neurological Hospital (Grenoble, France). In collaboration with the medical staff, and based on visual inspection, electrodes presenting pathological waveforms were discarded from the present study. All participants had normal vision without corrective glasses. All participants provided written informed consent, and the experimental procedures were approved by the local Ethical Committee (CPP Sud-Est V n° 09-CHU-12). Patient-specific clinical details can be found in S1 Table.

**Method Details**

*Electrode implantation and stereotactic EEG recordings*

Each participant was implanted with stereotactic electroencephalography (SEEG) electrodes (diameter of 0.8 mm). Depending on the implanted structure, electrodes were composed of 10 to 15 contacts that were 2 mm wide and 1.5 mm apart (DIXI Medical Instrument, Besançon, France). Intracranial EEG signals were recorded from a total of 778 intracerebral sites across all participants (Between 128 and 133 sites per participant). At the time of acquisition, a white matter electrode was used as reference, and data was sampled at 1024 Hz and bandpass filtered between 0.1 and 250 Hz. Electrode locations were determined in each individual participant using the stereotactic implantation scheme. The coordinates of each electrode contact were given following these references: origin (anterior commissure), anteroposterior axis (anterior commissure - posterior commissure), and vertical axis (interhemispheric plane). The electrodes were then localized in each individual participant using Talairach coordinates, which were then transformed to MNI coordinate system using standard procedures (i.e. tal2mni.m Matlab function) (Fig 1C). We then automatically assigned electrodes to brain regions based on three distinct atlases : Brodmann areas, the Automated Anatomical Labeling (AAL; 75), and the Multiresolution Intrinsic Segmentation Template (MIST; 101). The mapping from coordinates to brain areas (using this atlas) is publicly available in several toolboxes, including the one we used here (Visbrain, see (Combrisson et al., 2019).

*Delayed motor task*

At the beginning of each trial, participants were asked to fixate a central fixation point that appeared at the center of the screen, along with two lateral points for 500ms. Lateral points are always visible and were located within a 14° visual angle (-7° and +7° around the central point). Participants were then instructed to perform horizontal saccades toward one of the two targets, depending on a visually presented central cue appearing briefly for 250ms. In the FREE condition, the cue (outline diamond-shaped) indicated the participants were free to decide the direction (Right or

Left) of the saccade they would execute at the upcoming go signal (cue 2). In this condition (FREE), no specific instruction was given concerning the timing of decisions. In the INSTRUCTED condition, participants prepared a saccade towards the target indicated by the cue (empty arrow). As soon as the central cue disappeared a variable delay period began (3750, 5750 or 7750ms, selected with equal probability for each trial, i.e. 33,3%) during which the participants prepared the (chosen or instructed) saccade while fixating a central fixation point. The overall luminance and stimulus area of the first cue were matched across all three trial types, to exclude differential visual effects. Next, a GO signal (a central filled double-arrow in the FREE condition or an arrow pointing to one of the two targets in the INSTRUCTED condition) indicated that the participants could execute the saccade (Execution period). In the CONTROL condition, an empty central rectangle indicated that the participants should continue central fixation without preparing any saccade. A variable delay (3750, 5750 or 7750ms) was then followed by a GO signal indicating the direction of the saccade to be executed immediately, i.e. without prior preparation. After every saccade execution, no visual feedback about the trial performance was given, and participants had to fixate the central fixation point for 500ms. Next, everything disappeared from the screen during 1500 ms until the start of the next trial (inter-trial interval). Each trial type (FREE, CONTROL, INSTRUCTED) was presented with the same (33,3%) probability, and trials were pseudo-randomly interleaved. In all conditions, participants were asked to execute the saccade as soon as possible after the GO signal. We excluded trials in which participants took longer than 750ms to execute the saccade after the GO cue, and the EOG signal was visually inspected to exclude trials that contained abnormal eye movements and/or spontaneous saccades made during fixation or during the delay period (see S3 Fig). Across all participants approximately 75 % of the trials were retained for further analysis.

*Behavioral analysis*

Based on the EOG traces (see S2 Fig), we computed saccade onset latencies for each trial and for all participants in the ***Control***, ***Instructed*** and ***Free*** conditions. Saccade onset latencies were identified from EOG traces recorded during each experimental conditions using a routine semi-automatic saccade detection procedure: a custom Matlab (The Mathworks, Inc.) program provided an initial

automatic detection of saccade onsets and allowed for interactive manual adjustments of the marker latencies (see S2 Table). In order to test whether reaction times differed significantly across conditions, we used a two-tailed paired Student's t-test and compared mean reaction times for Control vs Instructed, Control vs Free, and Instructed vs Free conditions. Standard errors of the mean together with means, t-statistics and p-values were reported. To confirm these results in individual participant data, we used a two tailed unpaired Student's t-test to compare reaction times between condition on a trial-by-trial basis within each participant (Control vs Instructed, Control vs Free, and Instructed vs Free). To account for differences in numbers of trials per condition, we used a bootstrap procedure (n=100) each time randomly selecting values to match the condition with the least number of trials. Lastly, we conducted an analysis to evaluate trial history effects during the free choice condition. We computed n-1 conditional probabilities to determine whether the saccade direction (Left, L or Right, R) of trial n-1 influenced trial n in the Free choice condition. The statistical significance of the obtained conditional probabilities was evaluated by computing statistical thresholds using permutation tests (n=1000, $p<0.001$). A null distribution was generated by repeatedly (n=1000) computing conditional probabilities for each participant obtained after randomly permuting class labels (Left and Right).

*EOG Data preprocessing*

Oculomotor performance was followed online using horizontal and vertical electro-oculograms (EOG), allowing to measure the amplitude and the speed of saccades (see S2 Fig), as well as the errors made by each participant. Four electrodes placed around the eyes to measure horizontal and vertical eye movements with a sampling frequency of 1024 Hz. Saccade onsets were identified from EOG traces recorded during each experimental condition using a routine semi-automatic saccade detection procedure. A custom Matlab script identified saccade onsets by detecting the onset of the characteristic slope (by computing the derivative of the EOG signal). The automatic detection of saccade onset was then fine-tuned through interactive manual adjustments of the marker latencies. To make sure our results cannot be attributed to saccades made after the presentation of Cue 1 during the delay period, we used a two tailed paired Student's t-test at each moment in time to

compare mean right and left EOG responses, as well as mean responses during Free and Instructed conditions across all participants and found no significant differences,

*SEEG Data preprocessing*

SEEG data preprocessing was conducted according to our routine procedures (Bastin et al., 2017; Combrisson et al., 2017; Hamamé et al., 2014; Jerbi, Ossandón, et al., 2009; Jung et al., 2010). These included signal bipolarization, where each electrode site was re-referenced to its direct neighbor. Bipolar re-referencing can increase sensitivity and reduce artefacts by canceling out distant signals that are picked up by adjacent electrode contacts (e.g. mains power). The spatial resolution of bipolar SEEG electrodes was approximately 3 mm (Jerbi, Ossandón, et al., 2009; J. P. Lachaux et al., 2003). Next, using visual inspection and time-frequency explorations of the signal, we excluded electrodes containing pathological epileptic activity. The pre-processing led to a total of 543 bipolar derivations across all participants (see Fig 1B).

**Quantification and Statistical Analysis**

*Spectral analyses*

We conducted power analyses in several standard frequency bands defined as follows: theta (θ) [4–8 Hz], alpha (α) [8–15 Hz], beta (β) [16–30 Hz], low gamma (low γ) [30–60] and HG [60-140 Hz]. This was achieved by first filtering the raw EEG signals using a finite impulse response filtering (FIR1, order = 3) and then computing the Hilbert transform over 400 ms time windows with an overlap of 50ms. The power features used for classification were computed as mean power over 400ms time windows with an overlap of 50ms during the delay period (-500ms to 2500 ms), where t=0ms corresponds to the onset of Cue 1, and execution (-500ms to 1500ms) where t=0ms corresponds to the onset of Cue 2. The classification was applied on non-normalized power. For single trial representations, the same methods were used but using 60ms time windows with an overlap of 10ms. Whenever present,

baseline normalization was only used for visualization purposes (time-frequency maps and single trial representation). Baseline normalization was achieved for each frequency band, by subtracting then dividing by the mean of a 400 ms baseline window, i.e. the pre-stimulus rest period ([-500ms, -100ms]).

*Signal classification*

We set out to explore the feasibility of using multisite human LFP data (543 bipolar electrode sites) to perform classifications during motor planning and execution. To this end, we implemented a machine learning framework for trial-by-trial classification using spectral power. Several classification techniques were initially tested for the single feature classification procedure, including linear-discriminant analysis (LDA), k-nearest-neighbor (KNN) and support vector machine (SVM). The classification accuracy results were very similar across the three methods. The LDA algorithm (Fisher, 1936) was the fastest and was therefore chosen for this study given the computationally-demanding permutation tests used to evaluate classifier performance. In brief, for a two-dimensional problem, the LDA algorithm tries to find a hyperplane that maximizes the mean distance between the mean of the two classes while minimizing inter-class variance.

*Decoding accuracy and statistical evaluation of decoding performance*

Single-trial classification performance was evaluated in each participant separately. We used a standard stratified 10-fold cross-validation approach with Scikit-learn, a Python 3 package dedicated to machine-learning analyses (112). First, the data set was pseudo-randomly split into 10, equally-sized, observations: 9 segments were used for training the classifier, and the last one as the test set. This procedure was repeated 10 times, such that every observation in the data was used exactly once for testing, and at least once for training, but never at the same time. This strict separation of training and testing ensures the test data was naïve and did not violate basic classification principles (e.g., 108). The use of stratification seeks to ensure that the relative proportion of labels (or classes) in the whole data set is reasonably preserved within each of the segments after the split. Next, the

performance of the achieved decoding was calculated using the DA metric, which was computed as the mean correct classification across all folds. The statistical significance of the obtained decoding accuracies was evaluated by computing statistical thresholds using permutation tests (n=100, p<0.01). In other words, a null-distribution is generated by repeatedly (n=100) computing the classification accuracy obtained after randomly permuting class labels (Combrisson & Jerbi, 2015). In all our decoding analyses, we used maximum statistics to correct across electrodes, frequency bands and time with a statistical threshold at *p<0.01*.

*Cross-temporal generalization of HG decoding*

We explored the temporal dynamics of HG activity during the delay period for ***Free*** vs ***Control*** and ***Instructed*** vs ***Control*** conditions by probing cross-temporal generalization (King & Dehaene, 2014; Stokes, 2015). In principle, we employed the same LDA decoding approach as described above, except that the classifiers trained at a given time point were now tested at every other point in time, resulting in two-dimensional cross-temporal decoding matrices (see 11,51)). Once *t* LDA classifiers have been fitted (where *t* is the duration of a trial expressed in time samples), each classifier is tested on its decoding generalization at any time *t'*. This method thus leads to a temporal generalization matrix of *training time x generalization time* (see Fig 4). In each cell of the matrix, decoding performance is summarized by the decoding accuracy (DA). Classifiers trained and tested at the same time point correspond to the diagonal of this matrix and are thus referred to as "diagonal" decoding. The decoding performance obtained when *t'* differ from t is referred to as "off-diagonal" decoding. To identify where HG activity was significantly different between conditions in the temporal generalization matrices, we used the binomial cumulative distribution to derive statistical significance thresholds (see (Combrisson & Jerbi, 2015). Finally, we compared our results with the repertoire of canonical dynamical patterns in temporal generalization matrices established by previous studies (King & Dehaene, 2014; Stokes, 2015).

*Multifeature classification analysis*

To perform the multi-feature analysis, we use the Exhaustive Feature Selection (EFS) method from mlxtend (Raschka, 2018) applied for each frequency band, for each participant. The EFS algorithm will test all the possible combinations of the frequency bands and will select which feature or set of features allows for better decoding of our two conditions (***Free*** vs ***Instructed,*** see Fig 3E). The feature selection is scored on a stratified validation dataset consisting of one third of the data. The EFS is repeated with all possibilities of validation set and the best selected features are counted for each electrode.

*Statistical analyses of temporal dynamics (peak and duration)*

To statistically compare the peak of HG activity across the Instructed and Free conditions from all relevant sites during the delay period, we first extracted the peak of HG activity from all electrodes that exhibited significant decoding of Free vs Instructed conditions. We then compared the peak HG activity for all electrodes within participants using unpaired t-tests (Instructed - Free). This gave us t-values and p values for each individual participant (e.g., for HG activity, ***Instructed*** - ***Free***, 4/6 participants). We then averaged the peak HG activity across electrodes and used a paired t-test to assess whether the effect was statistically significant across participants, at the group level.

To assess whether activity was decoded earlier, peaked earlier and whether it was more sustained in the ***Free*** condition than in the ***Instructed*** condition, we first conducted two separate classifications (***Free*** vs ***Control*** and ***Instructed*** vs ***Control***). We then computed the timing at which each significant electrode (1) started to decode (based on first time bin of significant decoding) and (2) maximally decoded (based on the timing of the maximum accuracy) ***Free*** vs ***Control*** and ***Instructed*** vs ***Control*** conditions. We compared these timings for all electrodes within participants with an unpaired Student's t-test. This gave us t-values and p values for each participant. We then averaged the first significant timings across electrodes and used a paired Student's t-test to assess whether the effect was statistically significant across participants, at the group level. The same analysis was used to determine whether HG activity was more sustained in time in the ***Free*** condition, compared to the ***Instructed*** condition. To this end, we counted the total number of time points with significant

decoding between ***Free*** vs ***Control***, and ***Instructed*** vs ***Control*** and ran both within and across participant comparisons correlations between reaction times and HG activity.

In addition, we computed Pearson's rank correlation coefficients between reaction times and the onset of HG activity for each trial in the Free, Instructed and Control conditions during saccade execution. The onset of HG activity was determined in each trial by detecting the time point after which HG activity was greater than 2 standard deviations for at least two consecutive time bins. The statistical significance of correlations was established by using a two-sided test whose null hypothesis is that two sets of data are uncorrelated. The p-value thus indicates the probability of an uncorrelated system producing datasets that have a Pearson rank correlation at least as extreme as the one computed from these datasets.

*Data mapping to a 3-D standard cortical representation*

To facilitate the interpretation of the results, all significant task-based feature modulations and decoding results were remapped from the intracranial electrode sites onto a standard cortical representation. To achieve this, all electrode coordinates were transformed from individual Talairach space to standard MNI space using Visbrain (Combrisson et al., 2019), an open-source Python 3 package dedicated to brain signal visualization, to map the data from iEEG sites onto 3D images of transparent brains. This cortical representation technique is in line with methods used in previous iEEG studies (Bastin et al., 2017; Jerbi, Ossandón, et al., 2009; Ossandón et al., 2012) and allowed for brain-wide visualization of significant features and decoding performances.

**Data and Software Availability**

Electrophysiological data were analyzed using Python 3, in conjunction with toolboxes including Visbrain (Combrisson et al., 2019) for data visualisation and mlxtend (Raschka, 2018) as well as Scikit-learn (Pedregosa et al., 2012) for machine learning analyses. Data and custom Python analysis scripts are available upon reasonable request from Thomas Thiery (thomas.thiery@umontreal.ca).

The numerical data used in all figures are included in S1 Data.

## 3.6 References


Andersen, R. A., & Buneo, C. A. (2002). Intentional maps in posterior parietal cortex. *Annual Review of Neuroscience*, *25*, 189–220. https://doi.org/10.1146/annurev.neuro.25.112701.142922

Anderson, E. J., Jones, D. K., O'Gorman, R. L., Leemans, A., Catani, M., & Husain, M. (2012). Cortical network for gaze control in humans revealed using multimodal MRI. *Cerebral Cortex (New York, N.Y.: 1991)*, *22*(4), 765–775. https://doi.org/10.1093/cercor/bhr110

Ariani, G., Wurm, M. F., & Lingnau, A. (2015). Decoding Internally and Externally Driven Movement Plans. *Journal of Neuroscience*, *35*(42), 14160–14171. https://doi.org/10.1523/JNEUROSCI.0596-15.2015

Bastin, J., Deman, P., David, O., Gueguen, M., Benis, D., Minotti, L., Hoffman, D., Combrisson, E., Kujala, J., Perrone-Bertolotti, M., Kahane, P., Lachaux, J.-P., & Jerbi, K. (2017). Direct Recordings from Human Anterior Insula Reveal its Leading Role within the Error-Monitoring Network. *Cerebral Cortex (New York, N.Y.: 1991)*, *27*(2), 1545–1557. https://doi.org/10.1093/cercor/bhv352

Bastin, J., Lebranchu, P., Jerbi, K., Kahane, P., Orban, G., Lachaux, J.-P., & Berthoz, A. (2012). Direct recordings in human cortex reveal the dynamics of gamma-band [50-150 Hz] activity during pursuit eye movement control. *NeuroImage*, *63*(1), 339–347. https://doi.org/10.1016/j.neuroimage.2012.07.011

Berman, R. A., Colby, C. L., Genovese, C. R., Voyvodic, J. T., Luna, B., Thulborn, K. R., & Sweeney, J. A. (1999). Cortical networks subserving pursuit and saccadic eye movements in humans: An FMRI study. *Human Brain Mapping*, *8*(4), 209–225.

Billeke, P., Ossandon, T., Perrone-Bertolotti, M., Kahane, P., Bastin, J., Jerbi, K., Lachaux, J.-P., & Fuentealba, P. (n.d.). Human Anterior Insula Encodes Performance Feedback and Relays Prediction Error to the Medial Prefrontal Cortex. *Cerebral Cortex*. https://doi.org/10.1093/cercor/bhaa017

Blanke, O., & Seeck, M. (2003). Direction of saccadic and smooth eye movements induced by electrical stimulation of the human frontal eye field: Effect of orbital position. *Experimental Brain Research*, *150*(2), 174–183. https://doi.org/10.1007/s00221-003-1395-7

Carl, C., Hipp, J. F., König, P., & Engel, A. K. (2016). Spectral Signatures of Saccade Target Selection. *Brain Topography*, *29*(1), 130–148. https://doi.org/10.1007/s10548-015-0426-6

Christopoulos, V. N., Kagan, I., & Andersen, R. A. (2018). Lateral intraparietal area (LIP) is largely effector-specific in free-choice decisions. *Scientific Reports*, *8*(1), 8611. https://doi.org/10.1038/s41598-018-26366-9

Cisek, P., & Kalaska, J. F. (2005). Neural correlates of reaching decisions in dorsal premotor cortex: Specification of multiple direction choices and final selection of action. *Neuron*, *45*(5), 801–814. https://doi.org/10.1016/j.neuron.2005.01.027

Cisek, P., & Kalaska, J. F. (2010). Neural mechanisms for interacting with a world full of action choices. *Annual Review of Neuroscience*, *33*, 269–298. https://doi.org/10.1146/annurev.neuro.051508.135409

Coe, B., Tomihara, K., Matsuzawa, M., & Hikosaka, O. (2002). Visual and Anticipatory Bias in Three Cortical Eye Fields of the Monkey during an Adaptive Decision-Making Task. *Journal of Neuroscience*, *22*(12), 5081–5090. https://doi.org/10.1523/JNEUROSCI.22-12-05081.2002

Combrisson, E., & Jerbi, K. (2015). Exceeding chance level by chance: The caveat of theoretical chance levels in brain signal classification and statistical assessment of decoding accuracy. *Journal of Neuroscience Methods*, *250*, 126–136. https://doi.org/10.1016/j.jneumeth.2015.01.010

Combrisson, E., Perrone-Bertolotti, M., Soto, J. L., Alamian, G., Kahane, P., Lachaux, J.-P., Guillot, A., & Jerbi, K. (2017). From intentions to actions: Neural oscillations encode motor processes through phase, amplitude and phase-amplitude coupling. *NeuroImage*, *147*, 473–487. https://doi.org/10.1016/j.neuroimage.2016.11.042

Combrisson, E., Vallat, R., O'Reilly, C., Jas, M., Pascarella, A., Saive, A.-L., Thiery, T., Meunier, D., Altukhov, D., Lajnef, T., Ruby, P., Guillot, A., & Jerbi, K. (2019). Visbrain: A Multi-Purpose GPU-Accelerated Open-Source Suite for Multimodal Brain Data Visualization. *Frontiers in Neuroinformatics*, *13*, 14. https://doi.org/10.3389/fninf.2019.00014

Connolly, J. D., Goodale, M. A., Menon, R. S., & Munoz, D. P. (2002). Human fMRI evidence for the neural correlates of preparatory set. *Nature Neuroscience*, *5*(12), 1345–1352. https://doi.org/10.1038/nn969

Constantinidis, C., Funahashi, S., Lee, D., Murray, J. D., Qi, X.-L., Wang, M., & Arnsten, A. F. T. (2018). Persistent Spiking Activity Underlies Working Memory. *The Journal of Neuroscience*, *38*(32), 7020–7028. https://doi.org/10.1523/JNEUROSCI.2486-17.2018

Costello, M. G., Zhu, D., Salinas, E., & Stanford, T. R. (2013). Perceptual Modulation of Motor—But Not Visual—Responses in the Frontal Eye Field during an Urgent-Decision Task. *The Journal of Neuroscience*, *33*(41), 16394–16408. https://doi.org/10.1523/JNEUROSCI.1899-13.2013

Coulthard, E., Rudd, A., & Husain, M. (2008). Motor neglect associated with loss of action inhibition. *Journal of Neurology, Neurosurgery, and Psychiatry*, *79*(12), 1401–1404. https://doi.org/10.1136/jnnp.2007.140715

Cui, H., & Andersen, R. A. (2007). Posterior Parietal Cortex Encodes Autonomously Selected Motor Plans. *Neuron*, *56*(3), 552–559. https://doi.org/10.1016/j.neuron.2007.09.031

Curtis, C. E., & Connolly, J. D. (2008). Saccade preparation signals in the human frontal and parietal cortices. *Journal of Neurophysiology*, *99*(1), 133–145. https://doi.org/10.1152/jn.00899.2007

Curtis, C. E., & Lee, D. (2010). Beyond working memory: The role of persistent activity in decision making. *Trends in Cognitive Sciences*, *14*(5), 216–222. https://doi.org/10.1016/j.tics.2010.03.006

de Jong, B. M. (2011). Neurology of widely embedded free will. *Cortex; a Journal Devoted to the Study of the Nervous System and Behavior*, *47*(10), 1160–1165. https://doi.org/10.1016/j.cortex.2011.06.011

Dorris, M. C., & Glimcher, P. W. (2004). Activity in posterior parietal cortex is correlated with the relative subjective desirability of action. *Neuron*, *44*(2), 365–378. https://doi.org/10.1016/j.neuron.2004.09.009

Fisher, R. A. (1936). The Use of Multiple Measurements in Taxonomic Problems. *Annals of Eugenics*, *7*(2), 179–188. https://doi.org/10.1111/j.1469-1809.1936.tb02137.x

Fleming, S. M., Mars, R. B., Gladwin, T. E., & Haggard, P. (2009). When the brain changes its mind: Flexibility of action selection in instructed and free choices. *Cerebral Cortex (New York, N.Y.: 1991)*, *19*(10), 2352–2360. https://doi.org/10.1093/cercor/bhn252

Frost, D., & Pöppel, E. (1976). Different programming modes of human saccadic eye movements as a function of stimulus eccentricity: Indications of a functional subdivision of the visual field. *Biological Cybernetics*, *23*(1), 39–48. https://doi.org/10.1007/BF00344150

Gold, J. I., & Shadlen, M. N. (2007). The neural basis of decision making. *Annual Review of Neuroscience*, *30*, 535–574. https://doi.org/10.1146/annurev.neuro.29.051605.113038

Grent-'t-Jong, T., Oostenveld, R., Jensen, O., Medendorp, W. P., & Praamstra, P. (2014). Competitive interactions in sensorimotor cortex: Oscillations express separation between alternative movement targets. *Journal of Neurophysiology*, *112*(2), 224–232. https://doi.org/10.1152/jn.00127.2014

Haggard, P. (2019). The Neurocognitive Bases of Human Volition. *Annual Review of Psychology*, *70*(1), 9–28. https://doi.org/10.1146/annurev-psych-010418-103348

Hamamé, C. M., Vidal, J. R., Perrone-Bertolotti, M., Ossandón, T., Jerbi, K., Kahane, P., Bertrand, O., & Lachaux, J.-P. (2014). Functional selectivity in the human occipitotemporal cortex during natural vision: Evidence from combined intracranial EEG and eye-tracking. *NeuroImage*, *95*, 276–286. https://doi.org/10.1016/j.neuroimage.2014.03.025

Hwang, E. J., & Andersen, R. A. (2012). Spiking and LFP activity in PRR during symbolically instructed reaches. *Journal of Neurophysiology*, *107*(3), 836–849. https://doi.org/10.1152/jn.00063.2011

Jerbi, K., Freyermuth, S., Dalal, S., Kahane, P., Bertrand, O., Berthoz, A., & Lachaux, J.-P. (2009). Saccade Related Gamma-Band Activity in Intracerebral EEG: Dissociating Neural from Ocular Muscle Activity. *Brain Topography*, *22*(1), 18–23. https://doi.org/10.1007/s10548-009-0078-5

Jerbi, K., Ossandón, T., Hamamé, C. M., Senova, S., Dalal, S. S., Jung, J., Minotti, L., Bertrand, O., Berthoz, A., Kahane, P., & Lachaux, J.-P. (2009). Task-related gamma-band dynamics from an intracerebral perspective: Review and implications for surface EEG and MEG. *Human Brain Mapping*, *30*(6), 1758–1771. https://doi.org/10.1002/hbm.20750

Jung, J., Jerbi, K., Ossandon, T., Ryvlin, P., Isnard, J., Bertrand, O., Guénot, M., Mauguière, F., & Lachaux, J.-P. (2010). Brain responses to success and failure: Direct recordings from human cerebral cortex. *Human Brain Mapping*, *31*(8), 1217–1232. https://doi.org/10.1002/hbm.20930

Kable, J. W., & Glimcher, P. W. (2009). The Neurobiology of Decision: Consensus and Controversy. *Neuron*, *63*(6), 733–745. https://doi.org/10.1016/j.neuron.2009.09.003

Kagan, I., Iyer, A., Lindner, A., & Andersen, R. A. (2010). Space representation for eye movements is more contralateral in monkeys than in humans. *Proceedings of the National Academy of Sciences*, *107*(17), 7933–7938. https://doi.org/10.1073/pnas.1002825107

Kayser, C., Kim, M., Ugurbil, K., Kim, D.-S., & König, P. (2004). A comparison of hemodynamic and neural responses in cat visual cortex using complex stimuli. *Cerebral Cortex (New York, N.Y.: 1991)*, *14*(8), 881–891. https://doi.org/10.1093/cercor/bhh047

Khonsari, R. H., Lobel, E., Milea, D., Lehéricy, S., Pierrot-Deseilligny, C., & Berthoz, A. (2007a). Lateralized parietal activity during decision and preparation of saccades. *Neuroreport*, *18*(17), 1797–1800. https://doi.org/10.1097/WNR.0b013e3282f1a986

Khonsari, R. H., Lobel, E., Milea, D., Lehéricy, S., Pierrot-Deseilligny, C., & Berthoz, A. (2007b). Lateralized parietal activity during decision and preparation of saccades. *Neuroreport*, *18*(17), 1797–1800. https://doi.org/10.1097/WNR.0b013e3282f1a986

King, J.-R., & Dehaene, S. (2014). Characterizing the dynamics of mental representations: The temporal generalization method. *Trends in Cognitive Sciences*, *18*(4), 203–210. https://doi.org/10.1016/j.tics.2014.01.002

Klaes, C., Westendorff, S., Chakrabarti, S., & Gail, A. (2011). Choosing Goals, Not Rules: Deciding among Rule-Based Action Plans. *Neuron*, *70*(3), 536–548. https://doi.org/10.1016/j.neuron.2011.02.053

Kovach, C. K., Tsuchiya, N., Kawasaki, H., Oya, H., Howard, M. A., & Adolphs, R. (2011). Manifestation of ocular-muscle EMG contamination in human intracranial recordings. *NeuroImage*, *54*(1), 213–233. https://doi.org/10.1016/j.neuroimage.2010.08.002

Kucewicz, M. T., Berry, B. M., Kremen, V., Brinkmann, B. H., Sperling, M. R., Jobst, B. C., Gross, R. E., Lega, B., Sheth, S. A., Stein, J. M., Das, S. R., Gorniak, R., Stead, S. M., Rizzuto, D. S., Kahana, M. J., & Worrell, G. A. (2017a). Dissecting gamma frequency activity during human memory processing. *Brain: A Journal of Neurology*, *140*(5), 1337–1350. https://doi.org/10.1093/brain/awx043

Kucewicz, M. T., Berry, B. M., Kremen, V., Brinkmann, B. H., Sperling, M. R., Jobst, B. C., Gross, R. E., Lega, B., Sheth, S. A., Stein, J. M., Das, S. R., Gorniak, R., Stead, S. M., Rizzuto, D. S., Kahana, M. J., & Worrell, G. A. (2017b). Dissecting gamma frequency activity during human memory

processing. *Brain: A Journal of Neurology*, *140*(5), 1337–1350. https://doi.org/10.1093/brain/awx043

Lachaux, J. P., Rudrauf, D., & Kahane, P. (2003). Intracranial EEG and human brain mapping. *Journal of Physiology, Paris*, *97*(4–6), 613–628. https://doi.org/10.1016/j.jphysparis.2004.01.018

Lachaux, J.-P., Axmacher, N., Mormann, F., Halgren, E., & Crone, N. E. (2012). High-frequency neural activity and human cognition: Past, present and possible future of intracranial EEG research. *Progress in Neurobiology*, *98*(3), 279–301. https://doi.org/10.1016/j.pneurobio.2012.06.008

Lachaux, J.-P., Fonlupt, P., Kahane, P., Minotti, L., Hoffmann, D., Bertrand, O., & Baciu, M. (2007). Relationship between task-related gamma oscillations and BOLD signal: New insights from combined fMRI and intracranial EEG. *Human Brain Mapping*, *28*(12), 1368–1375. https://doi.org/10.1002/hbm.20352

Lachaux, J.-P., Hoffmann, D., Minotti, L., Berthoz, A., & Kahane, P. (2006). Intracerebral dynamics of saccade generation in the human frontal eye field and supplementary eye field. *NeuroImage*, *30*(4), 1302–1312. https://doi.org/10.1016/j.neuroimage.2005.11.023

Lemm, S., Blankertz, B., Dickhaus, T., & Müller, K.-R. (2011). Introduction to machine learning for brain imaging. *NeuroImage*, *56*(2), 387–399. https://doi.org/10.1016/j.neuroimage.2010.11.004

Leszczynski, M., & Schroeder, C. E. (2019). The Role of Neuronal Oscillations in Visual Active Sensing. *Frontiers in Integrative Neuroscience*, *13*. https://doi.org/10.3389/fnint.2019.00032

Logothetis, N. K., Pauls, J., Augath, M., Trinath, T., & Oeltermann, A. (2001). Neurophysiological investigation of the basis of the fMRI signal. *Nature*, *412*(6843), 150–157. https://doi.org/10.1038/35084005

Lundqvist, M., Herman, P., & Miller, E. K. (2018). Working Memory: Delay Activity, Yes! Persistent Activity? Maybe Not. *The Journal of Neuroscience*, *38*(32), 7013–7019. https://doi.org/10.1523/JNEUROSCI.2485-17.2018

Manning, J. R., Jacobs, J., Fried, I., & Kahana, M. J. (2009). Broadband shifts in local field potential power spectra are correlated with single-neuron spiking in humans. *The Journal of Neuroscience: The Official Journal of the Society for Neuroscience*, *29*(43), 13613–13620. https://doi.org/10.1523/JNEUROSCI.2041-09.2009

McDowell, J. E., Dyckman, K. A., Austin, B. P., & Clementz, B. A. (2008). Neurophysiology and neuroanatomy of reflexive and volitional saccades: Evidence from studies of humans. *Brain and Cognition*, *68*(3), 255–270. https://doi.org/10.1016/j.bandc.2008.08.016

Meyer, T., Qi, X.-L., & Constantinidis, C. (2007). Persistent discharges in the prefrontal cortex of monkeys naive to working memory tasks. *Cerebral Cortex (New York, N.Y.: 1991)*, *17 Suppl 1*, i70-76. https://doi.org/10.1093/cercor/bhm063

Milea, D., Lobel, E., Lehéricy, S., Leboucher, P., Pochon, J.-B., Pierrot-Deseilligny, C., & Berthoz, A. (2007a). Prefrontal cortex is involved in internal decision of forthcoming saccades. *Neuroreport*, *18*(12), 1221–1224. https://doi.org/10.1097/WNR.0b013e3281e72ce7

Milea, D., Lobel, E., Lehéricy, S., Leboucher, P., Pochon, J.-B., Pierrot-Deseilligny, C., & Berthoz, A. (2007b). Prefrontal cortex is involved in internal decision of forthcoming saccades. *Neuroreport*, *18*(12), 1221–1224. https://doi.org/10.1097/WNR.0b013e3281e72ce7

Mitzdorf, U. (1985). Current source-density method and application in cat cerebral cortex: Investigation of evoked potentials and EEG phenomena. *Physiological Reviews*, *65*(1), 37–100. https://doi.org/10.1152/physrev.1985.65.1.37

Mochizuki, K., & Funahashi, S. (2016). Prefrontal spatial working memory network predicts animal's decision making in a free choice saccade task. *Journal of Neurophysiology*, *115*(1), 127–142. https://doi.org/10.1152/jn.00255.2015

Moon, S. Y., Barton, J. J. S., Mikulski, S., Polli, F. E., Cain, M. S., Vangel, M., Hämäläinen, M. S., & Manoach, D. S. (2007). Where left becomes right: A magnetoencephalographic study of sensorimotor transformation for antisaccades. *NeuroImage*, *36*(4), 1313–1323. https://doi.org/10.1016/j.neuroimage.2007.04.040

Mukamel, R., Gelbard, H., Arieli, A., Hasson, U., Fried, I., & Malach, R. (2005a). Coupling between neuronal firing, field potentials, and FMRI in human auditory cortex. *Science (New York, N.Y.)*, *309*(5736), 951–954. https://doi.org/10.1126/science.1110913

Mukamel, R., Gelbard, H., Arieli, A., Hasson, U., Fried, I., & Malach, R. (2005b). Coupling between neuronal firing, field potentials, and FMRI in human auditory cortex. *Science (New York, N.Y.)*, *309*(5736), 951–954. https://doi.org/10.1126/science.1110913

Nachev, P., Kennard, C., & Husain, M. (2008). Functional role of the supplementary and pre-supplementary motor areas. *Nature Reviews Neuroscience*, *9*(11), 856–869. https://doi.org/10.1038/nrn2478

Nachev, P., Rees, G., Parton, A., Kennard, C., & Husain, M. (2005). Volition and conflict in human medial frontal cortex. *Current Biology : CB*, *15*(2), 122–128. https://doi.org/10.1016/j.cub.2005.01.006

Niessing, J., Ebisch, B., Schmidt, K. E., Niessing, M., Singer, W., & Galuske, R. A. W. (2005). Hemodynamic signals correlate tightly with synchronized gamma oscillations. *Science (New York, N.Y.)*, *309*(5736), 948–951. https://doi.org/10.1126/science.1110948

Nir, Y., Fisch, L., Mukamel, R., Gelbard-Sagiv, H., Arieli, A., Fried, I., & Malach, R. (2007). Coupling between neuronal firing rate, gamma LFP, and BOLD fMRI is related to interneuronal correlations. *Current Biology: CB*, *17*(15), 1275–1285. https://doi.org/10.1016/j.cub.2007.06.066

Ojemann, G. A., Ramsey, N. F., & Ojemann, J. (2013). Relation between functional magnetic resonance imaging (fMRI) and single neuron, local field potential (LFP) and electrocorticography (ECoG) activity in human cortex. *Frontiers in Human Neuroscience*, *7*. https://doi.org/10.3389/fnhum.2013.00034

Oliveira, F. T. P., Diedrichsen, J., Verstynen, T., Duque, J., & Ivry, R. B. (2010). Transcranial magnetic stimulation of posterior parietal cortex affects decisions of hand choice. *Proceedings of the National Academy of Sciences*, *107*(41), 17751–17756. https://doi.org/10.1073/pnas.1006223107

Olk, B., Chang, E., Kingstone, A., & Ro, T. (2006). Modulation of antisaccades by transcranial magnetic stimulation of the human frontal eye field. *Cerebral Cortex (New York, N.Y.: 1991)*, *16*(1), 76–82. https://doi.org/10.1093/cercor/bhi085

Ossandón, T., Jerbi, K., Vidal, J. R., Bayle, D. J., Henaff, M.-A., Jung, J., Minotti, L., Bertrand, O., Kahane, P., & Lachaux, J.-P. (2011). Transient Suppression of Broadband Gamma Power in the Default-Mode Network Is Correlated with Task Complexity and Subject Performance. *Journal of Neuroscience*, *31*(41), 14521–14530. https://doi.org/10.1523/JNEUROSCI.2483-11.2011

Ossandón, T., Vidal, J. R., Ciumas, C., Jerbi, K., Hamamé, C. M., Dalal, S. S., Bertrand, O., Minotti, L., Kahane, P., & Lachaux, J.-P. (2012). Efficient “pop-out” visual search elicits sustained broadband γ activity in the dorsal attention network. *The Journal of Neuroscience: The Official Journal of the Society for Neuroscience*, *32*(10), 3414–3421. https://doi.org/10.1523/JNEUROSCI.6048-11.2012

Pastor-Bernier, A., & Cisek, P. (2011). Neural correlates of biased competition in premotor cortex. *The Journal of Neuroscience: The Official Journal of the Society for Neuroscience*, *31*(19), 7083–7088. https://doi.org/10.1523/JNEUROSCI.5681-10.2011

Pastor-Bernier, A., Tremblay, E., & Cisek, P. (2012). Dorsal premotor cortex is involved in switching motor plans. *Frontiers in Neuroengineering*, *5*. https://doi.org/10.3389/fneng.2012.00005

Pedregosa, F., Varoquaux, G., Gramfort, A., Michel, V., Thirion, B., Grisel, O., Blondel, M., Müller, A., Nothman, J., Louppe, G., Prettenhofer, P., Weiss, R., Dubourg, V., Vanderplas, J., Passos, A., Cournapeau, D., Brucher, M., Perrot, M., & Duchesnay, É. (2012). *Scikit-learn: Machine Learning in Python*. https://arxiv.org/abs/1201.0490v4

Pesaran, B., Nelson, M. J., & Andersen, R. A. (2008). Free choice activates a decision circuit between frontal and parietal cortex. *Nature*, *453*(7193), 406–409. https://doi.org/10.1038/nature06849

Petit, L., Clark, V. P., Ingeholm, J., & Haxby, J. V. (1997). Dissociation of saccade-related and pursuit-related activation in human frontal eye fields as revealed by fMRI. *Journal of Neurophysiology*, *77*(6), 3386–3390. https://doi.org/10.1152/jn.1997.77.6.3386

Pierrot-Deseilligny, C., Ploner, C. J., Muri, R. M., Gaymard, B., & Rivaud-Pechoux, S. (2002). Effects of cortical lesions on saccadic: Eye movements in humans. *Annals of the New York Academy of Sciences*, *956*, 216–229. https://doi.org/10.1111/j.1749-6632.2002.tb02821.x

Platt, M. L., & Glimcher, P. W. (1999). Neural correlates of decision variables in parietal cortex. *Nature*, *400*(6741), 233–238. https://doi.org/10.1038/22268

Procyk, E., & Goldman-Rakic, P. S. (2006). Modulation of Dorsolateral Prefrontal Delay Activity during Self-Organized Behavior. *Journal of Neuroscience*, *26*(44), 11313–11323. https://doi.org/10.1523/JNEUROSCI.2157-06.2006

Raschka, S. (2018). *Model Evaluation, Model Selection, and Algorithm Selection in Machine Learning*. https://arxiv.org/abs/1811.12808v2

Ray, S., Crone, N. E., Niebur, E., Franaszczuk, P. J., & Hsiao, S. S. (2008). Neural Correlates of High-Gamma Oscillations (60–200 Hz) in Macaque Local Field Potentials and Their Potential Implications in Electrocorticography. *Journal of Neuroscience*, *28*(45), 11526–11536. https://doi.org/10.1523/JNEUROSCI.2848-08.2008

Ray, S., & Maunsell, J. H. R. (2011). Different Origins of Gamma Rhythm and High-Gamma Activity in Macaque Visual Cortex. *PLOS Biology*, *9*(4), e1000610. https://doi.org/10.1371/journal.pbio.1000610

Rowe, J. B., Toni, I., Josephs, O., Frackowiak, R. S., & Passingham, R. E. (2000). The prefrontal cortex: Response selection or maintenance within working memory? *Science (New York, N.Y.)*, *288*(5471), 1656–1660. https://doi.org/10.1126/science.288.5471.1656

Rushworth, M. F. S., Johansen-Berg, H., Göbel, S. M., & Devlin, J. T. (2003). The left parietal and premotor cortices: Motor attention and selection. *NeuroImage*, *20 Suppl 1*, S89-100.

Sakamoto, A., Lüders, H., & Burgess, R. (1991). Intracranial recordings of movement-related potentials to voluntary saccades. *Journal of Clinical Neurophysiology: Official Publication of the American Electroencephalographic Society*, *8*(2), 223–233.

Schall, J. D. (1991). Neuronal activity related to visually guided saccadic eye movements in the supplementary motor area of rhesus monkeys. *Journal of Neurophysiology*, *66*(2), 530–558. https://doi.org/10.1152/jn.1991.66.2.530

Schall, J. D., & Bichot, N. P. (1998). Neural correlates of visual and motor decision processes. *Current Opinion in Neurobiology*, *8*(2), 211–217.

Schluppeck, D. (2006). Sustained Activity in Topographic Areas of Human Posterior Parietal Cortex during Memory-Guided Saccades. *Journal of Neuroscience*, *26*(19), 5098–5108. https://doi.org/10.1523/JNEUROSCI.5330-05.2006

Sendhilnathan, N., Basu, D., & Murthy, A. (2017). Simultaneous analysis of the LFP and spiking activity reveals essential components of a visuomotor transformation in the frontal eye field. *Proceedings of the National Academy of Sciences*, *114*(24), 6370–6375. https://doi.org/10.1073/pnas.1703809114

Shadlen, M. N., & Newsome, W. T. (2001). Neural basis of a perceptual decision in the parietal cortex (area LIP) of the rhesus monkey. *Journal of Neurophysiology*, *86*(4), 1916–1936. https://doi.org/10.1152/jn.2001.86.4.1916

Shima, K., Aya, K., Mushiake, H., Inase, M., Aizawa, H., & Tanji, J. (1991). Two movement-related foci in the primate cingulate cortex observed in signal-triggered and self-paced forelimb movements. *Journal of Neurophysiology*, *65*(2), 188–202. https://doi.org/10.1152/jn.1991.65.2.188

Stokes, M. G. (2015). "Activity-silent" working memory in prefrontal cortex: A dynamic coding framework. *Trends in Cognitive Sciences*, *19*(7), 394–405. https://doi.org/10.1016/j.tics.2015.05.004

Sugrue, L. P., Corrado, G. S., & Newsome, W. T. (2004). Matching behavior and the representation of value in the parietal cortex. *Science (New York, N.Y.)*, *304*(5678), 1782–1787. https://doi.org/10.1126/science.1094765

Suriya-Arunroj, L., & Gail, A. (2019). Complementary encoding of priors in monkey frontoparietal network supports a dual process of decision-making. *ELife*, *8*, e47581. https://doi.org/10.7554/eLife.47581

Sweeney, J. A., Luna, B., Keedy, S. K., McDowell, J. E., & Clementz, B. A. (2007). fMRI Studies of Eye Movement Control: Investigating the Interaction of Cognitive and Sensorimotor Brain Systems. *NeuroImage*, *36*(Suppl 2), T54–T60. https://doi.org/10.1016/j.neuroimage.2007.03.018

Tobler, P. N., & Müri, R. M. (2002). Role of human frontal and supplementary eye fields in double step saccades. *NeuroReport*, *13*(2), 253.

Tzourio-Mazoyer, N., Landeau, B., Papathanassiou, D., Crivello, F., Etard, O., Delcroix, N., Mazoyer, B., & Joliot, M. (2002). Automated Anatomical Labeling of Activations in SPM Using a Macroscopic Anatomical Parcellation of the MNI MRI Single-Subject Brain. *NeuroImage*, *15*(1), 273–289. https://doi.org/10.1006/nimg.2001.0978

Urchs, S., Armoza, J., Moreau, C., Benhajali, Y., St-Aubin, J., Orban, P., & Bellec, P. (2019). MIST: A multi-resolution parcellation of functional brain networks. *MNI Open Research*, *1*, 3. https://doi.org/10.12688/mniopenres.12767.2

Van Der Werf, J., Buchholz, V. N., Jensen, O., & Medendorp, W. P. (2009). Neuronal synchronization in human parietal cortex during saccade planning. *Behavioural Brain Research*, *205*(2), 329–335. https://doi.org/10.1016/j.bbr.2009.06.011

Watanabe, K., Igaki, S., & Funahashi, S. (2006). Contributions of prefrontal cue-, delay-, and response-period activity to the decision process of saccade direction in a free-choice ODR task. *Neural Networks*, *19*(8), 1203–1222. https://doi.org/10.1016/j.neunet.2006.05.033

Werf, J. V. D., Jensen, O., Fries, P., & Medendorp, W. P. (2008). Gamma-Band Activity in Human Posterior Parietal Cortex Encodes the Motor Goal during Delayed Prosaccades and Antisaccades. *Journal of Neuroscience*, *28*(34), 8397–8405. https://doi.org/10.1523/JNEUROSCI.0630-08.2008

Werf, J. V. D., Jensen, O., Fries, P., & Medendorp, W. P. (2010). Neuronal Synchronization in Human Posterior Parietal Cortex during Reach Planning. *Journal of Neuroscience*, *30*(4), 1402–1412. https://doi.org/10.1523/JNEUROSCI.3448-09.2010

Wilke, M., Kagan, I., & Andersen, R. A. (2012). Functional imaging reveals rapid reorganization of cortical activity after parietal inactivation in monkeys. *Proceedings of the National Academy of Sciences*, *109*(21), 8274–8279. https://doi.org/10.1073/pnas.1204789109

Yamamoto, J., Ikeda, A., Satow, T., Matsuhashi, M., Baba, K., Yamane, F., Miyamoto, S., Mihara, T., Hori, T., Taki, W., Hashimoto, N., & Shibasaki, H. (2004). Human eye fields in the frontal lobe as studied by epicortical recording of movement-related cortical potentials. *Brain: A Journal of Neurology*, *127*(Pt 4), 873–887. https://doi.org/10.1093/brain/awh110

Yang, T., & Shadlen, M. N. (2007). Probabilistic reasoning by neurons. *Nature*, *447*(7148), 1075–1080. https://doi.org/10.1038/nature05852

Zapparoli, L., Seghezzi, S., Scifo, P., Zerbi, A., Banfi, G., Tettamanti, M., & Paulesu, E. (2018). Dissecting the neurofunctional bases of intentional action. *Proceedings of the National Academy of Sciences*, *115*(28), 7440–7445. https://doi.org/10.1073/pnas.1718891115

## 3.7 Supplementary Information

| | Handedness | Age | Gender | MRI | EZ localization | Surgery | Histology |
|---|---|---|---|---|---|---|---|
| **P1** | Right-handed | 30 | M | normal | right mesio-temporal | yes | heterotopia |
| **P2** | Right-handed | 33 | F | normal | right frontal (premotor) | yes | non specific |
| **P3** | Right-handed | 26 | M | normal | right frontal (dorsolateral premotor) | yes | non specific |
| **P4** | Right-handed | 35 | F | normal | bi-frontal epilepsy | no | na |
| **P5** | Right-handed | 18 | F | left hippocampal sclerosis | left mesio-temporal | yes | hippocampa sclerosis |
| **P6** | Right-handed | 20 | F | left frontal (rolandic) focal cortical dysplasia | left frontal (rolandic) | no | na |

**S1 Table.** Participant data: handedness, age, gender, and description of epilepsy type, etiology, as determined by the clinical staff of the Grenoble Neurological Hospital, Grenoble, France. The lesions (if any were observed) were determined based on the T1 images. Recording sites with epileptogenic activity were excluded from the analyses.

| | Mean Saccade Duration (ms) | Std Duration | Saccade speed (°/s) | Mean Latency (ms) | Std Latency | Number of Saccades |
|---|---|---|---|---|---|---|
| Patient 1: Control | 47 | 5.1 | 149 | 475 | 137 | 91 |
| Patient 1: Free | 48 | 5.6 | 146 | 341 | 128 | 104 |
| Patient 1: Instructed | 46 | 4.6 | 152 | 390 | 165 | 93 |
| | | | | | | |
| Patient 2: Control | 34 | 7.6 | 206 | 543 | 117 | 130 |
| Patient 2: Free | 37 | 6.4 | 189 | 361 | 75 | 117 |
| Patient 2: Instructed | 36 | 7.6 | 194 | 350 | 76 | 110 |
| | | | | | | |
| Patient 3: Control | 47 | 7.1 | 149 | 465 | 91 | 71 |
| Patient 3: Free | 47 | 8.4 | 149 | 368 | 68 | 58 |
| Patient 3: Instructed | 47 | 7.9 | 149 | 363 | 93 | 78 |
| | | | | | | |
| Patient 4: Control | 45 | 19.9 | 156 | 423 | 62 | 85 |
| Patient 4: Free | 45 | 17.5 | 156 | 316 | 93 | 87 |
| Patient 4: Instructed | 45 | 17.5 | 156 | 341 | 89 | 97 |
| | | | | | | |
| Patient 5: Control | 59 | 8.4 | 119 | 422 | 124 | 51 |
| Patient 5: Free | 59 | 9.4 | 119 | 418 | 144 | 37 |
| Patient 5: Instructed | 60 | 11.2 | 117 | 424 | 134 | 79 |
| | | | | | | |
| Patient 6: Control | 48 | 10.9 | 146 | 360 | 86 | 98 |
| Patient 6: Free | 48 | 11.7 | 146 | 276 | 60 | 100 |
| Patient 6: Instructed | 49 | 12.7 | 143 | 275 | 58 | 97 |

**S2 Table.** Behavioral results for all participants (n=6).

| | | Mean ***Ins.*** | Mean ***Free*** | *T* value | *p* value | Conditions |
|---|---|---|---|---|---|---|
| **HG peak (in %)** | **P1** | 38 | 27 | 3 | 0.005 | ***Free*** vs ***Instructed*** |
| | **P2** | 40 | 24 | 2 | 0.05 | |
| | **P3** | 38 | 23 | 0.8 | 0.4 | |
| | **P6** | 41 | 21 | 3.05 | 0.004 | |
| | **All Participants** | **39** | **24** | **8.34** | **0.003** | |

| | | Mean ***Ins.*** | Mean ***Free*** | *T* value | *p* value | Conditions |
|---|---|---|---|---|---|---|
| **HG peak latency (in ms)** | **P1** | 450 | 750 | 2.7 | 0.01 | ***Free*** vs ***Instructed*** |
| | **P2** | 500 | 700 | 5.5 | $3 \times 10^{-6}$ | |
| | **P3** | 450 | 700 | 2.1 | 0.17 | |
| | **P 6** | 500 | 1100 | 4.2 | 0.0001 | |
| | **All Participants** | **475** | **812** | **21** | **0.0002** | |

| | | Mean ***Ins.*** | Mean ***Free*** | *T* value | *p* value | Conditions |
|---|---|---|---|---|---|---|
| **First significant time (in ms)** | **P1** | 260 | 490 | 4.1 | 0.0003 | ***Free*** *vs* ***Control*** |
| | **P2** | 112 | 490 | 3.9 | 0.0002 | |
| | **P3** | 80 | 325 | 2.2 | 0.08 | |
| | **P6** | 157 | 558 | 4.4 | 0.0001 | ***Inst.*** *vs* ***Control*** |
| | **All Participants** | **152** | **465** | **7.1** | **0.006** | |

| | | Mean ***Ins.*** | Mean ***Free*** | *T* value | *p* value | Conditions |
|---|---|---|---|---|---|---|
| **Total of significant differences (in ms)** | **P1** | 407 | 478 | 1.5 | 0.14 | ***Free*** *vs* ***Control*** |
| | **P2** | 417 | 640 | 1.3 | 0.19 | |
| | **P3** | 190 | 600 | 1.5 | 0.18 | |
| | **P6** | 456 | 753 | 2.6 | 0.01 | ***Inst.*** *vs* ***Control*** |
| | **All Participants** | **368** | **618** | **3.52** | **0.04** | |

| | | Mean ***Ins.*** | Mean ***Free*** | *T* value | *p* value | Conditions |
|---|---|---|---|---|---|---|
| **Latency of peak DA (in ms)** | **P1** | 473 | 865 | 3.9 | 0.0005 | ***Free*** *vs* ***Control*** |
| | **P2** | 628 | 897 | 5.2 | $1.4 \times 10^{-6}$ | |
| | **P3** | 320 | 700 | 11.3 | $9.3 \times 10^{-5}$ | |
| | **P6** | 554 | 1019 | 4.6 | $5.1 \times 10^{-5}$ | ***Inst.*** *vs* ***Control*** |
| | **All Participants** | **527** | **822** | **3.39** | **0.027** | |

**S3 Table.** Statistical results for HG differences across and within individual participants.

| Electrodes | ID | X | Y | Z | BA | AAL | MIST | EARLY / LATE |
|---|---|---|---|---|---|---|---|---|
| **g'11-g'10** | P1 | -31 | 29 | 18 | BA48 | Frontal Inf Tri | Left inf fronl sulcus | EARLY |
| **e'2-e'1** | P1 | -1,105 | 28 | 32 | BA24 | Cingulum Mid | Left ant cing cortex dorsal | EARLY |
| **h'3-h'2** | P1 | -3,7 | 11 | 36 | BA24 | Cingulum Mid | Left ant cing cortex dorsal | EARLY |
| **h'4-h'3** | P1 | -7,3 | 11 | 36 | BA24 | Cingulum Mid | Left ant cing cortex dorsal | EARLY |
| **p8-p7** | P2 | 25 | -50 | 50 | BA7 | Parietal Inf | Right dorsal vis stream sup | EARLY |
| **p9-p8** | P2 | 29 | -50 | 50 | BA7 | Parietal Inf | Right dorsal vis stream sup | EARLY |
| **p10-p9** | P2 | 33 | -50 | 50 | BA40 | Parietal Inf | Right dorsal vis stream sup | EARLY |
| **b3-b2** | P2 | 5,8 | -6,2 | 56 | BA6 | Supp Motor Area | Right somatomotor network anteromedial | EARLY |
| **b10-b9** | P2 | 32 | -6,2 | 56 | BA6 | Precentral | Right frontal eye field | EARLY |
| **m4-m3** | P2 | 10 | 14 | 47 | BA32 | Supp Motor Area | Right pre supplementary motor cortex anterior | EARLY |
| **m8-m7** | P2 | 25 | 14 | 47 | BA8 | Frontal Mid | Right sup frontal sulcus | EARLY |
| **n9-n8** | P2 | 29 | 36 | 37 | BA9 | Frontal Mid | Right sup frontal sulcus | EARLY |
| **n10-n9** | P2 | 32,5 | 36 | 37 | BA9 | Frontal Mid | Right mid front gyrus post | EARLY |
| **n11-n10** | P2 | 36 | 36 | 37 | BA9 | Frontal Mid | Right mid front gyrus post | EARLY |
| **n12-n11** | P2 | 40 | 36 | 37 | BA46 | Frontal Mid | Right mid front gyrus post | EARLY |
| **f14-f13** | P2 | 48 | 52 | 22 | BA46 | Frontal Mid | Right mid front gyrus post | EARLY |
| **f15-f14** | P2 | 52 | 52 | 22 | BA46 | Frontal Mid | Right mid front gyrus post | EARLY |
| **x14-x13** | P2 | 25,5 | 32,5 | 22,5 | BA48 | Insula | Left insula | EARLY |
| **h'12-'11** | P6 | -44,5 | -2,2 | 34 | BA6 | Precentral | Left inferior frontal sulcus | EARLY |
| **e'3-e'2** | P6 | -9,3 | 11 | 39 | BA32 | Cingulum Mid | Left cing  sulcus posterior | EARLY |
| **e'4-e'3** | P6 | -13 | 11 | 39 | BA32 | Cingulum Mid | Left cing  sulcus posterior | EARLY |
| **a'2-a'1** | P6 | -6,2 | 8,6 | 47 | BA32 | Supp Motor Area | Left pre suppl motor cortex anterior | EARLY |
| **a'3-a'2** | P6 | -10 | 10,15 | 47 | BA32 | Supp Motor Area | Left pre suppl motor cortex anterior | EARLY |
| **a'4-a'3** | P6 | -13,5 | 11,5 | 47 | BA32 | Supp Motor Area | Left pre suppl motor cortex anterior | EARLY |
| **a'5-a'4** | P6 | -17 | 13 | 47 | BA32 | Frontal Sup | Left sup front sulcus ant | EARLY |
| **a'6-a'5** | P6 | -20,5 | 14,5 | 47,5 | BA8 | Frontal Sup | Left sup frontal sulcus ant | EARLY |
| **a'7-a'6** | P6 | -24 | 16 | 48 | BA8 | Frontal Sup | Left sup frontal sulcus ant | EARLY |
| **a'8-a'7** | P6 | -27,5 | 17,5 | 48 | BA8 | Frontal Mid | Left sup frontal sulcus ant | EARLY |
| **a'9-a'8** | P6 | -31 | 18,5 | 48 | BA8 | Frontal Mid | Left sup frontal sulcus ant | EARLY |
| **x10-x9** | P1 | 37,5 | 23,5 | 11 | BA48 | Frontal Inf Tri | Right ant insula anteroodorsal | LATE |
| **x'17-'16** | P1 | -22,5 | 51,5 | 23 | BA46 | Frontal Sup | Left mid frontal gyrus ant | EARLY AND LATE |
| **e'10-'9** | P1 | -30 | 28 | 32 | BA46 | Frontal Mid | Left superior frontal sulcus anterior | EARLY AND LATE |
| **e'14-'13** | P1 | -44,5 | 28 | 32 | BA45 | Frontal Mid | Left middle frontal gyrus anterior | EARLY AND LATE |
| **e'15-'14** | P1 | -48 | 28 | 32 | BA45 | Frontal Mid | Left middle frontal gyrus anterior | EARLY AND LATE |
| **m8-m7** | P6 | 25 | 2 | 53 | BA8 | Frontal Sup | Right frontal eye field | EARLY AND LATE |

**S4 Table.** Full list of all significant electrodes that have free-choice specific HG enhancements during the delay period, determined by conjunction analysis (cf Fig 5B).

| Electrodes | ID | *Free pvalues* | *Instructed pvalues* | *Control pvalues* | *X* | *Y* | *Z* | *BA* | *AAL* | *MIST* |
|---|---|---|---|---|---|---|---|---|---|---|
| **j5-j4** | P2 | 0,2 | 0,2 | 0,6 | 16 | -20 | 57 | BA6 | Supp Motor Area | Right frontal eye field |
| **j6-j5** | P2 | 0,2 | **< 0.01** | 0,4 | 19,5 | -20 | 57 | BA6 | Supp Motor Area | Right frontal eye field |
| **b9-b8** | P2 | 0,07 | 0,9 | 0,8 | 28,5 | -6,2 | 56 | BA6 | Precentral | Right frontal eye field |
| **j2-j1** | P2 | **< 0.01** | 0,6 | 0,3 | 4,2 | -20 | 57 | BA4 | Supp Motor Area | Right somatomotor network medial |
| **b3-b2** | P2 | **< 0.01** | **< 0.01** | **0,03** | 5,8 | -6,2 | 56 | BA6 | Supp Motor Area | Right somatomotor network anteromedial |
| **m3-m2** | P2 | 0,6 | 0,08 | 0,2 | 6,1 | 14 | 47 | BA32 | Supp Motor Area | Right pre supplementary motor cortex anterior |
| **m4-m3** | P2 | 0,6 | 0,9 | 0,4 | 10 | 14 | 47 | BA32 | Supp Motor Area | Right pre supplementary motor cortex anterior |
| **j9-j8** | P2 | **0,01** | 0,9 | 0,5 | 31 | -20 | 57 | BA4 | Precentral | Right_somatomotor_network_dorsolateral |
| **j8-j7** | P2 | 0,9 | 0,9 | 0,7 | 27 | -20 | 57 | BA6 | Precentral | Right_somatomotor_network_mediolateral |
| **j7-j6** | P2 | 0,9 | 0,5 | 0,3 | 23 | -20 | 57 | BA6 | Precentral | Right_somatomotor_network_mediolateral |
| **p14-p13** | P2 | 0,8 | 1 | 0,5 | 48 | -50 | 50 | BA40 | Parietal Inf | Right inferior parietal lobule |
| **p13-p12** | P2 | 0,9 | 0,5 | 0,9 | 44 | -50 | 50 | BA40 | Parietal Inf | Right intraparietal sulcus |
| **p10-p9** | P2 | 0,1 | 0,2 | 0,1 | 33 | -50 | 50 | BA40 | Parietal Inf | Right dorsal visual stream |
| **p9-p8** | P2 | 0,6 | 0,4 | 0,6 | 29 | -50 | 50 | BA7 | Parietal Inf | Right dorsal visual stream |
| **m13-m12** | P2 | 0,1 | 0,7 | **0,04** | 44 | 14 | 47 | BA9 | Frontal Mid | Right middle frontal gyrus posterior |
| **m14-m13** | P2 | 0,3 | 0,9 | 0,054 | 48 | 14 | 47 | BA9 | Frontal Mid | Right middle frontal gyrus posterior |
| **f9-f8** | P2 | 0,2 | 0,6 | 0,8 | 29 | 52 | 22 | BA46 | Frontal Mid | Right middle frontal gyrus anterior |
| **f10-f9** | P2 | 0,07 | 0,5 | 0,9 | 33 | 52 | 22 | BA46 | Frontal Mid | Right middle frontal gyrus anterior |
| **f14-f13** | P2 | 0,7 | 0,9 | 0,3 | 48 | 52 | 22 | BA46 | Frontal Mid | Right middle frontal gyrus anterior |
| **f5-f4** | P2 | 0,4 | 0,8 | 0,4 | 14 | 52 | 22 | BA32 | Frontal Sup | Right dmPFC anterororstral |
| **n8-n7** | P2 | 0,6 | 1 | 0,9 | 25 | 36 | 37 | BA9 | Frontal Sup | Right superior frontal sulcus |
| **n7-n6** | P2 | 0,8 | 0,7 | 0,8 | 21 | 36 | 37 | BA9 | Frontal Sup | Right superior frontal sulcus |
| **y2-y1** | P2 | 0,5 | 0,8 | 0,5 | 40,5 | -8,25 | -4,25 | BA48 | Insula | Right posterior insula ventral |
| **r5-r4** | P2 | 0,6 | 0,3 | 0,3 | 50 | 7,4 | 15 | BA6 | Rolandic Oper | Left vlPFC |
| | | | | | | | | | | |
| **q'7-q'6** | P5 | 0,2 | 0,1 | 0,1 | -50,5 | 18 | 14 | BA48 | Frontal Inf Oper | Left vlPFC |
| **q'8-q'7** | P5 | 0,2 | 0,4 | 1 | -54 | 18 | 14 | BA48 | Frontal Inf Oper | Left vlPFC |
| **h'15-h'14** | P5 | 0,6 | 0,4 | 1 | -53,5 | 18 | 26 | BA44 | Frontal Inf Tri | Left inferior frontal sulcus |
| **h'14-h'13** | P5 | 0,7 | 0,4 | 0,9 | -50 | 18 | 26 | BA48 | Frontal Inf Tri | Left inferior frontal sulcus |
| **h'11-h'10** | P5 | 0,3 | 0,3 | 0,9 | -38 | 18 | 26 | BA48 | Frontal Inf Tri | Left inferior frontal sulcus |

**S5 Table.** Statistical significance (p values) for correlation between HG onset and saccade onsets for all 29 sites that were determined by conjunction analyses (see Fig 7B). Significant p-values are highlighted in yellow.

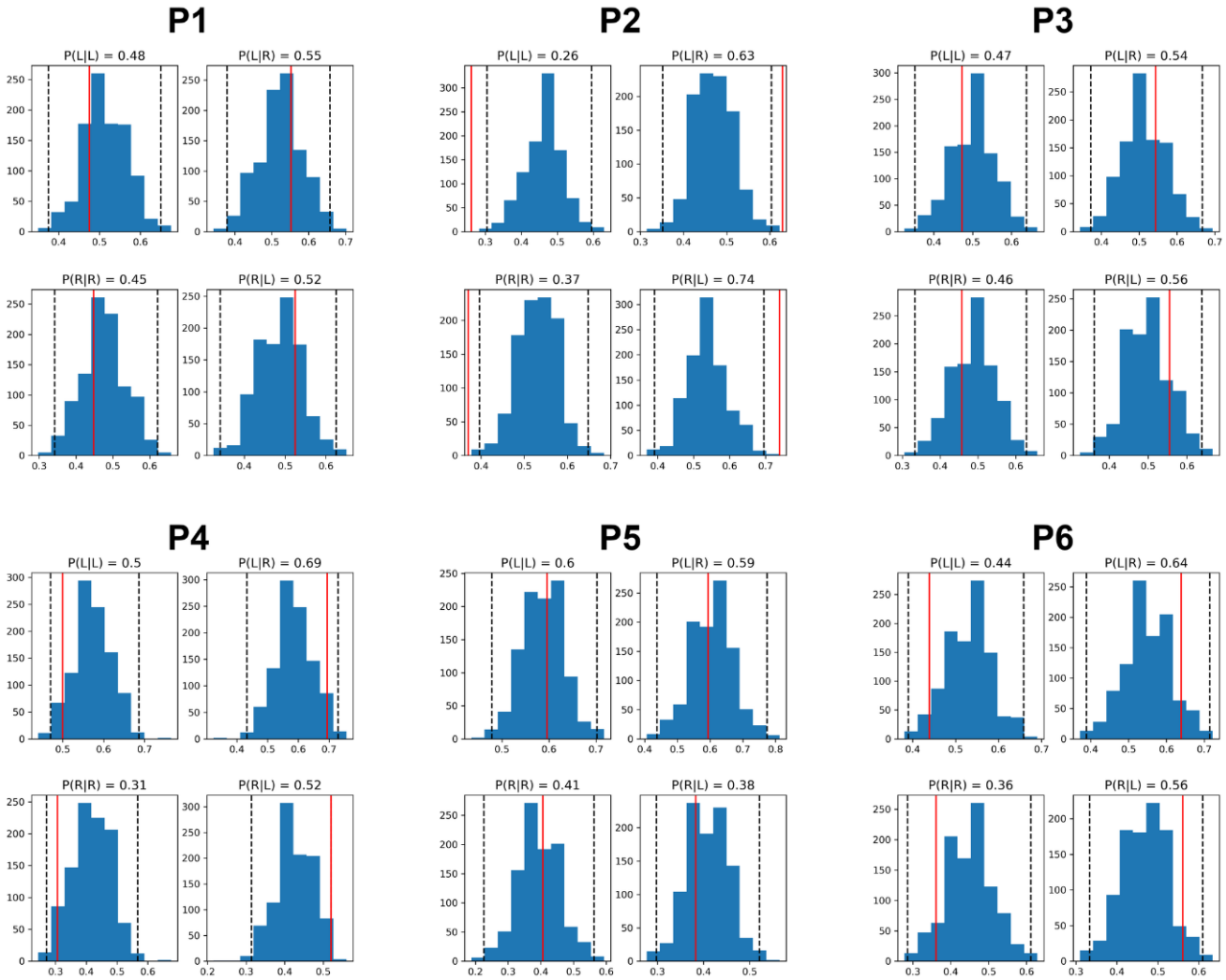


**S1 Fig. Statistical evaluation of choice history effects.** Conditional probabilities (*n-1*) were computed to determine whether the saccade direction (Left, L or Right, R) of trial *n-1* influenced trial *n* in the ***Free*** choice condition. For each participant, the value of conditional probabilities P(L|L), P(L|R), P(R|R) and P(R|L) are shown. The statistical significance of the obtained conditional probabilities was evaluated by computing statistical thresholds using permutation tests (n=1000, *p<0.001*). In other words, a null distribution is generated by repeatedly (n=1000) computing conditional probabilities for each participant obtained after randomly permuting class labels (Left and Right). We show that P2 was the only participant demonstrating a significant alternating behavior between left and right choices during the ***Free*** condition.

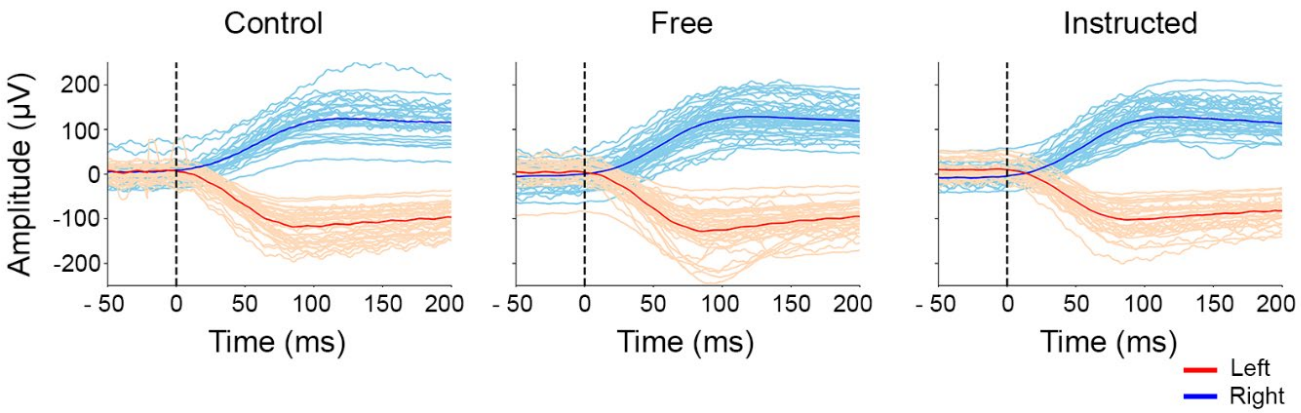


**S2 Fig.** EOG traces time-locked to saccade onset in one illustrative participant. Thin lines represent EOG traces for all trials and thick lines represent mean EOG traces locked on saccade onset for each condition (Control, Free, Instructed).

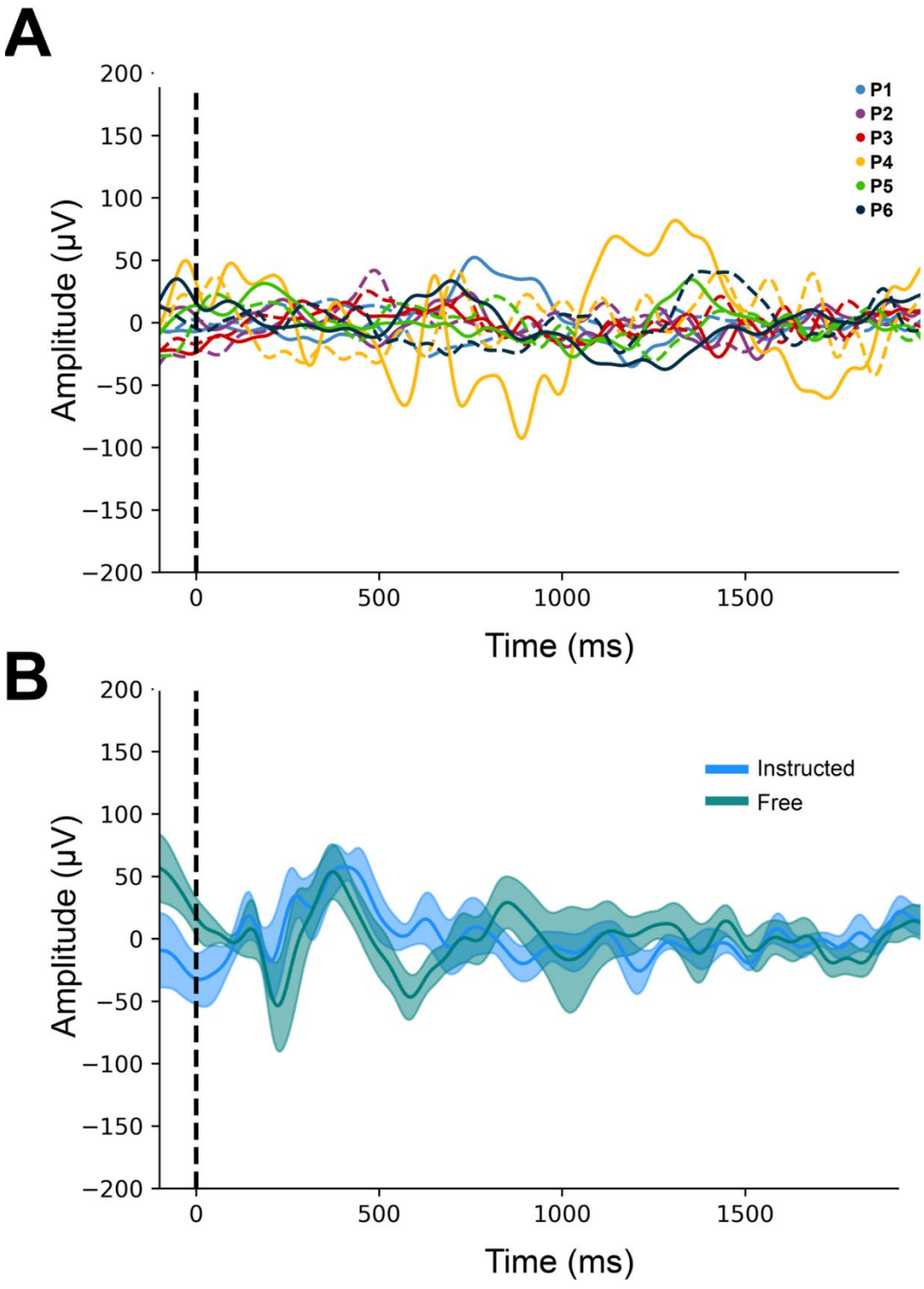


**S3 Fig.** (**A**) Mean EOG traces for all participants locked t stimulus onset (Cue 1) during the delay period. Each color is associated with a participant, dashed lines represent left saccades and full lines represent right saccades for all conditions. (**B**) Mean EOG traces for ***Instructed*** and ***Free*** conditions during the delay period. The data underlying panel **B** can be found in S1 Data.

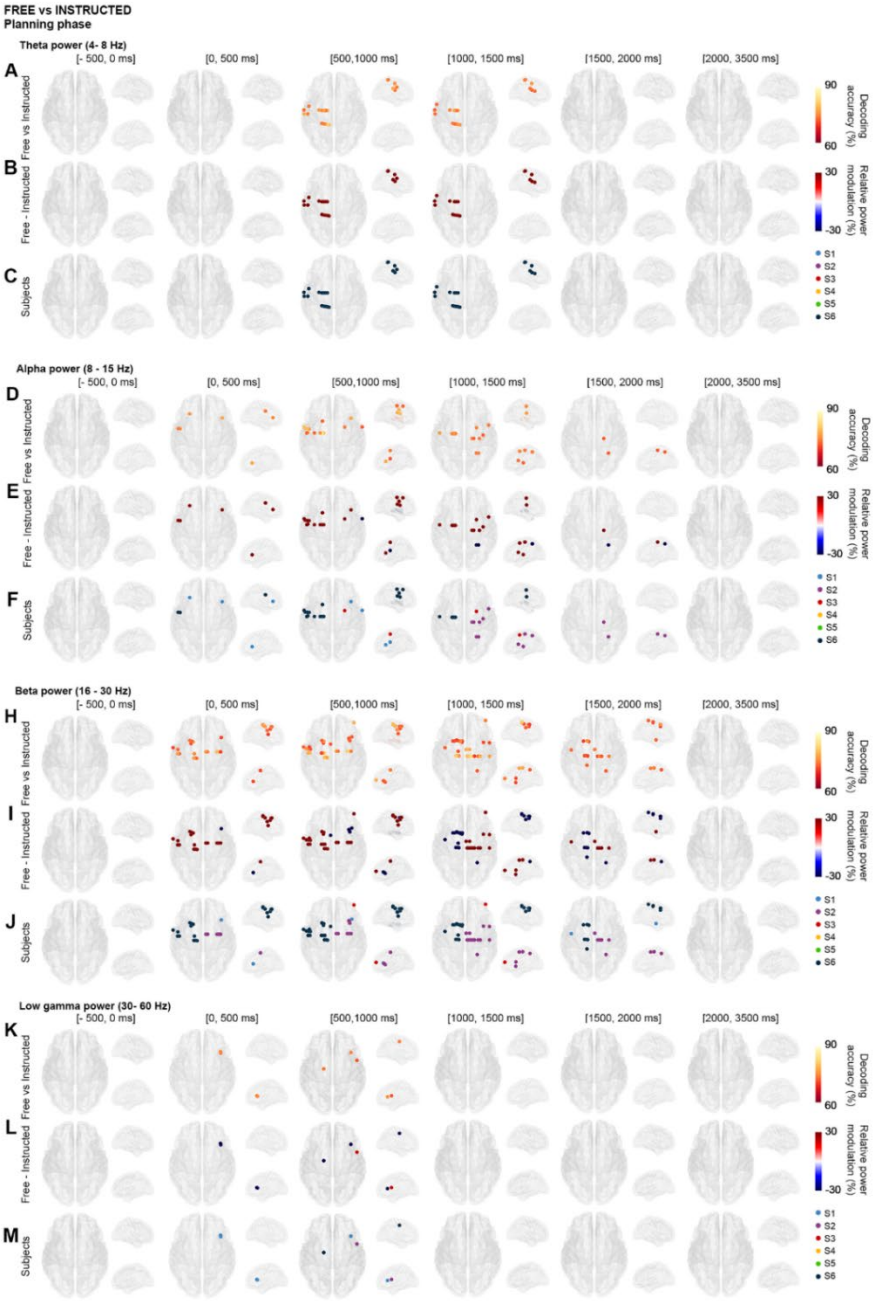


**S4 Fig. Decoding Free vs Instructed trials in θ, α, β and low γ frequency bands.** We compared high frequency neuronal activity in θ (4 -8 Hz), α (8 - 15 Hz), β (16 - 30 Hz), low γ (30 - 60 Hz) frequency bands for the ***Free*** and ***Instructed*** conditions during the planning phase in different time windows (baseline = -500 to 0 ms; 0 to 500 ms; 500 to 1000 ms; 1000 to 1500 ms; 1500 to 2000 ms; and 2000 to 3500 ms (**A, D, H, K**) Electrode-specific significant decoding accuracies (*corrected across electrodes, time and frequency bands using exhaustive permutations corrected with maximum statistics at $p < 0.01$*), (**B, E, I, L**) relative power changes (relative change = [Free - Instructed]/Instructed), and (**C, F, J, M, P**) colors belonging to individual participants are mapped to the corresponding electrode positions on transparent 3D brain images.

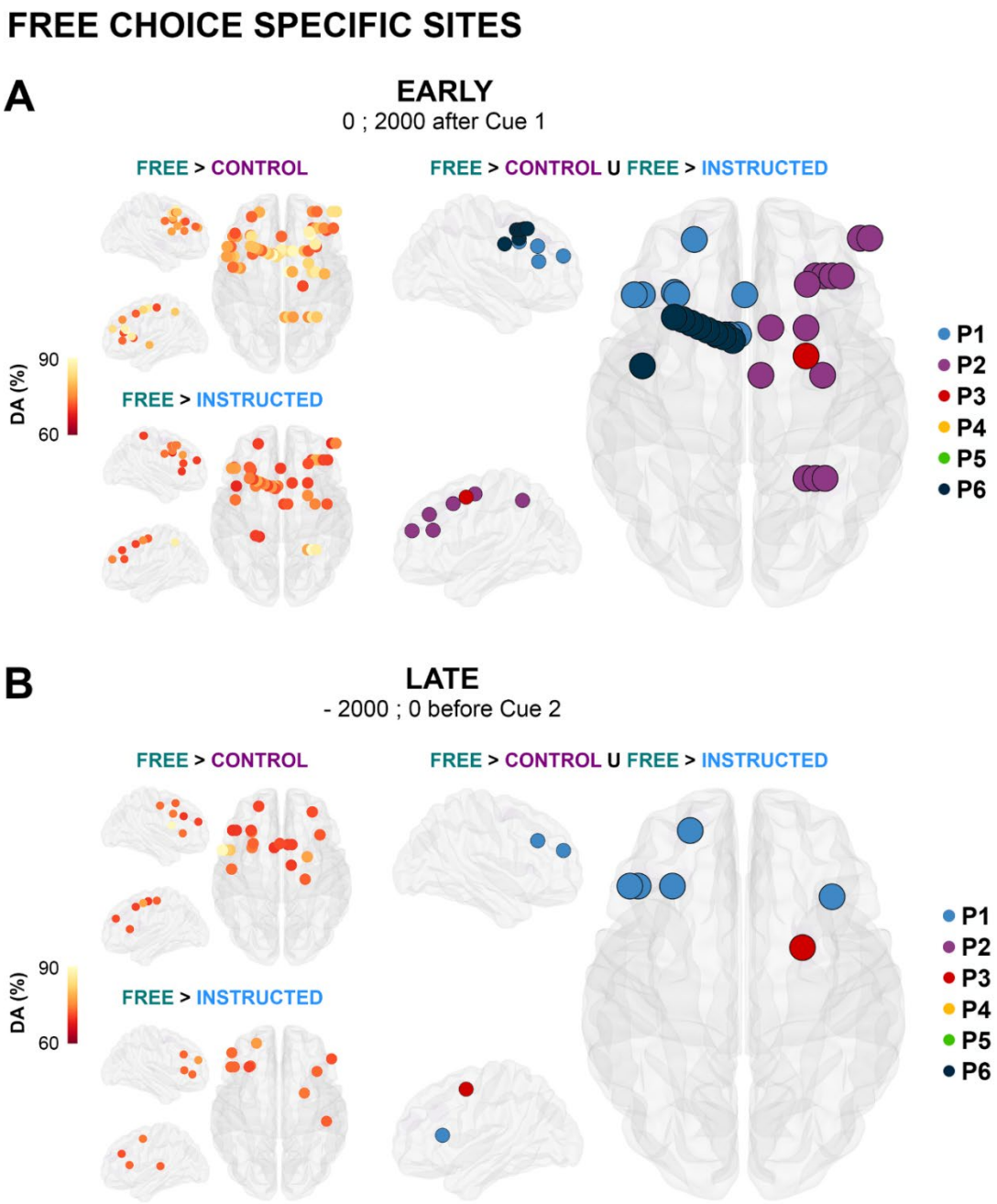


**S5 Fig. EARLY and LATE Free choice specific sites.** In **A**, electrodes with significant decoding accuracies (*p<0.01, corrected with permutations using maximum statistics across electrodes, frequency bands and time*) for all participants are mapped on transparent 3D brain images when HG activity is significantly stronger in the ***Free*** condition than in the ***Control*** condition (first row), and when HG activity is significantly stronger in the ***Free*** condition than in the ***Instructed*** condition (second row) during the delay period, from 0 to 2000 ms after Cue 1 (i.e., EARLY). We isolated a network of regions specifically involved in ***Free*** decisions showed in the right panel using a conjunction analysis (***Free*** > ***Control*** U ***Free*** > ***Instructed***). Electrodes are colored based on the participant to which they belong. **B.** The same analysis was conducted for the LATE part of the delay period, from -2000 to 0 ms second before Cue 2.

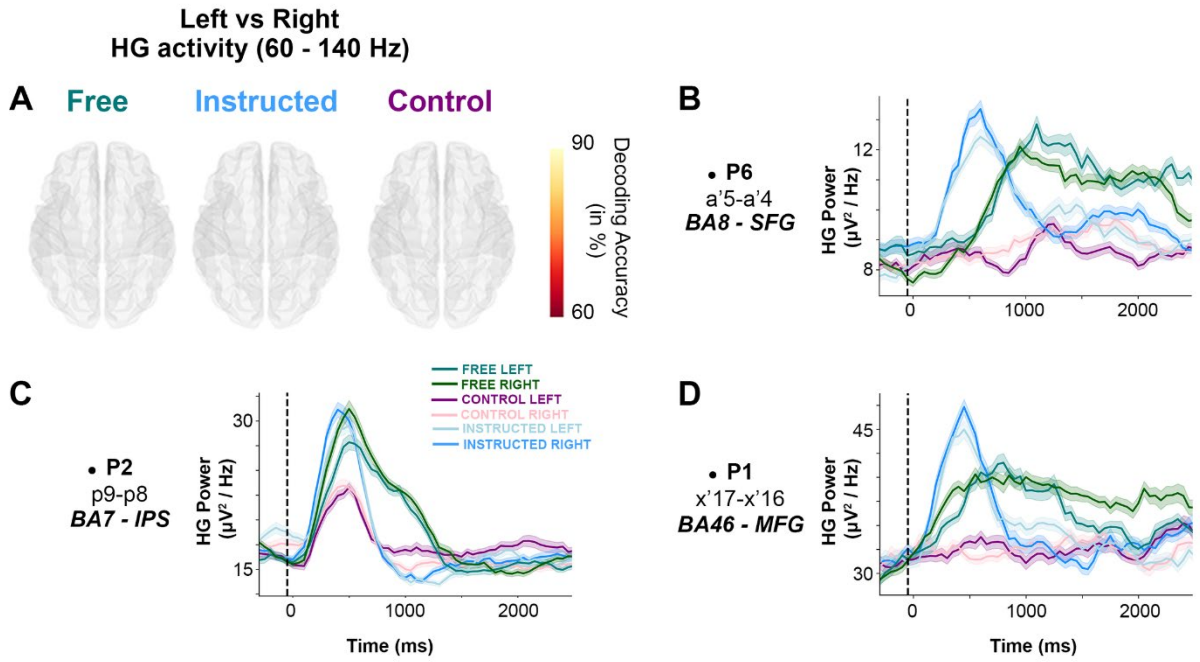


**S6 Fig. Left vs Right HG activity during the delay period. A.** Electrodes with significant decoding (*corrected across electrodes, time and frequency bands using exhaustive permutations corrected with maximum statistics at p < 0.01*) when comparing HG activity between *left* and *right choices* in the ***Free, Instructed and Control*** conditions during the delay period phase (0 to 2000ms after Cue 1) ) for all participants and mapped on transparent 3D brain images. **B, C, D.** For three individual electrodes, we plotted HG activity over time for ***Free*** (left and right), ***Instructed*** (left and right) and ***Control*** (left and right) conditions. We show that the capacity of electrodes to successfully decode ***Free*** vs ***Control*** and ***Free*** vs ***Instructed*** conditions based on HG activity on a single-trial basis is not determined by the content (left or right) of decisions. The data underlying panels **B**, **C** and **D** can be found in S1 Data.

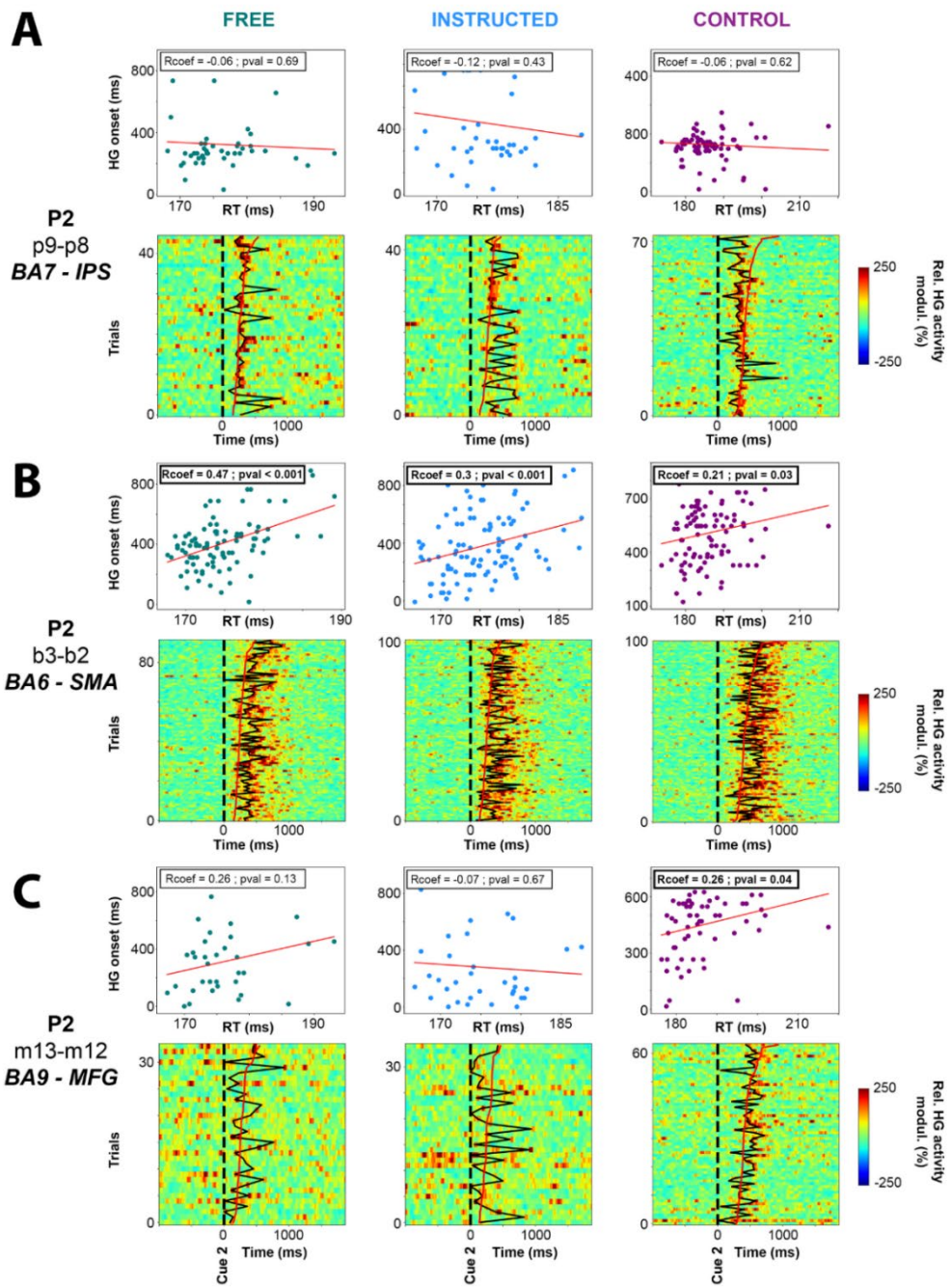


**S7 Fig. Correlations and single trials plots of HG activity during execution.** For three example electrodes located in the IPS (**A)**, SMA (**B)**, and MFG (**C**) : correlations between reaction times and the latencies of HG activity onset (upper rows) and single trial plots (lower rows) are show for the ***Free***, ***Instructed*** and ***Control*** conditions. On single trial plots, trials are sorted with respect to reactions times (RTs). RT latencies are represented by continuous red lines, and the latencies of HG activity onset are represented by continuous black lines (see Material and Methods). The data underlying this Figure can be found in S1 Data.

# Chapitre 4

# Article 2

# Decoding the neural correlates of dynamic decision-making in humans

Thomas Thiery[1], Pierre Rainville[1], Paul Cisek[1], Karim Jerbi[1]

[1] Université de Montréal, QC, Canada

Corresponding author: Thomas Thiery Email: thomas.thiery@umontreal.ca

Address: Department of Psychology, University of Montreal, C.P. 6128 succ. Centre- Ville, Montréal, QC, H3C 3J7, Canada

## Abstract

The brain evolved to guide behavior in a dynamic world, in which information about different choice options is often in flux, and one must find a balance between carefully deliberating versus quickly committing to one's current best guess. However, most research into the temporal aspects of decision making has focused on choices about information that is constant over time. While the use of such "static" scenarios provided valuable insights on how choices are made in the brain, they miss important aspects of situations encountered in ecological settings and are not well suited to disambiguate key components of decision-making. In the present study, we investigate brain wide electrophysiological correlates of "dynamic" choices in humans. We recorded brain signals of participants with MEG while they performed a forced-choice paradigm in which sensory information about the likelihood of the correct choice evolves over time within each trial, and subjects have the freedom to commit at any time, emphasizing either speed or accuracy. We then used a dimensionality reduction technique (PCA, Principal Component Analysis) to reveal and characterize the spatial, temporal, and spectral components of neural activity underlying the key processes contributing to decision-making. We show that alpha (9-13 Hz) and beta (16-24 Hz) principal components (PCs) are involved in ***tracking sensory information while participants were deliberating between two options*** in the sensorimotor, visual, and posterior cingulate cortex. We also highlight the role of alpha PCs in ***committing*** to a particular choice, while beta PCs were associated with ***motor execution*** once the decision was made. Finally, high frequency PCs (> 16 Hz) in subcortical areas including the cerebellum, pallidum, caudate nucleus and the thalamus indexed the implementation and adjustments of ***speed accuracy tradeoff policies*** when participants try to optimize successes per unit time.

## 4.2 Introduction

In our daily lives we make a wide variety of decisions. Some are abstract and long-term, such as choosing a career, and some are more mundane, such as whether to turn right or left at an intersection. In most cases there are risks, costs, and benefits to selecting a given course of action, and a rich body of work exists on how humans and other animals weigh these factors in making and committing to their choice. In particular, recent studies using functional MRI, electro-encephalography (EEG), and magnetoencephalography (MEG) have yielded important insights into the neural mechanisms of decision-making in humans[1–13]. For example, EEG and MEG studies have reported choice-predictive neuronal oscillations in motor, premotor and early visual cortex, thought to reflect accumulated sensory evidence[8–10,12,13]. While low frequency oscillations are thought to reflect global processing and feedforward information flow through the cortical hierarchy, high frequencies have been associated with local processing and feedback cortical pathways[19–26]. Beta oscillations (13-30 Hz) in particular are thought to play a crucial role in motor control and have been important for understanding the neural mechanisms underlying decisions between competing actions[27,28].

While these studies are building a strong foundation for our understanding of the neural bases of decisions, many questions remain unanswered. Prominent among these is the question of how the brain makes the transition from deliberating about the pros and cons of given options to committing to, and executing, a single choice. One potential answer comes from the well known “drift-diffusion model” (DDM), which suggests that commitment occurs when sensory (or value-based) evidence for one choice over the others is accumulated to some threshold level that controls the speed-accuracy trade-off[14,15], and at that point a response is chosen that is subsequently transformed into an action plan and executed. Consistent with this proposal, neural activity in many cortical and subcortical regions builds-up at a rate that is related to the evidence[16,17]. However, in most tasks studied to date, the evidence in favor of each given choice is constant over the course of a trial such that evidence accumulation reflects essentially the speed of perceptual processing/integration. An example is the widely used random dot motion discrimination task[18], in which subjects make a decision about the direction of coherent motion in a field of randomly moving dots. However, in conditions where motion coherence is stable across a given trial, it is notoriously difficult to distinguish neural activity build-up

that is due to evidence accumulation from build-up related to motor preparation, reward anticipation, the urge to make a choice, or simply the passage of time[29–34].

One approach for distinguishing processes related to the deliberation from other processes like motor preparation is to use "dynamic decision-making tasks". In such paradigms, sensory information in favor of competing responses varies over time within each trial. This makes it possible to isolate neural activity that follows the changing evidence from neural activity that is related to other processes, such as the preparation of a response after the choice is made. Such studies have suggested that the computation of sensory evidence is in fact quite fast, on the order of 200ms or so[35–37], and that most of the build-up of neural activity may be caused by a rising "urgency signal" that pushes the system to commit to a choice even if the evidence is weak[29,30,38]. This mechanism, sometimes referred to as "collapsing bounds", has been suggested as an effective policy for maximizing reward rates [39–43]. These effects question some of the assumptions of the DDM and call for a more refined account of distinctive processes contributing to decision making. One variation, called the "urgency gating model" (UGM)[30,33,39], suggests that evidence is computed quickly (emphasizing novel information), and combined with a context-dependent urgency signal that that dynamically adjusts the threshold for initiating movement. While this model produces behavioral and neural predictions that are nearly indistinguishable from the DDM in tasks with constant evidence[30,33], such as random dot motion discrimination, it makes very different predictions in tasks in which evidence is changing dynamically. In those conditions, results from numerous studies are better explained by the UGM than the DDM, at both a behavioral and neural level [5,10,30,33,38,39,44–46,37]. Furthermore, a series of electrophysiological studies in monkeys suggests that fast estimates of sensory evidence are computed in the prefrontal cortex[47], combined with an urgency signal from the basal ganglia[44], and then used to bias a competition evolving within the dorsal premotor and primary motor cortex[38,47]. The urgency signal is adjusted based on context[32,48] , including prior trial history[49], but always involves rising activity that drives the animal to eventually make a choice even if the evidence is ambiguous. In situations that require fast decisions, the urgency signal will be stronger and can be operationalized as shorter response time and increased error rates, consistent with classical speed-accuracy trade-off principles. While these findings have illuminated the mechanistic basis of decisions in a variety of conditions in non-human primates, it is not clear to what extent they may be specific to highly over-

trained monkeys[50]. Furthermore, local recordings do not inform about the large-scale distribution of these computations. In the present study, we address these outstanding issues by recording whole brain MEG activity of human subjects while they perform a dynamic decision-making task. We combine a dimensionality reduction technique (PCA, Principal Component Analysis) and machine learning to identify spectral, spatial, and temporal features of neuronal activity specifically related to (i) tracking sensory evidence during deliberation, (ii) committing to a particular choice, (iii) motor preparation and execution and (iv) control over speed-accuracy.

## 4.3 Results

In the tokens task, participants (N=28) pressed a button with their right or left index fingers based on their guess about which of two peripheral targets would receive the majority of 15 tokens jumping from a central circle to one of the two targets every 200 ms (Figure 1A). Participants were free to decide at any time and asked to get as many correct guesses as possible, motivating them to optimize successes per unit time. After a target was chosen, the remaining tokens accelerated, jumping every 150 ms in "slow" blocks or every 50 ms in "fast" blocks (Figure 1B). The design of the task thus presented a speed versus accuracy trade-off (SAT): subjects could choose to wait until all tokens have jumped (i.e., conservative decisions), or to take a guess before all tokens have jumped (i.e., hasty decisions) and save time, with the risk of having made the wrong choice. Each subject completed eight blocks, alternating between fast blocks which encourage hasty decisions (more time is saved by guessing quickly), and slow blocks which encourage more conservative decisions. Although subjects were told that each token jump was completely random, we interspersed among them three specific categories of trials characterized on the basis of the temporal pattern of jumps: Easy, ambiguous, and misleading trials (see Figure 1C). At the end of each trial, feedback indicating correct or incorrect choices was presented to subjects (Figure 1A, red or green circles). Before and after the tokens task, subjects performed a two-choice visuo-motor reaction-time task (two 2-minute blocks), in which the 15 tokens originally arranged in the center circle all simultaneously jumped ("GO signal) into one of the two peripheral targets (left or right) after a variable delay. The mean reaction time obtained during the visuo-motor reaction-time task was taken as an estimate of processing delays not related to decision-making and used to estimate decision time for each trial of the tokens task (*Button*

*Press Time – mean Reaction Time = Decision Time*, see Figure 1B). This experimental design allowed us to identify whole-brain dynamics involved in different aspects of decision-making, including the process of deliberation, the moment of commitment, and the adjustment of speed versus accuracy trade-offs.

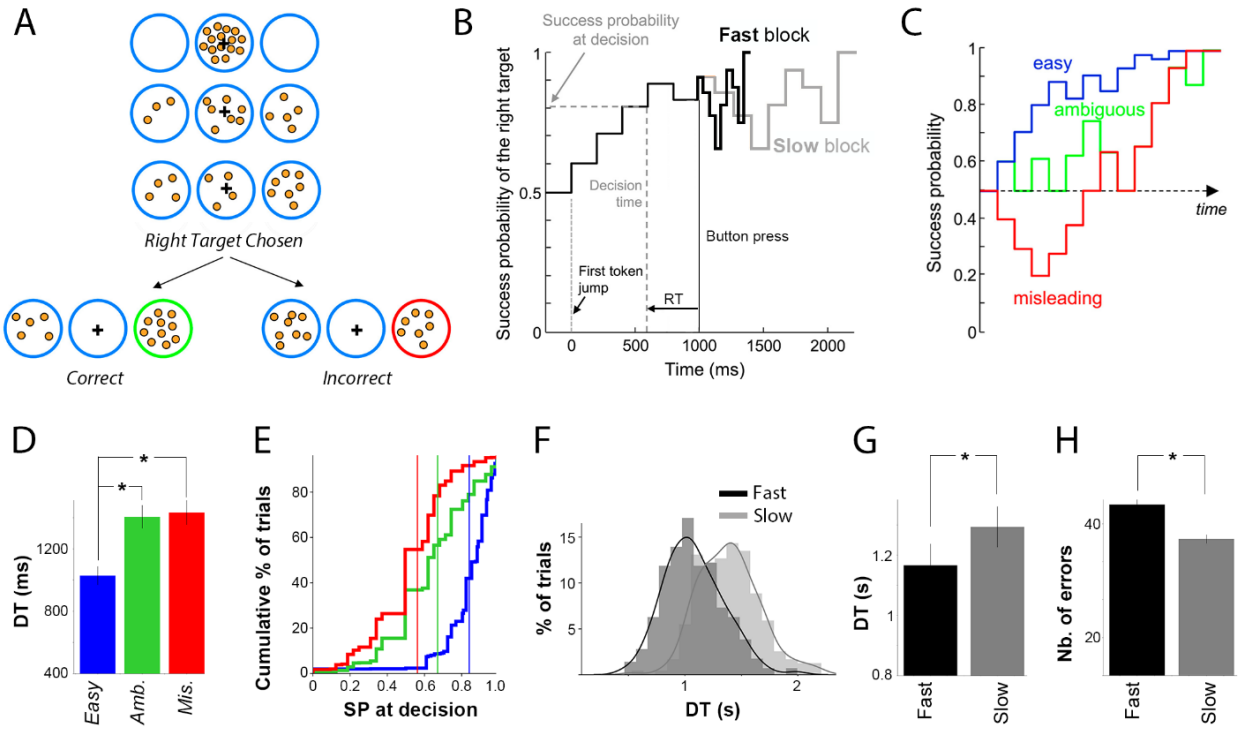


**Figure 1. Task and behavior. A.** The tokens task. Each row illustrates steps in an example trial, in which the right target is chosen. Two example outcomes are then illustrated, one in which the remaining tokens keep jumping to the right target (easy trial, correct choice), and one in which the remaining tokens jump to the left target (misleading trial, incorrect choice). **B.** Success probability (SP) profile of an example trial, in which the right target was chosen. Black trace indicates SP before the target is chosen, while tokens jump every 200 ms. After the target is chosen (button press, vertical black full line), the remaining tokens jump either every 150 ms (in slow blocks, grey trace) or every 50 ms (fast block, black trace). To yield an estimate of the decision time (DT, vertical gray dashed line), and the success probability at which the participant committed to his choice (horizontal gray dashed line), we subtract the mean RT calculated using a two-choice visuo-motor reaction-time task from button press time (horizontal black arrow). **C.** Example success probability profiles of "easy" (blue), "ambiguous" (green), or "misleading" (red) trials (see criteria in Methods). **D.** Mean decision time across subjects (N=28) in easy trials was significantly shorter than in ambiguous and misleading trials. **E.** Cumulative distributions of success probabilities at decision time for easy (blue), ambiguous (green) and misleading (red) trials for all subjects. Vertical lines indicate mean success probability. **F.** Distributions of the decision times of a representative subject for fast (black), and slow (grey) blocks. **G.** The mean decision time across participants (N=28) in fast blocks was significantly shorter than in slow blocks. **H.** Participants made significantly more errors in fast blocks compared to slow blocks.

**Behavioural analysis**

Decision time and success probability at the time of choice depended upon the sensory evidence provided by the distribution of tokens. Subjects made their decision significantly faster during easy trials (mean DT = 1028 ± 59 ms) than during both ambiguous (mean = 1405 ± 74 ms, Paired student t-test, easy *vs* ambiguous*, T value = -15.04; p = 1.19 e-14*) and misleading trials (mean = 1433 ± 79 ms, Paired student t-test, easy *vs* misleading, *T value = -13.1; p = 3.25 e-13*, Figure 1D), and their success probability at decision time was significantly higher in easy trials (Figure 1E). However, no significant differences were found between DT in ambiguous and misleading trials (Paired student t-test, ambiguous *vs* misleading*, T value = -1,84; p = 0.077).* Subjects also behaved more hastily and made their decision earlier in the fast blocks (mean DT = 1166 ± 71 ms) compared to slow blocks (mean = 1293 ± 68 ms, Paired student t-test, *T value = -6,08; p = 1.71 e-6)*, during which they were more conservative. Moreover, participants made significantly more mistakes in fast blocks (mean = 45.1 ± 9.9 errors) compared to slow blocks (mean = 36 ± 6 errors; Paired student t-test, errors in fast *vs* slow blocks, *T value = 6.1; p = 1.7 e-6*), consistent with a trade-off between speed and accuracy. The distribution of DTs in fast and slow blocks for one subject, mean DTs and mean errors across subjects are shown in Figure 1F, G, H. Note that the present behavioral results replicate previous observations in both humans[30] and rhesus monkeys[51].

**State space analysis of neuronal oscillations**

To study how modulations of neural activity dynamically reflect variables relevant to the performance of the tokens task we computed single-trial time-resolved spectral power envelopes in five frequency bands: theta (θ) [5–8 Hz], alpha (α) [9–13 Hz], beta (β) [16–24 Hz], gamma (γ) [30–60 Hz] and high gamma (high γ) [60–90 Hz] in the source space. The width of frequency bands was chosen based on results obtained with the FOOOF toolbox[52], allowing to detect oscillations (peaks) in the frequency domain by separating the periodic and aperiodic components of neural power spectra (see Supplementary Figure S1 and Material and Methods). We then focussed our analyses of brain oscillations in a specific low-dimensional subspace that captures across-trial variance which arises from subjects' choice (left or right choices), trial types (easy, ambiguous, or misleading trials), and

block-dependent SAT policies (fast or slow blocks), similar to analyses of neural spiking activity in monkeys[47]. We computed this task-related subspace using principal component analysis (PCA, see Supplementary Figure S2 for an illustration). This yielded an unbiased estimate of the most prominent features (that is, patterns of neural activity) in whole brain sources across all subjects for each frequency band. We restricted subsequent analyses to the subspace spanned by the first 20 principal components (PCs), though our conclusions are mostly based on the top 4. Compared to more standard power analyses, the PCs generated can be thought of as the 'building blocks' of the observed neural activity, in that the activity of any specific source is a linear combination (weighted average) of these components across the twelve groups of trials (slow/fast blocks x left/right choices x easy/ambiguous/misleading) used for the PCA. For example, Supplementary Figure S3 shows the comparison between power envelopes and PCs generated for the same frequency band (beta) and the same ROI (sensorimotor cortex). Note that a conventional power analysis would find the well-known beta suppression and rebound, which is captured by PC1, but it would not reveal additional features such as choice dependence, captured by PC2. Furthermore, by applying the analysis simultaneously across all brain sites, we do not need to pre-define ROIs but can let the data reveal the regions that contribute most to these distinct components of oscillatory power, as will be shown below.

The first four PCs for theta, alpha, beta, and gamma oscillations explained most of the variance in activity over time (explaining 83.5%, 86.5%, 94%, and 76.7% respectively), and Figure 2 shows their temporal profiles after aligning the data to button presses (see Supplementary Figure S4 for the first 8 PCs and Supplementary Figure S5 for the same PCs aligned on the first token jump for each frequency band, including high gamma). Then, we used a Linear Discriminant Analysis (LDA) classifier to probe the ability of these spectral features to significantly decode the three task-related conditions of choice, trial class, and SAT policy in a data-driven manner. The statistical significance of time-resolved decoding accuracy was determined using permutation tests, corrected for multiple comparisons across subjects and time ($p < 0.05$, corrected across time, see Methods section).

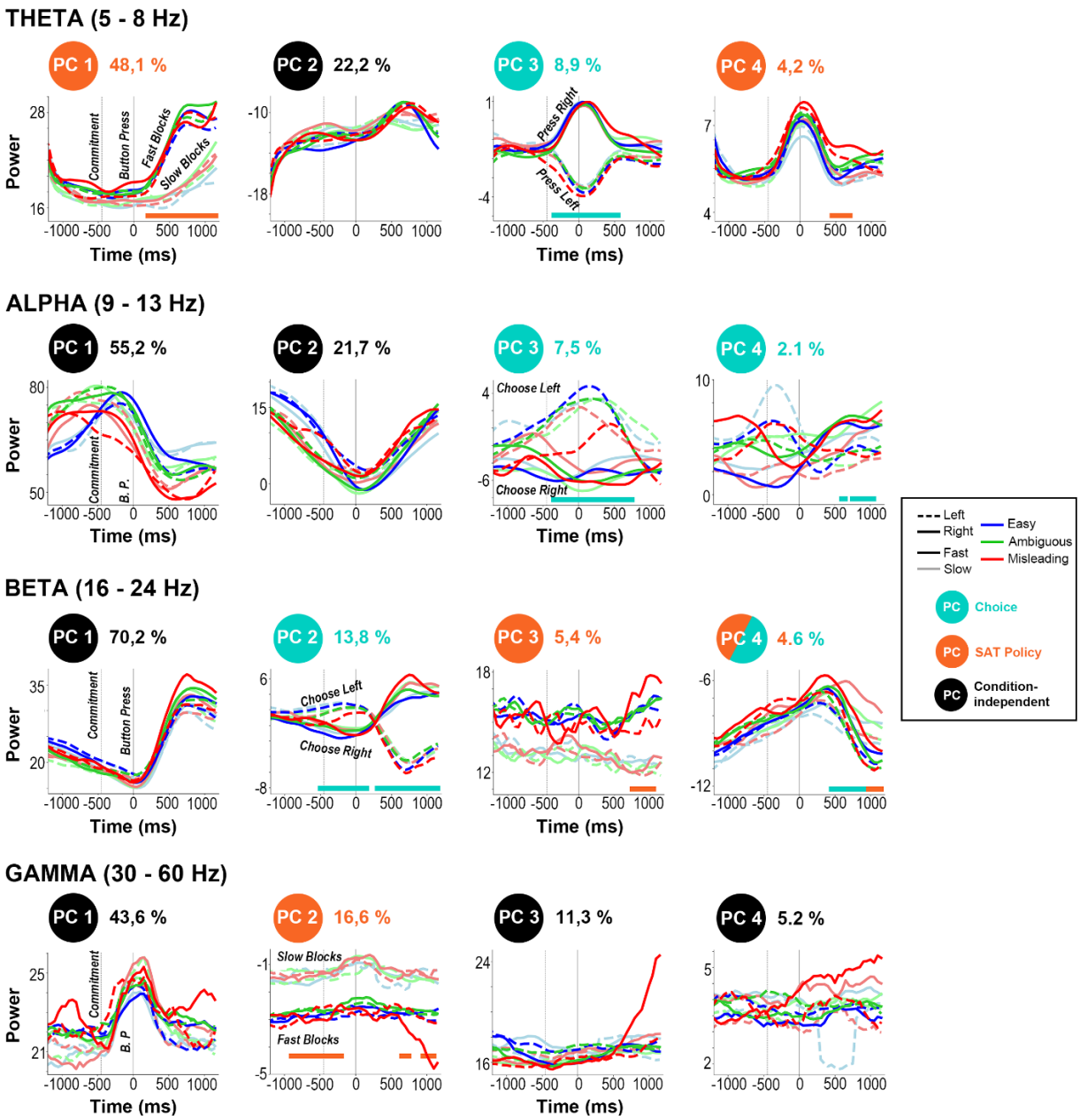


**Figure 2. First four PC components computed in theta (4 – 8 Hz), alpha (9 – 13 Hz), beta (16 – 24 Hz) and gamma (30 – 60 Hz) frequency bands** for easy (blue), ambiguous (green) and misleading (red) trials during fast (bright) and slow (dim) blocks, and for left (dashed) and right (solid) choices on data timelocked to button press (from -1250 to +1200 ms). In each panel, the second vertical dotted line indicates button press, and the first indicates the estimated moment of commitment (i.e., Decision Time, estimated as Button Press Time minus the mean Reaction Time across subjects in the Delayed Response task), 448ms earlier. Percentages next to PCs indicate the amount of variance explained, and PC circular labels are color-coded based on their ability to significantly decode between task-related conditions using an LDA classifier: choice made (left vs. right, turquoise), SAT policy (fast vs. slow block, orange), and condition-independent (black). Colored horizontal lines mark time intervals with significant effects.

**Alpha and beta patterns of neural activity track sensory evidence during deliberation**

First, we sought to identify principal components of neural activity involved in tracking sensory evidence over the course of deliberation. Out of the top 20 PCs computed for each frequency band of interest, we found that time courses (locked on button press) of Alpha PC3 (7.5% of explained variance) and Beta PC2 (13.8% of explained variance) were significantly correlated with the temporal profiles of success probabilities (see Methods) associated with easy (blue), ambiguous (green), and misleading (red) trials for right (solid) and left (dashed) choices (Alpha PC 3: $p < 0.05$ *for 5/6 profiles*, mean R = 0.78, std = 0.3 & Beta PC 2: $p < 0.05$ *for 5/6 profiles*, mean R = 0.83, std = 0.2, see Figure 3B and Supplementary Figure S8). As shown in Figure 3, in easy trials, strong sensory evidence (i.e., high success probability) is reflected by a quick increase in alpha PC3 and beta PC2 activity towards the subjects' ultimate choice (up for left choices, down for right choices). In ambiguous trials, these PCs fluctuate and then slowly increase towards the chosen target. In misleading trials, they initially ramp up towards the opposite target before they switch, around the same time in both frequency bands, to predict the correct target choice. Results from LDA classification between right and left choices also show that alpha PC3 and beta PC2 profiles could significantly predict the participant's choice from 350ms and from 500ms before the button press, respectively (left vs right, $p < 0.05$, *corrected across time*). Both PCs were thus identified as "choice components" (turquoise color code, Figure 3C, E).

To investigate which brain areas contributed most to these PCs, we projected the loading coefficients (i.e., weights computed in the PCA analysis) involved in generating those PCs onto 3D MNI brains in the MEG source space (see Figure 3D, F). We then used the HCPMMP1 atlas[53] to automatically assign sources to brain regions of interest (ROIs) and highlight similarities and differences between brain regions generating the two PCs tracking the state of sensory information to inform action choices. We show a clear lateralization of the top 5% of loading coefficients across all sources (referred to as "Leading Loading Coefficients, LLCs", see Methods as well as Supplementary Figures S6 and S7 to see Leading Coefficients and LLCs for the top 4 components of each frequency band, respectively) involved in generating both alpha PC3 (1073/8096 sources) and beta PC2 (860/8096 sources). Moreover, we found that beta PC2 was mostly generated by somatosensory and motor areas including Brodmann area 2, 3b, 4 and the anterior intraparietal area (AIP, see Supplementary Table S2), as well as premotor and superior parietal areas. On the other hand, alpha

PC3 was mostly generated by the posterior cingulate cortex, somatosensory and motor areas, but also included primary and early visual cortices (see Supplementary Table S1).

Of note, theta PC 3 was also identified as a choice-related component (see Figure 2) but it showed no significant correlations with success probabilities during the period of deliberation (mean R = -0.01, std = 0.8, *p>0.05 for 6/6 profiles*). Instead, theta PC3 peaked around the time of the button press, and the spatial distribution of its LLCs was found in the somatosensory, motor (35 % of LLCs, see Supplementary Table S1) and premotor (16%) cortex, advocating for their strong involvement in motor execution (button presses) once a decision had been made.

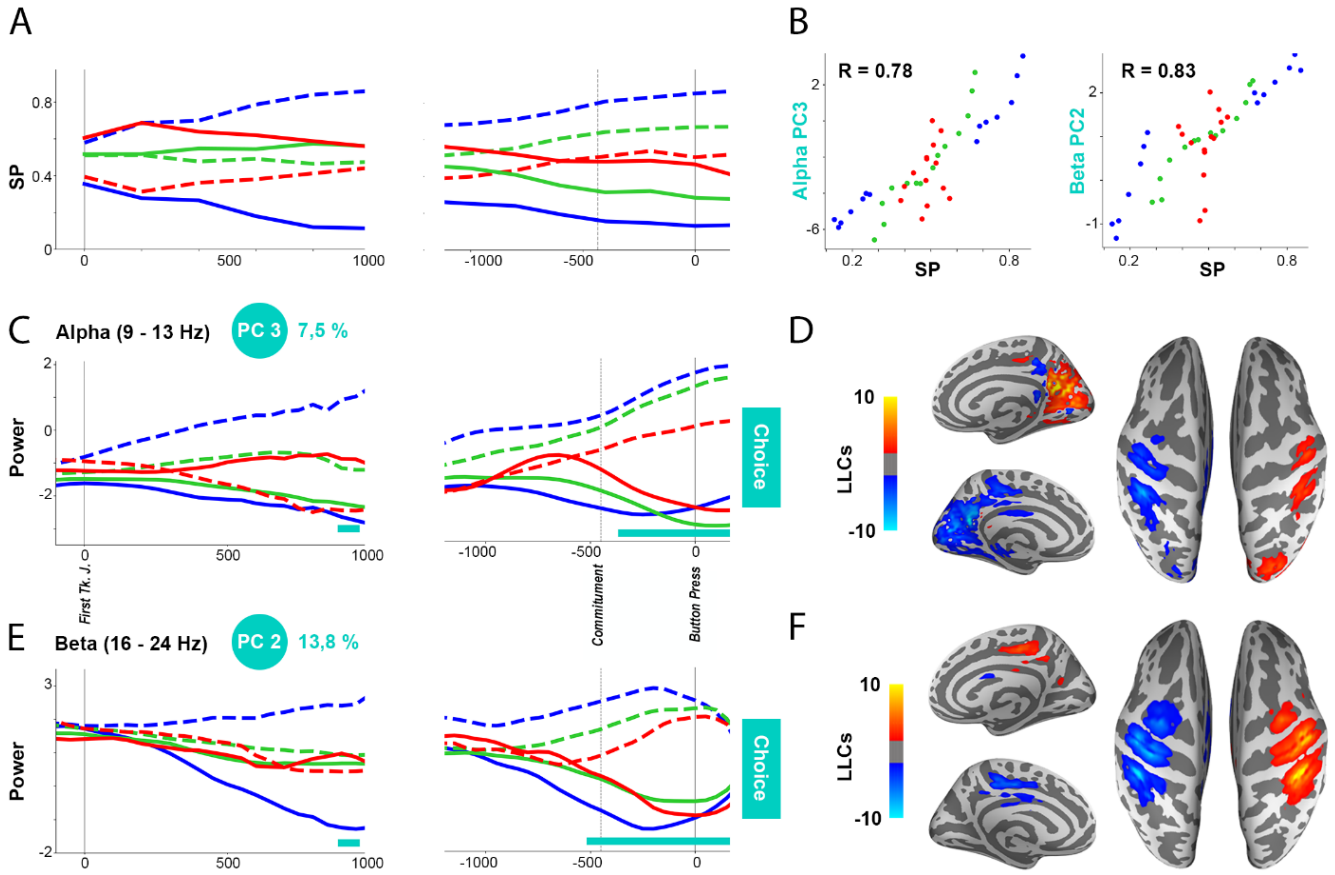


**Figure 3. Neural activity tracking sensory evidence during deliberation. A.** Mean success probability (SP) profiles across subjects and trial types (easy, ambiguous, and misleading trials), for left (dashed lines) and right choices (solid lines) locked on first token jump (first column) and button press (second column), computed every 200 ms. **B.** Scatter plots of mean SP versus mean alpha PC3 (left panel) and beta PC2 (right panel) locked on button press in easy (blue), ambiguous (green), and misleading (red) trials, for left and right choices, for each 200ms time bin. The correlation coefficient is R=0.78 (alpha PC3) and R=0.83 (beta PC2), p-values were below 0.05 for 5/6 profiles (see Supplementary Figure S8 for more details). **C.** Principal component Alpha PC3 locked on first token jump and button press during easy, ambiguous, and misleading trials for left (dashed lines) and right choices (solid lines). Horizontal lines mark time intervals with significant effects of choice (turquoise, left vs right), assessed by a Linear Discriminant Analysis (LDA) algorithm (using permutations corrected with maximum statistics at $p < 0.05$). **D.** Leading loading coefficients projected on 3D inflated MNI brains for alpha PC3. **E, F**. Same as **C** and **D**, for beta PC2.

**The role of alpha and beta neural trajectories in commitment and button press**

To help us further understand the functional role of alpha and beta PCs during dynamic decision-making, we plotted 3D trajectories of the evidence-related components alpha PC3 and beta PC2 against the top two components of each band (Figures 4 and 5), excluding SAT policy components (beta PC3). These were plotted for the different trial types (easy, ambiguous, and misleading) for left and right choices, and averaged across fast and slow blocks (to see trajectories for fast blocks and slow blocks independently, see Supplementary Figure S9). Figure 4A shows two views of the alpha band trajectories (see animated alpha trajectories in Supplementary Video S1), with the individual PCs shown in Figure 4B, and their respective leading loading coefficients (LLCs) in Figure 4C. We found that the first alpha PC was condition-independent and increased until it reached a peak before movement execution (button press), and its LLCs were located in the posterior cingulate cortex and the primary visual area V1 (63 % and 14% of LLCs, see Supplementary Table S1). Alpha PC2 showed a condition independent decrease in activity until button press and was mostly generated by somatomotor (areas 2, 3 and 4, 32% of LLCs) and posterior cingulate cortex (21 % of LLCs, see Supplementary Table S1). Finally, as noted above alpha PC3 tracked sensory evidence and was generated from the posterior cingulate cortex, somatosensory and motor areas, primary and early visual cortices, and the dorsal visual stream. We then showed that during the deliberation period, trajectories projected in a 3D neural state space track sensory evidence (success probabilities of easy, ambiguous and misleading trials, see previous paragraph), and unfold in what we call the "deliberation subspace"[47] (PC2/PC3), from bottom to top as time elapses and from left to right based on sensory evidence along alpha (Figure 4A, left panel). Importantly, we found that the moment of commitment (colored circles) corresponds to a sharp bend in alpha neural trajectories, after which they rapidly leave the deliberation subspace and move onto the PC1/PC2 subspace in which they evolve in a clockwise manner (arrows in Figure 4A, right panel). Notably, alpha neural trajectories do not bend at the time of button press (colored triangles in left panel) and are not sensitive to movement execution per se, since they only turn back towards the starting point > 500 ms after movement execution was completed (Figure 4A, right panel).

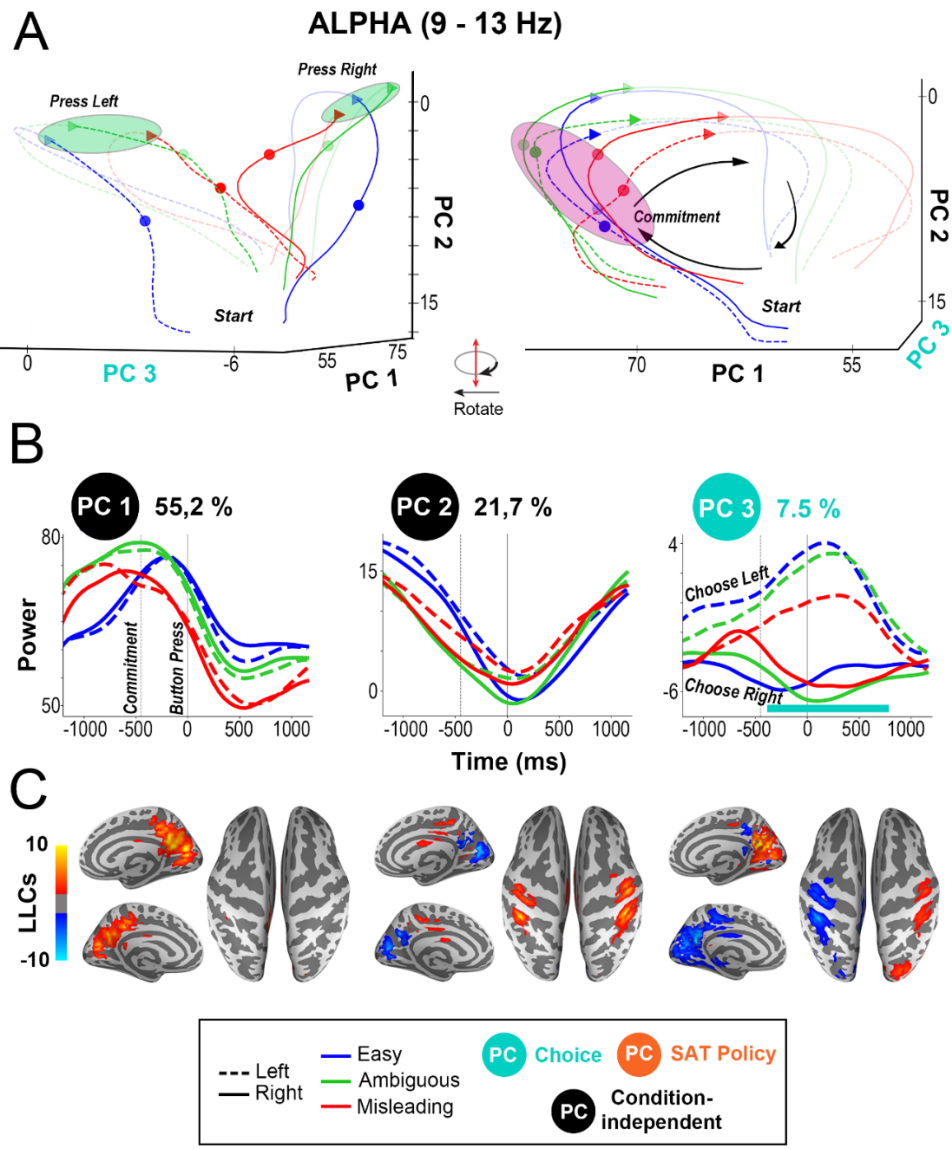


**Figure 4. Neural trajectories of alpha PCs in neural state space. A.** Neural trajectories of alpha PCs 1, 2 and 3 locked on button press [-1200 to 1200 ms], for left or right choices in easy, ambiguous, and misleading trials, averaged across fast and slow blocks. The right panel shows a 90 degrees rotation of the left panel. Small colored circles indicate the region in which commitment occurs, and small colored triangles indicate the time of button press for each individual trial types. Black arrows indicate how neural trajectories unfold over time. Purple ellipses indicate the region in which commitment occurs (indicated for individual trial types by small colored circles) and green ellipses indicate the time of button press (indicated for individual trial types by small colored triangles). **B.** Principal components Alpha PC1, 2 and 3 locked on button press during easy (blue), ambiguous (green) and misleading (red) trials for left (solid lines) and right choices (dashed lines). Horizontal lines mark time intervals with significant effects of choice (turquoise, left vs right) and SAT policy (orange, fast vs slow blocks), assessed by a Linear Discriminant Analysis (LDA) algorithm (using permutations corrected with maximum statistics at $p < 0.05$). **C.** Leading loading coefficients projected on 3D inflated MNI brains for PC1, 2 and 3 in the alpha band.

In contrast with the neural trajectories of alpha PCs, which bend around the time of commitment, the neural trajectories of beta PCs only bend at the time of button press, regardless of the task condition (see animated beta trajectories in Supplementary Video S2),. After button press, beta neural trajectories cross and separate between right and left choices, before turning back in the direction of the starting point (Figure 5A). We found that beta PC1 activity was condition independent and exhibited a gradual decrease before button press, reaching a (negative) maximum around button press onset. After button press, beta PC1 activity transiently increased (i.e., "rebounded") and peaked around 600 ms (see Figure 5B, left panel). Figure 5C shows that beta PC1 LLCs were mostly located in somatosensory motor regions (areas 2, 3a, 3b and 4, 42%, see Supplementary Table S1 and S2) and in the anterior part of the posterior cingulate cortex (areas 23c and 23d, 13%). Importantly, the beta PC1 temporal profile and LLCs are consistent with the extensive literature describing the typical patterns of beta oscillations before (i.e., gradual decrease), during (negative peak) and after (beta "rebound) voluntary movements[54]. Beta PC2 was found to significantly discriminate both left vs right decisions (i.e., choice component, $p < 0.05$, *corrected across time*), and was mostly generated by somatosensory and motor areas including Brodmann area 2, 3b, 4 and the anterior intraparietal area, as well as premotor and superior parietal areas. Finally, beta PC4 discriminated both left vs right choices and fast vs slow blocks, but only after the button press. Beta PC4 LLCs mostly originated from the posterior cingulate cortex (21% of LLCs), but also included somatosensory motor (11 %), subcortical regions (10%) and the inferior and superior parietal cortex (10% and 8%, see Supplementary Table S1).

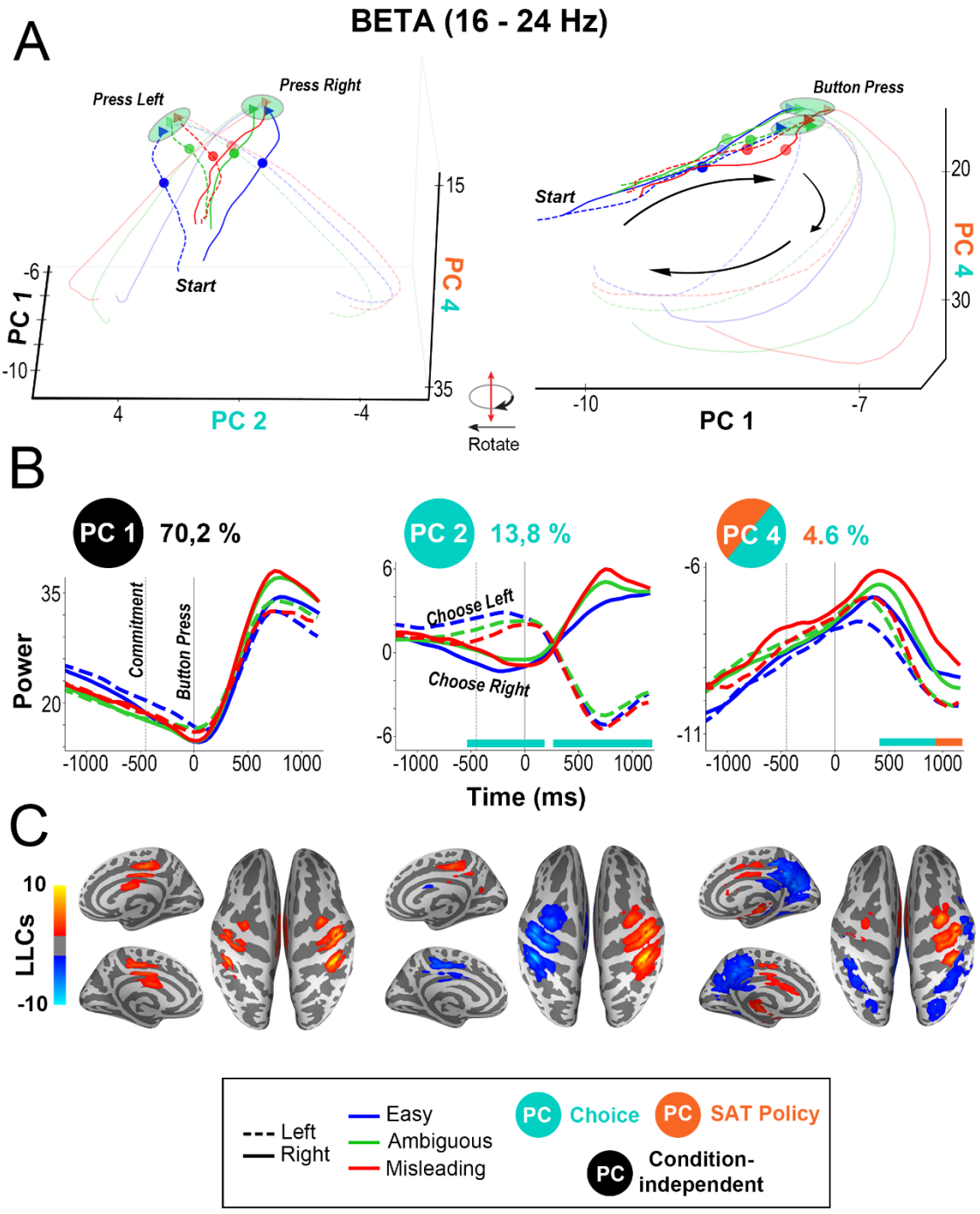


**Figure 5. Neural trajectories of beta PCs in neural state space.** Same as Figure 4, but for beta PCs 1, 2 and 4.

**Effect of speed-accuracy trade-off policy on subcortical brain structures**

Lastly, we looked for components that reflected adjustments in the subject's speed-accuracy trade-off policy. To do so, we used an LDA classifier to identify PCs that significantly discriminated fast and slow blocks for each frequency band. This procedure showed that theta-PC1, beta-PC3, and gamma-PC2 were identified as "SAT policy" components (fast vs slow, $p < 0.05$, corrected across time, see Figure 6). Beta PC3 and gamma PC2 displayed similar temporal profiles and reflected a shift in power distinguishing between the slow and fast blocks (even before the start of the trial, as shown in Supplementary Figure 3). Based on our LLCs analysis, we found that beta PC3 and gamma PC2 mostly originated from subcortical regions (see Figure 6 and Supplementary Table S1). On the other hand, theta PC1 only discriminated fast and slow blocks after button press onset, and their LLCs were located in subcortical brain structures (38.7 % of LLCs, see Supplementary Table S1), but also in the anterior cingulate cortex (15.7%) and in the orbitofrontal cortex (15.4%). To further understand the neural underpinnings of SAT policies in humans, we computed the source reconstructed MEG activity locked on the first token jump in the volume space of the following subcortical regions using the Freesurfer Aseg atlas[55]: caudate nucleus, putamen, globus pallidus, amygdala, cerebellum, and thalamus. We performed a PCA analysis independently for each region and in theta, alpha, beta, gamma, and high gamma frequency bands. Using an LDA classifier, we found that significant "SAT policy" principal components were only found in higher frequencies (beta, gamma and high gamma frequency bands), and originated from the cerebellum, globus pallidus, caudate nucleus and amygdala (see Figure 6D).

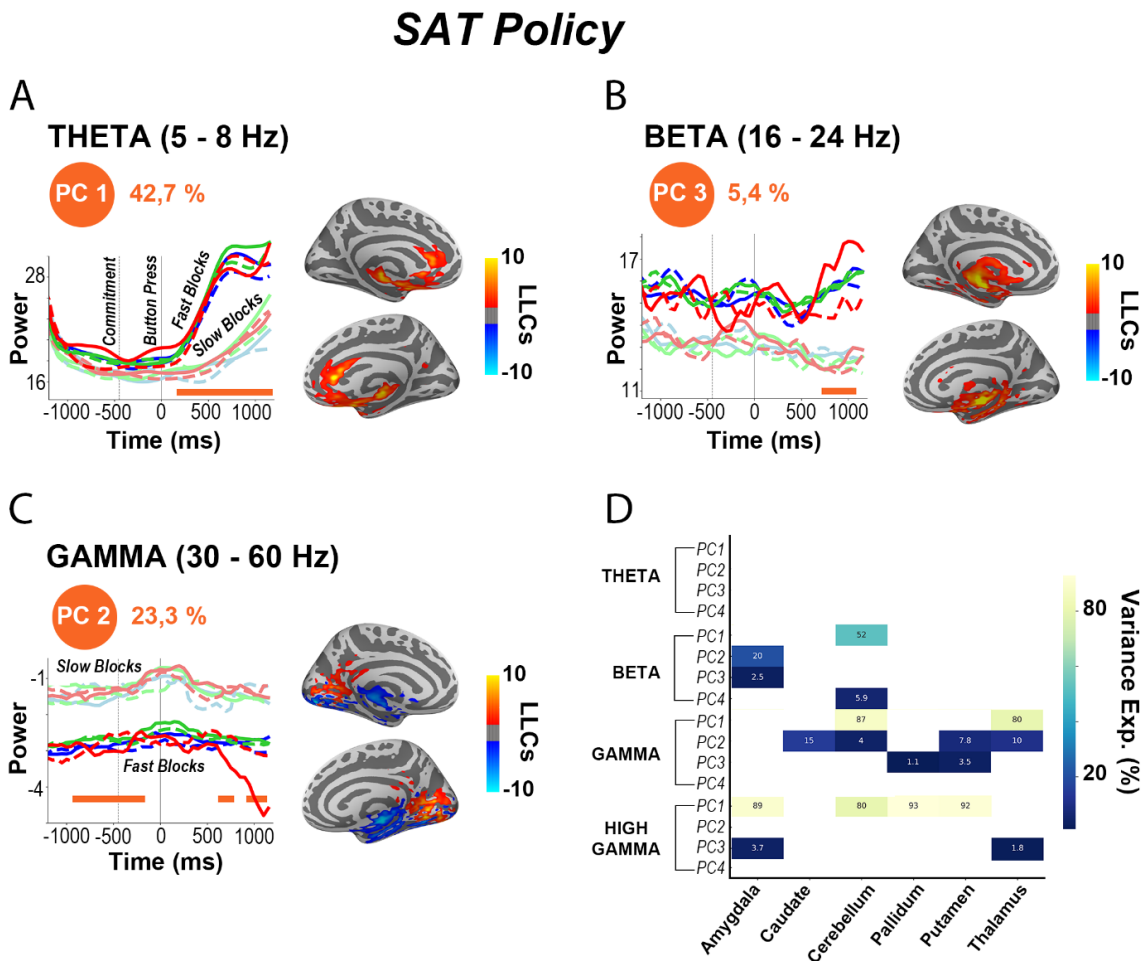


**Figure 6.** Leading Loading Coefficients (LLCs) projected on 3D inflated MNI brains and their associated neural trajectories locked on button press for the SAT-related principal components: (**A**) Theta PC1, (**B**) Beta PC3 and (**C**) Gamma PC2. Horizontal lines mark time intervals with significant effects of SAT policy (orange, fast vs slow blocks), assessed by a Linear Discriminant Analysis (LDA) algorithm (using permutations corrected with maximum statistics at $p < 0.05$). **D.** Heatmap representing significant (fast vs slow blocks, $p < 0.05$) SAT policy components for theta, beta, gamma and high gamma frequency bands per region based on the PCA analysis computed on data locked on the first token jump. The PCA analysis was computed independently for each of the following subcortical regions: Amygdala, Caudate, Cerebellum, Pallidum, Putamen and Thalamus for the first 4 PCs. Colors represent the percentage of variance explained for significant components.

## 4.4 Discussion

Decisions about actions are arguably the most fundamental kinds of decisions that animals, including humans, face in the natural world. For such decisions, choices are conditioned at least in part by the evidence available in the immediate environment but ongoing changes in the sensory landscape is rather the norm than the exception. However, most decision-making studies have used experimental paradigms in which the informational content of stimuli remains constant over the course of each trial[18,43]. The present paper provides the first report of neural correlates underlying dynamic decision-making in the human brain using whole brain MEG recordings. Using a dimensionality reduction technique allowed to clearly dissociate and characterize the temporal, spatial and spectral features of neural activity associated with key components of decision-making. In particular, tracking sensory evidence during deliberation was reflected by PCs in alpha and beta bands in the sensorimotor, visual, and posterior cingulate cortex. While alpha PCs activity in visual areas and PCC was associated with commitment to a particular choice, the beta PCs in sensorimotor areas indexed motor execution (i.e., button press). Lastly, we showed the involvement of high frequency PCs (> 16 Hz) generated from subcortical areas (cerebellum, pallidum, caudate nucleus and the thalamus) in speed accuracy tradeoff policies. In this discussion, results will be (1) interpreted in the context of the urgency-gating model and its neural underpinnings in non-human primates[38,44,47,48] and (2) compared to neurophysiological studies of action decision in humans[1–13].

***Tracking sensory evidence***

First, we showed that principal components (PCs) of activity in the alpha and beta frequency bands were highly correlated with the temporal profile of success probabilities given by the distribution of tokens having jumped in the right and left targets. These "sensory evidence PCs" originated from primary and early visual brain regions, the posterior cingulate cortex, and sensorimotor areas. These results converge with recent human studies using classical decision-making tasks with constant evidence to show that alpha and beta oscillations in visual[9] and sensorimotor regions[8,56,57] are crucial for processing sensory evidence. Results are also consistent with accounts suggesting that the PCC could be involved in estimating the need to change behavior in light of new

external requirements[58], including fast perceptual decisions[59]. Importantly, our results also confirm findings about the involvement of parietal, motor, and premotor regions in coding sensory evidence, as reported in non-human primates performing both classical[16] and dynamic[38] decision-making tasks. In particular, our results are consistent with studies that used direct single-unit recordings in non-human primates performing the tokens task, which showed the involvement of primary motor (M1) and premotor (PMd) areas in tracking sensory evidence during deliberation and in reaching commitment[38]. However, results did not provide evidence for a role of dlPFC in tracking the state of information given by the tokens' distribution[47]. As the dlPFC averages across cells with different preferences for right and left responses with no bias for contralateral responses, the lack of results might be due to the fact.

***Alpha oscillations reflect commitment while beta oscillations reflect motor execution***

Next, we showed that key decision-making events, namely commitment and motor execution, are reflected by frequency-specific brain activity. We found that the trajectories of alpha PCs in the neural state space "bent" before movement execution and close to the moment of commitment, indicating a role in resolving the competition and committing to a particular choice. This change of trajectories mostly came from alpha PC1, which showed increasing activity until reaching a peak before button press and was mostly generated in posterior regions such as visual cortex and the PCC. These results can be interpreted in the context of literature on the role of alpha oscillations in providing pulsed inhibition, reducing the processing capabilities of given brain areas[60]. In our study, the increased alpha activity in posterior regions could reflect the active and gradual suppression of sensory evidence processing. One possible interpretation is that the peak of alpha activity corresponds to the time of commitment, sensory evidence regions are maximally suppressed to allow a transition of the neural state toward movement preparation and execution.

In contrast, beta PCs did not show a notable change in trajectories at commitment time but instead exhibited a clear change at the button press. These were primarily generated and located in the sensorimotor cortex, suggesting a role in movement preparation and execution. This is consistent with the well-established link between beta frequencies and movement-related processing in the sensorimotor cortex[54]. In particular, the time course of beta PC1 was remarkably similar to the typical

decrease in amplitude until movement onset, followed by the increase at cessation of movements, commonly referred to as the "beta rebound"[8]. One hypothesis about the functional role of the beta rebound is that the post-movement period may be used by the sensorimotor cortex to recalibrate or reset the motor system to new conditions, in order to prepare for a subsequent movement[61]. Our findings support this view, as beta PCs in the neural state space clearly show changes of trajectories happening at the time of the beta rebound, redirecting neural activity towards its baseline level, at the start of a trial.

***High frequency activity in subcortical regions reflect adjustments of SAT policies***

Finally, we found that high frequency (beta, gamma, and high gamma) PCs in subcortical structures reflect adjustment of speed-accuracy trade-off policies. More specifically, we found significant differences between our two block-dependent conditions, encouraging participants toward a more conservative (slow blocks) or risky (fast blocks) SAT policy to optimize their success rate. State-of-the art deep source reconstruction methods suggested that these effects originated in the cerebellum, pallidum, caudate nucleus, amygdala, and thalamus. These observations provide the first experimental evidence that bridges the gap between two streams of research: ***(1)*** studies in which an urgency signal was found in classical random dot motion discrimination tasks when varying the time pressure in humans[10] and monkeys[62], and ***(2)*** studies supporting the presence of a neural signature that reflects SAT policies in the basal ganglia of humans[7–10,63] and monkeys[33].

***General conclusion***

In conclusion, dimensionality reduction of oscillatory power revealed and characterized the neural signatures of key dynamic decision-making processes that allow humans and animals to interact with an environment that can (and does) change continuously over time. Importantly, the use of a dynamic decision-making task made it possible to dissociate activity related to evidence, urgency, and motor preparation, providing new insights consistent with the urgency gating model about the processing of evidence in visual and sensorimotor regions [8,9,16,38,56,57] (Figure 3), speed-accuracy adjustments involving subcortical areas[7–10,63,64] (Figure 6), and the process of commitment in motor and premotor cortex[16,30,38,40,45,46]. Our results also cast new light on the functional roles of alpha and

beta oscillations in different brain circuits and how they contribute to the commitment to a choice versus its execution (see Figures 4-5). Finally, it is important to note that many of the PCs obtained in our study were remarkably similar to those found when dimensionality reduction was applied to the single-unit data from monkey PMd, M1, dlPFC, and pallidum[36]. This supports the proposal that similar mechanisms are involved when decisions are made by highly trained monkeys versus untrained human subjects, and that the prospects are very promising for unifying the conclusions of single-unit studies in animals with whole-brain human magnetoencephalography.

**Acknowledgments**

KJ is supported by funding from the Canada Research Chairs program and a Discovery Grant (RGPIN-2015-04854) from the Natural Sciences and Engineering Research Council of Canada, a New Investigators Award from the Fonds de Recherche du Québec - Nature et Technologies (2018-NC-206005) and an IVADO- Apogée fundamental research project grant. TT was supported by IVADO Excellence Scholarship – PhD, and a scholarship from FRQS paid by PR in the context of the “Chercheur national – aide à la formation” program. PC received funding from NSERC Grant RGPIN/05245.

## 4.5 Methods

**KEY RESOURCES TABLE**

| REAGENT or RESOURCE | SOURCE | IDENTIFIER |
|---|---|---|
| **Experimental Models: Organisms/Strains** | | |
| Humans | N/A | N/A |
| **Software and Algorithms** | | |
| Python 3.7 | Anaconda | https://www.anaconda.com/ |
| Matlab 2019b | Mathworks | https://www.mathworks.com/product/matlab.html |
| Labview | NI | http://www.ni.com/fr-fr/shop/labview.html |
| Visbrain | N/A | doi: 10.3389/fninf.2019.00014 |
| Scikit-Learn | N/A | https://scikit-learn.org/stable/ |
| **Other** | | |
| MEG system | CTF | https://www.ctf.com/ |

**LEAD CONTACT AND MATERIALS AVAILABILITY**

Further information and requests for resources and reagents should be directed to and will be fulfilled by the Lead Contact, Thomas Thiery (thomas.thiery@umontreal.ca).

**EXPERIMENTAL MODEL AND SUBJECT DETAILS**

**Subjects**

Thirty-two subjects (aged 18-34, mean age 25.7) participated in this study. 15 were male, and one male was left-handed. Two were excluded before the start of analysis because of large head movement (extent of displacement during one session > 20 mm), and one because of myographic artifacts during MEG scanning. Data from another subject was unusable due to an interruption of the MEG system during the experiment, leaving 28 subjects in total for further analyses. All subjects had normal or corrected-to-normal vision, no history of psychiatric or neurological disorders, and had provided written informed consent prior to the start of the experiment, which was approved by the Research Ethics Committee at University of Montreal, under ethics number CER VN 18-19-05.

**Behavioral Task**

In the MEG scanner, subjects had to perform two behavioral tasks: the "tokens" task and the two choice visuo-motor reaction-time task.

In the tokens task (Figure 1A), 32 healthy subjects between 18 and 34 years old were presented with a central circle and two peripheral target circles (180° apart). At the beginning of each trial, 15 small tokens were randomly arranged in the central circle and began to jump, one-by-one every 200 ms ("predecision" interval), from the center circle to one of the two peripheral targets. The subject's task was to press a button (left or right) to choose the target he/she believed would ultimately receive most of the tokens. Importantly, the subject could make the decision at any time, and once the choice was reported, the remaining tokens jumped more quickly to their final targets. In separate 5-minute blocks, this "postdecision interval" was set to either 50 ms (in the "fast" blocks) or to 150 ms (in the "slow" blocks). Each subject completed eight blocks, alternating between fast blocks, which encourage hasty behavior, and slow blocks, which encourage more conservative behavior. The task was designed so trials could be classified into three classes of interest: easy, ambiguous and misleading (see next section for more details). Importantly, participants were not given any instruction about speed or accuracy and never told explicitly about block and trial differences, and were only instructed to maximize success rate by making as many correct choices as they could in a given period of time (5 minutes). On each trial, once all tokens had jumped, visual feedback was provided (the chosen target turns green for correct or red for error choices), but there was no feedback or instruction regarding the timing of choices.

In the visuo-motor reaction-time task (two 2-minute blocks before and after the "tokens" task), the 15 tokens originally arranged in the center circle simultaneously jump into one of the two peripheral targets (left or right) after a variable delay. This "GO signal" instructed the subjects to press the button corresponding to the target in which all the tokens have jumped as fast as possible.

**Behavioral Data Analysis**

In the tokens task we can compute, at each moment in time, the success probability $p_i(t)$ associated with choosing each target *i*. For instance, if at a particular moment in time the right target contains $N_R$ tokens, whereas the left contains $N_L$ tokens, and there are $N_C$ tokens remaining in the center, then the probability that the target on the right will ultimately be the correct one (i.e., the success probability of guessing correctly) is the following:

$$p(R|N_R, N_L, N_C) = \frac{N_C!}{2^{N_C}} \sum_{k=0}^{\min(N_C, 7-N_L)} \frac{1}{k!(N_C-k)!} \qquad \textbf{Equation 1}$$

Calculating this quantity for the 15 token jumps allows us to construct the success probability profile $p_i(t)$ associated with each trial (Figure 1B).

As far as the subjects knew, the correct target and the individual token movements were completely random. However, to test specific hypotheses about the dynamics of decision making, we interspersed among the fully random trials three specific trial types characterized by particular temporal profiles of success probability. Subjects were not told about the existence of these trials, but 15% of trials were so-called "easy" trials, in which success probability (SP) had to exceed 0.6 after two token jumps, 0.75 after five token jumps and 0.75 after eight token jumps, quickly driving the success probability $p_i(t)$ for each toward either 0 or 1. Another 15% of trials were "ambiguous", in which SP was 0.5 after two jumps, between 0.4 and 0.65 after three token jumps, and then between 0.35 and 0.65 after five jumps, making the $p_i(t)$ function stay near 0.5 until late in the trial. Another 10% of trials were called "misleading" trials, in which the SP had to be below 0.4 after three token jumps. The remaining 60% of trials were fully randomized. Thus, the final distribution of trials was as follows: 60% random, 15% easy, 15% ambiguous, and 10% misleading. We used SP to classify random trials into a posteriori classes of trials (e.g., "easy," "ambiguous," and "misleading" trials) embedded in the sequence (Figure 1C), yielding an average of 26% easy, 22% ambiguous and 11% misleading trials.

Reaction time in the tokens task was calculated as the time of button press relative to the time of the first token jump. Decision time (DT) was estimated by subtracting from the reaction time the subject's mean reaction time from the visuo-motor reaction-time task. We could then compute for each trial

the duration of a decision as well as its SP, computed using ***Equation 1***, at the time of the decision (Figure 1B).

## QUANTIFICATION AND STATISTICAL ANALYSIS

### MEG acquisition and preprocessing

Data was acquired from subjects in a seated position using a 275-channel VSM/CTF MEG system with a sampling rate of 2400 Hz (no high-pass filter, 660 Hz anti-aliasing online low-pass filter). Three head positioning coils were attached to fiducial anatomical locations (nasion, left/right pre-auricular points) to track head movements during recordings. Head shape and the locations of head position coils were digitized (Polhemus Fastrak, Polhemus Inc., VT, USA) prior to MEG data collection, for co-registration of MEG channel locations with anatomical T1-weighted MRI. Eye movements and blinks were recorded using 2 bipolar electro-oculographic (EOG) channels. EOG leads were placed above and below one eye (vertical channel); the second channel was placed laterally to the two eyes (horizontal channel). Heart activity was recorded with one channel (ECG), with electrical reference at the opposite clavicle.

We computed 20 independent components (Independent Component Analysis, ICA[65]) from the continuous MEG data filtered between 0.5 and 150 Hz, notch filtered at 60 and 120 Hz, and down sampled to 600 Hz. We identified components capturing artifacts from eye-blinks, saccades and heartbeats based on the correlation of ICA component time-series and ECG/EOG channels. We computed a projector from the identified mixing/unmixing matrices ($\mathbf{\Phi}/\mathbf{\Phi}^{+}$) as $\mathbf{I} - \mathbf{\Phi}\mathbf{\Phi}^{+}$ and applied it to the raw unfiltered MEG data to remove contributions from these artifact sources. Subsequently, noisy MEG channels were identified by visually inspecting their power spectrum and removing those that showed excessive power across a broad band of frequencies. The raw data were further visually inspected to detect and exclude time segments with excessive noise e.g., from jaw clenching or eye saccades contamination not captured by any ICA component.

## MEG analyses

### *MEG Source reconstruction*

A T1-weighted MRI of the brain (1.5 T, 3D MP-RAGE, 0.8 mm isotropic, sagittal orientation (160), TR= 2200 ms, TE= 2.3 ms; FoV= 256) was obtained from each subject after the MEG session. For subsequent cortically constrained source analyses, the nasion and the left and right pre-auricular points were first marked manually in each subject's MRI volume. These were used as an initial starting point for registration of the MEG activity to the structural T1 image. An iterative closest point rigid-body registration method implemented in MNE python[66] improved the anatomical alignment using the additional scalp points. The registration was visually verified. Forward models were generated from the segmented and meshed MRI (decimation = 6, conductivity = [0.3, 0.006, 0.3]) using Freesurfer segmentation pipeline (with default parameter settings[55]) and MNE[66]. The individual high-resolution cortical surfaces (about 120,000 vertices) were downsampled to 8,196 triangle vertices to serve as image supports and define the MEG source space. The epoch data were additionally baseline corrected by subtracting the mean across all time points and epochs for each channel between −200 and 0 ms before the first token jump, and a shrunk co-variance[67] was estimated across all trials from this time window. The inverse operators were generated using the dynamic Statistical Parametric Mapping method (dSPM, using the Tikhonov regularization coefficient lambda2 = 1), applied at the single-trial level. To perform group analyses, the surface vertices of individual subjects were morphed towards vertices in a reference "fsaverage" space from freesurfer (see surfer.nmr.mgh.harvard.edu/fswiki/fsaverager).

### *MEG Spectral analyses*

We first used the FOOOF toolbox[52], a model-driven method used to parameterize neural power spectra as a combination of an aperiodic component and putative periodic oscillatory peaks of our MEG data. The benefit of using FOOOF for measuring neuronal oscillations is that peaks in the power spectrum are characterized in terms of their specific center frequency, power and bandwidth without requiring predefining specific bands of interest and controlling for the aperiodic component. This method was applied to sensor-level data across all subjects, from -1500ms to +2000ms around button

press, in the frequency range from 1 to 35 Hz (see full report in Supplementary Figure S1). Based on the results given by the FOOOF framework, we chose the following frequency bands: theta (θ) [5–8 Hz], alpha (α) [9–13 Hz], beta (β) [16–24 Hz], and we split high frequency bands into gamma (γ) [30–60] and high gamma (γ) [60–90]. We then extracted the time resolved power by filtering the source reconstructed raw MEG signals using a finite impulse response filtering (FIR1, order = 3) and then computing the Hilbert transform. The signal was then averaged over 500 ms time windows with an overlap of 50 ms. This was computed from 500 ms before to 1000 ms after the first token jump, and from 1500 ms before to 2000 ms after button press, feedback, and decision time. Whenever present, baseline normalization was only used for visualization purposes (time-frequency maps and single trial representation). Baseline normalization was achieved for each frequency band, by subtracting then dividing by the mean of a 400 ms baseline window, i.e., the pre-stimulus rest period ([-500 ms, -100 ms]) before the first token jump.

***MEG Principal Component Analysis***

To calculate the principal components of neural activity, we used the source reconstructed power data computed from 1200 ms before to 600 ms after button press individually for each frequency band. This time window was chosen so it incorporates the token onset movement across all participants and trials. We then grouped trials into twelve non-overlapping classes based on block type (fast or slow), choice (left or right), and trial types (easy, ambiguous or misleading). In each group, power envelopes were averaged together for each frequency band, regardless of whether the choice was correct, or the reaction time was early or late. For each of these twelve classes, we constructed a 28x61x8196 (for the range [-1250; +1200 ms] relative to button press onset) 3D tensor where dimensions correspond to subjects, time bins and sources, respectively. We then concatenated these twelve classes into a 20496 x 8196 sources (where 20496 = 12 conditions x 28 subjects x 61 time bins and 8196 is the number of source nodes) matrix on which we performed standard Principal Component Analysis (using the pca function in Matlab 2019b), yielding a matrix of weights (“Loading Coefficients”) across all 8196 sources and PCs as well as the variance explained by each PC, for each frequency band. For further analysis, we only kept the top 20 PCs, which explained 95.3% of the total variance across frequency bands (theta:

95.1%, alpha: 97%, beta: 98.1%, gamma: 95.5%, high gamma: 96.5%) though as will be shown below, most of the interpretation will focus on the first four PCs, which explained 84.2% of the total variance across frequency bands (theta: 83.5%, alpha: 86.5%, beta: 94%, gamma: 76.7% and high gamma: 80.3%).

The time courses of PCs for each of the twelve experimental conditions were computed by taking the product of loading coefficients and original power data (locked on the first token jump, on decision time or on button press), for each subject and for each frequency band. To localize the distribution of weights that contributed most to each PC, we projected the top 5% of loading coefficients ("Leading Loadings Coefficients", LLCs) onto sources of 3D inflated standard MNI brains. Specifically, we created a distribution of the absolute values of all loading coefficients, and only kept top 5% of sources based on their loading coefficient (absolute) value. Importantly, we ran the same procedure using 3% and 10%, and obtained similar results.

***Correlation analyses***

We computed Pearson correlation coefficients (R) and their associated *p-values* between the time-courses of mean success probabilities (SPs) and the time courses of the top 20 PCs for easy, ambiguous, and misleading trials and for left and right choices averaged across fast and slow blocks (6 conditions), for each frequency band separately. SPs and PCs were computed every 200 ms from 0 to 1000 ms after first token jump and from -1200 ms to 0 ms before button press onset (see Supplementary Figure S8).

**Decoding analyses**

***Signal classification***

We set out to evaluate whether time courses of principal components derived from the PCA analysis could significantly classify effects of decision (Left vs Right), sensory evidence (Easy vs Ambiguous vs Misleading), and SAT policy (Fast vs Slow) during dynamic perceptual decision making. To this end, we

implemented a machine learning framework for classification using matrices where dimensions correspond to subjects (n=28), conditions (n=2 for Left vs Right and Fast vs Slow, or n=3 for Easy vs Ambiguous vs Misleading), and time bins. LDA classifications were repeated for each frequency band (θ, α, β and γ), and for data locked on the first token jump, on decision time or on button press).

Several classification techniques were initially tested for the single feature classification procedure, including linear-discriminant analysis (LDA), k-nearest-neighbor (KNN) and support vector machine (SVM). The classification accuracy results were similar across the three methods. The LDA algorithm (Fisher, 1936) was the fastest and was therefore chosen for this study given the computationally demanding permutation tests used to evaluate classifier performance. In brief, for a binary classification problem, the LDA algorithm tries to find a hyperplane that maximizes the mean distance between the mean of the two classes while minimizing inter-class variance.

***Decoding accuracy and statistical evaluation of decoding performance***

At the group level, the performance of the proposed classification method was evaluated using a Leave-One-Subject-Out (LOSO) cross-validation procedure. This procedure is a special case of k-fold cross-validation, where all individuals except one are used for training, and the classifier is tested on the data from the omitted participant (i.e., test data). This procedure is repeated iteratively, each time leaving a different individual out of the training. The LOSO cross-validation method efficiently uses data and provides an asymptotically unbiased estimate of the averaged classification error probability over all possible training sets[68]. The statistical significance of the obtained decoding accuracies was evaluated by computing statistical thresholds using permutation tests ($p < 0.05$). In other words, a null distribution is generated by repeatedly ($n = 1000$) computing the classification accuracy obtained after randomly permuting class labels[69].

## 4.6 References


Andersen, L. M., Jerbi, K., & Dalal, S. S. (2020). Can EEG and MEG detect signals from the human cerebellum? *NeuroImage*, *215*, 116817. https://doi.org/10.1016/j.neuroimage.2020.116817

Bastos, A. M., Vezoli, J., Bosman, C. A., Schoffelen, J.-M., Oostenveld, R., Dowdall, J. R., De Weerd, P., Kennedy, H., & Fries, P. (2015). Visual Areas Exert Feedforward and Feedback Influences through Distinct Frequency Channels. *Neuron*, *85*(2), 390–401. https://doi.org/10.1016/j.neuron.2014.12.018

Bitzer, S., Park, H., Maess, B., von Kriegstein, K., & Kiebel, S. J. (2020). Representation of Perceptual Evidence in the Human Brain Assessed by Fast, Within-Trial Dynamic Stimuli. *Frontiers in Human Neuroscience*, *14*. https://doi.org/10.3389/fnhum.2020.00009

Boehm, U., Hawkins, G. E., Brown, S., van Rijn, H., & Wagenmakers, E.-J. (2016). Of monkeys and men: Impatience in perceptual decision-making. *Psychonomic Bulletin & Review*, *23*, 738–749. https://doi.org/10.3758/s13423-015-0958-5

Bogacz, R., Wagenmakers, E.-J., Forstmann, B. U., & Nieuwenhuis, S. (2010). The neural basis of the speed-accuracy tradeoff. *Trends in Neurosciences*, *33*(1), 10–16. https://doi.org/10.1016/j.tins.2009.09.002

Britten, K. H., Shadlen, M. N., Newsome, W. T., & Movshon, J. A. (1992). The analysis of visual motion: A comparison of neuronal and psychophysical performance. *Journal of Neuroscience*, *12*(12), 4745–4765.

Buffalo, E. A., Fries, P., Landman, R., Buschman, T. J., & Desimone, R. (2011). Laminar differences in gamma and alpha coherence in the ventral stream. *Proceedings of the National Academy of Sciences*, *108*(27), 11262–11267.

Carland, M. A., Marcos, E., Thura, D., & Cisek, P. (2015). Evidence against perfect integration of sensory information during perceptual decision making. *Journal of Neurophysiology*, *115*(2), 915–930. https://doi.org/10.1152/jn.00264.2015

Carland, M. A., Thura, D., & Cisek, P. (2019). The Urge to Decide and Act: Implications for Brain Function and Dysfunction. *The Neuroscientist*, *25*(5), 491–511. https://doi.org/10.1177/1073858419841553

Churchland, A. K., Kiani, R., & Shadlen, M. N. (2008). Decision-making with multiple alternatives. *Nature Neuroscience*, *11*(6), 693–702. https://doi.org/10.1038/nn.2123

Cisek, P., Puskas, G. A., & El-Murr, S. (2009). Decisions in Changing Conditions: The Urgency-Gating Model. *Journal of Neuroscience*, *29*(37), 11560–11571. https://doi.org/10.1523/JNEUROSCI.1844-09.2009

Combrisson, E., & Jerbi, K. (2015). Exceeding chance level by chance: The caveat of theoretical chance levels in brain signal classification and statistical assessment of decoding accuracy. *Journal of Neuroscience Methods*, *250*, 126–136. https://doi.org/10.1016/j.jneumeth.2015.01.010

de Lange, F. P., Rahnev, D. A., Donner, T. H., & Lau, H. (2013). Prestimulus oscillatory activity over motor cortex reflects perceptual expectations. *The Journal of Neuroscience: The Official Journal of the Society for Neuroscience*, *33*(4), 1400–1410. https://doi.org/10.1523/JNEUROSCI.1094-12.2013

Delorme, A., Sejnowski, T., & Makeig, S. (2007). Enhanced detection of artifacts in EEG data using higher-order statistics and independent component analysis. *NeuroImage*, *34*(4), 1443–1449. https://doi.org/10.1016/j.neuroimage.2006.11.004

Ditterich, J. (2006). Evidence for time-variant decision making. *The European Journal of Neuroscience*, *24*(12), 3628–3641. https://doi.org/10.1111/j.1460-9568.2006.05221.x

Donner, T. H., Siegel, M., Fries, P., & Engel, A. K. (2009). Buildup of Choice-Predictive Activity in Human Motor Cortex during Perceptual Decision Making. *Current Biology*, *19*(18), 1581–1585. https://doi.org/10.1016/j.cub.2009.07.066

Donoghue, T., Haller, M., Peterson, E. J., Varma, P., Sebastian, P., Gao, R., Noto, T., Lara, A. H., Wallis, J. D., Knight, R. T., Shestyuk, A., & Voytek, B. (2020). Parameterizing neural power spectra into periodic and aperiodic components. *Nature Neuroscience*, *23*(12), 1655–1665. https://doi.org/10.1038/s41593-020-00744-x

Drugowitsch, J., Moreno-Bote, R., Churchland, A. K., Shadlen, M. N., & Pouget, A. (2012). The Cost of Accumulating Evidence in Perceptual Decision Making. *The Journal of Neuroscience*, *32*(11), 3612–3628. https://doi.org/10.1523/JNEUROSCI.4010-11.2012

Engel, A. K., & Fries, P. (2010). Beta-band oscillations—Signalling the status quo? *Current Opinion in Neurobiology*, *20*(2), 156–165. https://doi.org/10.1016/j.conb.2010.02.015

Engemann, D. A., & Gramfort, A. (2015). Automated model selection in covariance estimation and spatial whitening of MEG and EEG signals. *NeuroImage*, *108*, 328–342. https://doi.org/10.1016/j.neuroimage.2014.12.040

Fischl, B. (2012). FreeSurfer. *NeuroImage*, *62*(2), 774–781. https://doi.org/10.1016/j.neuroimage.2012.01.021

Gaetz, W., & Cheyne, D. (2006). Localization of sensorimotor cortical rhythms induced by tactile stimulation using spatially filtered MEG. *NeuroImage*, *30*(3), 899–908. https://doi.org/10.1016/j.neuroimage.2005.10.009

Ghose, G. M. (2006). Strategies optimize the detection of motion transients. *Journal of Vision*, *6*(4), 429–440. https://doi.org/10.1167/6.4.10

Glasser, M. F., Coalson, T. S., Robinson, E. C., Hacker, C. D., Harwell, J., Yacoub, E., Ugurbil, K., Andersson, J., Beckmann, C. F., Jenkinson, M., Smith, S. M., & Van Essen, D. C. (2016). A multi-modal parcellation of human cerebral cortex. *Nature*, *536*(7615), 171–178. https://doi.org/10.1038/nature18933

Gluth, S., Rieskamp, J., & Büchel, C. (2012). Deciding When to Decide: Time-Variant Sequential Sampling Models Explain the Emergence of Value-Based Decisions in the Human Brain. *Journal of Neuroscience*, *32*(31), 10686–10698. https://doi.org/10.1523/JNEUROSCI.0727-12.2012

Gold, J. I., & Shadlen, M. N. (2007). The neural basis of decision making. *Annual Review of Neuroscience*, *30*, 535–574. https://doi.org/10.1146/annurev.neuro.29.051605.113038

Gould, I. C., Nobre, A. C., Wyart, V., & Rushworth, M. F. S. (2012). Effects of Decision Variables and Intraparietal Stimulation on Sensorimotor Oscillatory Activity in the Human Brain. *Journal of Neuroscience*, *32*(40), 13805–13818. https://doi.org/10.1523/JNEUROSCI.2200-12.2012

Gramfort, A., Luessi, M., Larson, E., Engemann, D. A., Strohmeier, D., Brodbeck, C., Goj, R., Jas, M., Brooks, T., Parkkonen, L., & Hämäläinen, M. (2013). MEG and EEG data analysis with MNE-Python. *Frontiers in Neuroscience*, *7*. https://doi.org/10.3389/fnins.2013.00267

Hawkins, G. E., Wagenmakers, E.-J., Ratcliff, R., & Brown, S. D. (2015). Discriminating evidence accumulation from urgency signals in speeded decision making. *Journal of Neurophysiology*, *114*(1), 40–47. https://doi.org/10.1152/jn.00088.2015

Huk, A. C., Katz, L. N., & Yates, J. L. (2017). The Role of the Lateral Intraparietal Area in (the Study of) Decision Making. *Annual Review of Neuroscience*, *40*(1), 349–372. https://doi.org/10.1146/annurev-neuro-072116-031508

Jensen, O., & Mazaheri, A. (2010). Shaping Functional Architecture by Oscillatory Alpha Activity: Gating by Inhibition. *Frontiers in Human Neuroscience*, *4*. https://doi.org/10.3389/fnhum.2010.00186

Kable, J. W., & Glimcher, P. W. (2009). The Neurobiology of Decision: Consensus and Controversy. *Neuron*, *63*(6), 733–745. https://doi.org/10.1016/j.neuron.2009.09.003

Kelly, S. P., & O'Connell, R. G. (2015). The neural processes underlying perceptual decision making in humans: Recent progress and future directions. *Journal of Physiology, Paris*, *109*(1–3), 27–37. https://doi.org/10.1016/j.jphysparis.2014.08.003

Kilavik, B. E., Zaepffel, M., Brovelli, A., MacKay, W. A., & Riehle, A. (2013). The ups and downs of beta oscillations in sensorimotor cortex. *Experimental Neurology*, *245*, 15–26. https://doi.org/10.1016/j.expneurol.2012.09.014

Kolling, N., Behrens, T. E. J., Mars, R. B., & Rushworth, M. F. S. (2012). Neural mechanisms of foraging. *Science (New York, N.Y.)*, *336*(6077), 95–98. https://doi.org/10.1126/science.1216930

Levy, D. J., & Glimcher, P. W. (2012). The root of all value: A neural common currency for choice. *Current Opinion in Neurobiology*, *22*(6), 1027–1038. https://doi.org/10.1016/j.conb.2012.06.001

Ludwig, C. J. H., Gilchrist, I. D., McSorley, E., & Baddeley, R. J. (2005). The Temporal Impulse Response Underlying Saccadic Decisions. *The Journal of Neuroscience*, *25*(43), 9907–9912. https://doi.org/10.1523/JNEUROSCI.2197-05.2005

Malhotra, G. (20170413). Overcoming indecision by changing the decision boundary. *Journal of Experimental Psychology: General*, *146*(6), 776. https://doi.org/10.1037/xge0000286

Markov, N. T., Vezoli, J., Chameau, P., Falchier, A., Quilodran, R., Huissoud, C., Lamy, C., Misery, P., Giroud, P., Ullman, S., Barone, P., Dehay, C., Knoblauch, K., & Kennedy, H. (2014). Anatomy of hierarchy: Feedforward and feedback pathways in macaque visual cortex. *The Journal of Comparative Neurology*, *522*(1), 225–259. https://doi.org/10.1002/cne.23458

McClure, S. M., Laibson, D. I., Loewenstein, G., & Cohen, J. D. (2004). Separate neural systems value immediate and delayed monetary rewards. *Science (New York, N.Y.)*, *306*(5695), 503–507. https://doi.org/10.1126/science.1100907

Mejias, J. F., Murray, J. D., Kennedy, H., & Wang, X.-J. (2016). Feedforward and feedback frequency-dependent interactions in a large-scale laminar network of the primate cortex. *Science Advances*, *2*(11), e1601335. https://doi.org/10.1126/sciadv.1601335

Mendonça, A. G., Drugowitsch, J., Vicente, M. I., DeWitt, E. E. J., Pouget, A., & Mainen, Z. F. (2020). The impact of learning on perceptual decisions and its implication for speed-accuracy tradeoffs. *Nature Communications*, *11*(1), 2757. https://doi.org/10.1038/s41467-020-16196-7

Michalareas, G., Vezoli, J., van Pelt, S., Schoffelen, J.-M., Kennedy, H., & Fries, P. (2016). Alpha-beta and gamma rhythms subserve feedback and feedforward influences among human visual cortical areas. *Neuron*, *89*(2), 384–397. https://doi.org/10.1016/j.neuron.2015.12.018

Murphy, P. R., Boonstra, E., & Nieuwenhuis, S. (2016). Global gain modulation generates time-dependent urgency during perceptual choice in humans. *Nature Communications*, *7*(1), 13526. https://doi.org/10.1038/ncomms13526

O'Connell, R. G., Dockree, P. M., & Kelly, S. P. (2012). A supramodal accumulation-to-bound signal that determines perceptual decisions in humans. *Nature Neuroscience*, *15*(12), 1729. https://doi.org/10.1038/nn.3248

O'Connell, R. G., Shadlen, M. N., Wong-Lin, K., & Kelly, S. P. (2018). Bridging Neural and Computational Viewpoints on Perceptual Decision-Making. *Trends in Neurosciences*, *41*(11), 838–852. https://doi.org/10.1016/j.tins.2018.06.005

Palestro, J. J., Weichart, E., Sederberg, P. B., & Turner, B. M. (2018). Some task demands induce collapsing bounds: Evidence from a behavioral analysis. *Psychonomic Bulletin & Review*, *25*(4), 1225–1248. https://doi.org/10.3758/s13423-018-1479-9

Pearson, J. M., Heilbronner, S. R., Barack, D. L., Hayden, B. Y., & Platt, M. L. (2011). Posterior cingulate cortex: Adapting behavior to a changing world. *Trends in Cognitive Sciences*, *15*(4), 143–151. https://doi.org/10.1016/j.tics.2011.02.002

Rangel, A., & Hare, T. (2010). Neural computations associated with goal-directed choice. *Current Opinion in Neurobiology*, *20*(2), 262–270. https://doi.org/10.1016/j.conb.2010.03.001

Ratcliff, R. (1978). A Theory of Memory Retrieval. *Psychological Review*, *85*(2), 59–108.

Ratcliff, R., & McKoon, G. (2008). The Diffusion Decision Model: Theory and Data for Two-Choice Decision Tasks. *Neural Computation*, *20*(4), 873–922. https://doi.org/10.1162/neco.2008.12-06-420

Roitman, J. D., & Shadlen, M. N. (2002). Response of Neurons in the Lateral Intraparietal Area during a Combined Visual Discrimination Reaction Time Task. *Journal of Neuroscience*, *22*(21), 9475–9489. https://doi.org/10.1523/JNEUROSCI.22-21-09475.2002

Sherman, M. A., Lee, S., Law, R., Haegens, S., Thorn, C. A., Hämäläinen, M. S., Moore, C. I., & Jones, S. R. (2016). Neural mechanisms of transient neocortical beta rhythms: Converging evidence from humans, computational modeling, monkeys, and mice. *Proceedings of the National Academy of Sciences*, *113*(33), E4885–E4894.

Spaak, E., Bonnefond, M., Maier, A., Leopold, D. A., & Jensen, O. (2012). Layer-Specific Entrainment of Gamma-Band Neural Activity by the Alpha Rhythm in Monkey Visual Cortex. *Current Biology*, *22*(24), 2313–2318. https://doi.org/10.1016/j.cub.2012.10.020

Tajima, S., Drugowitsch, J., Patel, N., & Pouget, A. (2019). Optimal policy for multi-alternative decisions. *Nature Neuroscience*, *22*(9), 1503–1511. https://doi.org/10.1038/s41593-019-0453-9

Theodoridis, S., & Koutroumbas, K. (2009). *Pattern recognition* (4. ed). Elsevier Acad. Press.

Thura, D. (2016). How to discriminate conclusively among different models of decision making? *Journal of Neurophysiology*, *115*(5), 2251–2254. https://doi.org/10.1152/jn.00911.2015

Thura, D., Beauregard-Racine, J., Fradet, C.-W., & Cisek, P. (2012). Decision making by urgency gating: Theory and experimental support. *Journal of Neurophysiology*. https://doi.org/10.1152/jn.01071.2011

Thura, D., Cabana, J.-F., Feghaly, A., & Cisek, P. (2020). Unified neural dynamics of decisions and actions in the cerebral cortex and basal ganglia. *BioRxiv*, 2020.10.22.350280. https://doi.org/10.1101/2020.10.22.350280

Thura, D., & Cisek, P. (2014). Deliberation and Commitment in the Premotor and Primary Motor Cortex during Dynamic Decision Making. *Neuron*, *81*(6), 1401–1416. https://doi.org/10.1016/j.neuron.2014.01.031

Thura, D., & Cisek, P. (2016). Modulation of Premotor and Primary Motor Cortical Activity during Volitional Adjustments of Speed-Accuracy Trade-Offs. *Journal of Neuroscience*, *36*(3), 938–956. https://doi.org/10.1523/JNEUROSCI.2230-15.2016

Thura, D., & Cisek, P. (2017). The Basal Ganglia Do Not Select Reach Targets but Control the Urgency of Commitment. *Neuron*, *95*(5), 1160-1170.e5. https://doi.org/10.1016/j.neuron.2017.07.039

Thura, D., Cos, I., Trung, J., & Cisek, P. (2014). Context-Dependent Urgency Influences Speed–Accuracy Trade-Offs in Decision-Making and Movement Execution. *Journal of Neuroscience*, *34*(49), 16442–16454. https://doi.org/10.1523/JNEUROSCI.0162-14.2014

Thura, D., Guberman, G., & Cisek, P. (2017). Trial-to-trial adjustments of speed-accuracy trade-offs in premotor and primary motor cortex. *Journal of Neurophysiology*. https://doi.org/10.1152/jn.00726.2016

Trueblood, J. S., Heathcote, A., Evans, N. J., & Holmes, W. R. (2021). Urgency, leakage, and the relative nature of information processing in decision-making. *Psychological Review*, *128*(1), 160–186. https://doi.org/10.1037/rev0000255

van Kerkoerle, T., Self, M. W., Dagnino, B., Gariel-Mathis, M.-A., Poort, J., van der Togt, C., & Roelfsema, P. R. (2014). Alpha and gamma oscillations characterize feedback and feedforward processing in monkey visual cortex. *Proceedings of the National Academy of Sciences*, *111*(40), 14332–14341.

van Maanen, L., Fontanesi, L., Hawkins, G. E., & Forstmann, B. U. (2016). Striatal activation reflects urgency in perceptual decision making. *NeuroImage*, *139*, 294–303. https://doi.org/10.1016/j.neuroimage.2016.06.045

Varela, F., Lachaux, J.-P., Rodriguez, E., & Martinerie, J. (2001). The brainweb: Phase synchronization and large-scale integration. *Nature Reviews Neuroscience*, *2*(4), 229–239. https://doi.org/10.1038/35067550

Wilming, N., Murphy, P. R., Meyniel, F., & Donner, T. H. (2020). Large-scale dynamics of perceptual decision information across human cortex. *Nature Communications*, *11*(1), 5109. https://doi.org/10.1038/s41467-020-18826-6

## 4.7 Supplementary Material

**https://www.dropbox.com/scl/fi/indsoe08aguvkveuh1csz/00_Table_S1.xlsx?dl=0&rlkey=6ov9zzv22ttzxqm2517oeyzmo**

**Table S1. Leading Loading Coefficients assigned to Regions of interest (ROIs)** using the HCPMMP1 combined atlas[53].

**https://www.dropbox.com/s/fno2fspnw2cx8f3/00_Table_S2.xlsx?dl=0**

**Table S2. Leading Loading Coefficients assigned to Regions of interest (ROIs)** using the HCPMMP1 atlas[53].

```
================================================================================

                              FOOOF - GROUP RESULTS

                    Number of power spectra in the Group: 7644

              The model was run on the frequency range 1 - 35 Hz
                         Frequency Resolution is 0.50 Hz

                    Power spectra were fit without a knee.

                              Aperiodic Fit Values:
              Exponents - Min: -0.754, Max:  2.540, Mean: 1.004

              In total 25438 peaks were extracted from the group

                              Goodness of fit metrics:
                  R2s -  Min:  0.024, Max:  0.998, Mean: 0.975
                Errors -  Min:  0.015, Max:  0.436, Mean: 0.041

================================================================================
```

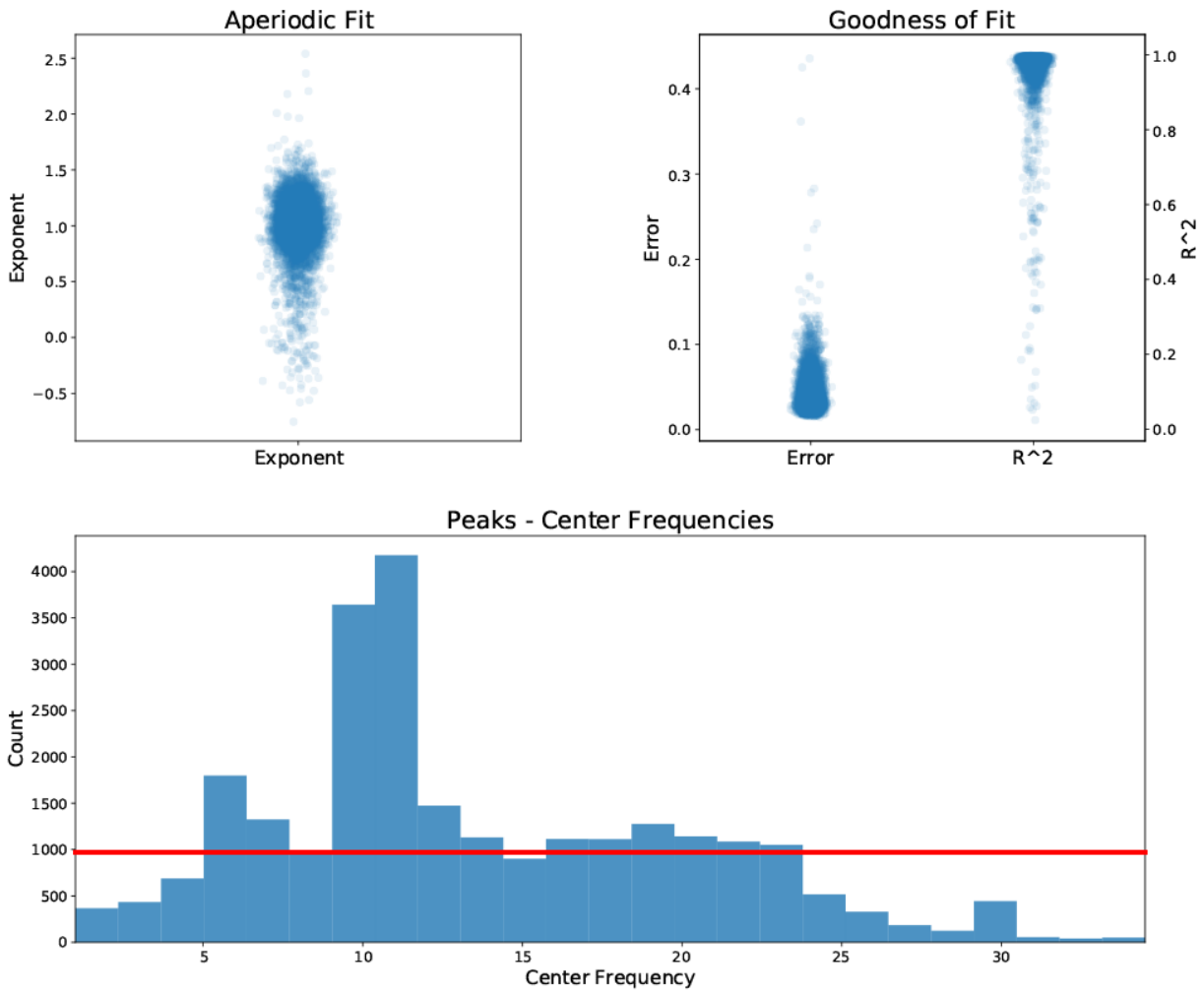


**Figure S1. FOOOF toolbox report.** To determine the width of your frequency bands for theta, alpha and beta we fit a model on power spectra (n=7644) from all subjects based on the sensor-level data (28 subjects * 273 channels) locked on button press (-1500ms to +2000ms). We chose to group frequencies into three bands: theta [5-8 Hz], alpha [9-13 Hz] and beta [16-24 Hz].

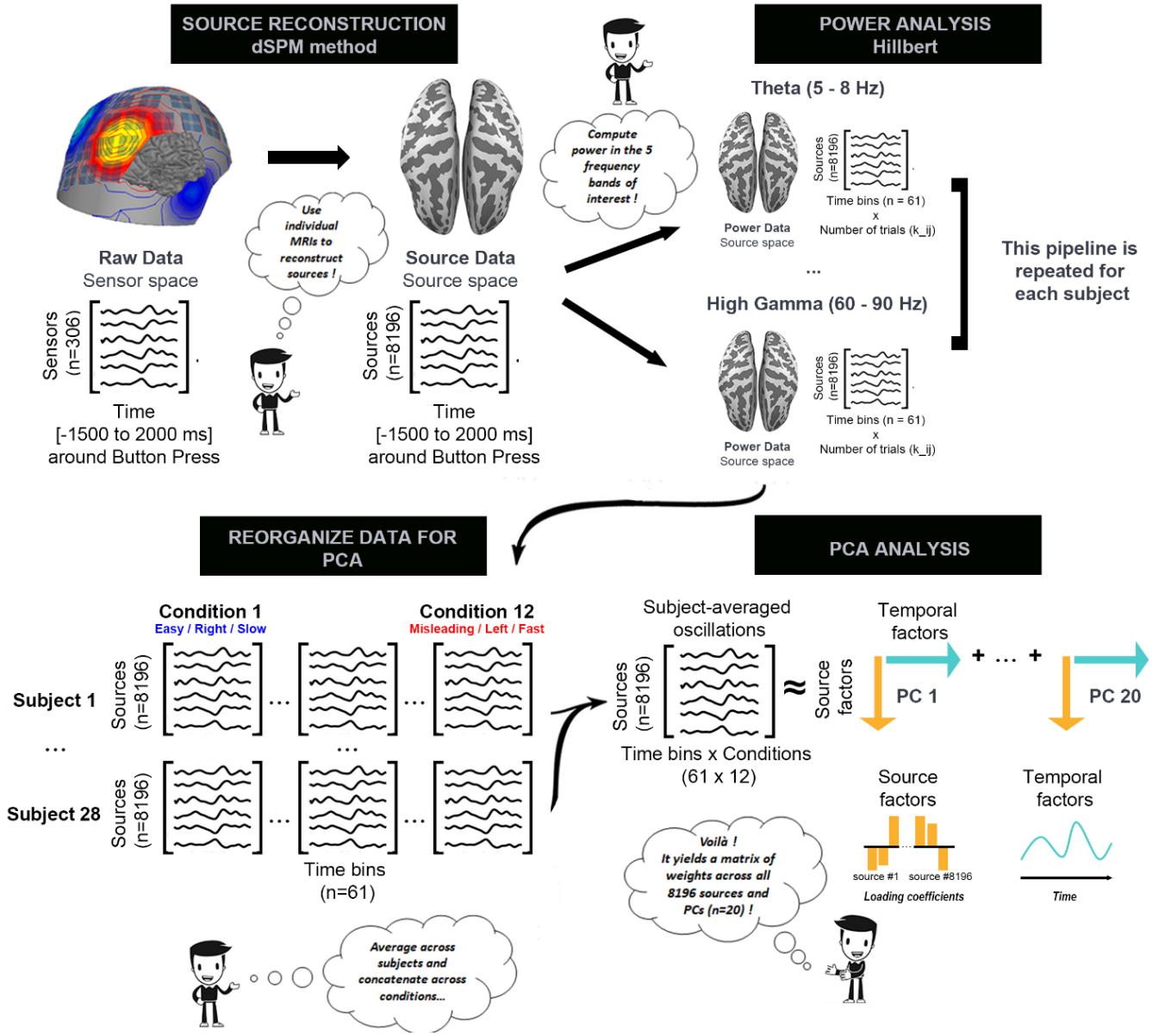


**Figure S2. Illustration of the PCA analysis** performed on the source-reconstructed MEG data. We first used the preprocessed raw MEG data in the sensor space combined with the individual T1 MRI images to reconstruct sources. We then computed power envelopes in 5 frequency bands of interest, using the Hilbert method with sliding windows (width, overlap), and kept the trial dimensions (k represents the number of trials, *i* the condition from 1 to 12, and *j* the subject number from 1 to 28). We then reorganized the data to obtain the following 3D tensor for each frequency band :12 conditions (averaged across trials in each condition) x 8196 sources (averaged across subjects) x 61 time bins, and we performed the PCA analysis to obtain a matrix of weights ("Loading Coefficients") across all 8196 sources and principal components (PC) as well as the variance explained by each PC, for each frequency band.

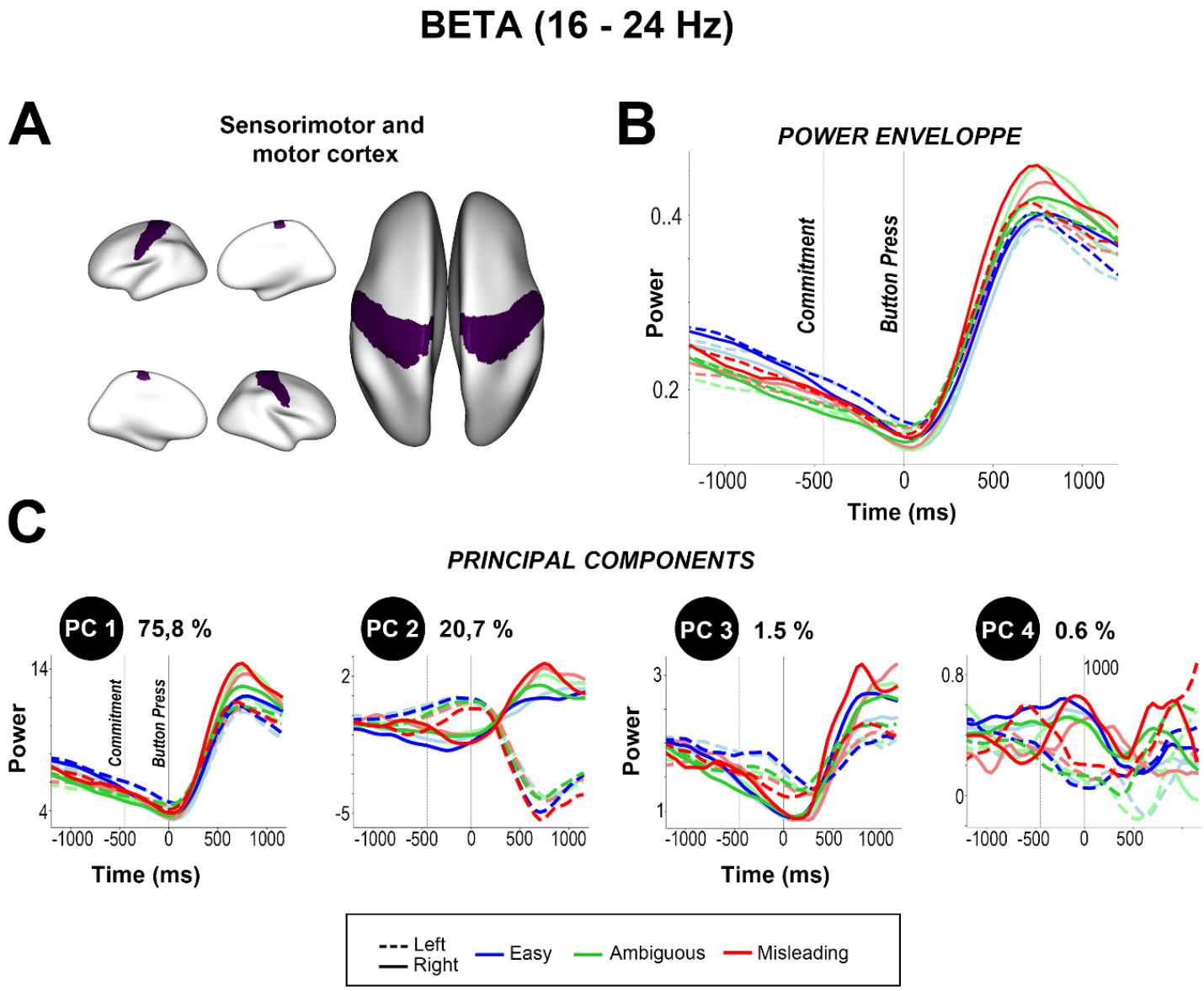


**Figure S3. Comparison between beta (16-24 Hz) power envelopes (B) and principal components (C)** in the sensorimotor and motor cortex (A), averaged across trials and participants for easy, ambiguous and misleading trials, and for left and right choices.

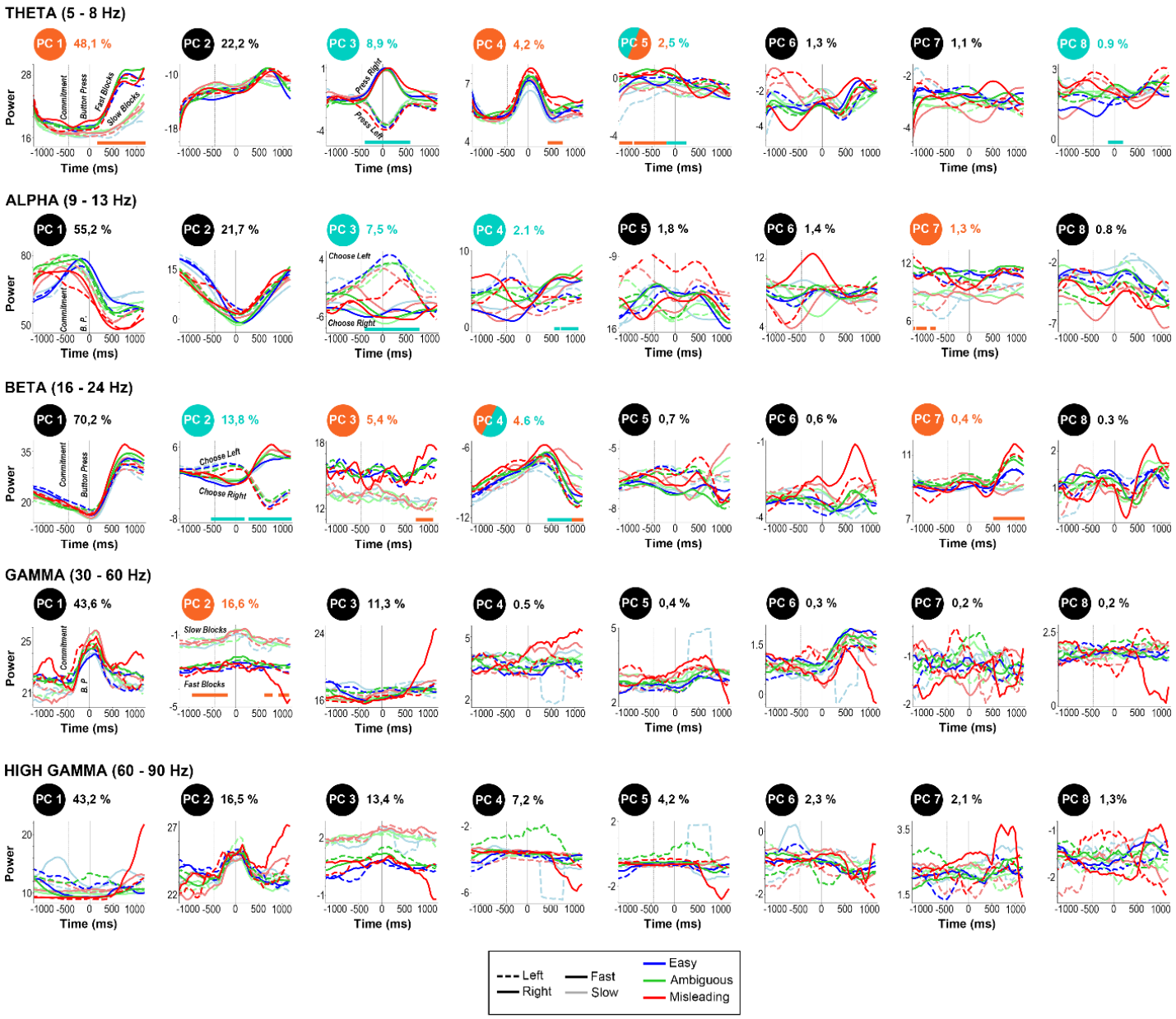


**Figure S4. First eight PC components computed in theta (4 – 8 Hz), alpha (8 - 15 Hz), beta (15 – 30 Hz), gamma and high gamma (30 - 60 Hz) frequency bands** for easy (blue), ambiguous (green) and misleading (red) trials during fast (bright) and slow (transparent) blocks, and for left (continuous) and right (dashed) choices on data time locked on button press (from -1250 to 1200 ms). In each panel, the second vertical dotted line indicates button press, and the first indicates the estimated moment of commitment (i.e., mean decision time across subjects obtained in the Delayed Response task), 448ms earlier. Percentages next to PCs indicate the amount of variance explained.

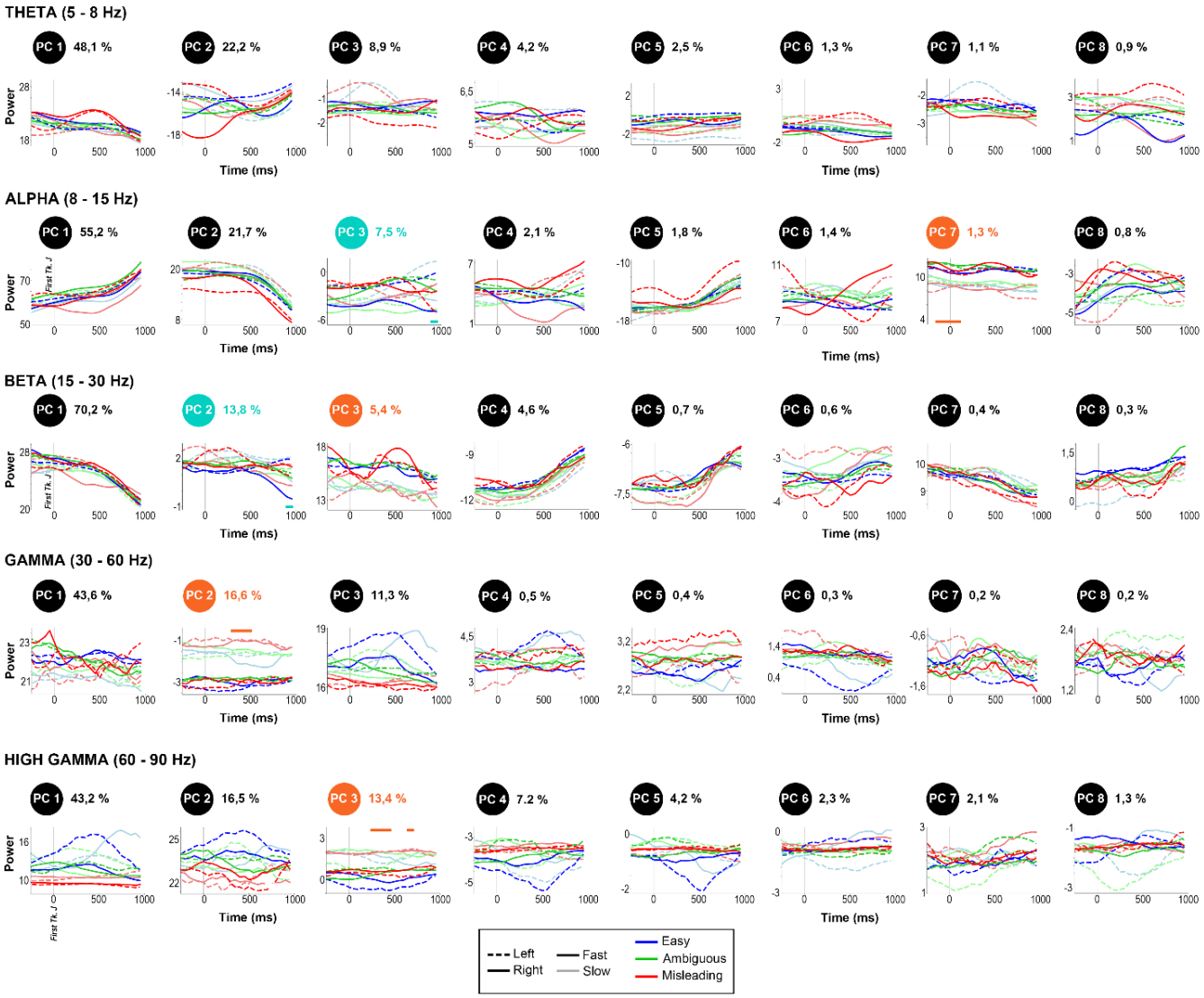


**Figure S5. First eight PC components computed in theta (4 – 8 Hz), alpha (8 - 15 Hz), beta (15 – 30 Hz), gamma (30 - 60 Hz) and high gamma (60 – 90 Hz) frequency bands** for easy (blue), ambiguous (green) and misleading (red) trials during fast (bright) and slow (transparent) blocks, and for left (continuous) and right (dashed) choices on data time locked on first token jump (from -200 to 1000 ms). Percentages next to PCs indicate the amount of variance explained.

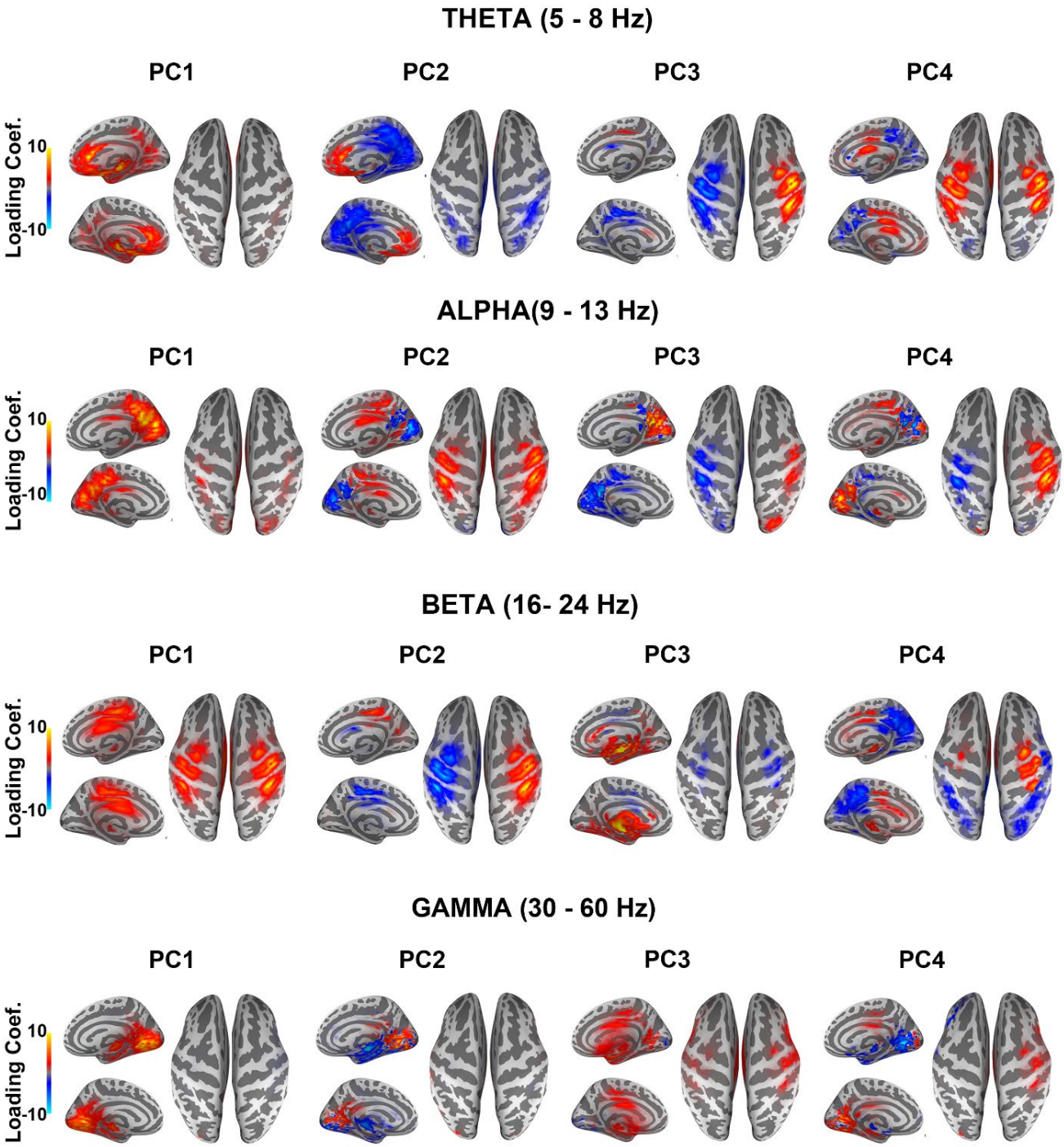


**Figure S6. Loading coefficients** projected on 3D inflated MNI brains in the MEG source space for the first 4 components in theta, alpha, beta and gamma frequency bands.

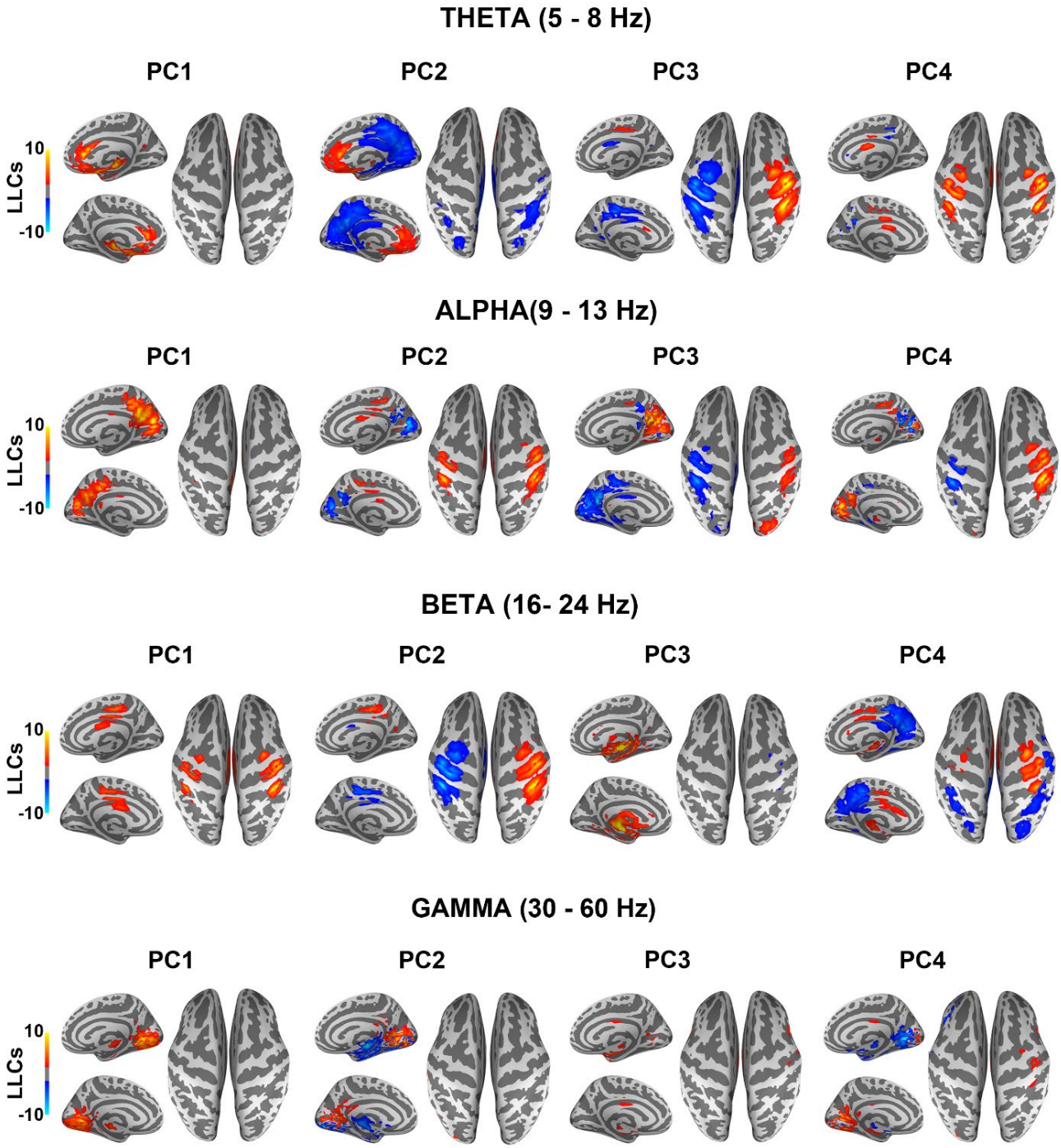


**Figure S7. Leading Loading coefficients (LLCs, top 5%)** projected on 3D inflated MNI brains in the MEG source space for the first 4 components in theta, alpha, beta and gamma frequency bands.

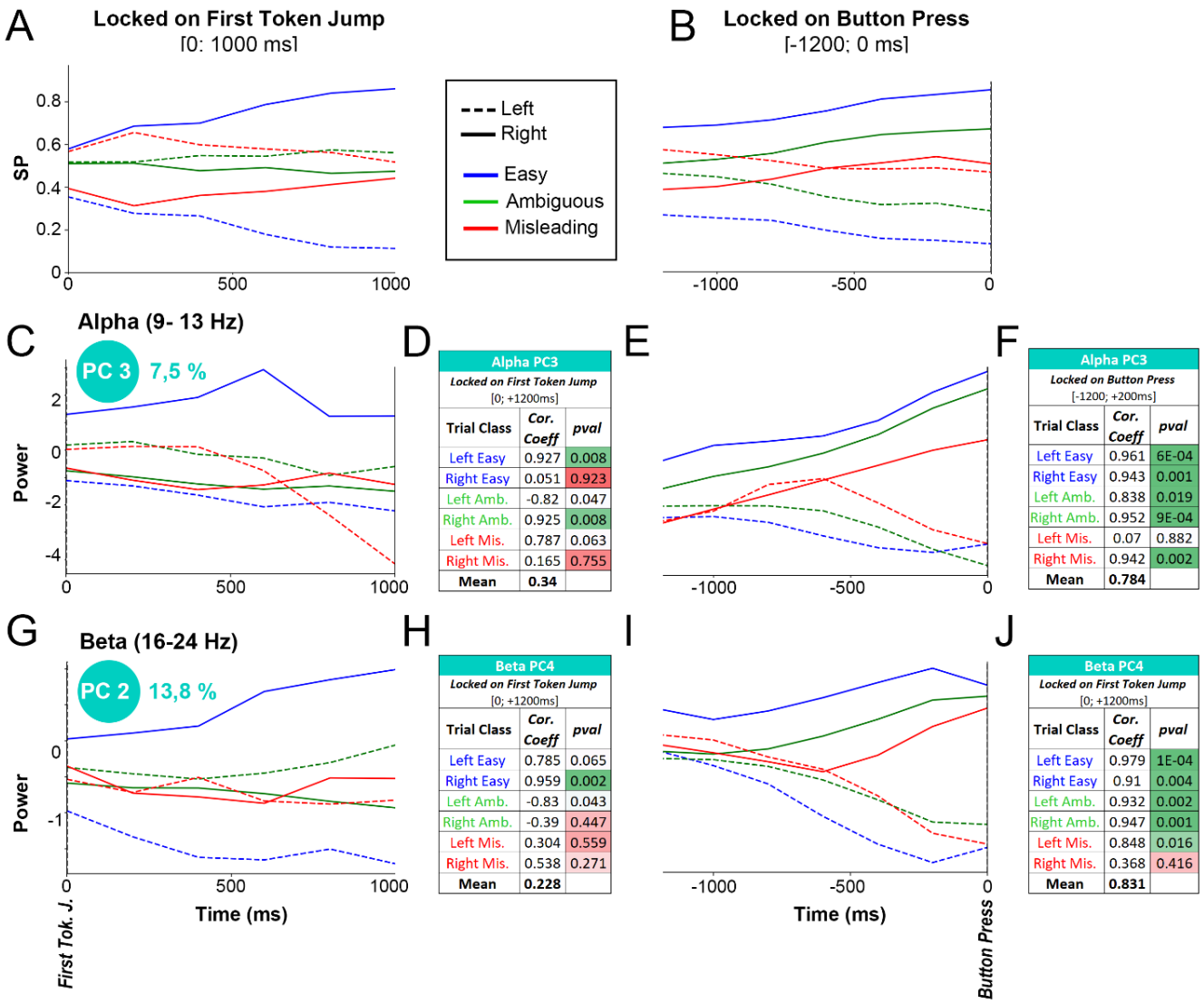


| Alpha PC3 | | |
|---|---|---|
| *Locked on First Token Jump* [0; +1200ms] | | |
| **Trial Class** | ***Cor. Coeff*** | ***pval*** |
| Left Easy | 0.927 | 0.008 |
| Right Easy | 0.051 | 0.923 |
| Left Amb. | -0.82 | 0.047 |
| Right Amb. | 0.925 | 0.008 |
| Left Mis. | 0.787 | 0.063 |
| Right Mis. | 0.165 | 0.755 |
| **Mean** | **0.34** | |

| Alpha PC3 | | |
|---|---|---|
| *Locked on Button Press* [-1200; +200ms] | | |
| **Trial Class** | ***Cor. Coeff*** | ***pval*** |
| Left Easy | 0.961 | 6E-04 |
| Right Easy | 0.943 | 0.001 |
| Left Amb. | 0.838 | 0.019 |
| Right Amb. | 0.952 | 9E-04 |
| Left Mis. | 0.07 | 0.882 |
| Right Mis. | 0.942 | 0.002 |
| **Mean** | **0.784** | |

| Beta PC4 | | |
|---|---|---|
| *Locked on First Token Jump* [0; +1200ms] | | |
| **Trial Class** | ***Cor. Coeff*** | ***pval*** |
| Left Easy | 0.785 | 0.065 |
| Right Easy | 0.959 | 0.002 |
| Left Amb. | -0.83 | 0.043 |
| Right Amb. | -0.39 | 0.447 |
| Left Mis. | 0.304 | 0.559 |
| Right Mis. | 0.538 | 0.271 |
| **Mean** | **0.228** | |

| Beta PC4 | | |
|---|---|---|
| *Locked on First Token Jump* [0; +1200ms] | | |
| **Trial Class** | ***Cor. Coeff*** | ***pval*** |
| Left Easy | 0.979 | 1E-04 |
| Right Easy | 0.91 | 0.004 |
| Left Amb. | 0.932 | 0.002 |
| Right Amb. | 0.947 | 0.001 |
| Left Mis. | 0.848 | 0.016 |
| Right Mis. | 0.368 | 0.416 |
| **Mean** | **0.831** | |

**Figure S8. Correlation between success probabilities and PCs.** Success probabilities locked on first token jump [0; 1000 ms] (**A**) and lockedon button press [-1200; 0 ms] (**B**). Alpha PC3 and beta PC4 temporal profiles locked on first token jump (**C**, **G**) and on button press (**E**, **I**) averaged across fast and slow blocks for easy, ambiguous, and misleading trials and for left and right choices. Tables **D**, **F**, **H** and **J** show correlation coefficients and *p-values* between SPs and alpha PC3/beta PC4 locked on first token jump (**D/H**) and button press (**F/J**).

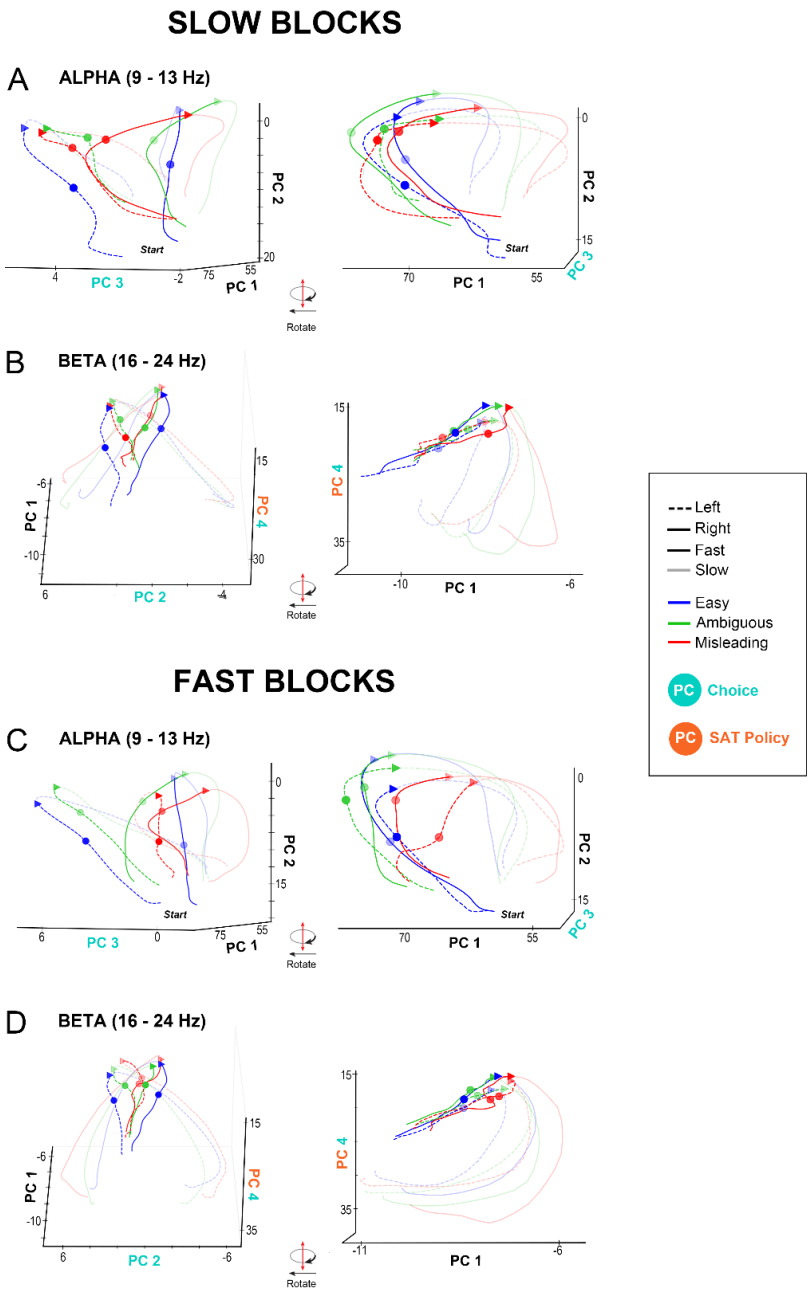


**Figure S9. Neural trajectories of alpha and beta PCs in neural state space for fast and slow blocks.** Neural trajectories of alpha PCs 1, 2 and 3 and beta PCs 1, 3 and 4, locked on button press [-1200 to 1200 ms], for left or right choices in easy, ambiguous, and misleading trials, for slow (**A**, **B**) and fast blocks (**C**, **D**). Small colored circles indicate the region in which commitment occurs, and small colored triangles indicate the time of button press for each individual trial types. Black arrows indicate how neural trajectories unfold over time. Purple ellipses indicate the region in which commitment occurs (indicated for individual trial types by small colored circles) and green ellipses indicate the time of button press (indicated for individual trial types by small colored triangles). Right panel corresponds to a 90 degrees rotation of left panel.

# Chapitre 4

# Discussion générale

Ce travail de thèse, à travers les deux articles présentés, avait pour objectif de mettre en lumière les processus neuronaux qui caractérisent le processus de délibération et de décision entre plusieurs actions possibles chez l'humain. En utilisant deux paradigmes expérimentaux différents, et deux techniques d'enregistrement des signaux électrophysiologiques, soit l'EEG intracrânien et la MEG, nous avons pu aborder le processus de délibération sous plusieurs angles. L'objectif de cette discussion générale est de résumer les résultats principaux des deux articles de cette thèse, de discuter des implications de ces résultats dans le domaine de la prise de décision en neurosciences cognitives, et enfin de présenter les perspectives futures sous la forme d'un projet intitulé Cross The Ocean.

### 4.1 Choisir librement, simplement

Le premier article de cette thèse a pris le parti d'étudier la prise de décision entre deux actions dans un scénario particulièrement simple, afin d'arriver à étudier l'essence même d'une délibération entre deux options qui ont une valeur égale. Le paradigme expérimental, en permettant de dissocier la phase de délibération et la phase d'exécution du mouvement (saccade oculaire) à proprement parler, a permis de montrer les dynamiques neuronales qui caractérisent le fait de faire un choix libre et volontaire. En comparant le choix libre à (1) une condition dans laquelle les patients devaient planifier un mouvement selon une instruction donnée par un indice et (2) une condition contrôle dans laquelle les participants devaient « ne rien faire de spécial » pendant la phase de planification, nous avons pu isoler les corrélats neuronaux spécifiques du choix libre, en excluant l'activité neuronale liée à la préparation motrice, ou à l'apparition d'indices visuels. Le résultat principal de cette étude est l'observation d'une augmentation soutenue dans le temps de l'activité neuronale de haute fréquence (60-140 Hz) dans les aires frontales et pariétales lors d'un choix libre et volontaire. Cette augmentation soutenue était spécifique du choix libre puisque (1) dans la condition contrôle, aucune augmentation de l'activité haute fréquence n'était observée lors de la phase de planification, et (2) lorsque les participants devaient planifier un mouvement sur la base d'instructions données par un indice visuel, une augmentation de l'activité haute fréquence était également observée, mais celle-ci n'était pas soutenue à travers le temps. Ces résultats mettent en évidence l'importance de la

dynamique temporelle de l'activité neuronale lors du processus de délibération entre deux actions lors d'un choix libre et volontaire. Des analyses plus poussées ont aussi permis de déterminer que cette activité haute fréquence soutenue n'était pas générée par le fait de garder les alternatives possibles en mémoire, mais bien au processus de délibération en tant que tel. L'interprétation la plus probable des résultats obtenus lors de cette étude, en s'appuyant sur les théories existantes sur la sélection d'actions comme l'hypothèse de la compétition d'affordances (Shadlen et Newsome, 2001 ; Cisek, 2007 ; Costello et coll., 2013 ; Coulthard et coll., 2008 ; Cui et Andersen, 2008 ; Oliveira et coll., 2010 ; Pastor-Bernier et Cisek, 2011), est la suivante : lorsque les participants peuvent choisir entre deux options, ils délibèrent, et l'augmentation soutenue de l'activité haute fréquence dans les aires frontales et pariétales reflète la compétition entre plusieurs alternatives possibles (en l'occurrence, faire une saccade à droite ou à gauche). Cette compétition peut durer plusieurs secondes, jusqu'à ce qu'elle soit résolue, ce qui correspond au moment de s'engager dans un choix donné (à gauche ou à droite). Une baisse de l'activité relative est alors observée, avec un « retour à la normale » vers le niveau d'activité de base lorsque la compétition est résolue et que le choix a été fait. Lorsque la direction du mouvement est imposée par un indice visuel extérieur, aucune délibération n'intervient dans le sens ou le choix est « fait pour nous ». L'activité haute fréquence augmente alors pour une durée très courte et n'est pas soutenue dans le temps. En d'autres termes, on peut imaginer que la compétition entre deux options est tellement biaisée par l'apparition d'un indice extérieur indiquant la direction de la saccade subséquente, que l'activité neuronale n'augmente que très brièvement avant de retourner à son niveau de base.

Un autre aspect crucial de cette première étude concerne l'analyse de l'activité liée à l'exécution de la saccade oculaire, intervenant après l'apparition d'un deuxième indice visuel, le « go signal ». Dans cet article, nous avons montré que l'activité haute fréquence de certaines régions frontales, pariétales et motrices, impliquées dans la sélection entre plusieurs actions lors de phase de planification était aussi responsable de l'exécution du mouvement moteur, soit une saccade oculaire. De plus, nous avons montré que le processus de sélection d'action lors de la phase de planification avait une influence directe sur l'activité des régions frontopariétales et motrices lors de l'exécution du mouvement moteur. En effet, lors des conditions dans lesquelles les participants avaient sélectionné une action, soit en faisant un choix libre, soit en suivant les instructions données par l'indice visuel, l'activité haute

fréquence au moment de l'exécution était plus faible que lors de la condition contrôle. Rappelons que lors de la condition contrôle les participants voyaient un premier indice visuel leur indiquant de « ne rien faire de spécial » pendant la phase de planification, puis, après un certain délai, voyaient apparaître le deuxième indice visuel (le go signal) leur indiquant de faire une saccade dans une direction donnée. Nos résultats indiquent donc un potentiel mécanisme de chevauchement: lorsque des ressources ont été mobilisées pendant la phase de planification pour sélectionner une action, celles-ci ne sont pas autant réutilisées lors de la phase d'exécution. Ces résultats sont particulièrement intéressants, puisqu'ils vont à l'encontre des théories cognitivistes selon lesquelles la perception, la cognition et l'action sont considérées comme des processus distincts et fonctionnant en séquentiel (Fodor, 1983 ; Pylyshyn, 1984). En effet, alors même que les exigences expérimentales du paradigme utilisé font en sorte que l'étape de planification et l'étape de l'exécution soient strictement séparées, nous avons observé un chevauchement et une dynamique de déplacement dynamique **d**e l'activité neuronale des régions responsables de ces deux processus. Ces observations sont donc en faveur des théories selon lesquelles la prise de décision est un processus intégré: (1) le processus de compétition entre les alternatives possibles se déroulerait dans les mêmes régions cérébrales que celles qui spécifient les actions (Cisek, 2006, 2007a), et (2) la prise de décision, loin d'être un processus cognitif abstrait et isolé, influencerait directement l'activité du système sensorimoteur (Gold et Shadlen, 2000, Platt et Glimcher, 1999, Salinas et Romo, 1998, Wallis et Miller, 2003).

Enfin, l'ensemble des résultats de cet article permettent d'établir un lien entre l'activité neuronale enregistrée (1) chez le singe (enregistrement unitaire) lors de la préparation et l'exécution de saccades oculaires (Schall et Bichot, 1998 ; Platt et Glimcher, 1999 ; Coe et coll., 2002 ; Dorris et Glimcher, 2004 ; Sugrue et coll., 2004), et (2) chez l'humain à l'aide de techniques de neuroimagerie non invasive comme l'IRMf (Milea et coll., 2007 ; Khonsari et al., 2007) et la MEG (Carl et coll., 2016), en bénéficiant d'une résolution spatiale, temporelle et fréquentielle inégalable. En effet, plusieurs études ont suggéré que l'activité haute fréquence reflète une augmentation globale d'activité neuronale dans le tissu cortical sous-jacent, pourrait donc être définie comme un marqueur de l'activité unitaire mesurée chez le singe (Kucewicz et coll., 2017 ; Manning et al., 2009 ; Mukamel et coll., 2005 ; Nir et coll., 2007 ; Ray & Mansell, 2011 ; Ray et coll., 2008). En accord avec ces travaux, nous pensons que l'activité haut gamma soutenue observée lors du choix libre dans notre étude reflète l'activité unitaire

de réseaux neuronaux locaux dans les couches superficielles du cortex qui peut être enregistrée chez le primate non humain. D'autre part, nous avons aussi proposé un lien entre l'activité haut gamma et le signal BOLD enregistré par l'IRMf grâce à deux études en particulier, utilisant exactement le même paradigme expérimental que dans l'article présenté (Milea et coll., 2007 ; Khonsari, 2007). Les résultats de celles-ci indiquaient une augmentation du signal BOLD (signal qui reflète les variations de la quantité d'oxygène transporté par l'hémoglobine en fonction de l'activité neuronale du cerveau) spécifique au choix libre dans les aires préfrontales (cortex dorsolatéral préfrontal), frontales (champs oculaires) et pariétales (sulculs intrapariétal). La correspondance spatiale entre les résultats de l'article présenté dans cette thèse et ceux de l'étude IRMf est remarquable, et confirme l'implication de ces régions lors du processus de délibération, tout en renforçant le lien entre l'activité haute fréquence (mesurée par l'EEG intracrânien) et le signal BOLD mesuré par l'IRMf (Kayser et coll., 1991 ; Lachaux et al., 2007 ; 2012 ; Logothethis et coll., 2001 ; Mukamel et coll., 2005 ; Niessing et coll., 2005 ; Ojemann et coll., 2013). De plus, l'utilisation de l'EEG intracrânien a permis de caractériser les dynamiques temporelles et fréquentielles de l'activité neuronale, ce qui n'est pas possible avec l'IRMf à cause de limitations inhérentes à la méthode d'acquisition du signal cérébral.

### 4.2 Vers une approche plus écologique de la prise de décision dynamique

Dans le deuxième article de ce travail de thèse, nous avons utilisé la magnétoencéphalographie pour enregistrer le signal cérébral de participants humains alors qu'ils effectuaient une tâche de prise de décision dynamique : la tâche des jetons. Dans cette tâche, l'objectif était de deviner laquelle des deux cibles périphériques (gauche ou droite) allait recevoir la majorité des 15 jetons, qui sautent du cercle central à l'une des deux cibles toutes les 200 ms. Les sujets pouvaient répondre à n'importe quel moment, leur objectif étant d'obtenir le plus de bonnes réponses possibles le plus rapidement possible (voir Figure 6 pour plus de détails). L'évidence sensorielle en faveur ou contre un choix donné (gauche ou droite par exemple) variait au cours du temps, au sein d'un même essai, se rapprochant ainsi de situations réelles dans lesquelles l'information provenant du monde extérieur dans lequel on évolue peut changer à tout moment. Ces changements dans l'évidence sensorielle exigent une certaine flexibilité, et nécessitent l'implémentation d'un compromis entre vitesse et précision afin de

maximiser la fréquence de récompenses. En effet, lors de situations écologiques, il est souvent crucial de faire le choix le plus juste possible, mais aussi le plus rapidement possible, afin d'optimiser non pas chaque décision indépendamment, mais plutôt la fréquence de succès résultant des choix que nous faisons. L'objectif principal du deuxième article était donc d'analyser les caractéristiques fondamentales du processus décisionnel lors de situations dynamiques de prise de décision, soit la ***délibération*** entre plusieurs actions, ***l'engagement dans un choix***, ***l'exécution du mouvement moteur*** permettant d'exprimer ce choix, et enfin ***l'implémentation d'un compromis entre vitesse et précision*** afin d'optimiser son taux de succès. Pour ce faire, nous avons extrait les oscillations cérébrales du signal MEG (voir encadré page 30), dans les bandes de fréquences suivantes : thêta (5-8 Hz), alpha (9-13 Hz), bêta (16-24 Hz), gamma (30-60 Hz) et haut gamma (60–100 Hz). Nous avons ensuite utilisé une technique de réduction de dimensionnalité, l'analyse en composantes principales (PCA), pour identifier les composantes principales des oscillations de l'activité cérébrale, correspondant à chacun des processus fondamentaux intervenant lors de prise de décision dynamique. Cette méthode d'analyse, de plus en plus utilisées au cours de ces dernières années chez l'animal, permet d'identifier et de caractériser les composantes principales de l'activité neuronale qui expliquent une part significative de la variance neuronale (Cunningham & Yu, 2014; Gallego et al., 2017). En réduisant la dimensionalité de l'activité neuronale observée, il est alors possible de représenter les changements de trajectoires des composantes principales dans un espace neuronal à faible dimensionnalité, et de lier ces changements aux processus cognitifs sous-jacents comme l'exécution d'un mouvement moteur (Churchland et al., 2010, 2012; Kaufman et al., 2014), la discrimination d'odeur dans le système olfactif (Broome et al., 2006; Mazor & Laurent, 2005; Saha et al., 2013), ou encore la prise de décision (Briggman et al., 2005; Harvey et al., 2012; Stokes et al., 2013), et notamment la sélection et l'intégration de l'input sensoriel dans le cortex préfrontal chez le singe (Mante et al., 2013). Dans ce travail de thèse, nous avons utilisé la PCA sur des données MEG chez l'humain et montré que certaines composantes des oscillations alpha et bêta dans les régions visuelles et sensorimotrices permettaient de coder les changements de ***l'évidence sensorielle*** provoqués par les sauts successifs de jetons lors de la ***délibération***. D'autre part, nous avons mis en évidence le rôle des oscillations alpha dans ***l'engagement dans un choix donné***, et le rôle des oscillations bêta dans la préparation et ***l'exécution du mouvement moteur permettant d'exprimer son choix*** (appui bouton avec l'index gauche ou droit).

Enfin, nous avons montré que l'activité cérébrale dans les hautes fréquences dans les régions sous-corticales était modulée en fonction du ***compromis vitesse/précision*** adopté par les participants.

Nous avons pu interpréter ces résultats à la lumière des études réalisées chez des singes effectuant la même tâche expérimentale et du modèle d'urgence, formulé de la manière suivante :

$$x_i(t) = g \cdot E_i(t) \cdot u(t)$$

L'activité neuronale $x_i(t)$ est donc le produit *(1)* d'un signal d'urgence $u(t)$, indépendant de l'évidence sensorielle provenant du stimulus et dont le but est de « pousser » à agir, et *(2)* de l'évidence sensorielle $E_i(t)$, filtrée par un filtre passe-bas et qui intègre uniquement l'information nouvelle. Celle-ci est obtenue via l'analyse perceptive afin d'identifier l'alternative la plus avantageuse. La dynamique temporelle des composantes dans les bandes alpha et beta au sein des régions visuelles, du PCC et des régions sensorimotrices correspondraient au paramètre $\boldsymbol{E_i(t)}$, permettant de coder l'évidence sensorielle, et plus précisément la probabilité de succès en fonction de la distribution des jetons ayant déjà sauté dans l'une des deux cibles (droite ou gauche). Ces résultats sont en accord avec la littérature sur le rôle des oscillations alpha et bêta dans le traitement de l'information sensorielle au sein des régions visuelles (Murphy et coll., 2016 ; Wilming et al., 2020) et sensorimotrices (Donner et coll., 2009 ; Gould et coll., 2012 ; de Lange et coll., 2013) chez l'humain. Plus récemment, une étude a aussi mis en avant le rôle du cortex cingulaire postérieur (PCC) dans le traitement et l'accumulation d'évidence sensorielle (Bitzer et coll., 2020). Cette région, peu mentionnée dans les études existantes dans le domaine de la prise de décision, pourrait effectivement jouer un rôle crucial dans le processus décisionnel puisqu'elle permettrait d'estimer le besoin de changer son comportement en fonction de nouvelles exigences dictées par l'environnement externe (Pearson et coll., 2011). Ces résultats viennent aussi confirmer certains résultats obtenus dans les études effectuées chez le singe, notamment par rapport au rôle des neurones situés dans les régions sensorimotrices dans le codage de l'évidence sensorielle lors des tâches classiques (Gold et Shadlen, 2007) et dynamiques (Thura et coll., 2014). En revanche, des résultats récents chez le singe ont montré que les neurones situés dans le dlPFC permettaient aussi de suivre l'évidence sensorielle au cours du temps, ce que nous n'avons pas observé dans notre étude. Selon nous, cette

différence interespèces est particulièrement intéressante, et pourrait être expliquée par les différences anatomiques bien connues entre l'humain et le singe au niveau du cortex préfrontal. Ces dissimilitudes pourraient aussi être dues à au surentraînement des singes à la tâche des jetons, puisque ceux-ci doivent passer plusieurs centaines d'heures avant de maîtriser le paradigme expérimental, alors que les humains sont capables de l'effectuer sans aucun entraînement préalable. L'activité du dlPFC présente chez le singe, mais pas chez l'humain pourrait donc refléter une différence dans la mobilisation des ressources cognitives demandées par la tâche. Mesurer l'importance et le rôle du dlPFC au cours de l'apprentissage chez le singe et chez l'humain pourrait permettre de répondre à cette question. Cette interprétation serait en accord avec les nombreux travaux ayant établi le rôle du dlPFC dans le contrôle cognitif et l'apprentissage (Ridderinkhofa et coll., 2004).

Ensuite, nous avons montré que même si certaines composantes des oscillations alpha et bêta permettaient de suivre l'évidence sensorielle, l'activité dans ces bandes de fréquence se distinguait par ailleurs. En effet, les composantes principales des oscillations dans la bande alpha indiquaient une activité liée au fait de s'engager dans un choix en particulier, générée par les régions postérieures internes qui incluent les régions visuelles, le cortex cingulaire postérieur, le cuneus, et le précuneus. Ces résultats peuvent être interprétés à la lumière de la littérature sur le rôle fonctionnel des oscillations alpha dans l'inhibition, permettant de réduire les capacités de traitement de certaines aires cérébrales au profit d'autres (Jensen et Mazaheri, 2010). D'après nos données, l'augmentation de l'activité alpha permettrait de supprimer l'activité des régions postérieures et le traitement de l'évidence sensorielle : le pic d'activité alpha correspondrait alors au moment de l'engagement dans un choix, et permettrait de mobiliser les ressources nécessaires pour déclencher l'exécution d'un mouvement moteur. L'exécution du mouvement moteur permettant d'appuyer sur un bouton pour signifier son choix, d'après nos résultats, serait générée par les oscillations dans la bande bêta dans les aires sensorimotrices. En effet, la dynamique temporelle des CPs bêta correspond aux signatures caractéristiques de la préparation et de l'exécution motrice lors de mouvements volontaires (Kivalik et coll., 2013) : une baisse d'activité bêta jusqu'au mouvement moteur, typique de la préparation motrice, est suivie d'un « rebond » bêta, qui permettrait de restaurer l'activité du réseau sensorimoteur à son niveau de base (Gaetz and Cheyne, 2006). Cette interprétation du rebond bêta

correspond à la trajectoire des CPs bêta dans l'espace neuronal, qui se « courbent » pour revenir à leur point de départ après l'exécution de l'appui bouton (figure 5 dans notre article 2).

Enfin, le signal d'urgence $\boldsymbol{u}(\boldsymbol{t})$, serait pour sa part modulé par le compromis vitesse/décision au sein des régions sous-corticales dans les bandes de haute fréquence (bêta, gamma, haut gamma). Plus précisément, une différence significative était observée entre l'activité pendant les blocs d'essais favorisant des réponses plus lentes et plus prudentes et les blocs d'essais favorisant des réponses plus rapides et plus risquées dans le cervelet, le pallidum, le noyau caudé et le thalamus. Ces résultats viennent confirmer l'existence d'un signal d'urgence neuronal pour ajuster le compromis vitesse/précision en fonction des demandes de l'environnement et la pression temporelle chez le primate non humain (Churchland et coll., 2008 ; Heitz et Schall, 2012 ; Hanks et coll., 2014), y compris lorsque ceux-ci réalisaient la tâche des jetons (Thura et Cisek, 2014 ; 2016). Peu d'études sur les mécanismes neuronaux permettant d'implémenter un compromis entre vitesse et précision ont été réalisées chez l'humain à ce jour, mais récemment, Murphy et coll. ont utilisé des enregistrements EEG lors d'une tâche KPMA avec ou sans pression temporelle. Les résultats de leur étude corroborent les nôtres en montrant l'implémentation d'un signal d'urgence représenté au niveau des capteurs situés au-dessus des régions motrices latérales dans la bande alpha (8-14 Hz).

Dans l'ensemble, notre étude a pour la première fois permis de caractériser les signatures neuronales de la prise de décision dynamique chez l'humain, permettant ainsi d'étendre nos connaissances sur les mécanismes qui permettent d'interagir avec un environnement qui évolue au cours du temps. Nos résultats viennent confirmer et étendre les postulats du modèle d'urgence, en montrant qu'il existe des corrélats neuronaux reflétant (1) les modulations du compromis vitesse précision dans les régions sous-corticales et (2) les fluctuations de l'évidence sensorielle au cours du temps dans un réseau de régions visuelles et sensorimotrices. Ces deux composantes permettent l'implémentation d'une compétition entre les options possibles au sein du système sensorimoteur, qui résulte en un engagement dans un choix reflété par l'activité alpha, et un mouvement moteur reflété par l'activité bêta. Nos résultats vont dans le sens des théories qui considèrent la prise de décision comme étant un processus intégré, parallèle, et distribué à travers plusieurs régions cérébrales clefs (Cisek et coll., 2007).

### 4.3 Perspectives

Ce travail de thèse avait pour objectif de mettre en lumière les mécanismes neuronaux qui sous-tendent la prise de décision chez l'être humain, avec la volonté assumée d'étudier les décisions se rapprochant le plus possible de situations naturelles. Alors que le premier article a utilisé une tâche de décision simple, dans laquelle il était possible de séparer le processus de délibération du processus d'exécution d'une action, le deuxième article a utilisé une tâche de décision dynamique, dans laquelle les stimuli représentaient une information sensorielle qui peut changer brusquement au cours du temps. Ces travaux de recherche ont permis de susciter de nombreuses réflexions à propos des multiples facettes de la prise de décision. Dans cette partie, nous proposons d'en aborder quelques-unes.

D'abord, l'un des aspects cruciaux de la prise de décision abordés dans cette thèse concerne la relation qu'elle entretient avec la notion de libre arbitre. En effet, une décision pourrait être considérée comme « libre » par défaut. Si l'on ne peut pas choisir, alors par définition on ne prend pas de décisions. Pourtant, notre premier article et bien d'autres études suggèrent une interprétation plus nuancée du sens que l'on donne au libre arbitre. Dans notre étude, on considère qu'une décision libre, est une décision ou le sujet choisit d'effectuer une saccade vers la gauche ou vers la droite, par rapport à une autre condition (« guidée ») ou un indice visuel indique au sujet la direction vers laquelle il devra effectuer une saccade. Même dans un scénario aussi simple, il est légitime de se demander si la décision dans la première condition est vraiment libre (Haggard, 2019). Par exemple, lorsque le sujet n'a le choix qu'entre deux options : la décision serait-elle plus libre si celui-ci avait le choix entre 10 options ? Et 100 ? Ces réflexions permettent d'introduire des notions comme le degré de liberté (Lavazza, 2016). On pourrait penser que la condition « libre » de notre expérience a plus de degrés de liberté que la condition « guidée ». Mais moins de degrés de liberté qu'une situation où l'on aurait le choix entre plusieurs ingrédients pour préparer un repas. Bien sûr, le degré de liberté n'augmente pas linéairement en fonction du nombre d'options, et l'on peut imaginer qu'avoir milles options nous rendrait moins libre qu'en avoir trois à cause de la difficulté inhérente à un nombre d'options trop élevé. De plus, de nombreuses études ont montré que le libre arbitre s'apparenterait plutôt à un

sentiment d'agence (c. à d., l'impression d'être la cause d'effets observables) qu'à une réalité factuelle (Harris, 2012; Wegner, 2002). En psychologie d'abord, puis en neuroscience, cette idée a été mise à l'épreuve par de nombreuses expériences cherchant à mieux comprendre la dynamique de l'activité cérébrale au moment de prendre une décision librement (Libet, 1999), c'est-à-dire avant d'effectuer une action pour concrétiser un choix donné. Plus récemment, des chercheurs ont montré que l'activité cérébrale lors d'une action effectuée volontairement pouvait varier en fonction des croyances des participants sur leur sentiment d'agence. Par exemple, une activité cérébrale différente a été observée si le participant pensait que le bouton sur lequel il appuie avait provoqué un bip sonore, ou s'il pensait qu'il n'y avait aucun lien entre les deux (Haggard, 2008, 2019; Soon et al., 2008). Les perspectives qu'offrent ces études pour notre compréhension de la prise de décision sont innombrables, et pourraient permettre de répondre à des questions longtemps abordées par les philosophes en utilisant des méthodes quantitatives.

Ce travail de thèse a aussi voulu montrer l'importance des méthodes d'acquisition et d'analyse du signal cérébral, en insistant sur l'avantage important qu'ont les techniques d'enregistrement électrophysiologiques et non invasives chez l'humain. En effet, dans l'étude de la prise de décision, l'information est cruciale, et souvent les techniques bénéficiant d'une résolution temporelle plus faible comme l'IRMf ne sont pas en mesure de détecter des changements rapides dans le traitement de l'évidence sensorielle. De plus, l'utilisation de techniques comme la MEG permettent de capturer le signal cérébral de tout le cortex, contrairement aux enregistrements unicellulaires chez le primate, qui se concentrent sur une région spécifique. Dans les deux études de cette thèse, nous avons montré que des réseaux de régions étaient impliqués dans les processus majeurs de la prise de décision : une activité cérébrale soutenue dans un réseau fronto-pariétal permet de caractériser les décisions libres (voir article 1), un ensemble de régions sensorimotrices permet de délibérer entre plusieurs options puis d'effectuer un mouvement (voir article 2), etc. Ces résultats sont en accord avec les théories qui soutiennent que l'idée qu'une région équivaut à une fonction serait simpliste, et que le cerveau devrait plutôt être envisagé en tant que réseau dynamique (Varela et coll., 2001). Il serait intéressant, des de futures études, d'étudier les interactions entre ces différentes régions, en utilisant des méthodes de connectivité fonctionnelles (mesures de cohérence, de phase) et effectives (connectivité

de Granger, outils issus de la théorie de l'information) pour quantifier les interactions des différentes régions cérébrales qui sous-tendent les mécanismes à l'origine de nos prises de décision.

Enfin, cette thèse prend le parti d'adopter une perspective écologique afin d'insister sur son importance dans le domaine des neurosciences contemporaines. En effet, le second article inclus dans ce travail de thèse propose d'aborder la prise de décision dynamique, afin de mieux comprendre les mécanismes comportementaux et cérébraux impliqués lors de situations plus proches de celles qu'on peut rencontrer dans un environnement naturel. Cette approche écologique a historiquement occupé une place relativement faible dans le domaine des neurosciences, pour des raisons conceptuelles (que nous avons explicitées dans l'introduction), mais surtout pour des raisons techniques. Encore aujourd'hui, le fait de devoir limiter le plus possible des mouvements des participants humains ou non humains lors d'enregistrements cérébraux constitue une limite majeure au développement de paradigmes expérimentaux plus écologiques. Pourtant, récemment, certains chercheurs et ingénieurs ont redoublé de créativité pour inventer des solutions permettant d'enregistrer l'activité cérébrale de singes entièrement libres de leurs mouvements (Courellis et coll., 2019; Ludvig et al., 2001), ou d'humains se déplaçant dans une pièce ou à travers un campus accompagnés d'un sac à dos dans lequel se trouve un système d'enregistrement iEEG (Aghajan et coll., 2017; Topalovic et al., 2020). De nouvelles technologies d'acquisition du signal non invasives ont également fait leur apparition au cours des dernières années, avec par exemple la conception de nouveaux capteurs MEG appelés SQUID, pouvant être fixés directement sur le crâne, ce qui permet de suivre les mouvements du crâne et produit moins d'artefacts (Boto et coll., 2016). Une autre approche consiste à utiliser des environnements virtuels immersifs ou sous forme de jeux vidéo. Cette approche est adoptée par de plus en plus de chercheurs, surtout dans le domaine de la navigation, car elle permet de reproduire des situations écologiques tout en gardant un contrôle très précis des paramètres qui définissent le design expérimental (Bellmund et coll., 2020). Dans la partie suivante, nous proposons un exemple de projet qui utilise le jeu vidéo 3D pour étudier la prise de décision lors de situations naturelles.

### 4.4 Le projet Cross The Ocean

Pour aller plus loin dans la caractérisation des processus mentaux au sein d'environnements écologiques et naturels, la dernière partie de ce travail de thèse a pour objectif de présenter un projet qui a pour objectif de proposer un exemple des nombreuses études qui pourraient découler des apports théoriques et méthodologiques de la thèse qui a été présenté. Le projet Cross The Ocean a pour objectif d'aller encore plus loin dans l'analyse de nos prises de décisions lorsque nous nous trouvons dans des situations écologiques. En effet, celui-ci propose d'utiliser une tâche expérimentale sous la forme d'un jeu vidéo dans lequel les participants incarnent un avatar dans un monde virtuel en 3D. Cette utilisation du jeu vidéo permet d'évoluer dans un monde virtuel se rapprochant au plus près de situations que nous sommes susceptibles de vivre réellement lorsque nous prenons des décisions dans des milieux écologiques. Le but du jeu Cross The Ocean est simple : comme son nom l'indique, l'avatar contrôlé par les participants doit traverser l'océan le plus vite possible, en sautant de pierre en pierre sans tomber dans l'eau empoisonnée pour atteindre sa maison, située sur une île paradisiaque (voir Figure 9). Pour reproduire des conditions de contrainte temporelle similaires à celles du second article présenté dans cette thèse, on pourrait également implémenter une « marée montante », qui forcerait les participants à aller le plus vite possible (i.e., signal d'urgence).

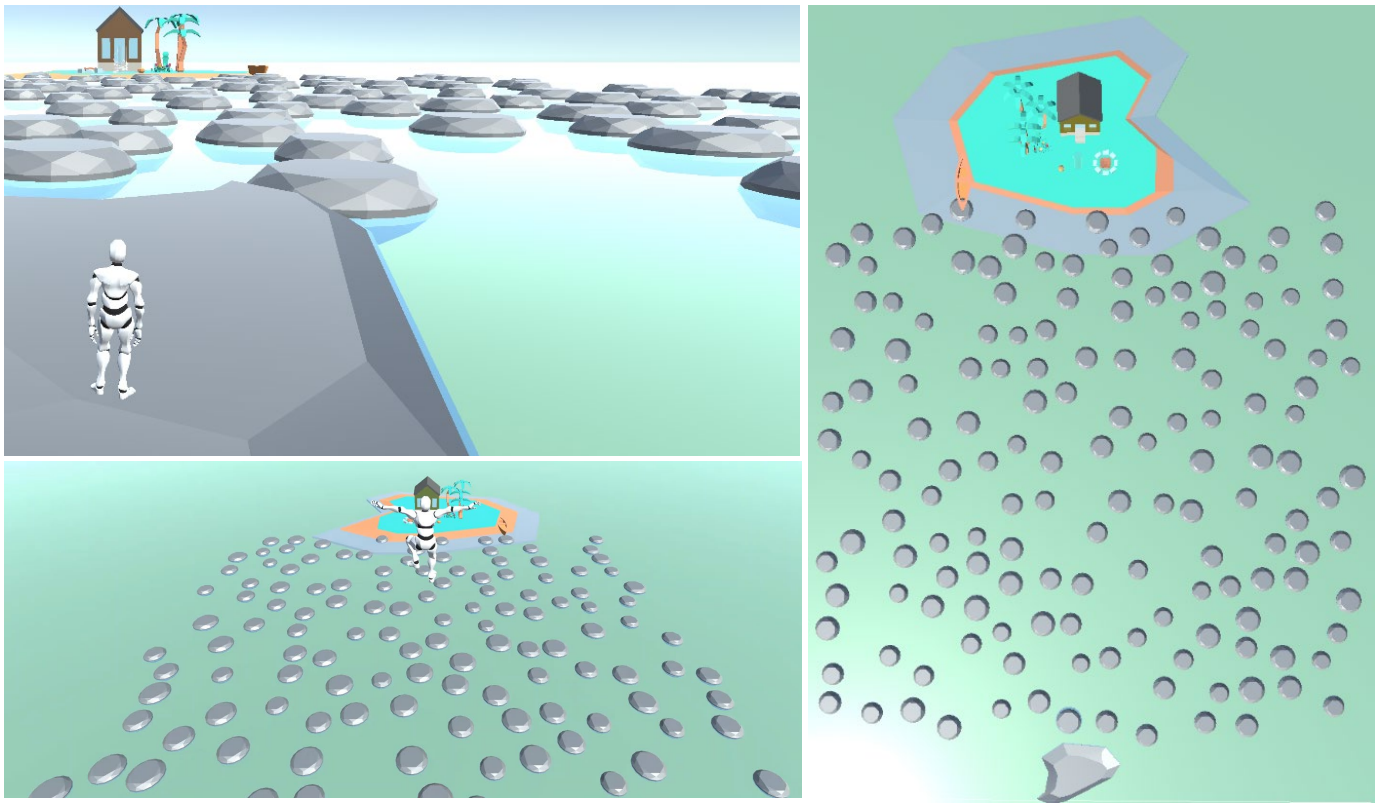

**Figure 9. Capture d'écran du jeu vidéo 3D Cross The Ocean**, dans lequel les participants contrôlent un avatar et doivent sauteur de pierre en pierre pour atteindre leur l'île le plus vite possible, sans tomber dans l'eau empoisonnée.

À chaque essai, l'objectif est donc d'atteindre l'île le plus vite possible, en prenant des décisions qui s'enchaînent, sur le qui-vive, pour choisir de sauter sur certaines pierres plutôt que d'autres en fonction de leur « valeur », c'est-à-dire leur potentiel de faire avancer l'avatar vers l'objectif le plus vite possibles et sans tomber dans l'eau. Les décisions que doivent prendre les participants sont donc conditionnées par les possibilités d'action, ou affordances, directement déterminées par la géométrie de l'environnement (c.-à-d., l'emplacement des pierres) dans lequel l'avatar évolue. Le premier volet de ce projet a pour ambition de modéliser les comportements d'humains qui jouent à Cross The Ocean, en répondant aux questions suivantes : comment choisissent-ils les pierres sur lesquelles ils vont sauter pour atteindre leur objectif au plus vite ? Le font-ils de manière optimale ? À quel point arrivent-ils à planifier ce qu'ils vont faire dans le futur, en prenant en compte les pierres qui sont plus loin d'eux ? Quel est le rôle de l'apprentissage ? L'approche que nous avons choisie pour aborder des interrogations consiste à entraîner plusieurs agents artificiels sur le jeu Cross The Ocean, afin de

comparer leurs performances à celles des participants, comme le taux de succès et le temps qu'ils mettent pour atteindre leur objectif, l'île paradisiaque. Un agent artificiel performant devrait donc être en mesure d'utiliser un modèle simple afin (1) d'évaluer sa propre capacité à pouvoir naviguer au sein de son environnement et (2) de mesurer la qualité des actions qu'il a entrepris (en évaluant la distance parcourue par rapport à l'objectif). Dans des travaux préliminaires, nous avons montré que cela peut être réalisé par un agent qui utilise un modèle « convolutionnel à déploiements » (« Convolutional successor rollouts ») pour naviguer efficacement à travers son environnement. Ce modèle combine l'utilisation (1) d'un simple filtre 2D autour de l'avatar (voir Figure 10), qu'il est facilement possible de superposer à l'environnement visible localement pour évaluer les possibilités d'actions et (2) d'un moyen de planifier ses actions futures, en se déployant à travers l'environnement pour évaluer et maintenir en mémoire la valeur des pierres qui sont devant lui. L'utilisation d'agents artificiels permet d'ajuster les paramètres du modèle qu'ils utilisent en se basant sur les données comportementales des participants humains. Cela permettra de quantifier précisément les règles dont se servent les participants au cours de leur apprentissage du jeu, mais aussi le degré de planification requis pour emprunter la meilleure trajectoire possible, ou encore les différentes stratégies utilisées par les individus.

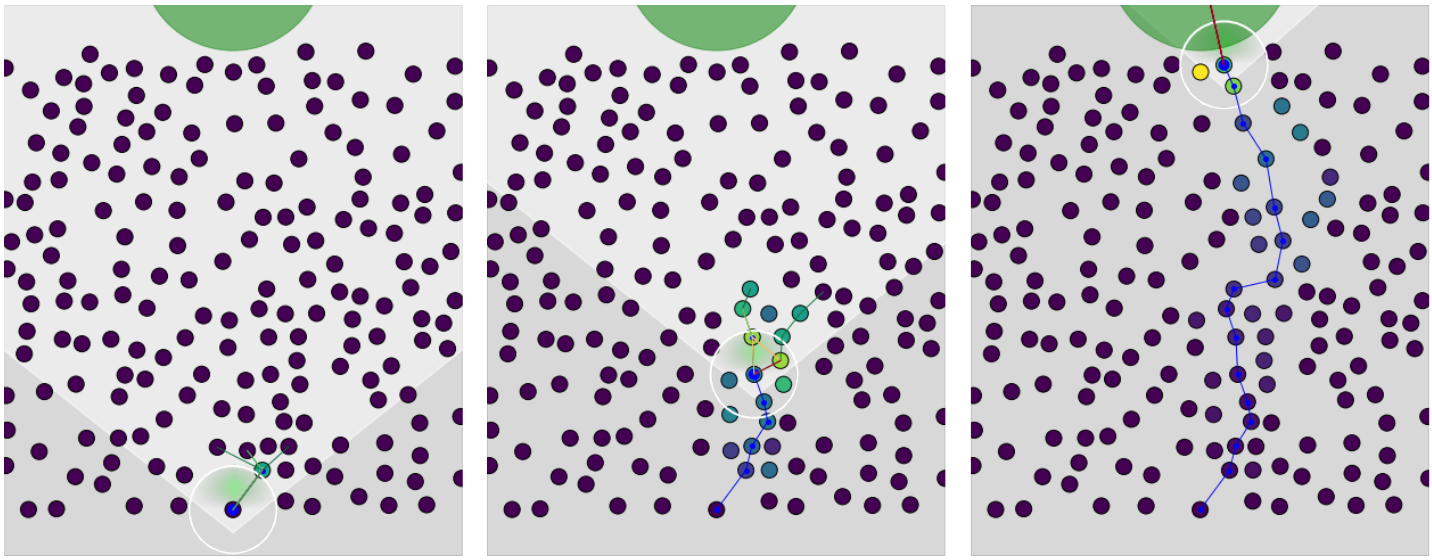

**Figure 10. Capture d'écran du jeu vidéo 3D Cross The Ocean**, dans lequel les participants contrôlent un avatar et doivent sauteur de pierre en pierre pour atteindre leur l'île le plus vite possible, sans tomber dans l'eau empoisonnée.

Une fois que nous aurons caractérisé et modélisé le comportement de participants humains lorsqu'ils jouent à Cross The Ocean, le deuxième objectif principal du projet est de mesurer le signal cérébral EEG (intracrânien) et MEG afin de caractériser les processus neuronaux qui sous-tendent la navigation et la prise de décision lors de situations écologiques chez l'humain. Cette recherche permettra de faire le lien entre deux lignes de recherches qui ont été menées séparément dans le domaine des neurosciences cognitives : soit l'étude des corrélats neuronaux à l'origine des représentations ***allocentriques*** (centré sur l'environnement, vue du dessus comme sur une carte) et ***égocentriques*** (centré sur soi, vue « à la première personne ») de l'environnement. En effet, une première ligne de recherche, établie par les travaux fondateurs d'O'Keefe et Nadel (1978), a permis de mettre en lumière le rôle crucial de l'hippocampe et ses structures corticales adjacentes dans les représentations ***allocentriques*** de l'environnement lors de tâches de navigation spatiale chez le rongeur. Certains neurones situés dans l'hippocampe, appelés « cellules de localisation » (c.-à-d., « place cells »), s'activent uniquement lorsque le rongeur passe à un endroit spécifique de l'espace (O'Keefe et Dostrovsky, Brain Res., 1971). D'autres neurones, les « cellules de grille » (« grid cells ») dans le cortex entorhinal médian, s'activent dans un ensemble de petites régions (champs d'activation) qui sont à peu près de taille égale et sont disposées dans un arrangement triangulaire périodique qui couvre l'ensemble de l'environnement disponible. Ce maillage de l'environnement spatial, représenté dans le cerveau grâce aux cellules de localisation et de grille permet donc de se situer dans l'espace. Au cours des dernières années, les chercheurs ont mis en lumière plusieurs autres cellules qui codent pour les propriétés allocentriques de l'environnement spatial dans l'hippocampe : certaines cellules codent pour la direction de la tête, pour la position de l'animal par rapport à un objet ou une récompense (Taube et coll., J. Neurosci., 1990 ; Lever et coll., J. Neurosci., 2009 ; Gauthier et Tank, Neuron, 2018). Chez l'humain, un codage qui correspond aux cellules de grille a récemment été observé chez l'homme à l'aide d'enregistrements unitaires chez des patients épileptiques (Ekstrom, Nature, 2003 ; Jacobs et al., Nat. Neurosci., 2013) et de techniques d'imagerie cérébrale non invasive comme l'IRMf (Doeller et coll., Nature, 2010) et la MEG (Nau et al., Nat. Neurosci., 2018). Une seconde ligne de recherche indépendante s'est développée en parallèle, ayant pour objet d'étude la représentation des éléments situés dans un espace donnée par rapport à son propre corps (égocentrique). En effet, les neurones du

cortex pariétal et sensorimoteur permettent de coder l'emplacement d'un objet par rapport à soi : à gauche ou à droite, proche ou loin, en haut ou en bas (Amorapanth et coll., 2010 ; Colby et Goldberg, 1999 ; Schindler et Bartels, 2013 ; Spiers et Maguire, 2007). À la lumière de l'hypothèse de la compétition d'affordances, ces résultats permettent de mieux comprendre comment le cerveau représente les différents objets, et les différentes possibilités d'actions avant de prendre une décision. Selon la littérature, le cortex pariétal pourrait donc être impliqué dans la représentation égocentrique des affordances, afin que celles-ci puissent entrer en compétition jusqu'à ce que l'une d'entre elles l'emporte, et que la décision soit prise.

Le projet Cross The Ocean est ancré dans le constat suivant : lors de situations du monde réel, lorsque vous faites du sport, que vous marchez dans une foule pour trouver un ami à un concert ou que vous partez en vacances en voiture, il est raisonnable de partir du principe que les représentations allocentriques (formation hippocampale) et égocentriques (cortex pariétal et sensorimoteur) soient sollicitées simultanément pour atteindre vos objectifs et marquer un but, profiter du concert à côté de vos amis ou arriver à votre destination de vacances rêvée. Pourtant, ces deux types de représentations et leurs corrélats neuronaux ont été étudiés séparément. La plupart des études de navigation ont été menées à l'aide de paradigmes expérimentaux dans lesquels les affordances ne sont pas explicitement spécifiées par la géométrie de l'environnement (p. ex., les arènes, les labyrinthes). Choisir où aller ou quoi faire est donc souvent déterminé par une récompense placée arbitrairement à un endroit donné. En contrepartie, les études d'imagerie cérébrale visant à comprendre les fondements neuronaux des décisions entre plusieurs actions chez l'humain n'impliquent que très peu souvent une dimension de navigation spatiale, à cause des limitations de mouvement lors de protocoles de neuroimagerie invasifs et non invasifs. En utilisant un jeu vidéo 3D comme Cross The Ocean, l'objectif est d'élucider les interactions entre les systèmes cérébraux allocentriques et égocentriques lors de prise de décision dynamique dans un environnement écologique.

Dans ce travail de thèse, nous nous sommes intéressés aux dynamiques cérébrales qui reflètent les processus décisionnels chez l'humain. Pour ce faire, nous avons combiné des enregistrements de l'activité électrophysiologique du cerveau (EEG intracrânien et MEG) et des techniques computationnelles avancées pour analyser ces données, comme l'apprentissage machine ou des méthodes de réduction de dimensionnalité. Cela nous a permis d'identifier, de caractériser, et de

dissocier les processus clés qui interviennent lors de la prise de décision, y compris lors de situations plus proches du monde réel, lorsque nous devons délibérer en prenant en compte les changements dynamiques de l'information sensorielle que nous percevons. C'est dans cette perspective plus générale que ce travail s'inscrit, avec la volonté assumée de s'ancrer dans une perspective évolutionniste et écologique, et en soutenant la proposition que les décisions naissent d'une interaction dynamique entre la perception et l'action, plutôt que de cloisonner le processus de décision comme faisant partie d'une entité abstraite que serait la cognition. Cette thèse devrait être envisagée comme un point de départ pour d'autres travaux de recherches, qui auront pour objectif ***(1)*** d'étudier l'activité cérébrale lors de situations se rapprochant encore davantage de scénarii naturels (cf. le jeu vidéo Cross The Ocean), et ***(2)*** de profiter des enregistrements à l'échelle du cerveau en entier pour aller plus loin dans l'étude de l'interaction entre plusieurs régions cérébrales lors de la prise de décision chez l'humain, en utilisant des méthodes de connectivité fonctionnelles (mesures de cohérence, de phase) et dirigées (connectivité de Granger, outils issus de la théorie de l'information). Ce travail contribuera à l'avancement de notre compréhension des mécanismes neuronaux impliqués dans nos prises de décisions lors de situations de la vie de tous les jours chez l'humain.

# Références Bibliographiques


Akeju, O., Westover, M. B., Pavone, K. J., Sampson, A. L., Hartnack, K. E., Brown, E. N., & Purdon, P. L. (2014). Effects of Sevoflurane and Propofol on Frontal Electroencephalogram Power and Coherence. *Anesthesiology: The Journal of the American Society of Anesthesiologists*, *121*(5), 990–998. https://doi.org/10.1097/ALN.0000000000000436

Alkire, M. T., Hudetz, A. G., & Tononi, G. (2008). Consciousness and anesthesia. *Science (New York, N.Y.)*, *322*(5903), 876–880. https://doi.org/10.1126/science.1149213

Andersen, R. A., & Buneo, C. A. (2002). Intentional maps in posterior parietal cortex. *Annual Review of Neuroscience*, *25*, 189–220. https://doi.org/10.1146/annurev.neuro.25.112701.142922

Anderson, E. J., Jones, D. K., O'Gorman, R. L., Leemans, A., Catani, M., & Husain, M. (2012). Cortical network for gaze control in humans revealed using multimodal MRI. *Cerebral Cortex (New York, N.Y.: 1991)*, *22*(4), 765–775. https://doi.org/10.1093/cercor/bhr110

Ariani, G., Wurm, M. F., & Lingnau, A. (2015). Decoding Internally and Externally Driven Movement Plans. *Journal of Neuroscience*, *35*(42), 14160–14171. https://doi.org/10.1523/JNEUROSCI.0596-15.2015

Bak, P., Tang, C., & Wiesenfeld, K. (1987). Self-organized criticality: An explanation of the 1/f noise. *Physical Review Letters*, *59*(4), 381–384. https://doi.org/10.1103/PhysRevLett.59.381

Barttfeld, P., Uhrig, L., Sitt, J. D., Sigman, M., Jarraya, B., & Dehaene, S. (2015). Signature of consciousness in the dynamics of resting-state brain activity. *Proceedings of the National Academy of Sciences*, *112*(3), 887–892. https://doi.org/10.1073/pnas.1418031112

Bastin, J., Deman, P., David, O., Gueguen, M., Benis, D., Minotti, L., Hoffman, D., Combrisson, E., Kujala, J., Perrone-Bertolotti, M., Kahane, P., Lachaux, J.-P., & Jerbi, K. (2017). Direct Recordings from Human Anterior Insula Reveal its Leading Role within the Error-Monitoring

Network. *Cerebral Cortex (New York, N.Y.: 1991)*, *27*(2), 1545–1557. https://doi.org/10.1093/cercor/bhv352

Bastin, J., Lebranchu, P., Jerbi, K., Kahane, P., Orban, G., Lachaux, J.-P., & Berthoz, A. (2012). Direct recordings in human cortex reveal the dynamics of gamma-band [50-150 Hz] activity during pursuit eye movement control. *NeuroImage*, *63*(1), 339–347. https://doi.org/10.1016/j.neuroimage.2012.07.011

Beggs, J. M., & Plenz, D. (2003). Neuronal avalanches in neocortical circuits. *The Journal of Neuroscience: The Official Journal of the Society for Neuroscience*, *23*(35), 11167–11177.

Berman, R. A., Colby, C. L., Genovese, C. R., Voyvodic, J. T., Luna, B., Thulborn, K. R., & Sweeney, J. A. (1999). Cortical networks subserving pursuit and saccadic eye movements in humans: An FMRI study. *Human Brain Mapping*, *8*(4), 209–225.

Berthouze, L., James, L. M., & Farmer, S. F. (2010). Human EEG shows long-range temporal correlations of oscillation amplitude in Theta, Alpha and Beta bands across a wide age range. *Clinical Neurophysiology: Official Journal of the International Federation of Clinical Neurophysiology*, *121*(8), 1187–1197. https://doi.org/10.1016/j.clinph.2010.02.163

Billeke, P., Ossandon, T., Perrone-Bertolotti, M., Kahane, P., Bastin, J., Jerbi, K., Lachaux, J.-P., & Fuentealba, P. (n.d.). Human Anterior Insula Encodes Performance Feedback and Relays Prediction Error to the Medial Prefrontal Cortex. *Cerebral Cortex*. https://doi.org/10.1093/cercor/bhaa017

Blain-Moraes, S., Tarnal, V., Vanini, G., Alexander, A., Rosen, D., Shortal, B., Janke, E., & Mashour, G. A. (2015). Neurophysiological correlates of sevoflurane-induced unconsciousness. *Anesthesiology*, *122*(2), 307–316. https://doi.org/10.1097/ALN.0000000000000482

Blanke, O., & Seeck, M. (2003). Direction of saccadic and smooth eye movements induced by electrical stimulation of the human frontal eye field: Effect of orbital position. *Experimental Brain Research*, *150*(2), 174–183. https://doi.org/10.1007/s00221-003-1395-7

Boly, M., Massimini, M., Garrido, M. I., Gosseries, O., Noirhomme, Q., Laureys, S., & Soddu, A. (2012). Brain connectivity in disorders of consciousness. *Brain Connectivity*, *2*(1), 1–10. https://doi.org/10.1089/brain.2011.0049

Bonhomme, V., Vanhaudenhuyse, A., Demertzi, A., Bruno, M.-A., Jaquet, O., Bahri, M. A., Plenevaux, A., Boly, M., Boveroux, P., Soddu, A., Brichant, J. F., Maquet, P., & Laureys, S. (2016). Resting-state Network-specific Breakdown of Functional Connectivity during Ketamine Alteration of Consciousness in Volunteers. *Anesthesiology*, *125*(5), 873–888. https://doi.org/10.1097/ALN.0000000000001275

Bornas, X., Fiol-Veny, A., Balle, M., Morillas-Romero, A., & Tortella-Feliu, M. (2015). Long range temporal correlations in EEG oscillations of subclinically depressed individuals: Their association with brooding and suppression. *Cognitive Neurodynamics*, *9*(1), 53–62. https://doi.org/10.1007/s11571-014-9313-1

Boveroux, P., Vanhaudenhuyse, A., Bruno, M.-A., Noirhomme, Q., Lauwick, S., Luxen, A., Degueldre, C., Plenevaux, A., Schnakers, C., Phillips, C., Brichant, J.-F., Bonhomme, V., Maquet, P., Greicius, M. D., Laureys, S., & Boly, M. (2010). Breakdown of within- and between-network resting state functional magnetic resonance imaging connectivity during propofol-induced loss of consciousness. *Anesthesiology*, *113*(5), 1038–1053. https://doi.org/10.1097/ALN.0b013e3181f697f5

Briggman, K. L., Abarbanel, H. D. I., & Kristan, W. B. (2005). Optical Imaging of Neuronal Populations During Decision-Making. *Science*, *307*(5711), 896–901. https://doi.org/10.1126/science.1103736

Broome, B. M., Jayaraman, V., & Laurent, G. (2006). Encoding and decoding of overlapping odor sequences. *Neuron*, *51*(4), 467–482. https://doi.org/10.1016/j.neuron.2006.07.018

Carl, C., Hipp, J. F., König, P., & Engel, A. K. (2016). Spectral Signatures of Saccade Target Selection. *Brain Topography*, *29*(1), 130–148. https://doi.org/10.1007/s10548-015-0426-6

Casali, A. G., Gosseries, O., Rosanova, M., Boly, M., Sarasso, S., Casali, K. R., Casarotto, S., Bruno, M.-A., Laureys, S., Tononi, G., & Massimini, M. (2013). A theoretically based index of consciousness independent of sensory processing and behavior. *Science Translational Medicine*, *5*(198), 198ra105. https://doi.org/10.1126/scitranslmed.3006294

Ching, S., Cimenser, A., Purdon, P. L., Brown, E. N., & Kopell, N. J. (2010). Thalamocortical model for a propofol-induced alpha-rhythm associated with loss of consciousness. *Proceedings of the National Academy of Sciences of the United States of America*, *107*(52), 22665–22670. https://doi.org/10.1073/pnas.1017069108

Christopoulos, V. N., Kagan, I., & Andersen, R. A. (2018). Lateral intraparietal area (LIP) is largely effector-specific in free-choice decisions. *Scientific Reports*, *8*(1), 8611. https://doi.org/10.1038/s41598-018-26366-9

Churchland, M. M., Cunningham, J. P., Kaufman, M. T., Foster, J. D., Nuyujukian, P., Ryu, S. I., & Shenoy, K. V. (2012). Neural population dynamics during reaching. *Nature*, *487*(7405), 51–56. https://doi.org/10.1038/nature11129

Churchland, M. M., Yu, B. M., Cunningham, J. P., Sugrue, L. P., Cohen, M. R., Corrado, G. S., Newsome, W. T., Clark, A. M., Hosseini, P., Scott, B. B., Bradley, D. C., Smith, M. A., Kohn, A., Movshon, J. A., Armstrong, K. M., Moore, T., Chang, S. W., Snyder, L. H., Lisberger, S. G., … Shenoy, K. V. (2010). Stimulus onset quenches neural variability: A widespread cortical phenomenon. *Nature Neuroscience*, *13*(3), 369–378. https://doi.org/10.1038/nn.2501

Cimenser, A., Purdon, P. L., Pierce, E. T., Walsh, J. L., Salazar-Gomez, A. F., Harrell, P. G., Tavares-Stoeckel, C., Habeeb, K., & Brown, E. N. (2011). Tracking brain states under general anesthesia by using global coherence analysis. *Proceedings of the National Academy of Sciences*, *108*(21), 8832–8837. https://doi.org/10.1073/pnas.1017041108

Cisek, P., & Kalaska, J. F. (2005). Neural correlates of reaching decisions in dorsal premotor cortex: Specification of multiple direction choices and final selection of action. *Neuron*, *45*(5), 801–814. https://doi.org/10.1016/j.neuron.2005.01.027

Cisek, P., & Kalaska, J. F. (2010). Neural mechanisms for interacting with a world full of action choices. *Annual Review of Neuroscience*, *33*, 269–298. https://doi.org/10.1146/annurev.neuro.051508.135409

Ciuciu, P., Varoquaux, G., Abry, P., Sadaghiani, S., & Kleinschmidt, A. (2012). Scale-Free and Multifractal Time Dynamics of fMRI Signals during Rest and Task. *Frontiers in Physiology*, *3*, 186. https://doi.org/10.3389/fphys.2012.00186

Coe, B., Tomihara, K., Matsuzawa, M., & Hikosaka, O. (2002). Visual and Anticipatory Bias in Three Cortical Eye Fields of the Monkey during an Adaptive Decision-Making Task. *Journal of Neuroscience*, *22*(12), 5081–5090. https://doi.org/10.1523/JNEUROSCI.22-12-05081.2002

Combrisson, E., & Jerbi, K. (2015). Exceeding chance level by chance: The caveat of theoretical chance levels in brain signal classification and statistical assessment of decoding accuracy. *Journal of Neuroscience Methods*, *250*, 126–136. https://doi.org/10.1016/j.jneumeth.2015.01.010

Combrisson, E., Perrone-Bertolotti, M., Soto, J. L., Alamian, G., Kahane, P., Lachaux, J.-P., Guillot, A., & Jerbi, K. (2017). From intentions to actions: Neural oscillations encode motor processes through phase, amplitude and phase-amplitude coupling. *NeuroImage*, *147*, 473–487. https://doi.org/10.1016/j.neuroimage.2016.11.042

Combrisson, E., Vallat, R., O'Reilly, C., Jas, M., Pascarella, A., Saive, A.-L., Thiery, T., Meunier, D., Altukhov, D., Lajnef, T., Ruby, P., Guillot, A., & Jerbi, K. (2019). Visbrain: A Multi-Purpose GPU-Accelerated Open-Source Suite for Multimodal Brain Data Visualization. *Frontiers in Neuroinformatics*, *13*, 14. https://doi.org/10.3389/fninf.2019.00014

Connolly, J. D., Goodale, M. A., Menon, R. S., & Munoz, D. P. (2002). Human fMRI evidence for the neural correlates of preparatory set. *Nature Neuroscience*, *5*(12), 1345–1352. https://doi.org/10.1038/nn969

Constantinidis, C., Funahashi, S., Lee, D., Murray, J. D., Qi, X.-L., Wang, M., & Arnsten, A. F. T. (2018). Persistent Spiking Activity Underlies Working Memory. *The Journal of Neuroscience*, *38*(32), 7020–7028. https://doi.org/10.1523/JNEUROSCI.2486-17.2018

Costello, M. G., Zhu, D., Salinas, E., & Stanford, T. R. (2013). Perceptual Modulation of Motor—But Not Visual—Responses in the Frontal Eye Field during an Urgent-Decision Task. *The Journal of Neuroscience*, *33*(41), 16394–16408. https://doi.org/10.1523/JNEUROSCI.1899-13.2013

Coulthard, E., Rudd, A., & Husain, M. (2008). Motor neglect associated with loss of action inhibition. *Journal of Neurology, Neurosurgery, and Psychiatry*, *79*(12), 1401–1404. https://doi.org/10.1136/jnnp.2007.140715

Cui, H., & Andersen, R. A. (2007). Posterior Parietal Cortex Encodes Autonomously Selected Motor Plans. *Neuron*, *56*(3), 552–559. https://doi.org/10.1016/j.neuron.2007.09.031

Cunningham, J. P., & Yu, B. M. (2014). Dimensionality reduction for large-scale neural recordings. *Nature Neuroscience*, *17*(11), 1500–1509. https://doi.org/10.1038/nn.3776

Curtis, C. E., & Connolly, J. D. (2008). Saccade preparation signals in the human frontal and parietal cortices. *Journal of Neurophysiology*, *99*(1), 133–145. https://doi.org/10.1152/jn.00899.2007

Curtis, C. E., & Lee, D. (2010). Beyond working memory: The role of persistent activity in decision making. *Trends in Cognitive Sciences*, *14*(5), 216–222. https://doi.org/10.1016/j.tics.2010.03.006

de Jong, B. M. (2011). Neurology of widely embedded free will. *Cortex; a Journal Devoted to the Study of the Nervous System and Behavior*, *47*(10), 1160–1165. https://doi.org/10.1016/j.cortex.2011.06.011

Dehaene, S., & Changeux, J.-P. (2011). Experimental and theoretical approaches to conscious processing. *Neuron*, *70*(2), 200–227. https://doi.org/10.1016/j.neuron.2011.03.018

Dorris, M. C., & Glimcher, P. W. (2004). Activity in posterior parietal cortex is correlated with the relative subjective desirability of action. *Neuron*, *44*(2), 365–378. https://doi.org/10.1016/j.neuron.2004.09.009

Engel, A. K., & Fries, P. (2010). Beta-band oscillations—Signalling the status quo? *Current Opinion in Neurobiology*, *20*(2), 156–165. https://doi.org/10.1016/j.conb.2010.02.015

Fedele, T., Blagovechtchenski, E., Nazarova, M., Iscan, Z., Moiseeva, V., & Nikulin, V. V. (2016). Long-Range Temporal Correlations in the amplitude of alpha oscillations predict and reflect strength of intracortical facilitation: Combined TMS and EEG study. *Neuroscience*, *331*, 109–119. https://doi.org/10.1016/j.neuroscience.2016.06.015

Feshchenko, V. A., Veselis, R. A., & Reinsel, R. A. (2004). Propofol-induced alpha rhythm. *Neuropsychobiology*, *50*(3), 257–266. https://doi.org/10.1159/000079981

Fisher, R. A. (1936). The Use of Multiple Measurements in Taxonomic Problems. *Annals of Eugenics*, *7*(2), 179–188. https://doi.org/10.1111/j.1469-1809.1936.tb02137.x

Fleming, S. M., Mars, R. B., Gladwin, T. E., & Haggard, P. (2009). When the brain changes its mind: Flexibility of action selection in instructed and free choices. *Cerebral Cortex (New York, N.Y.: 1991)*, *19*(10), 2352–2360. https://doi.org/10.1093/cercor/bhn252

Franks, N. P. (2008). General anaesthesia: From molecular targets to neuronal pathways of sleep and arousal. *Nature Reviews. Neuroscience*, *9*(5), 370–386. https://doi.org/10.1038/nrn2372

Frost, D., & Pöppel, E. (1976). Different programming modes of human saccadic eye movements as a function of stimulus eccentricity: Indications of a functional subdivision of the visual field. *Biological Cybernetics*, *23*(1), 39–48. https://doi.org/10.1007/BF00344150

Funahashi, M., Higuchi, H., Miyawaki, T., Shimada, M., & Matsuo, R. (2001). Propofol suppresses a hyperpolarization-activated inward current in rat hippocampal CA1 neurons. *Neuroscience Letters*, *311*(3), 177–180. https://doi.org/10.1016/S0304-3940(01)02169-3

Gallego, J. A., Perich, M. G., Miller, L. E., & Solla, S. A. (2017). Neural Manifolds for the Control of Movement. *Neuron*, *94*(5), 978–984. https://doi.org/10.1016/j.neuron.2017.05.025

Gao, J., Hu, J., Tung, W.-W., Cao, Y., Sarshar, N., & Roychowdhury, V. P. (2006). Assessment of long-range correlation in time series: How to avoid pitfalls. *Physical Review E*, *73*(1), 016117. https://doi.org/10.1103/PhysRevE.73.016117

Gifani, P., Rabiee, H. R., Hashemi, M. R., Taslimi, P., & Ghanbari, M. (2006). Nonlinear analysis of anesthesia dynamics by Fractal Scaling Exponent. *Conference Proceedings: ... Annual International Conference of the IEEE Engineering in Medicine and Biology Society. IEEE Engineering in Medicine and Biology Society. Annual Conference*, *1*, 6225–6228. https://doi.org/10.1109/IEMBS.2006.260501

Gold, J. I., & Shadlen, M. N. (2007). The neural basis of decision making. *Annual Review of Neuroscience*, *30*, 535–574. https://doi.org/10.1146/annurev.neuro.29.051605.113038

Grent-'t-Jong, T., Oostenveld, R., Jensen, O., Medendorp, W. P., & Praamstra, P. (2014). Competitive interactions in sensorimotor cortex: Oscillations express separation between alternative movement targets. *Journal of Neurophysiology*, *112*(2), 224–232. https://doi.org/10.1152/jn.00127.2014

Gugino, L. D., Chabot, R. J., Prichep, L. S., John, E. R., Formanek, V., & Aglio, L. S. (2001). Quantitative EEG changes associated with loss and return of consciousness in healthy adult volunteers anaesthetized with propofol or sevoflurane. *British Journal of Anaesthesia*, *87*(3), 421–428.

Haggard, P. (2019). The Neurocognitive Bases of Human Volition. *Annual Review of Psychology*, *70*(1), 9–28. https://doi.org/10.1146/annurev-psych-010418-103348

Hamamé, C. M., Vidal, J. R., Perrone-Bertolotti, M., Ossandón, T., Jerbi, K., Kahane, P., Bertrand, O., & Lachaux, J.-P. (2014). Functional selectivity in the human occipitotemporal cortex during natural vision: Evidence from combined intracranial EEG and eye-tracking. *NeuroImage*, *95*, 276–286. https://doi.org/10.1016/j.neuroimage.2014.03.025

Harvey, C. D., Coen, P., & Tank, D. W. (2012). Choice-specific sequences in parietal cortex during a virtual-navigation decision task. *Nature*, *484*(7392), 62–68. https://doi.org/10.1038/nature10918

He, B. J. (2014). Scale-free brain activity: Past, present, and future. *Trends in Cognitive Sciences*, *18*(9), 480–487. https://doi.org/10.1016/j.tics.2014.04.003

Hudetz, A. G., Liu, X., & Pillay, S. (2015). Dynamic Repertoire of Intrinsic Brain States Is Reduced in Propofol-Induced Unconsciousness. *Brain Connectivity*, *5*(1), 10–22. https://doi.org/10.1089/brain.2014.0230

Hwang, E. J., & Andersen, R. A. (2012). Spiking and LFP activity in PRR during symbolically instructed reaches. *Journal of Neurophysiology*, *107*(3), 836–849. https://doi.org/10.1152/jn.00063.2011

Jerbi, K., Freyermuth, S., Dalal, S., Kahane, P., Bertrand, O., Berthoz, A., & Lachaux, J.-P. (2009). Saccade Related Gamma-Band Activity in Intracerebral EEG: Dissociating Neural from Ocular Muscle Activity. *Brain Topography*, *22*(1), 18–23. https://doi.org/10.1007/s10548-009-0078-5

Jerbi, K., Ossandón, T., Hamamé, C. M., Senova, S., Dalal, S. S., Jung, J., Minotti, L., Bertrand, O., Berthoz, A., Kahane, P., & Lachaux, J.-P. (2009). Task-related gamma-band dynamics from an intracerebral perspective: Review and implications for surface EEG and MEG. *Human Brain Mapping*, *30*(6), 1758–1771. https://doi.org/10.1002/hbm.20750

John, E. R., & Prichep, L. S. (2005). The anesthetic cascade: A theory of how anesthesia suppresses consciousness. *Anesthesiology*, *102*(2), 447–471.

Jordan, D., Ilg, R., Riedl, V., Schorer, A., Grimberg, S., Neufang, S., Omerovic, A., Berger, S., Untergehrer, G., Preibisch, C., Schulz, E., Schuster, T., Schröter, M., Spoormaker, V., Zimmer, C., Hemmer, B., Wohlschläger, A., Kochs, E. F., & Schneider, G. (2013). Simultaneous electroencephalographic and functional magnetic resonance imaging indicate impaired cortical top-down processing in association with anesthetic-induced unconsciousness. *Anesthesiology*, *119*(5), 1031–1042. https://doi.org/10.1097/ALN.0b013e3182a7ca92

Jospin, M., Caminal, P., Jensen, E. W., Litvan, H., Vallverdu, M., Struys, M. M. R. F., Vereecke, H. E. M., & Kaplan, D. T. (2007). Detrended Fluctuation Analysis of EEG as a Measure of Depth of Anesthesia. *IEEE Transactions on Biomedical Engineering*, *54*(5), 840–846. https://doi.org/10.1109/TBME.2007.893453

Jung, J., Jerbi, K., Ossandon, T., Ryvlin, P., Isnard, J., Bertrand, O., Guénot, M., Mauguière, F., & Lachaux, J.-P. (2010). Brain responses to success and failure: Direct recordings from human cerebral cortex. *Human Brain Mapping*, *31*(8), 1217–1232. https://doi.org/10.1002/hbm.20930

Kable, J. W., & Glimcher, P. W. (2009). The Neurobiology of Decision: Consensus and Controversy. *Neuron*, *63*(6), 733–745. https://doi.org/10.1016/j.neuron.2009.09.003

Kagan, I., Iyer, A., Lindner, A., & Andersen, R. A. (2010). Space representation for eye movements is more contralateral in monkeys than in humans. *Proceedings of the National Academy of Sciences*, *107*(17), 7933–7938. https://doi.org/10.1073/pnas.1002825107

Kahneman, D., & Tversky, A. (1990). *Prospect theory: An analysis of decision under risk* (p. 170). Cambridge University Press.

Kantelhardt, J. W., Koscielny-Bunde, E., Rego, H. H. A., Havlin, S., & Bunde, A. (2001). Detecting Long-range Correlations with Detrended Fluctuation Analysis. *Physica A: Statistical Mechanics and Its Applications*, *295*(3–4), 441–454. https://doi.org/10.1016/S0378-4371(01)00144-3

Kaskinoro, K., Maksimow, A., Georgiadis, S., Långsjö, J., Scheinin, H., Karjalainen, P., & Jääskeläinen, S. K. (2015). Electroencephalogram reactivity to verbal command after dexmedetomidine, propofol and sevoflurane-induced unresponsiveness. *Anaesthesia*, *70*(2), 190–204. https://doi.org/10.1111/anae.12868

Kaufman, M. T., Churchland, M. M., Ryu, S. I., & Shenoy, K. V. (2014). Cortical activity in the null space: Permitting preparation without movement. *Nature Neuroscience*, *17*(3), 440–448. https://doi.org/10.1038/nn.3643

Kayser, C., Kim, M., Ugurbil, K., Kim, D.-S., & König, P. (2004). A comparison of hemodynamic and neural responses in cat visual cortex using complex stimuli. *Cerebral Cortex (New York, N.Y.: 1991)*, *14*(8), 881–891. https://doi.org/10.1093/cercor/bhh047

Khonsari, R. H., Lobel, E., Milea, D., Lehéricy, S., Pierrot-Deseilligny, C., & Berthoz, A. (2007a). Lateralized parietal activity during decision and preparation of saccades. *Neuroreport*, *18*(17), 1797–1800. https://doi.org/10.1097/WNR.0b013e3282f1a986

Khonsari, R. H., Lobel, E., Milea, D., Lehéricy, S., Pierrot-Deseilligny, C., & Berthoz, A. (2007b). Lateralized parietal activity during decision and preparation of saccades. *Neuroreport*, *18*(17), 1797–1800. https://doi.org/10.1097/WNR.0b013e3282f1a986

King, J.-R., & Dehaene, S. (2014). Characterizing the dynamics of mental representations: The temporal generalization method. *Trends in Cognitive Sciences*, *18*(4), 203–210. https://doi.org/10.1016/j.tics.2014.01.002

Kinouchi, O., & Copelli, M. (2006). Optimal dynamical range of excitable networks at criticality. *Nature Physics*, *2*(5), 348–351. https://doi.org/10.1038/nphys289

Klaes, C., Westendorff, S., Chakrabarti, S., & Gail, A. (2011). Choosing Goals, Not Rules: Deciding among Rule-Based Action Plans. *Neuron*, *70*(3), 536–548. https://doi.org/10.1016/j.neuron.2011.02.053

Koch, C. (2004). *The quest for consciousness: A neurobiological approach*. Roberts and Co.

Kovach, C. K., Tsuchiya, N., Kawasaki, H., Oya, H., Howard, M. A., & Adolphs, R. (2011). Manifestation of ocular-muscle EMG contamination in human intracranial recordings. *NeuroImage*, *54*(1), 213–233. https://doi.org/10.1016/j.neuroimage.2010.08.002

Krzemiński, D., Kamiński, M., Marchewka, A., & Bola, M. (2017). Breakdown of long-range temporal correlations in brain oscillations during general anesthesia. *NeuroImage*, *159*(Supplement C), 146–158. https://doi.org/10.1016/j.neuroimage.2017.07.047

Kucewicz, M. T., Berry, B. M., Kremen, V., Brinkmann, B. H., Sperling, M. R., Jobst, B. C., Gross, R. E., Lega, B., Sheth, S. A., Stein, J. M., Das, S. R., Gorniak, R., Stead, S. M., Rizzuto, D. S., Kahana, M. J., & Worrell, G. A. (2017a). Dissecting gamma frequency activity during human memory processing. *Brain: A Journal of Neurology*, *140*(5), 1337–1350. https://doi.org/10.1093/brain/awx043

Kucewicz, M. T., Berry, B. M., Kremen, V., Brinkmann, B. H., Sperling, M. R., Jobst, B. C., Gross, R. E., Lega, B., Sheth, S. A., Stein, J. M., Das, S. R., Gorniak, R., Stead, S. M., Rizzuto, D. S., Kahana, M. J., & Worrell, G. A. (2017b). Dissecting gamma frequency activity during human

memory processing. *Brain: A Journal of Neurology*, *140*(5), 1337–1350. https://doi.org/10.1093/brain/awx043

Lachaux, J. P., Rudrauf, D., & Kahane, P. (2003). Intracranial EEG and human brain mapping. *Journal of Physiology, Paris*, *97*(4–6), 613–628. https://doi.org/10.1016/j.jphysparis.2004.01.018

Lachaux, J.-P., Axmacher, N., Mormann, F., Halgren, E., & Crone, N. E. (2012). High-frequency neural activity and human cognition: Past, present and possible future of intracranial EEG research. *Progress in Neurobiology*, *98*(3), 279–301. https://doi.org/10.1016/j.pneurobio.2012.06.008

Lachaux, J.-P., Fonlupt, P., Kahane, P., Minotti, L., Hoffmann, D., Bertrand, O., & Baciu, M. (2007). Relationship between task-related gamma oscillations and BOLD signal: New insights from combined fMRI and intracranial EEG. *Human Brain Mapping*, *28*(12), 1368–1375. https://doi.org/10.1002/hbm.20352

Lachaux, J.-P., Hoffmann, D., Minotti, L., Berthoz, A., & Kahane, P. (2006). Intracerebral dynamics of saccade generation in the human frontal eye field and supplementary eye field. *NeuroImage*, *30*(4), 1302–1312. https://doi.org/10.1016/j.neuroimage.2005.11.023

Lalitha, V., & Eswaran, C. (2007). Automated detection of anesthetic depth levels using chaotic features with artificial neural networks. *Journal of Medical Systems*, *31*(6), 445–452.

Laureys, S., & Tononi, G. (Eds.). (2009). *The neurology of consciousness: Cognitive neuroscience and neuropathology* (1st ed). Elsevier/Academic Press.

Lavazza, A. (2016). Free Will and Neuroscience: From Explaining Freedom Away to New Ways of Operationalizing and Measuring It. *Frontiers in Human Neuroscience*, *10*, 262. https://doi.org/10.3389/fnhum.2016.00262

Lee, U., Ku, S., Noh, G., Baek, S., Choi, B., & Mashour, G. A. (2013). Disruption of frontal-parietal communication by ketamine, propofol, and sevoflurane. *Anesthesiology*, *118*(6), 1264–1275. https://doi.org/10.1097/ALN.0b013e31829103f5

Lee, U., Mashour, G. A., Kim, S., Noh, G.-J., & Choi, B.-M. (2009). Propofol induction reduces the capacity for neural information integration: Implications for the mechanism of consciousness

and general anesthesia. *Consciousness and Cognition*, *18*(1), 56–64. https://doi.org/10.1016/j.concog.2008.10.005

Lee, U., Oh, G., Kim, S., Noh, G., Choi, B., & Mashour, G. A. (2010). Brain networks maintain a scale-free organization across consciousness, anesthesia, and recovery: Evidence for adaptive reconfiguration. *Anesthesiology*, *113*(5), 1081–1091. https://doi.org/10.1097/ALN.0b013e3181f229b5

Lemm, S., Blankertz, B., Dickhaus, T., & Müller, K.-R. (2011). Introduction to machine learning for brain imaging. *NeuroImage*, *56*(2), 387–399. https://doi.org/10.1016/j.neuroimage.2010.11.004

Leszczynski, M., & Schroeder, C. E. (2019). The Role of Neuronal Oscillations in Visual Active Sensing. *Frontiers in Integrative Neuroscience*, *13*. https://doi.org/10.3389/fnint.2019.00032

Li, X., Wang, F., & Wu, G. (2017). Monitoring Depth of Anesthesia Using Detrended Fluctuation Analysis Based on EEG Signals. *Journal of Medical and Biological Engineering*, *37*(2), 171–180. https://doi.org/10.1007/s40846-016-0196-y

Liang, Z., Wang, Y., Sun, X., Li, D., Voss, L. J., Sleigh, J. W., Hagihira, S., & Li, X. (2015). EEG entropy measures in anesthesia. *Frontiers in Computational Neuroscience*, *9*. https://doi.org/10.3389/fncom.2015.00016

Linkenkaer-Hansen, K., Monto, S., Rytsälä, H., Suominen, K., Isometsä, E., & Kähkönen, S. (2005). Breakdown of Long-Range Temporal Correlations in Theta Oscillations in Patients with Major Depressive Disorder. *Journal of Neuroscience*, *25*(44), 10131–10137. https://doi.org/10.1523/JNEUROSCI.3244-05.2005

Linkenkaer-Hansen, K., Nikouline, V. V., Palva, J. M., & Ilmoniemi, R. J. (2001). Long-range temporal correlations and scaling behavior in human brain oscillations. *The Journal of Neuroscience: The Official Journal of the Society for Neuroscience*, *21*(4), 1370–1377.

Linkenkaer-Hansen, K., Nikulin, V. V., Palva, S., Ilmoniemi, R. J., & Palva, J. M. (2004). Prestimulus Oscillations Enhance Psychophysical Performance in Humans. *Journal of Neuroscience*, *24*(45), 10186–10190. https://doi.org/10.1523/JNEUROSCI.2584-04.2004

Linkenkaer-Hansen, K., Smit, D. J. A., Barkil, A., Beijsterveldt, T. E. M. van, Brussaard, A. B., Boomsma, D. I., Ooyen, A. van, & Geus, E. J. C. de. (2007). Genetic Contributions to Long-Range Temporal Correlations in Ongoing Oscillations. *Journal of Neuroscience*, *27*(50), 13882–13889. https://doi.org/10.1523/JNEUROSCI.3083-07.2007

Logothetis, N. K., Pauls, J., Augath, M., Trinath, T., & Oeltermann, A. (2001). Neurophysiological investigation of the basis of the fMRI signal. *Nature*, *412*(6843), 150–157. https://doi.org/10.1038/35084005

Lundqvist, M., Herman, P., & Miller, E. K. (2018). Working Memory: Delay Activity, Yes! Persistent Activity? Maybe Not. *The Journal of Neuroscience*, *38*(32), 7013–7019. https://doi.org/10.1523/JNEUROSCI.2485-17.2018

Lux, T., & Marchesi, M. (1999). Scaling and criticality in a stochastic multi-agent model of a financial market. *Nature*, *397*(6719), 498–500. https://doi.org/10.1038/17290

Manning, J. R., Jacobs, J., Fried, I., & Kahana, M. J. (2009). Broadband shifts in local field potential power spectra are correlated with single-neuron spiking in humans. *The Journal of Neuroscience: The Official Journal of the Society for Neuroscience*, *29*(43), 13613–13620. https://doi.org/10.1523/JNEUROSCI.2041-09.2009

Mante, V., Sussillo, D., Shenoy, K. V., & Newsome, W. T. (2013). Context-dependent computation by recurrent dynamics in prefrontal cortex. *Nature*, *503*(7474), 78–84. https://doi.org/10.1038/nature12742

Mashour, G. A. (2013). Cognitive unbinding: A neuroscientific paradigm of general anesthesia and related states of unconsciousness. *Neuroscience & Biobehavioral Reviews*, *37*(10), 2751–2759. https://doi.org/10.1016/j.neubiorev.2013.09.009

Mashour, G. A., Shanks, A., Tremper, K. K., Kheterpal, S., Turner, C. R., Ramachandran, S. K., Picton, P., Schueller, C., Morris, M., Vandervest, J. C., Lin, N., & Avidan, M. S. (2012). Prevention of intraoperative awareness with explicit recall in an unselected surgical population:

A randomized comparative effectiveness trial. *Anesthesiology*, *117*(4), 717–725. https://doi.org/10.1097/ALN.0b013e31826904a6

Mazor, O., & Laurent, G. (2005). Transient Dynamics versus Fixed Points in Odor Representations by Locust Antennal Lobe Projection Neurons. *Neuron*, *48*(4), 661–673. https://doi.org/10.1016/j.neuron.2005.09.032

McDowell, J. E., Dyckman, K. A., Austin, B. P., & Clementz, B. A. (2008). Neurophysiology and neuroanatomy of reflexive and volitional saccades: Evidence from studies of humans. *Brain and Cognition*, *68*(3), 255–270. https://doi.org/10.1016/j.bandc.2008.08.016

Meisel, C., Bailey, K., Achermann, P., & Plenz, D. (2017). Decline of long-range temporal correlations in the human brain during sustained wakefulness. *Scientific Reports*, *7*. https://doi.org/10.1038/s41598-017-12140-w

Meyer, T., Qi, X.-L., & Constantinidis, C. (2007). Persistent discharges in the prefrontal cortex of monkeys naive to working memory tasks. *Cerebral Cortex (New York, N.Y.: 1991)*, *17 Suppl 1*, i70-76. https://doi.org/10.1093/cercor/bhm063

Milea, D., Lobel, E., Lehéricy, S., Leboucher, P., Pochon, J.-B., Pierrot-Deseilligny, C., & Berthoz, A. (2007a). Prefrontal cortex is involved in internal decision of forthcoming saccades. *Neuroreport*, *18*(12), 1221–1224. https://doi.org/10.1097/WNR.0b013e3281e72ce7

Milea, D., Lobel, E., Lehéricy, S., Leboucher, P., Pochon, J.-B., Pierrot-Deseilligny, C., & Berthoz, A. (2007b). Prefrontal cortex is involved in internal decision of forthcoming saccades. *Neuroreport*, *18*(12), 1221–1224. https://doi.org/10.1097/WNR.0b013e3281e72ce7

Mitzdorf, U. (1985). Current source-density method and application in cat cerebral cortex: Investigation of evoked potentials and EEG phenomena. *Physiological Reviews*, *65*(1), 37–100. https://doi.org/10.1152/physrev.1985.65.1.37

Mochizuki, K., & Funahashi, S. (2016). Prefrontal spatial working memory network predicts animal's decision making in a free choice saccade task. *Journal of Neurophysiology*, *115*(1), 127–142. https://doi.org/10.1152/jn.00255.2015

Montez, T., Poil, S.-S., Jones, B. F., Manshanden, I., Verbunt, J. P. A., van Dijk, B. W., Brussaard, A. B., van Ooyen, A., Stam, C. J., Scheltens, P., & Linkenkaer-Hansen, K. (2009). Altered temporal correlations in parietal alpha and prefrontal theta oscillations in early-stage Alzheimer disease. *Proceedings of the National Academy of Sciences of the United States of America*, *106*(5), 1614–1619. https://doi.org/10.1073/pnas.0811699106

Monto, S., Vanhatalo, S., Holmes, M. D., & Palva, J. M. (2007). Epileptogenic neocortical networks are revealed by abnormal temporal dynamics in seizure-free subdural EEG. *Cerebral Cortex (New York, N.Y.: 1991)*, *17*(6), 1386–1393. https://doi.org/10.1093/cercor/bhl049

Moon, S. Y., Barton, J. J. S., Mikulski, S., Polli, F. E., Cain, M. S., Vangel, M., Hämäläinen, M. S., & Manoach, D. S. (2007). Where left becomes right: A magnetoencephalographic study of sensorimotor transformation for antisaccades. *NeuroImage*, *36*(4), 1313–1323. https://doi.org/10.1016/j.neuroimage.2007.04.040

Mukamel, E. A., Pirondini, E., Babadi, B., Wong, K. F. K., Pierce, E. T., Harrell, P. G., Walsh, J. L., Salazar-Gomez, A. F., Cash, S. S., Eskandar, E. N., Weiner, V. S., Brown, E. N., & Purdon, P. L. (2014). A Transition in Brain State during Propofol-Induced Unconsciousness. *Journal of Neuroscience*, *34*(3), 839–845. https://doi.org/10.1523/JNEUROSCI.5813-12.2014

Mukamel, R., Gelbard, H., Arieli, A., Hasson, U., Fried, I., & Malach, R. (2005a). Coupling between neuronal firing, field potentials, and FMRI in human auditory cortex. *Science (New York, N.Y.)*, *309*(5736), 951–954. https://doi.org/10.1126/science.1110913

Mukamel, R., Gelbard, H., Arieli, A., Hasson, U., Fried, I., & Malach, R. (2005b). Coupling between neuronal firing, field potentials, and FMRI in human auditory cortex. *Science (New York, N.Y.)*, *309*(5736), 951–954. https://doi.org/10.1126/science.1110913

Murphy, P. R., Wilming, N., Hernandez-Bocanegra, D. C., Prat-Ortega, G., & Donner, T. H. (2021). Adaptive circuit dynamics across human cortex during evidence accumulation in changing environments. *Nature Neuroscience*, 1–11. https://doi.org/10.1038/s41593-021-00839-z

Nachev, P., Kennard, C., & Husain, M. (2008). Functional role of the supplementary and pre-supplementary motor areas. *Nature Reviews Neuroscience*, *9*(11), 856–869. https://doi.org/10.1038/nrn2478

Nachev, P., Rees, G., Parton, A., Kennard, C., & Husain, M. (2005). Volition and conflict in human medial frontal cortex. *Current Biology : CB*, *15*(2), 122–128. https://doi.org/10.1016/j.cub.2005.01.006

Nguyen-Ky, T., Wen, P., & Li, Y. (2010). An improved detrended moving-average method for monitoring the depth of anesthesia. *IEEE Transactions on Bio-Medical Engineering*, *57*(10), 2369–2378. https://doi.org/10.1109/TBME.2010.2053929

Niedermeyer, E., & Silva, F. H. L. da. (2005). *Electroencephalography: Basic Principles, Clinical Applications, and Related Fields*. Lippincott Williams & Wilkins.

Niessing, J., Ebisch, B., Schmidt, K. E., Niessing, M., Singer, W., & Galuske, R. A. W. (2005). Hemodynamic signals correlate tightly with synchronized gamma oscillations. *Science (New York, N.Y.)*, *309*(5736), 948–951. https://doi.org/10.1126/science.1110948

Nikulin, V. V., & Brismar, T. (2004). Long-range temporal correlations in alpha and beta oscillations: Effect of arousal level and test-retest reliability. *Clinical Neurophysiology: Official Journal of the International Federation of Clinical Neurophysiology*, *115*(8), 1896–1908. https://doi.org/10.1016/j.clinph.2004.03.019

Nikulin, V. V., & Brismar, T. (2005). Long-range temporal correlations in electroencephalographic oscillations: Relation to topography, frequency band, age and gender. *Neuroscience*, *130*(2), 549–558. https://doi.org/10.1016/j.neuroscience.2004.10.007

Nikulin, V. V., Jönsson, E. G., & Brismar, T. (2012). Attenuation of long-range temporal correlations in the amplitude dynamics of alpha and beta neuronal oscillations in patients with schizophrenia. *NeuroImage*, *61*(1), 162–169. https://doi.org/10.1016/j.neuroimage.2012.03.008

Nir, Y., Fisch, L., Mukamel, R., Gelbard-Sagiv, H., Arieli, A., Fried, I., & Malach, R. (2007). Coupling between neuronal firing rate, gamma LFP, and BOLD fMRI is related to interneuronal

correlations. *Current Biology: CB*, *17*(15), 1275–1285. https://doi.org/10.1016/j.cub.2007.06.066

Ojemann, G. A., Ramsey, N. F., & Ojemann, J. (2013). Relation between functional magnetic resonance imaging (fMRI) and single neuron, local field potential (LFP) and electrocorticography (ECoG) activity in human cortex. *Frontiers in Human Neuroscience*, *7*. https://doi.org/10.3389/fnhum.2013.00034

Oliveira, F. T. P., Diedrichsen, J., Verstynen, T., Duque, J., & Ivry, R. B. (2010). Transcranial magnetic stimulation of posterior parietal cortex affects decisions of hand choice. *Proceedings of the National Academy of Sciences*, *107*(41), 17751–17756. https://doi.org/10.1073/pnas.1006223107

Olk, B., Chang, E., Kingstone, A., & Ro, T. (2006). Modulation of antisaccades by transcranial magnetic stimulation of the human frontal eye field. *Cerebral Cortex (New York, N.Y.: 1991)*, *16*(1), 76–82. https://doi.org/10.1093/cercor/bhi085

Ossandón, T., Jerbi, K., Vidal, J. R., Bayle, D. J., Henaff, M.-A., Jung, J., Minotti, L., Bertrand, O., Kahane, P., & Lachaux, J.-P. (2011). Transient Suppression of Broadband Gamma Power in the Default-Mode Network Is Correlated with Task Complexity and Subject Performance. *Journal of Neuroscience*, *31*(41), 14521–14530. https://doi.org/10.1523/JNEUROSCI.2483-11.2011

Ossandón, T., Vidal, J. R., Ciumas, C., Jerbi, K., Hamamé, C. M., Dalal, S. S., Bertrand, O., Minotti, L., Kahane, P., & Lachaux, J.-P. (2012). Efficient “pop-out” visual search elicits sustained broadband γ activity in the dorsal attention network. *The Journal of Neuroscience: The Official Journal of the Society for Neuroscience*, *32*(10), 3414–3421. https://doi.org/10.1523/JNEUROSCI.6048-11.2012

Pal, D., Silverstein, B. H., Lee, H., & Mashour, G. A. (2016). Neural Correlates of Wakefulness, Sleep, and General Anesthesia: An Experimental Study in Rat. *Anesthesiology*, *125*(5), 929–942. https://doi.org/10.1097/ALN.0000000000001342

Palanca, B. J. A., Mitra, A., Larson-Prior, L., Snyder, A. Z., Avidan, M. S., & Raichle, M. E. (2015). Resting-state Functional Magnetic Resonance Imaging Correlates of Sevoflurane-induced Unconsciousness. *Anesthesiology*, *123*(2), 346–356. https://doi.org/10.1097/ALN.0000000000000731

Pastor-Bernier, A., & Cisek, P. (2011). Neural correlates of biased competition in premotor cortex. *The Journal of Neuroscience: The Official Journal of the Society for Neuroscience*, *31*(19), 7083–7088. https://doi.org/10.1523/JNEUROSCI.5681-10.2011

Pastor-Bernier, A., Tremblay, E., & Cisek, P. (2012). Dorsal premotor cortex is involved in switching motor plans. *Frontiers in Neuroengineering*, *5*. https://doi.org/10.3389/fneng.2012.00005

Pavone, K. J., Su, L., Gao, L., Eromo, E., Vazquez, R., Rhee, J., Hobbs, L. E., Ibala, R., Demircioglu, G., Purdon, P. L., Brown, E. N., & Akeju, O. (2017). Lack of Responsiveness during the Onset and Offset of Sevoflurane Anesthesia Is Associated with Decreased Awake-Alpha Oscillation Power. *Frontiers in Systems Neuroscience*, *11*. https://doi.org/10.3389/fnsys.2017.00038

Pedregosa, F., Varoquaux, G., Gramfort, A., Michel, V., Thirion, B., Grisel, O., Blondel, M., Müller, A., Nothman, J., Louppe, G., Prettenhofer, P., Weiss, R., Dubourg, V., Vanderplas, J., Passos, A., Cournapeau, D., Brucher, M., Perrot, M., & Duchesnay, É. (2012). *Scikit-learn: Machine Learning in Python*. https://arxiv.org/abs/1201.0490v4

Peng, C. K., Havlin, S., Stanley, H. E., & Goldberger, A. L. (1995). Quantification of scaling exponents and crossover phenomena in nonstationary heartbeat time series. *Chaos (Woodbury, N.Y.)*, *5*(1), 82–87. https://doi.org/10.1063/1.166141

Pesaran, B., Nelson, M. J., & Andersen, R. A. (2008). Free choice activates a decision circuit between frontal and parietal cortex. *Nature*, *453*(7193), 406–409. https://doi.org/10.1038/nature06849

Petit, L., Clark, V. P., Ingeholm, J., & Haxby, J. V. (1997). Dissociation of saccade-related and pursuit-related activation in human frontal eye fields as revealed by fMRI. *Journal of Neurophysiology*, *77*(6), 3386–3390. https://doi.org/10.1152/jn.1997.77.6.3386

Pierrot-Deseilligny, C., Ploner, C. J., Muri, R. M., Gaymard, B., & Rivaud-Pechoux, S. (2002). Effects of cortical lesions on saccadic: Eye movements in humans. *Annals of the New York Academy of Sciences*, *956*, 216–229. https://doi.org/10.1111/j.1749-6632.2002.tb02821.x

Platt, M. L., & Glimcher, P. W. (1999). Neural correlates of decision variables in parietal cortex. *Nature*, *400*(6741), 233–238. https://doi.org/10.1038/22268

Poil, S.-S., Hardstone, R., Mansvelder, H. D., & Linkenkaer-Hansen, K. (2012). Critical-state dynamics of avalanches and oscillations jointly emerge from balanced excitation/inhibition in neuronal networks. *The Journal of Neuroscience: The Official Journal of the Society for Neuroscience*, *32*(29), 9817–9823. https://doi.org/10.1523/JNEUROSCI.5990-11.2012

Procyk, E., & Goldman-Rakic, P. S. (2006). Modulation of Dorsolateral Prefrontal Delay Activity during Self-Organized Behavior. *Journal of Neuroscience*, *26*(44), 11313–11323. https://doi.org/10.1523/JNEUROSCI.2157-06.2006

Purdon, P. L., Pavone, K. J., Akeju, O., Smith, A. C., Sampson, A. L., Lee, J., Zhou, D. W., Solt, K., & Brown, E. N. (2015). The Ageing Brain: Age-dependent changes in the electroencephalogram during propofol and sevoflurane general anaesthesia. *British Journal of Anaesthesia*, *115 Suppl 1*, i46–i57. https://doi.org/10.1093/bja/aev213

Purdon, P. L., Pierce, E. T., Mukamel, E. A., Prerau, M. J., Walsh, J. L., Wong, K. F. K., Salazar-Gomez, A. F., Harrell, P. G., Sampson, A. L., Cimenser, A., Ching, S., Kopell, N. J., Tavares-Stoeckel, C., Habeeb, K., Merhar, R., & Brown, E. N. (2013). Electroencephalogram signatures of loss and recovery of consciousness from propofol. *Proceedings of the National Academy of Sciences of the United States of America*, *110*(12), E1142–E1151. https://doi.org/10.1073/pnas.1221180110

Ranft, A., Golkowski, D., Kiel, T., Riedl, V., Kohl, P., Rohrer, G., Pientka, J., Berger, S., Thul, A., Maurer, M., Preibisch, C., Zimmer, C., Mashour, G. A., Kochs, E. F., Jordan, D., & Ilg, R. (2016). Neural Correlates of Sevoflurane-induced Unconsciousness Identified by Simultaneous

Functional Magnetic Resonance Imaging and Electroencephalography. *Anesthesiology*, *125*(5), 861–872. https://doi.org/10.1097/ALN.0000000000001322

Raschka, S. (2018). *Model Evaluation, Model Selection, and Algorithm Selection in Machine Learning*. https://arxiv.org/abs/1811.12808v2

Ray, S., Crone, N. E., Niebur, E., Franaszczuk, P. J., & Hsiao, S. S. (2008). Neural Correlates of High-Gamma Oscillations (60–200 Hz) in Macaque Local Field Potentials and Their Potential Implications in Electrocorticography. *Journal of Neuroscience*, *28*(45), 11526–11536. https://doi.org/10.1523/JNEUROSCI.2848-08.2008

Ray, S., & Maunsell, J. H. R. (2011). Different Origins of Gamma Rhythm and High-Gamma Activity in Macaque Visual Cortex. *PLOS Biology*, *9*(4), e1000610. https://doi.org/10.1371/journal.pbio.1000610

Rowe, J. B., Toni, I., Josephs, O., Frackowiak, R. S., & Passingham, R. E. (2000). The prefrontal cortex: Response selection or maintenance within working memory? *Science (New York, N.Y.)*, *288*(5471), 1656–1660. https://doi.org/10.1126/science.288.5471.1656

Rushworth, M. F. S., Johansen-Berg, H., Göbel, S. M., & Devlin, J. T. (2003). The left parietal and premotor cortices: Motor attention and selection. *NeuroImage*, *20 Suppl 1*, S89-100.

Saha, D., Leong, K., Li, C., Peterson, S., Siegel, G., & Raman, B. (2013). A spatiotemporal coding mechanism for background-invariant odor recognition. *Nature Neuroscience*, *16*(12), 1830–1839. https://doi.org/10.1038/nn.3570

Sakamoto, A., Lüders, H., & Burgess, R. (1991). Intracranial recordings of movement-related potentials to voluntary saccades. *Journal of Clinical Neurophysiology: Official Publication of the American Electroencephalographic Society*, *8*(2), 223–233.

Sanders, R. D., Tononi, G., Laureys, S., & Sleigh, J. W. (2012). Unresponsiveness ≠ unconsciousness. *Anesthesiology*, *116*(4), 946–959. https://doi.org/10.1097/ALN.0b013e318249d0a7

Sarasso, S., Boly, M., Napolitani, M., Gosseries, O., Charland-Verville, V., Casarotto, S., Rosanova, M., Casali, A. G., Brichant, J.-F., Boveroux, P., Rex, S., Tononi, G., Laureys, S., & Massimini,

M. (2015). Consciousness and Complexity during Unresponsiveness Induced by Propofol, Xenon, and Ketamine. *Current Biology: CB*, *25*(23), 3099–3105. https://doi.org/10.1016/j.cub.2015.10.014

Schall, J. D. (1991). Neuronal activity related to visually guided saccadic eye movements in the supplementary motor area of rhesus monkeys. *Journal of Neurophysiology*, *66*(2), 530–558. https://doi.org/10.1152/jn.1991.66.2.530

Schall, J. D., & Bichot, N. P. (1998). Neural correlates of visual and motor decision processes. *Current Opinion in Neurobiology*, *8*(2), 211–217.

Schluppeck, D. (2006). Sustained Activity in Topographic Areas of Human Posterior Parietal Cortex during Memory-Guided Saccades. *Journal of Neuroscience*, *26*(19), 5098–5108. https://doi.org/10.1523/JNEUROSCI.5330-05.2006

Sendhilnathan, N., Basu, D., & Murthy, A. (2017). Simultaneous analysis of the LFP and spiking activity reveals essential components of a visuomotor transformation in the frontal eye field. *Proceedings of the National Academy of Sciences*, *114*(24), 6370–6375. https://doi.org/10.1073/pnas.1703809114

Shadlen, M. N., & Newsome, W. T. (2001). Neural basis of a perceptual decision in the parietal cortex (area LIP) of the rhesus monkey. *Journal of Neurophysiology*, *86*(4), 1916–1936. https://doi.org/10.1152/jn.2001.86.4.1916

Shew, W. L., & Plenz, D. (2013). The functional benefits of criticality in the cortex. *The Neuroscientist: A Review Journal Bringing Neurobiology, Neurology and Psychiatry*, *19*(1), 88–100. https://doi.org/10.1177/1073858412445487

Shew, W. L., Yang, H., Petermann, T., Roy, R., & Plenz, D. (2009). Neuronal Avalanches Imply Maximum Dynamic Range in Cortical Networks at Criticality. *The Journal of Neuroscience*, *29*(49), 15595–15600. https://doi.org/10.1523/JNEUROSCI.3864-09.2009

Shew, W. L., Yang, H., Yu, S., Roy, R., & Plenz, D. (2011). Information capacity and transmission are maximized in balanced cortical networks with neuronal avalanches. *The Journal of*

*Neuroscience: The Official Journal of the Society for Neuroscience*, *31*(1), 55–63. https://doi.org/10.1523/JNEUROSCI.4637-10.2011

Shima, K., Aya, K., Mushiake, H., Inase, M., Aizawa, H., & Tanji, J. (1991). Two movement-related foci in the primate cingulate cortex observed in signal-triggered and self-paced forelimb movements. *Journal of Neurophysiology*, *65*(2), 188–202. https://doi.org/10.1152/jn.1991.65.2.188

Slezin, V. B., Korsakova, E. A., Dytjatkovsky, M. A., Schultz, E. A., Arystova, T. A., & Siivola, J. R. (2007). Multifractal analysis as an aid in the diagnostics of mental disorders. *Nordic Journal of Psychiatry*, *61*(5), 339–342. https://doi.org/10.1080/08039480701643175

Solovey, G., Alonso, L. M., Yanagawa, T., Fujii, N., Magnasco, M. O., Cecchi, G. A., & Proekt, A. (2015). Loss of Consciousness Is Associated with Stabilization of Cortical Activity. *The Journal of Neuroscience: The Official Journal of the Society for Neuroscience*, *35*(30), 10866–10877. https://doi.org/10.1523/JNEUROSCI.4895-14.2015

Stokes, M. G. (2015). “Activity-silent” working memory in prefrontal cortex: A dynamic coding framework. *Trends in Cognitive Sciences*, *19*(7), 394–405. https://doi.org/10.1016/j.tics.2015.05.004

Stokes, M. G., Kusunoki, M., Sigala, N., Nili, H., Gaffan, D., & Duncan, J. (2013). Dynamic coding for cognitive control in prefrontal cortex. *Neuron*, *78*(2), 364–375. https://doi.org/10.1016/j.neuron.2013.01.039

Sugrue, L. P., Corrado, G. S., & Newsome, W. T. (2004). Matching behavior and the representation of value in the parietal cortex. *Science (New York, N.Y.)*, *304*(5678), 1782–1787. https://doi.org/10.1126/science.1094765

Suriya-Arunroj, L., & Gail, A. (2019). Complementary encoding of priors in monkey frontoparietal network supports a dual process of decision-making. *ELife*, *8*, e47581. https://doi.org/10.7554/eLife.47581

Suzuki, A., Katoh, T., & Ikeda, K. (1998). The effect of adenosine triphosphate on sevoflurane requirements for minimum alveolar anesthetic concentration and minimum alveolar anesthetic concentration-awake. *Anesthesia and Analgesia*, *86*(1), 179–183.

Sweeney, J. A., Luna, B., Keedy, S. K., McDowell, J. E., & Clementz, B. A. (2007). fMRI Studies of Eye Movement Control: Investigating the Interaction of Cognitive and Sensorimotor Brain Systems. *NeuroImage*, *36*(Suppl 2), T54–T60. https://doi.org/10.1016/j.neuroimage.2007.03.018

Theodoridis, S., & Koutroumbas, K. (2009). *Pattern recognition* (4. ed). Elsevier Acad. Press.

Tobler, P. N., & Müri, R. M. (2002). Role of human frontal and supplementary eye fields in double step saccades. *NeuroReport*, *13*(2), 253.

Tononi, G., Boly, M., Massimini, M., & Koch, C. (2016). Integrated information theory: From consciousness to its physical substrate. *Nature Reviews Neuroscience*, *17*(7), 450–461. https://doi.org/10.1038/nrn.2016.44

Tononi, G., & Koch, C. (2015). Consciousness: Here, there and everywhere? *Phil. Trans. R. Soc. B*, *370*(1668), 20140167. https://doi.org/10.1098/rstb.2014.0167

Tsuchiya, N., Wilke, M., Frässle, S., & Lamme, V. A. F. (2015). No-Report Paradigms: Extracting the True Neural Correlates of Consciousness. *Trends in Cognitive Sciences*, *19*(12), 757–770. https://doi.org/10.1016/j.tics.2015.10.002

Tzourio-Mazoyer, N., Landeau, B., Papathanassiou, D., Crivello, F., Etard, O., Delcroix, N., Mazoyer, B., & Joliot, M. (2002). Automated Anatomical Labeling of Activations in SPM Using a Macroscopic Anatomical Parcellation of the MNI MRI Single-Subject Brain. *NeuroImage*, *15*(1), 273–289. https://doi.org/10.1006/nimg.2001.0978

Urchs, S., Armoza, J., Moreau, C., Benhajali, Y., St-Aubin, J., Orban, P., & Bellec, P. (2019). MIST: A multi-resolution parcellation of functional brain networks. *MNI Open Research*, *1*, 3. https://doi.org/10.12688/mniopenres.12767.2

Van Der Werf, J., Buchholz, V. N., Jensen, O., & Medendorp, W. P. (2009). Neuronal synchronization in human parietal cortex during saccade planning. *Behavioural Brain Research*, *205*(2), 329–335. https://doi.org/10.1016/j.bbr.2009.06.011

Vijayan, S., Ching, S., Purdon, P. L., Brown, E. N., & Kopell, N. J. (2013). Thalamocortical mechanisms for the anteriorization of α rhythms during propofol-induced unconsciousness. *The Journal of Neuroscience: The Official Journal of the Society for Neuroscience*, *33*(27), 11070–11075. https://doi.org/10.1523/JNEUROSCI.5670-12.2013

Wang, J., Noh, G.-J., Choi, B.-M., Ku, S.-W., Joo, P., Jung, W.-S., Kim, S., & Lee, H. (2017). Suppressed neural complexity during ketamine- and propofol-induced unconsciousness. *Neuroscience Letters*, *653*, 320–325. https://doi.org/10.1016/j.neulet.2017.05.045

Watanabe, K., Igaki, S., & Funahashi, S. (2006). Contributions of prefrontal cue-, delay-, and response-period activity to the decision process of saccade direction in a free-choice ODR task. *Neural Networks*, *19*(8), 1203–1222. https://doi.org/10.1016/j.neunet.2006.05.033

Werf, J. V. D., Jensen, O., Fries, P., & Medendorp, W. P. (2008). Gamma-Band Activity in Human Posterior Parietal Cortex Encodes the Motor Goal during Delayed Prosaccades and Antisaccades. *Journal of Neuroscience*, *28*(34), 8397–8405. https://doi.org/10.1523/JNEUROSCI.0630-08.2008

Werf, J. V. D., Jensen, O., Fries, P., & Medendorp, W. P. (2010). Neuronal Synchronization in Human Posterior Parietal Cortex during Reach Planning. *Journal of Neuroscience*, *30*(4), 1402–1412. https://doi.org/10.1523/JNEUROSCI.3448-09.2010

Wilke, M., Kagan, I., & Andersen, R. A. (2012). Functional imaging reveals rapid reorganization of cortical activity after parietal inactivation in monkeys. *Proceedings of the National Academy of Sciences*, *109*(21), 8274–8279. https://doi.org/10.1073/pnas.1204789109

Yamamoto, J., Ikeda, A., Satow, T., Matsuhashi, M., Baba, K., Yamane, F., Miyamoto, S., Mihara, T., Hori, T., Taki, W., Hashimoto, N., & Shibasaki, H. (2004). Human eye fields in the frontal lobe

as studied by epicortical recording of movement-related cortical potentials. *Brain: A Journal of Neurology*, *127*(Pt 4), 873–887. https://doi.org/10.1093/brain/awh110

Yang, T., & Shadlen, M. N. (2007). Probabilistic reasoning by neurons. *Nature*, *447*(7148), 1075–1080. https://doi.org/10.1038/nature05852

Ying, S.-W., Abbas, S. Y., Harrison, N. L., & Goldstein, P. A. (2006). Propofol block of Ih contributes to the suppression of neuronal excitability and rhythmic burst firing in thalamocortical neurons. *European Journal of Neuroscience*, *23*(2), 465–480. https://doi.org/10.1111/j.1460-9568.2005.04587.x

Zapparoli, L., Seghezzi, S., Scifo, P., Zerbi, A., Banfi, G., Tettamanti, M., & Paulesu, E. (2018). Dissecting the neurofunctional bases of intentional action. *Proceedings of the National Academy of Sciences*, *115*(28), 7440–7445. https://doi.org/10.1073/pnas.1718891115

# Annexe A

# Article supplémentaire

## A. 1 Présentation de l'annexe A.

L'annexe A présente un article qui a été écrit dans le cadre de mon doctorat, sous la supervision du Dr. Karim Jerbi et du Dr. Rainville. Cet article a permis de mettre en lumière les changements d'oscillations neuronales associées à la prise ou à la perte de conscience induite par l'anesthésie. Cet article a permis de développer des méthodes d'analyses du signal EEG, des outils d'apprentissage machine, et de développer une compréhension des oscillations neuronales qui ont été indispensables pour la suite de mon doctorat, et pour les articles principaux présentés dans cette thèse.

# Long-range temporal correlations in the brain distinguish conscious wakefulness from induced unconsciousness

Thomas Thiery[1], Tarek Lajnef[1], Etienne Combrisson[1,2,3], Arthur Dehgan[1], Pierre Rainville[1], George A. Mashour[5], Stefanie Blain-Moraes[6], Karim Jerbi[1]

1 Psychology Department, University of Montreal, QC, Canada

2 Center of Research and Innovation in Sport, Mental Processes and Motor Performance, University Claude Bernard Lyon I, University of Lyon, Villeurbanne, France

3 Brain Dynamics and Cognition, Lyon Neuroscience Research Center, INSERM U1028, UMR 5292, University of Lyon, Villeurbanne, France

4 Department of Stomatology, University of Montreal, QC, Canada

5 Center for Consciousness Science, Department of Anesthesiology, University of Michigan, USA

6 School of Physical and Occupational Therapy, McGill University, Montreal, QC, Canada

Keywords: Consciousness, Unconsciousness, EEG, Oscillations, Detrended fluctuation analysis (DFA), Alpha oscillations, Anesthesia

Corresponding author: Thomas Thiery Email: thomas.thiery@umontreal.ca

Address: Department of Psychology, University of Montreal, C.P. 6128 succ. Centre- Ville, Montréal, QC, H3C 3J7, Canada

# Abstract

Rhythmic neuronal synchronization across large-scale networks is thought to play a key role in the regulation of conscious states. Changes in neuronal oscillation amplitude across states of consciousness have been widely reported, but little is known about possible changes in the temporal dynamics of these oscillations. The temporal structure of brain oscillations may provide novel insights into the neural mechanisms underlying consciousness. To address this question, we examined long-range temporal correlations (LRTC) of EEG oscillation amplitudes recorded during both wakefulness and anesthetic-induced unconsciousness. Importantly, the time-varying EEG oscillation envelopes were assessed over the course of a sevoflurane sedation protocol during which the participants alternated between states of consciousness and unconsciousness. Both spectral power and LRTC in oscillation amplitude were computed across multiple frequency bands. State-dependent differences in these features were assessed using non-parametric tests and supervised machine learning. We found that periods of unconsciousness were associated with increases in LRTC in beta (15–30Hz) amplitude over frontocentral channels and with a suppression of alpha (8–13Hz) amplitude over occipitoparietal electrodes. Moreover, classifiers trained to predict states of consciousness on single epochs demonstrated that the combination of beta LRTC with alpha amplitude provided the highest classification accuracy (above 80%). These results suggest that loss of consciousness is accompanied by an augmentation of temporal persistence in neuronal oscillation amplitude, which may reflect an increase in regularity and a decrease in network repertoire compared to the brain's activity during resting-state consciousness.

**Introduction**

Anesthetics are a useful tool for the study of human consciousness, as they can be titrated to pharmacologically induce the loss of consciousness (LOC) and the recovery of consciousness (ROC) in a controlled experimental design. Anesthetic-induced LOC usually coincides with a disruption of the brain's ability to integrate information (Alkire et al., 2008). Consistent with this view, studies have shown decreased EEG complexity at the time where consciousness was lost (Lee et al., 2010; Sarasso et al., 2015; Wang et al., 2017), as well as a changes in EEG global coherence (Akeju et al., 2014; Cimenser et al., 2011; John & Prichep, 2005). Analysis of EEG during propofol- and sevoflurane-induced unconsciousness further indicates a breakdown of the spatiotemporal organization around the gamma band (Pal et al., 2016), and a decreased frontoparietal connectivity associated with propofol, sevoflurane and ketamine-induced unconsciousness (Lee et al., 2009b, 2013 ; Boveroux et al., 2010 ; Jordan et al., 2013 ; Palanca et al., 2015 ; Bonhomme et al., 2016 ; Ranft et al., 2016). Additionally, several studies have demonstrated the importance of posterior alpha suppression and alpha anteriorization during anesthetic-induced unconsciousness (Blain-Moraes et al., 2015; Feshchenko et al., 2004; Gugino et al., 2001; Pavone et al., 2017; Purdon et al., 2015). These studies have focused on properties of local oscillations (e.g. power) and the functional connectivity between brain regions, but less is known about changes in long-range temporal properties of brain oscillations associated with states of consciousness.

The brain has been characterized according to its scale-invariant properties, reflected by a 1/f-like spectrum (Bak et al., 1987). This power-law scaling reflects arrhythmic brain activity with no predominant temporal scale (i.e., scale-free), and has been reported in MEG, EEG and fMRI data (Ciuciu et al., 2012; He, 2014). Some studies have used multiscale formalisms applied to the raw EEG signal, and have emphasized the relevance of scaling properties of the raw signal to predict the depth of anesthesia and measure the level of consciousness (Gifani et al., 2006; Jospin et al., 2007; Lalitha & Eswaran, 2007; Li et al., 2017; Liang et al., 2015; Nguyen-Ky et al., 2010). Interestingly, their results were close to the classical bispectral index values (BIS), which is commonly used to identify anesthesia states in clinical settings. While critical states can be detected in BOLD and raw EEG signal, it can also be observed in the amplitude-envelope of oscillations.

Beyond assessing scale-free dynamics of the raw brain signals, a growing body of literature provides evidence for the importance of investigating the scaling properties of brain signal amplitudes (i.e. envelopes) in specific frequency bands (Linkenkaer-Hansen et al., 2001). This allows us to probe their long-range temporal correlations (LRTC) and thereby provides a measure of how rhythmic neuronal activity propagates in time. Several studies have demonstrated the presence of LRTC in the amplitude dynamics of theta, alpha and beta frequency bands (Linkenkaer-Hansen et al., 2004, Nikulin and Brismar, 2004, 2005; Fedele et al., 2016) across a wide age range (Berthouze et al., 2010). Interestingly, pathological alterations of LRTC in brain oscillations were previously shown in Alzheimer's disease (Montez et al., 2009), major depressive disorder (Bornas et al., 2015; Linkenkaer-Hansen et al., 2005), schizophrenia (Nikulin et al., 2012; Slezin et al., 2007) and epilepsy patients (Monto et al., 2007). However, whether and how LRTC in specific frequency bands are modulated across states of consciousness remains unknown.

In the present study, we investigated the association of the LRTC of brain oscillations with varying states of consciousness. We hypothesized that reduced information processing during unconsciousness would be associated with increased brain signal regularity, which should translate into increased LRTC in the frequency bands most relevant for information integration. Secondly, we hypothesized that LRTC effects would not necessarily coincide with changes in mean spectral power in terms of frequency range and spatial distribution. To this end, we evaluated changes in the long-range temporal structure of band-limited EEG amplitude fluctuations (as well as standard mean spectral amplitude) during sevoflurane-induced unconsciousness in healthy participants. Importantly, this study protocol employed a gradual increase in the level of sevoflurane to bring participants to the border of conscious state transitions, leading to multiple successive switches between the state of consciousness and unconsciousness.

## Materials and methods

### Participants

Ten healthy volunteers were recruited and provided their written and informed consent after a careful discussion of risks and benefits to participate in this study. The study was conducted at the University

of Michigan Medical School and approved by the Institutional Review Board (HUM00061087). Two volunteers withdrew during administration of sevoflurane due to discomfort and one subject's EEG data were suboptimal due to excessive motion. Therefore, data from seven healthy volunteers (four males, 20 to 23 yrs. old) were included in the analysis. These data were previously published in a study investigating alpha anteriorization, cross-frequency coupling, and long-range phase correlations (Blain-Moraes et al., 2015). They have been re-analyzed in this study to test a distinct hypothesis.

**Anesthetic protocol**

Each experiment was conducted by two trained anesthesiologists. At the beginning of sevoflurane administration, participants were instructed to squeeze an object in either their left hand or right hand while instructions were delivered every 30 seconds through an audio loop. Left and right commands were randomized. Participants kept their eyes closed during waking states throughout the experiment and received sevoflurane anesthesia by a secured face mask with an initial concentration of 0.4% in high-flow oxygen. The protocol of sevoflurane administration follows the procedure introduced by Suzuki and colleagues (Suzuki et al., 1998). Sevoflurane was administered at a given level for a 15-min equilibration period to achieve steady state, followed by 10 minutes at the target concentration. Sevoflurane concentration was increased by increments of 0.2% until loss of consciousness (LOC) was achieved. After 10min of unconsciousness, the reverse protocol (equilibration followed by steady-state period in increments of 0.2%) was employed until the participant regained consciousness. After recovery of consciousness (ROC), anesthetic concentration was still titrated downward until end-tidal values were 0%. More details concerning the anesthetic protocol are available in Blain-Moraes and colleagues (Blain-Moraes et al., 2015).

**Behavioral State Analysis**

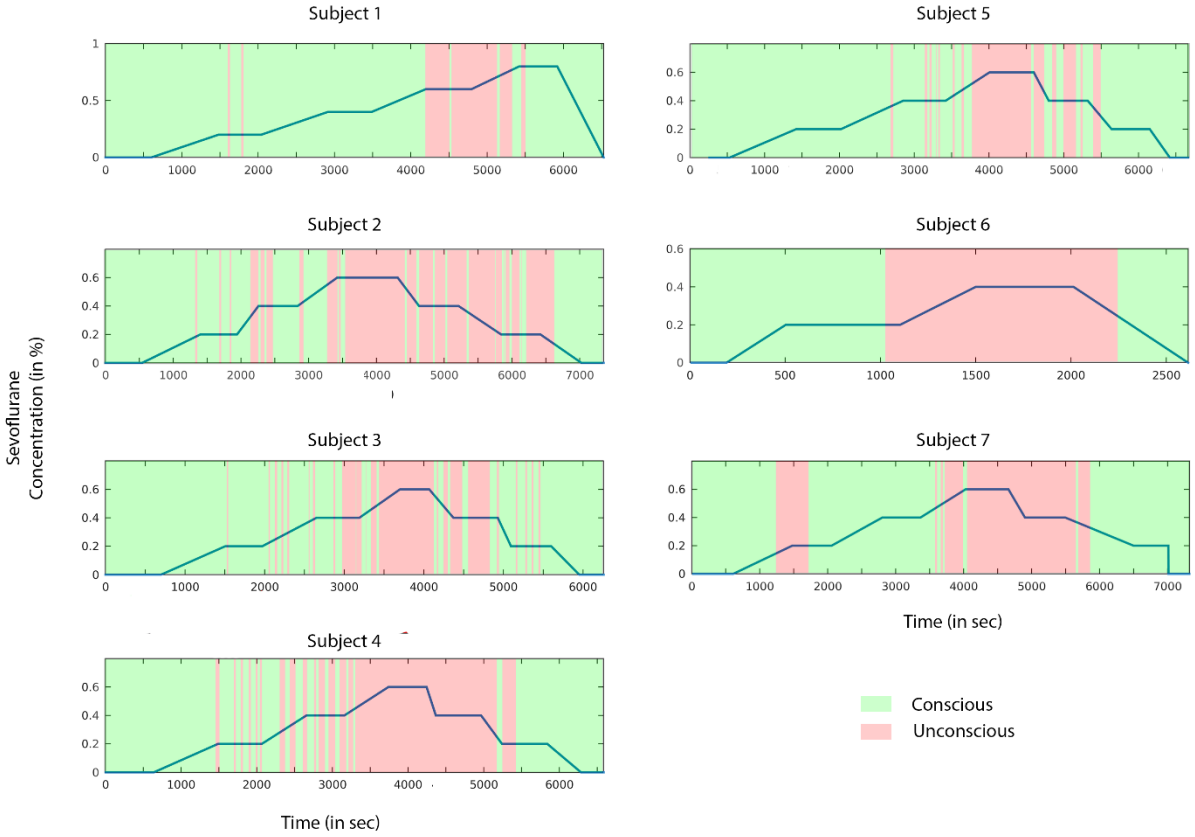


**Figure 1. Pharmacological and behavioral profiles.** The blue line represents the sevoflurane concentration during the experimental session for all participants. Conscious (green) and unconscious (red) segments were determined based on the responsiveness of participants.

Before sevoflurane exposure, the participants were given objects in each hand that would emit a sound when squeezed. They were instructed to squeeze the object in either their left hand or right hand when sevoflurane administration began; left/right commands were randomized and instructions were delivered every 30 seconds. Response presence or absence was observed and recorded in the data collection software by two investigators throughout the experimental period. To compare and pool data across participants, data segments were split into two categories using two types of behavioral time markers: LOC corresponded to the first failure to respond to an auditory command and ROC to the first positive response to an auditory command following LOC. We then defined in each subject the consciousness vs unconsciousness data segments based on these individual

responsiveness profiles: (1) Conscious periods were defined as those directly preceding LOC or following ROC markers and (2) Unconscious periods were defined as those between LOC and ROC.

**EEG recordings and pre-processing**

The EEG was acquired using a 64-channel sensor net from Electrical Geodesics, Inc. (Eugene, OR) and all channels were referenced to the vertex. Electrode impedances were kept below 50 kΩ and EEG signals were collected at a sampling rate of 500 Hz. EEG signals were re-referenced to an average reference and visually inspected to reject epochs and channels with noise or non-physiological artefacts. We used the individual responsiveness profiles to discriminate conscious from unconscious segments in the raw EEG data. For each subject, we ended up with two separated raw datasets, one for the conscious condition and one for the unconscious condition. We then segmented the data from both conditions in 60-second epochs with no overlap in order to match the number of samples we obtained in the detrended fluctuation analysis (DFA) (see next section). The average length of conscious epochs was 68 (± 20), while the average length of unconscious epochs was 34 (± 13).

**Instantaneous amplitude of neuronal oscillations**

The instantaneous amplitude of the EEG signals was computed in five different frequency bands: delta (1 – 4 Hz), theta (4 - 7Hz), alpha (8 – 13 Hz), beta (15 - 30 Hz) and gamma (30-60 Hz). This was achieved by first filtering the raw EEG signals using a finite impulse response filtering (FIR1, order = 3) and then computing the Hilbert transform. Fig. 2A shows an example of the raw signal, and Fig. 2B shows the filtered signal and its instantaneous amplitude in the beta band. The amplitude was obtained for each 60-s epoch and for each channel and condition separately (conscious and unconscious). Then, the overall mean amplitude of neuronal oscillations in each frequency band was computed by averaging the amplitude values across all available data samples for each channel and condition (conscious and unconscious) separately.

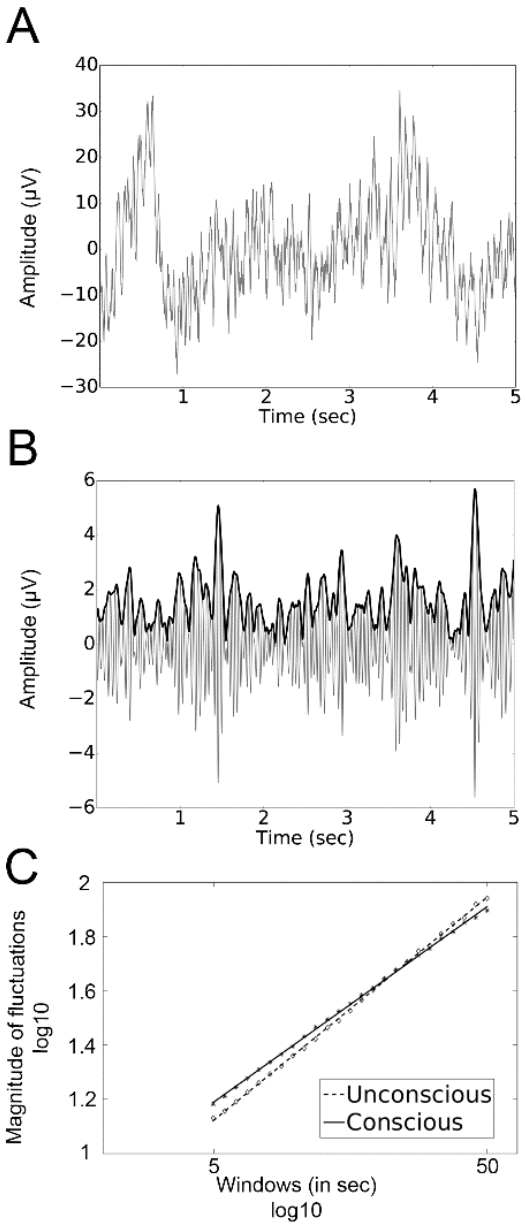


**Figure 2. Estimating scaling behavior in oscillatory amplitude using DFA.** (A) A 5-second sample of raw signal from electrode Cz. (B) The filtered signal (continuous grey line) and instantaneous amplitude (bold black line) of neuronal oscillations in the beta frequency range. (C). The DFA method measures the root-mean-square fluctuation of the integrated and linearly detrended signals as a function of time-window size. The slope of the fluctuation function for consciousness (continuous line) and unconsciousness (dotted line) for all subject on electrode Cz

**Detrended Fluctuation Analysis (DFA)**

The presence of LRTC indicates that the temporal auto-correlations attenuate very slowly in time, according to a power-law. Thus, slow attenuation of LRTC is an indication of how neuronal events develop over time. It provides information about the long-term temporal structure of the complex patterns of ongoing activity, which in turn is thought to be related to the integrity of multiple interconnected populations of neurons (Nikulin et al., 2012). In EEG recordings, DFA can be applied to detect long-range temporal correlations (auto-correlations) either in the raw time-domain signals or alternatively in the temporal dynamics of the signal envelope (amplitude) in a given frequency band (Kantelhardt et al., 2001; Peng et al., 1995). In the present study, DFA was used to analyze the decay of temporal auto-correlations in the time range of 5–50 s. The processing of broadband EEG signal to enable quantification of LRTC using DFA has been explained in detail elsewhere (Linkenkaer-Hansen et al., 2001; Nikulin & Brismar, 2005). In brief, the DFA measures the scaling of the root-mean-square fluctuation of the integrated and linearly detrended signals, F(t), as a function of time window size t (Fig. 2C). The DFA exponent is the slope of the fluctuation function shown in Fig. 2C. A DFA scaling exponent, also termed the "self-similarity parameter" (Lux & Marchesi, 1999), is extracted with linear regression in double-logarithmic coordinates using a least-squares algorithm. A scaling exponent between 0.5 and 1.0 indicates a greater persistence of temporal correlations (i.e. temporal autocorrelations), while scaling exponents between 0 and 0.5 reflect decreased signal persistence (i.e. temporal anti-correlations). An uncorrelated signal is characterized by an exponent of 0.5. This method is thought to have several advantages over other options such as the Generalized Hurst Exponent or the autocorrelation function (Peng et al., 1995), since it requires less strict assumptions about the stationarity of the signal and provides greater accuracy in the estimates of correlations (Gao et al., 2006; Linkenkaer-Hansen et al., 2007). Previous studies have shown that electrophysiological brain signals generally have scaling exponents above 0.5 (Berthouze et al., 2010; Fedele et al., 2016; Linkenkaer-Hansen et al., 2001, 2004; Nikulin & Brismar, 2004, 2005). Here we measured LRTC in the signal on single 60-second epochs. As DFA can be affected by the length of the signal it is calculated on, we conducted an additional analysis were LRTC were computed on the whole signal. Importantly, we found similar results in both cases.

**Statistical Analysis**

We conducted a two-sided permutation based pseudo t-test corrected with maximum statistics using exhaustive permutations (number of permutations = 128) on amplitude values and scaling exponent values. For most subjects, conscious and unconscious conditions were significantly unbalanced, resulting in a larger number of conscious samples. To address this issue, we randomly selected conscious samples in order to match the number of unconscious samples for each subject separately before performing the statistical analysis. We repeated this procedure 100 times, with different segments randomly chosen every time, and observed stable results across repetitions.

**Control Analysis: Effect of sevoflurane concentration**

To verify whether changes in oscillatory amplitude and scaling exponents can be entirely explained by changes in sevoflurane concentration rather than states of consciousness, an additional analysis was conducted. We used the sevoflurane concentration to discriminate periods of higher sevoflurane concentration (> 0.4) and lower sevoflurane concentration (< 0.4) segments in the raw EEG data across the entire recordings, during the state of consciousness only. The threshold of 0.4 was chosen by taking the median split of sevoflurane concentration (min = 0, max = 0.8). For each participant, this procedure led to two raw datasets, one for the higher sevoflurane condition and one for the lower sevoflurane condition. We computed LRTC and the instantaneous amplitude of neural oscillations using the same methods as those used for the comparison between consciousness and unconsciousness conditions. Then, we assessed statistical differences between lower and higher sevoflurane concentration at the group level using a two-sided permutation-based pseudo t-test corrected with maximum statistics using exhaustive permutations on amplitude values and scaling exponent values.

**Machine Learning Analysis**

In addition to investigating the contrasts between consciousness and unconsciousness using standard statistical assessments, we also assessed whether the neural markers (i.e., alpha amplitude and beta scaling exponent) that we identified as being relevant through comparisons between means also carried discriminative information at the level of single 60-second epochs, which we also refer to as trials. To this end, we implemented a machine learning (ML) framework for trial-by-trial classification of consciousness states using spectral amplitude and scaling exponent values as features. To avoid classification bias that arises from unbalanced classes, all ML analyses were performed on balanced sets of epochs where we randomly selected conscious samples in order to match the number of unconscious samples available for each subject. This random selection was repeated 100 times and decoding performance was computed as the mean of all classification accuracies across repetitions. To avoid any bias from unbalanced classes, we used equal numbers of epochs in each class within each individual. This led to an observation space of dimension n=476 for the cross-subject ML framework.

Two classification procedures were explored in this study. First, the machine-learning procedure was conducted by using single feature classification in order to identify the most relevant features discriminating conscious and unconscious conditions. We then used multi-feature classification to evaluate whether the decoding accuracies could be enhanced when combining multiple features and electrodes within each classification.

*Single Feature Classification:* Several classification techniques were initially tested for the single feature classification procedure, including linear-discriminant analysis (LDA), k-nearest-neighbor (KNN) and support vector machine (SVM). The results were very similar across the methods, with slightly better and faster results using LDA, which was therefore chosen for this study. Within- and across-subject classification of conscious versus unconscious states were performed using LDA (Fisher, 1936).

In brief, for a two-dimensional problem, the LDA algorithm tries to find a hyperplane that maximizes the mean distance between the mean of the two classes while minimizing inter-class variance.

*Computation of decoding accuracy via cross-validation*: At the group level, the performance of the proposed classification method was evaluated using a Leave-One-Subject-Out (LOSO) cross-validation procedure. This procedure is a special case of k-fold cross validation, where all individuals except one are used for training, and the classifier is tested on the data from the omitted participant (i.e., test data). This procedure is repeated iteratively, each time leaving a different individual out of the training. The LOSO cross-validation method efficiently uses data and provides an asymptotically unbiased estimate of the averaged classification error probability over all possible training sets (Theodoridis & Koutroumbas, 2009). The statistical significance of the obtained decoding accuracies was evaluated by computing statistical thresholds using permutation tests ($n=1000$, $p<0.001$). In other words, a null-distribution is generated by repeatedly ($n=1000$) computing the classification accuracy obtained after randomly permuting class labels (Combrisson & Jerbi, 2015).

*Multi-Feature classification*: A multi-feature (MF) classification procedure was employed to determine if (and to which extent) correct classification rate can be enhanced by combining features across types (oscillation amplitude and LRTC) and/or across all electrodes. We tried several MF strategies including K-best, Forward Feature Selection, Backward Feature Elimination, and Sequential Forward Feature Selection. Optimal classification performance was obtained by using LDA. This was done within the training set, in order to conserve a strict separation between training/hyper-parameter selection and the hold-out set. The performance of the proposed classification method was evaluated using a Leave-One-Subject-Out (LOSO) cross-validation procedure. This procedure is repeated as many times as there were participants, each time leaving a different individual out of the training data. Given that we had 7 participants; the procedure was completed in 7 iterations, with each iteration producing either a correct or an incorrect classification of the untrained, test data set. As for all other analyses, we randomly selected conscious epochs in order to match the number of unconscious samples for each

subject, and repeated our analyses 100 times. We then averaged the decoding accuracies across repetitions. Finally, we tested the statistical significance of all reported results using maximum statistics and derived significance thresholds using permutation testing (n=1000, P<0.001).

**Results**

The scaling behavior of oscillation amplitude dynamics of conscious (n=477, mean per subject = 68 ± 21) and unconscious (n=238, mean per subject = 34 ± 14) epochs was obtained using DFA in all participants. Fig. 1C shows an illustrative example of how scaling behavior (i.e., an estimate of the scaling exponent) was derived for beta-band amplitude dynamics at electrode CZ for conscious and unconscious conditions. The plot shows data for 5 to 50s. The linear relationship between the logarithm of the time scale and the logarithm of the amplitude fluctuations reflects power law scaling. The spatial distribution of the scaling exponents for delta, theta, alpha, beta and gamma oscillations is presented in Fig. 3. Importantly, scaling exponents values were all between 0.5 and 1, which is consistent with the presence of LRTC in all frequency bands and for both conscious and unconscious states. This observation is in agreement with previous findings (Nikulin and Brismar, 2005, Linkenkaer et al., 2001). Moreover, when comparing scaling exponents between conscious and unconscious epochs, significant differences were found uniquely for beta oscillation envelope ($p < 0.05$, corrected). The electrodes showing this effect formed a cluster over frontocentral areas.

**Posterior alpha power also distinguishes between states of consciousness**

The spatial topographies of oscillation amplitude (similar to spectral power) for delta, theta, alpha, beta and gamma bands in consciousness and unconsciousness are shown in Fig. 4. The only frequency band in which we observed a significant change in mean oscillation amplitude was the alpha (8-13 Hz) band. Compared to consciousness, unconsciousness was associated with a significant drop in alpha amplitude over posterior brain areas ($p < 0.05$). No such effects were found in the beta band where significant changes in LRTC were observed.

Importantly, we conducted an additional analysis to investigate whether changes in scaling exponents and oscillation amplitude could be driven by changes in sevoflurane concentration rather than states of consciousness. As shown in the supplementary figures, changes in sevoflurane concentration did not lead to significant changes in either scaling exponents (Fig. S1) or the instantaneous amplitude of neural oscillations (Fig. S2).

**Classification accuracy of states of consciousness is maximal when both beta LRTC and alpha power are combined**

We conducted a ML analysis to probe the robustness of the LRTC and amplitude changes across levels of consciousness. For both single feature and multi feature classification, we restricted the choice of the classifier either to an LDA or a SVM (with a linear or RBF kernel). The LDA provided higher decoding accuracy compared to other options. As a consequence, we used an LDA algorithm in our ML pipelines. This analysis revealed that beta-band LRTC and alpha amplitude could both be used to correctly predict consciousness from unconsciousness on single trials (Fig.5). The multi-feature analysis also gave the best results using LDA and a Sequential Forward Feature Selection. Multivariate classification using data from all electrodes yielded decoding accuracies of 75.22 % for beta LRTC and 79.05 % for alpha amplitude using single-trial LDA and LOSO cross-validation. Consistent with our findings in the LRTC analysis, while beta scaling exponents provided significant decoding on frontocentral channels, alpha oscillation amplitude led to significant decoding primarily over posterior regions. Interestingly, the spatial patterns of single-trial decoding accuracy (left panels in Fig 5) closely match the topographies of differences obtained using statistical comparisons of means (Fig 3 and 4). Moreover, performing multi-site multi-feature decoding combining the beta scaling exponents and alpha amplitudes in a common classification framework increased the overall decoding accuracy to 80.72 % (Fig 5. C). This increase, compared to the decoding accuracy obtained when using either beta LRTC or alpha amplitude individually, may indicate that LRTC and oscillation amplitude features reflect changes in distinct mechanisms underlying consciousness.

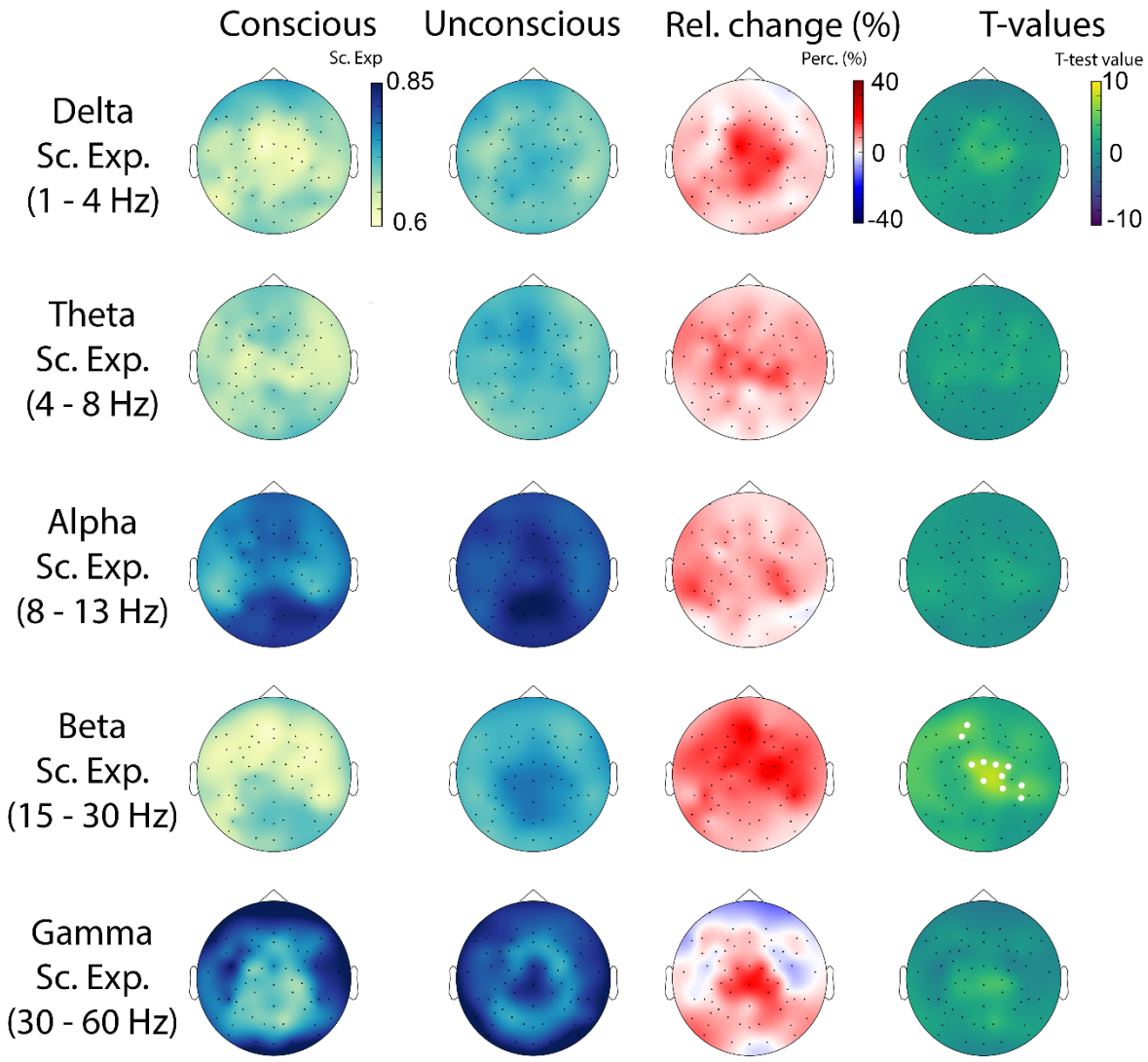


**Figure 3.** Topographical plots showing the spatial distribution of mean values for delta, theta, alpha, beta and gamma scaling exponents for conscious and unconscious conditions, and the percent relative change (Relative Change=[Unconsc-Consc]/Consc). Topographical maps of statistical differences between consciousness and unconsciousness at the group level are also shown. White dots represent the statistical significance derived for the sample size using exhaustive permutations corrected with maximum statistics at $p<0.05$.

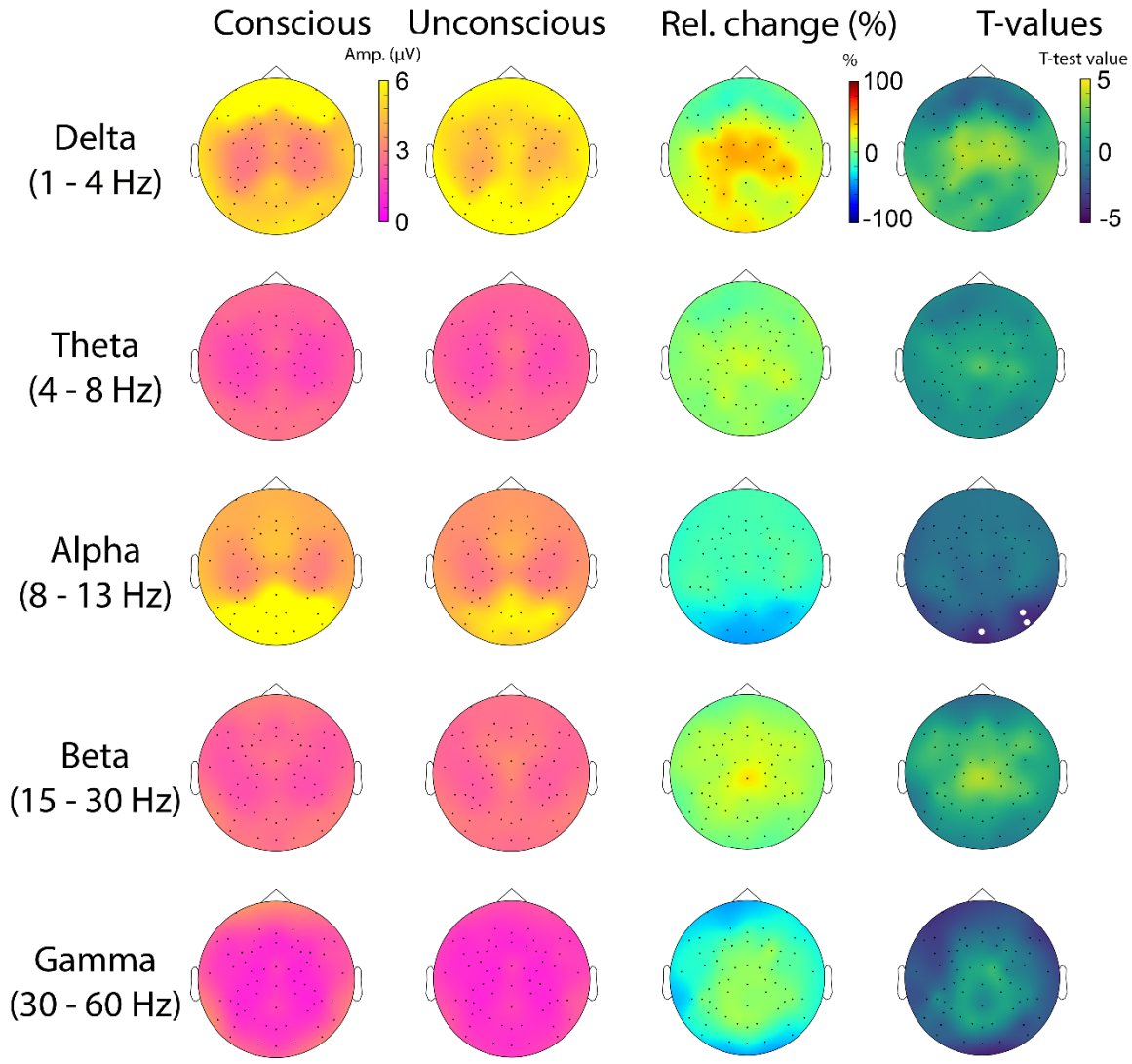


**Figure 4.** Topographical plots showing the spatial distribution of mean values for delta, theta, alpha, beta and gamma amplitudes for conscious and unconscious conditions, and the percent relative change (Relative = [Unconsc-Consc]/Consc). Topographical maps of statistical differences between consciousness and unconsciousness at the group level are also shown. White dots represent the statistical significance derived for the sample size using exhaustive permutations corrected with maximum statistics at $p<0.05$.

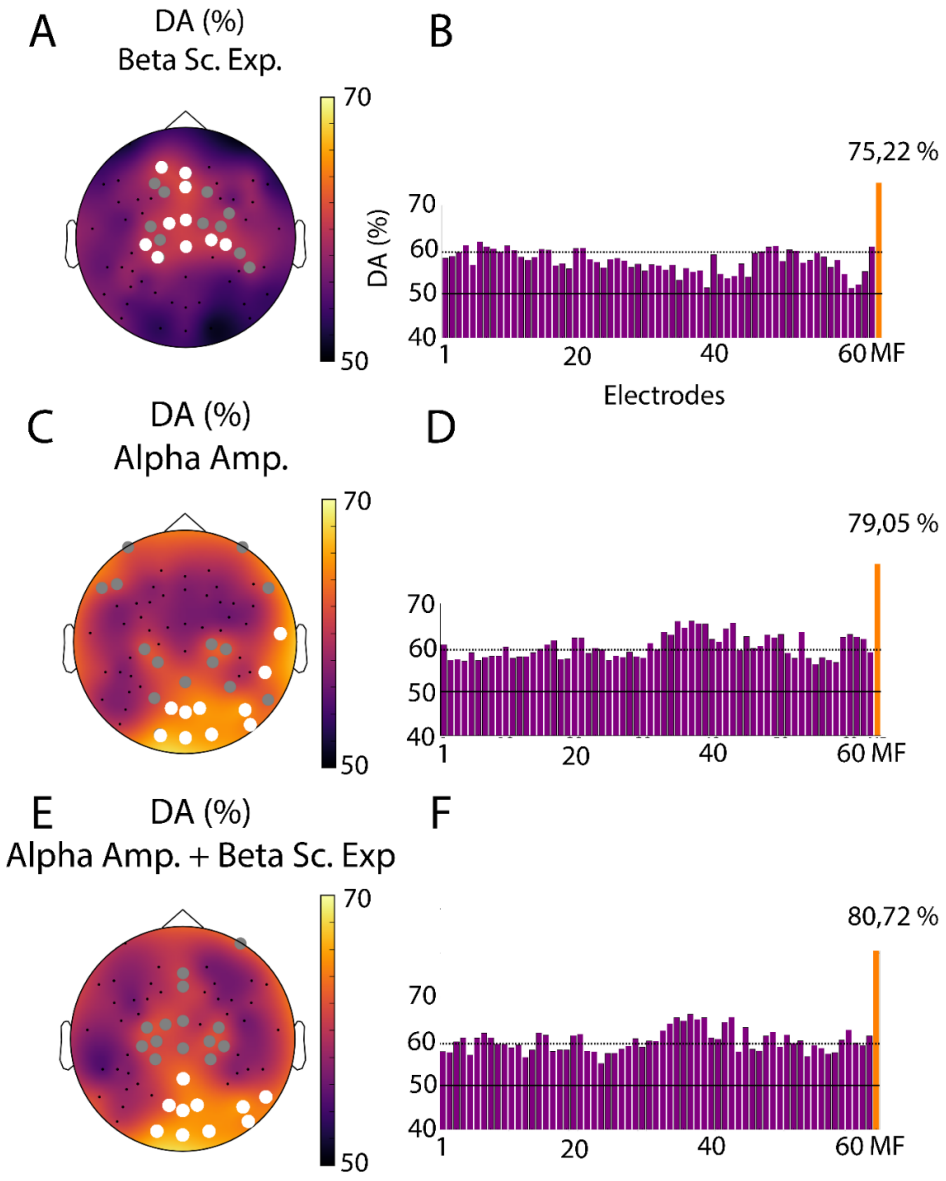


**Figure 5. Topographical maps of single-trial decoding performance (Conscious vs. Unconscious).** Topographical maps (left) and bar charts (right) of the single-feature decoding accuracy (DA) for the beta band scaling exponents (A,B), alpha amplitude (C,D), as well as the beta scaling exponent and the alpha amplitude combined (E,F). All circles in panels (A), (C) and (E) indicate electrodes where the DA was statistically significant ($p<0.001$, corrected). Among these, the ten that had the highest decoding accuracies are labeled with a white circle. The continuous horizontal lines on the bar charts depict the theoretical chance level (50%), while the dotted lines represent the statistical significance threshold ($p<0.001$, corrected). The orange bar to the right of each bar plot represents the decoding accuracy obtained with the multi-feature decoding method described above.

## Discussion

Although spectral power has been repeatedly shown to be modulated across states of consciousness, much less is known about whether the long-range temporal properties of such oscillations vary across levels of consciousness. Given that unconsciousness is associated with a decrease in neuronal excitability and diminished information integration capacity, we hypothesized that loss of consciousness should be associated with modulations in LRTC of relevant EEG rhythms. The results reported here using anesthetic-induced unconsciousness confirm this hypothesis and provide the first evidence for an increase in LRTC in the envelope of frontocentral beta oscillations during shallow unconsciousness. Spectral power in the beta frequency range did not change. However, a significant drop in posterior alpha power was found. The diverging spatial and spectral patterns observed with LRTC and oscillation amplitude suggest that these two features reflect distinct properties of brain dynamics that may be altered during unconsciousness. Conversely, the amplitude of neuronal oscillations and their scaling behavior may underlie different mechanisms critical to maintaining consciousness.

### Unconsciousness is associated with increased beta LRTC

The values of the scaling exponents of our DFA analysis are globally in agreement with values reported in previous studies and are thus consistent with the presence of LRTC in neuronal oscillations recorded with EEG/MEG (Linkenkaer-Hansen et al., 2001, 2004; Nikulin & Brismar, 2004, 2005). The increase in scaling exponents in beta band during unconsciousness reflects greater temporal correlation in the amplitude envelope of the EEG at this frequency, and is often described as increased persistence in the signal. It has been hypothesized that this trend towards regularity may reflect a drop in neuronal excitability which may in turn constrain cognitive flexibility (Alkire et al., 2008; He, 2014). The reported rise in beta-band LRTC during anesthetic-induced unresponsiveness is consistent with this explanation.

The electrode sites that showed statistically significant increases of beta LRTC in the present study were broadly located over frontocentral brain regions. Incidentally, this area overlaps with the location of putative generators of sensorimotor beta oscillations (Niedermeyer & Silva, 2005), which have been linked to signaling unchanging motor or cognitive states (Engel & Fries, 2010). The possibility that increased beta LRTC could indicate reduced switching between such states is a plausible hypothesis but it cannot be demonstrated with the currently reported data. Our assessment of changes in oscillation amplitude did not show any state-based differences in the beta band between consciousness and unconsciousness. This precludes an alternative interpretation of the results based on motor related activations. An additional analysis conducted on the mu (9-11 Hz) rhythm, with the methods previously described, did not yield any significant effects in amplitude or LRTC. The fact that amplitude and LRTC differences between consciousness and unconsciousness were only visible in the beta range and not in the mu and alpha frequency bands makes an account based on motor-related activity highly unlikely.

Several studies have applied multi-scale formalisms to the raw EEG signal to monitor the depth of anesthesia (Gifani et al., 2006; Jospin et al., 2007; Lalitha & Eswaran, 2007; Liang et al., 2015; Nguyen-Ky et al., 2010). Findings from these studies suggest that the quantification of scaling exponents by applying DFA to the raw EEG signal leads to comparable, and sometimes better, classification of the depth of anesthesia compared to assessments using other known measures such as bispectral index (BIS). The objective of the present study is different. Rather than seeking to find a metric to assess the depth of anesthetic-induced anesthesia, we set out to assess modulations in the scale-free properties of neural oscillations when participants alternate between wakefulness and light sedation. By doing this we aimed to gain novel insights into the role of brain oscillations in levels of consciousness by comparing their LRTC during states of consciousness and unconsciousness. Our study is the first to use DFA specifically on band-limited oscillation amplitude signals (envelopes) in humans during wakefulness and sevoflurane-induced unconsciousness.

In a recent study, Krzemiński et al (2017) used DFA on the amplitude of local field potentials (LFP) in monkeys and observed a decrease of LRTC during unconsciousness induced by anesthetics. The discrepancies between their results and ours could be due to a number of reasons. First, the anesthetic agents used to induce general anesthesia in monkeys differed from the one used here; the

authors used propofol, ketamine, medetomidine, or ketamine and medetomidine while we used sevoflurane. Moreover, in our study the participants were purposely maintained on the border of conscious/unconscious state transitions through a light-sedation protocol, whereas the monkeys in the study by Krzemiński et al (2017) underwent deep anesthesia. Lastly, the processes underlying consciousness and unconsciousness may differ between humans and primates.

To our knowledge, the present study is the first to detect a modulation in LRTC in beta oscillation amplitudes during unconsciousness. Overall, the increased beta-band LRTC we found is consistent with predictions based on the literature, and provides further evidence supporting the theory that anesthetics induce unconsciousness by reducing information integration and the repertoire of available cortical activation patterns (Alkire et al., 2008; Barttfeld et al., 2015; Casali et al., 2013; Hudetz et al., 2015; Solovey et al., 2015; Wang et al., 2017).

For the first time, the present study provides evidence for an increase in LRTC of beta-band oscillation amplitude during unconsciousness. This finding demonstrates that the loss of consciousness is accompanied by an augmentation of temporal persistence in neuronal oscillation amplitude, reflecting increased regularity in brain activity.

**Suppression of posterior alpha amplitude during anesthetic-induced unconsciousness**

Our assessment of mean oscillation amplitudes showed a significant suppression of occipital alpha, as expected from previous experimental and modeling work in anesthetic-induced unconsciousness (Blain-Moraes et al., 2015; Feshchenko et al., 2004; Gugino et al., 2001; Pavone et al., 2017; Purdon et al., 2015). Although the neurobiological basis of this occipital alpha suppression during anesthesia is not fully understood, computational models suggests that alpha suppression may be caused by alterations of hyperpolarization-activated membrane currents in the thalamus (Ying et al., 2006; Vijayan et al., 2013). Combining this occipital alpha model with a model of GABAergic inhibition enhancement involved in frontal alpha generation also accounts for alpha anteriorization (Ching et al., 2010; Purdon et al., 2013; Vijayan et al., 2013; Mukamel et al., 2014). The shallow unconsciousness induced here using low concentrations of sevoflurane only led to a drop in occipital alpha but not in

alpha anteriorization, as reported previously for this data (Blain-Moraes et al., 2015) and in other analyses (Kaskinoro et al., 2015).

**Supervised classification confirms distinct contributions of oscillations and LRTC**

The application of a supervised learning framework allowed us to determine which features, among those discussed above, were useful for short single-trial decoding of consciousness and unconsciousness. Being able to decode conscious and unconscious states on a single-trial basis is important for clinical monitoring and the prevention of intraoperative awareness with explicit recall (Mashour et al., 2012). Our results also demonstrate that combining alpha amplitude and beta LRTC features across multiple sites yields higher decoding than using just one or the other. Furthermore, EEG channels that showed significant classification using alpha amplitudes were located over occipitoparietal cortex. This is consistent with the account of Tononi and Koch (2015), suggesting that the NCC are primarily localized to a posterior cortical hot zone that includes sensory areas. By contrast, the beta LRTC decoding results suggest the additional involvement of frontocentral areas. This finding seems to corroborate the hypothesis that a frontoparietal circuit is ignited during consciousness (Dehaene and Changeux, 2011). Further studies are needed to confirm and extend these findings. Indeed, recent results from no-report paradigms challenge the ignition of a frontoparietal network as NCC, as it may be elicited by various components such as attention, working memory or expectations (Tsuchiya et al., 2015).

**LRTC in anesthesia and implications for NCC**

Our findings are consistent with previous investigations of the neuronal mechanisms underlying consciousness and anesthetic-induced unconsciousness, and with existing hypotheses of the mechanisms of unconsciousness such as the cognitive unbinding theory (Mashour, 2013) and the

integrated information theory (Tononi et al., 2016). Various candidates for NCC have been reported including an frontoparietal ignition network (Dehaene and Changeux, 2011) or alternately a posterior cortical hot zone (Koch et al., 2016), and often involve local and cortico-cortical oscillatory synchronization phenomena (Tononi and Koch, 2015). The present study is the first to provide evidence for an increase in LRTC of beta-band oscillation amplitude during unconsciousness. In recent years, LRTC of EEG or MEG oscillation amplitudes has been used to investigate the neural dynamics for a number of conditions such as Alzheimer's disease, schizophrenia and depression (Linkenkaer-Hansen et al., 2005; Montez et al., 2009; Nikulin et al., 2012). Our findings suggest that the scaling behavior of brain oscillation amplitude may constitute a distinctive feature characterizing the NCC through a characterization of the temporal properties of local and large-scale rhythmic synchronization.

**Limitations and future directions**

This study uses an anesthetic to induce unconsciousness, raising the possibility that the changes in beta amplitude LRTC are specific to the drug, as opposed to the state of consciousness of the participants. Our control analyses (cf. supplementary figures) demonstrate that changes in EEG oscillation amplitude and LRTC cannot be entirely explained by changes in sevoflurane concentration and thus likely reflect changes in the state of consciousness. Another valuable approach to tackle this question would be to assess changes in EEG during unconsciousness induced by molecularly distinct anesthetics or during sleep. Indeed, sleep can also be considered as a physiological state in which both the level and content of consciousness are reduced. Indeed, sleep can also be considered as physiological state in which both the level and content of consciousness are reduced. Several studies have applied DFA to the raw EEG signal during sleep and showed increased scaling exponent during deep sleep compared to wakefulness sleep (Lee 2002, Zorick 2013, Kim 2009, Lee 2004). Additionally, in a recent study, authors applied DFA on neuronal oscillations and demonstrated that LRTCs decline as sleep deprivation progresses, and then increased during sleep (Meisel et al., 2017). By demonstrating the importance of sleep to maintain LRTCs in the human brain, the authors postulate

that sleep reorganizes cortical networks towards critical dynamics for optimal functioning. Overall, these results suggest potentially similar processes between anesthetic and sleep induced unconsciousness. However, the natural increased LRTCs during sleep might have a functional role in bringing back cortical networks towards critical dynamics, while anesthetics might induce an abnormal increased regularity in brain signals, which may in turn reflect a drop in neuronal excitability, thus constraining cognitive flexibility.

Moreover, in our paradigm, participants were considered conscious or unconscious based on their degree of motor responsiveness to a verbal command, which is a false equivalency (Sanders et al., 2012). This study also had a small number of subjects, in part due to the demanding nature of the gradual-induction experimental paradigm. We accounted for this limitation by applying a single-epoch ML approach using all data segments aggregated across all participants (n=476) while controlling for biases due to subjects' idiosyncrasies using the LOSO procedure in order to confirm and extend the observations made through standard statistical comparisons of means. Additionally, one possible opportunity for improvement would be to explore in more detail the anatomical substrates of the changes reported here. With access to individual anatomical MRI data and a larger group of participants, one could more reliably localize sources of the EEG signals and probe the scaling and power changes in cortical source space.

This study represents a first step in investigating the significance of LRTC as a potential candidate for the NCC. Indeed, DFA scaling exponents can be considered as a potential window onto criticality of consciousness. The presence of LRTC has been linked to the criticality phenomenon in neuronal networks, which implies that the system is at a metastable state with a delicate balance between excitation and inhibition (Shew and Plenz, 2013). It is plausible that the increased LRTC during unconsciousness is associated with an imbalance between excitation and inhibition in neuronal networks, resulting in a loss of dynamic range (Shew et al., 2009), information transfer and capacity in the brain (Shew et al., 2011). Further studies are needed to assess the extent of LRTC changes across a variety of conditions involving alterations of consciousness and to determine the specific underlying neuronal mechanisms and functional meanings of LRTC.

**Acknowledgments**

TT was supported by a scholarship from Fonds de Recherche Nature et Technologies (FRQNT). KJ is supported by funding from the Canada Research Chairs program and a Discovery Grant (RGPIN-2015-04854) awarded by the Natural Sciences and Engineering Research Council of Canada. SBM is supported by a Discovery Grant (RGPIN-2016-03817) awarded by the Natural Sciences and Engineering Research Council of Canada, and a New Investigators Award from the Fonds de recherché du Quebec – Nature et technologies. The data acquisition was supported by the National Institutes of Health, Bethesda, Maryland, Grant R01GM098578 (to GAM) and the Department of Anesthesiology, University of Michigan.

**Competing Interests**

The authors declare that they do not have competing interest regarding the publication of this paper.

**References**


Akeju, O., Westover, M. B., Pavone, K. J., Sampson, A. L., Hartnack, K. E., Brown, E. N., & Purdon, P. L. (2014). Effects of Sevoflurane and Propofol on Frontal Electroencephalogram Power and Coherence. *Anesthesiology: The Journal of the American Society of Anesthesiologists*, *121*(5), 990–998. https://doi.org/10.1097/ALN.0000000000000436

Alkire, M. T., Hudetz, A. G., & Tononi, G. (2008). Consciousness and anesthesia. *Science (New York, N.Y.)*, *322*(5903), 876–880. https://doi.org/10.1126/science.1149213

Bak, P., Tang, C., & Wiesenfeld, K. (1987). Self-organized criticality: An explanation of the 1/f noise. *Physical Review Letters*, *59*(4), 381–384. https://doi.org/10.1103/PhysRevLett.59.381

Barttfeld, P., Uhrig, L., Sitt, J. D., Sigman, M., Jarraya, B., & Dehaene, S. (2015). Signature of consciousness in the dynamics of resting-state brain activity. *Proceedings of the National Academy of Sciences*, *112*(3), 887–892. https://doi.org/10.1073/pnas.1418031112

Beggs, J. M., & Plenz, D. (2003). Neuronal avalanches in neocortical circuits. *The Journal of Neuroscience: The Official Journal of the Society for Neuroscience*, *23*(35), 11167–11177.

Berthouze, L., James, L. M., & Farmer, S. F. (2010). Human EEG shows long-range temporal correlations of oscillation amplitude in Theta, Alpha and Beta bands across a wide age range. *Clinical Neurophysiology: Official Journal of the International Federation of Clinical Neurophysiology*, *121*(8), 1187–1197. https://doi.org/10.1016/j.clinph.2010.02.163

Blain-Moraes, S., Tarnal, V., Vanini, G., Alexander, A., Rosen, D., Shortal, B., Janke, E., & Mashour, G. A. (2015). Neurophysiological correlates of sevoflurane-induced unconsciousness. *Anesthesiology*, *122*(2), 307–316. https://doi.org/10.1097/ALN.0000000000000482

Boly, M., Massimini, M., Garrido, M. I., Gosseries, O., Noirhomme, Q., Laureys, S., & Soddu, A. (2012). Brain connectivity in disorders of consciousness. *Brain Connectivity*, *2*(1), 1–10. https://doi.org/10.1089/brain.2011.0049

Bonhomme, V., Vanhaudenhuyse, A., Demertzi, A., Bruno, M.-A., Jaquet, O., Bahri, M. A., Plenevaux, A., Boly, M., Boveroux, P., Soddu, A., Brichant, J. F., Maquet, P., & Laureys, S. (2016). Resting-state Network-specific Breakdown of Functional Connectivity during Ketamine Alteration of Consciousness in Volunteers. *Anesthesiology*, *125*(5), 873–888. https://doi.org/10.1097/ALN.0000000000001275

Bornas, X., Fiol-Veny, A., Balle, M., Morillas-Romero, A., & Tortella-Feliu, M. (2015). Long range temporal correlations in EEG oscillations of subclinically depressed individuals: Their association with brooding and suppression. *Cognitive Neurodynamics*, *9*(1), 53–62. https://doi.org/10.1007/s11571-014-9313-1

Boveroux, P., Vanhaudenhuyse, A., Bruno, M.-A., Noirhomme, Q., Lauwick, S., Luxen, A., Degueldre, C., Plenevaux, A., Schnakers, C., Phillips, C., Brichant, J.-F., Bonhomme, V., Maquet, P., Greicius, M. D., Laureys, S., & Boly, M. (2010). Breakdown of within- and between-network resting state functional magnetic resonance imaging connectivity during propofol-induced loss of consciousness. *Anesthesiology*, *113*(5), 1038–1053. https://doi.org/10.1097/ALN.0b013e3181f697f5

Casali, A. G., Gosseries, O., Rosanova, M., Boly, M., Sarasso, S., Casali, K. R., Casarotto, S., Bruno, M.-A., Laureys, S., Tononi, G., & Massimini, M. (2013). A theoretically based index of consciousness independent of sensory processing and behavior. *Science Translational Medicine*, *5*(198), 198ra105. https://doi.org/10.1126/scitranslmed.3006294

Ching, S., Cimenser, A., Purdon, P. L., Brown, E. N., & Kopell, N. J. (2010). Thalamocortical model for a propofol-induced alpha-rhythm associated with loss of consciousness. *Proceedings of the National Academy of Sciences of the United States of America*, *107*(52), 22665–22670. https://doi.org/10.1073/pnas.1017069108

Cimenser, A., Purdon, P. L., Pierce, E. T., Walsh, J. L., Salazar-Gomez, A. F., Harrell, P. G., Tavares-Stoeckel, C., Habeeb, K., & Brown, E. N. (2011). Tracking brain states under general anesthesia by using global coherence analysis. *Proceedings of the National Academy of Sciences*, *108*(21), 8832–8837. https://doi.org/10.1073/pnas.1017041108

Ciuciu, P., Varoquaux, G., Abry, P., Sadaghiani, S., & Kleinschmidt, A. (2012). Scale-Free and Multifractal Time Dynamics of fMRI Signals during Rest and Task. *Frontiers in Physiology*, *3*, 186. https://doi.org/10.3389/fphys.2012.00186

Combrisson, E., & Jerbi, K. (2015). Exceeding chance level by chance: The caveat of theoretical chance levels in brain signal classification and statistical assessment of decoding accuracy. *Journal of Neuroscience Methods*, *250*, 126–136. https://doi.org/10.1016/j.jneumeth.2015.01.010

Dehaene, S., & Changeux, J.-P. (2011). Experimental and theoretical approaches to conscious processing. *Neuron*, *70*(2), 200–227. https://doi.org/10.1016/j.neuron.2011.03.018

Engel, A. K., & Fries, P. (2010). Beta-band oscillations—Signalling the status quo? *Current Opinion in Neurobiology*, *20*(2), 156–165. https://doi.org/10.1016/j.conb.2010.02.015

Fedele, T., Blagovechtchenski, E., Nazarova, M., Iscan, Z., Moiseeva, V., & Nikulin, V. V. (2016). Long-Range Temporal Correlations in the amplitude of alpha oscillations predict and reflect strength of intracortical facilitation: Combined TMS and EEG study. *Neuroscience*, *331*, 109–119. https://doi.org/10.1016/j.neuroscience.2016.06.015

Feshchenko, V. A., Veselis, R. A., & Reinsel, R. A. (2004). Propofol-induced alpha rhythm. *Neuropsychobiology*, *50*(3), 257–266. https://doi.org/10.1159/000079981

Fisher, R. A. (1936). The Use of Multiple Measurements in Taxonomic Problems. *Annals of Eugenics*, *7*(2), 179–188. https://doi.org/10.1111/j.1469-1809.1936.tb02137.x

Franks, N. P. (2008). General anaesthesia: From molecular targets to neuronal pathways of sleep and arousal. *Nature Reviews. Neuroscience*, *9*(5), 370–386. https://doi.org/10.1038/nrn2372

Funahashi, M., Higuchi, H., Miyawaki, T., Shimada, M., & Matsuo, R. (2001). Propofol suppresses a hyperpolarization-activated inward current in rat hippocampal CA1 neurons. *Neuroscience Letters*, *311*(3), 177–180. https://doi.org/10.1016/S0304-3940(01)02169-3

Gao, J., Hu, J., Tung, W.-W., Cao, Y., Sarshar, N., & Roychowdhury, V. P. (2006). Assessment of long-range correlation in time series: How to avoid pitfalls. *Physical Review E*, *73*(1), 016117. https://doi.org/10.1103/PhysRevE.73.016117

Gifani, P., Rabiee, H. R., Hashemi, M. R., Taslimi, P., & Ghanbari, M. (2006). Nonlinear analysis of anesthesia dynamics by Fractal Scaling Exponent. *Conference Proceedings: ... Annual International Conference of the IEEE Engineering in Medicine and Biology Society. IEEE Engineering in Medicine and Biology Society. Annual Conference*, *1*, 6225–6228. https://doi.org/10.1109/IEMBS.2006.260501

Gugino, L. D., Chabot, R. J., Prichep, L. S., John, E. R., Formanek, V., & Aglio, L. S. (2001). Quantitative EEG changes associated with loss and return of consciousness in healthy adult volunteers anaesthetized with propofol or sevoflurane. *British Journal of Anaesthesia*, *87*(3), 421–428.

He, B. J. (2014). Scale-free brain activity: Past, present, and future. *Trends in Cognitive Sciences*, *18*(9), 480–487. https://doi.org/10.1016/j.tics.2014.04.003

Hudetz, A. G., Liu, X., & Pillay, S. (2015). Dynamic Repertoire of Intrinsic Brain States Is Reduced in Propofol-Induced Unconsciousness. *Brain Connectivity*, *5*(1), 10–22. https://doi.org/10.1089/brain.2014.0230

John, E. R., & Prichep, L. S. (2005). The anesthetic cascade: A theory of how anesthesia suppresses consciousness. *Anesthesiology*, *102*(2), 447–471.

Jordan, D., Ilg, R., Riedl, V., Schorer, A., Grimberg, S., Neufang, S., Omerovic, A., Berger, S., Untergehrer, G., Preibisch, C., Schulz, E., Schuster, T., Schröter, M., Spoormaker, V., Zimmer, C., Hemmer, B., Wohlschläger, A., Kochs, E. F., & Schneider, G. (2013). Simultaneous electroencephalographic and functional magnetic resonance imaging indicate impaired cortical top-down processing in association with anesthetic-induced unconsciousness. *Anesthesiology*, *119*(5), 1031–1042. https://doi.org/10.1097/ALN.0b013e3182a7ca92

Jospin, M., Caminal, P., Jensen, E. W., Litvan, H., Vallverdu, M., Struys, M. M. R. F., Vereecke, H. E. M., & Kaplan, D. T. (2007). Detrended Fluctuation Analysis of EEG as a Measure of Depth of Anesthesia. *IEEE Transactions on Biomedical Engineering*, *54*(5), 840–846. https://doi.org/10.1109/TBME.2007.893453

Kantelhardt, J. W., Koscielny-Bunde, E., Rego, H. H. A., Havlin, S., & Bunde, A. (2001). Detecting Long-range Correlations with Detrended Fluctuation Analysis. *Physica A: Statistical Mechanics and Its Applications*, *295*(3–4), 441–454. https://doi.org/10.1016/S0378-4371(01)00144-3

Kaskinoro, K., Maksimow, A., Georgiadis, S., Långsjö, J., Scheinin, H., Karjalainen, P., & Jääskeläinen, S. K. (2015). Electroencephalogram reactivity to verbal command after dexmedetomidine, propofol and sevoflurane-induced unresponsiveness. *Anaesthesia*, *70*(2), 190–204. https://doi.org/10.1111/anae.12868

Kinouchi, O., & Copelli, M. (2006). Optimal dynamical range of excitable networks at criticality. *Nature Physics*, *2*(5), 348–351. https://doi.org/10.1038/nphys289

Koch, C. (2004). *The quest for consciousness: A neurobiological approach*. Roberts and Co.

Krzemiński, D., Kamiński, M., Marchewka, A., & Bola, M. (2017). Breakdown of long-range temporal correlations in brain oscillations during general anesthesia. *NeuroImage*, *159*(Supplement C), 146–158. https://doi.org/10.1016/j.neuroimage.2017.07.047

Lalitha, V., & Eswaran, C. (2007). Automated detection of anesthetic depth levels using chaotic features with artificial neural networks. *Journal of Medical Systems*, *31*(6), 445–452.

Laureys, S., & Tononi, G. (Eds.). (2009). *The neurology of consciousness: Cognitive neuroscience and neuropathology* (1st ed). Elsevier/Academic Press.

Lee, U., Ku, S., Noh, G., Baek, S., Choi, B., & Mashour, G. A. (2013). Disruption of frontal-parietal communication by ketamine, propofol, and sevoflurane. *Anesthesiology*, *118*(6), 1264–1275. https://doi.org/10.1097/ALN.0b013e31829103f5

Lee, U., Mashour, G. A., Kim, S., Noh, G.-J., & Choi, B.-M. (2009). Propofol induction reduces the capacity for neural information integration: Implications for the mechanism of consciousness and general anesthesia. *Consciousness and Cognition*, *18*(1), 56–64. https://doi.org/10.1016/j.concog.2008.10.005

Lee, U., Oh, G., Kim, S., Noh, G., Choi, B., & Mashour, G. A. (2010). Brain networks maintain a scale-free organization across consciousness, anesthesia, and recovery: Evidence for adaptive reconfiguration. *Anesthesiology*, *113*(5), 1081–1091. https://doi.org/10.1097/ALN.0b013e3181f229b5

Li, X., Wang, F., & Wu, G. (2017). Monitoring Depth of Anesthesia Using Detrended Fluctuation Analysis Based on EEG Signals. *Journal of Medical and Biological Engineering*, *37*(2), 171–180. https://doi.org/10.1007/s40846-016-0196-y

Liang, Z., Wang, Y., Sun, X., Li, D., Voss, L. J., Sleigh, J. W., Hagihira, S., & Li, X. (2015). EEG entropy measures in anesthesia. *Frontiers in Computational Neuroscience*, *9*. https://doi.org/10.3389/fncom.2015.00016

Linkenkaer-Hansen, K., Monto, S., Rytsälä, H., Suominen, K., Isometsä, E., & Kähkönen, S. (2005). Breakdown of Long-Range Temporal Correlations in Theta Oscillations in Patients with Major Depressive Disorder. *Journal of Neuroscience*, *25*(44), 10131–10137. https://doi.org/10.1523/JNEUROSCI.3244-05.2005

Linkenkaer-Hansen, K., Nikouline, V. V., Palva, J. M., & Ilmoniemi, R. J. (2001). Long-range temporal correlations and scaling behavior in human brain oscillations. *The Journal of Neuroscience: The Official Journal of the Society for Neuroscience*, *21*(4), 1370–1377.

Linkenkaer-Hansen, K., Nikulin, V. V., Palva, S., Ilmoniemi, R. J., & Palva, J. M. (2004). Prestimulus Oscillations Enhance Psychophysical Performance in Humans. *Journal of Neuroscience*, *24*(45), 10186–10190. https://doi.org/10.1523/JNEUROSCI.2584-04.2004

Linkenkaer-Hansen, K., Smit, D. J. A., Barkil, A., Beijsterveldt, T. E. M. van, Brussaard, A. B., Boomsma, D. I., Ooyen, A. van, & Geus, E. J. C. de. (2007). Genetic Contributions to Long-Range Temporal Correlations in Ongoing Oscillations. *Journal of Neuroscience*, *27*(50), 13882–13889. https://doi.org/10.1523/JNEUROSCI.3083-07.2007

Lux, T., & Marchesi, M. (1999). Scaling and criticality in a stochastic multi-agent model of a financial market. *Nature*, *397*(6719), 498–500. https://doi.org/10.1038/17290

Mashour, G. A. (2013). Cognitive unbinding: A neuroscientific paradigm of general anesthesia and related states of unconsciousness. *Neuroscience & Biobehavioral Reviews*, *37*(10), 2751–2759. https://doi.org/10.1016/j.neubiorev.2013.09.009

Mashour, G. A., Shanks, A., Tremper, K. K., Kheterpal, S., Turner, C. R., Ramachandran, S. K., Picton, P., Schueller, C., Morris, M., Vandervest, J. C., Lin, N., & Avidan, M. S. (2012). Prevention of intraoperative awareness with explicit recall in an unselected surgical population: A randomized comparative effectiveness trial. *Anesthesiology*, *117*(4), 717–725. https://doi.org/10.1097/ALN.0b013e31826904a6

Meisel, C., Bailey, K., Achermann, P., & Plenz, D. (2017). Decline of long-range temporal correlations in the human brain during sustained wakefulness. *Scientific Reports*, *7*. https://doi.org/10.1038/s41598-017-12140-w

Montez, T., Poil, S.-S., Jones, B. F., Manshanden, I., Verbunt, J. P. A., van Dijk, B. W., Brussaard, A. B., van Ooyen, A., Stam, C. J., Scheltens, P., & Linkenkaer-Hansen, K. (2009). Altered temporal correlations in parietal alpha and prefrontal theta oscillations in early-stage Alzheimer disease. *Proceedings of the National Academy of Sciences of the United States of America*, *106*(5), 1614–1619. https://doi.org/10.1073/pnas.0811699106

Monto, S., Vanhatalo, S., Holmes, M. D., & Palva, J. M. (2007). Epileptogenic neocortical networks are revealed by abnormal temporal dynamics in seizure-free subdural EEG. *Cerebral Cortex (New York, N.Y.: 1991)*, *17*(6), 1386–1393. https://doi.org/10.1093/cercor/bhl049

Mukamel, E. A., Pirondini, E., Babadi, B., Wong, K. F. K., Pierce, E. T., Harrell, P. G., Walsh, J. L., Salazar-Gomez, A. F., Cash, S. S., Eskandar, E. N., Weiner, V. S., Brown, E. N., & Purdon, P. L. (2014). A Transition in Brain State during Propofol-Induced Unconsciousness. *Journal of Neuroscience*, *34*(3), 839–845. https://doi.org/10.1523/JNEUROSCI.5813-12.2014

Nguyen-Ky, T., Wen, P., & Li, Y. (2010). An improved detrended moving-average method for monitoring the depth of anesthesia. *IEEE Transactions on Bio-Medical Engineering*, *57*(10), 2369–2378. https://doi.org/10.1109/TBME.2010.2053929

Niedermeyer, E., & Silva, F. H. L. da. (2005). *Electroencephalography: Basic Principles, Clinical Applications, and Related Fields*. Lippincott Williams & Wilkins.

Nikulin, V. V., & Brismar, T. (2004). Long-range temporal correlations in alpha and beta oscillations: Effect of arousal level and test-retest reliability. *Clinical Neurophysiology: Official Journal of the International Federation of Clinical Neurophysiology*, *115*(8), 1896–1908. https://doi.org/10.1016/j.clinph.2004.03.019

Nikulin, V. V., & Brismar, T. (2005). Long-range temporal correlations in electroencephalographic oscillations: Relation to topography, frequency band, age and gender. *Neuroscience*, *130*(2), 549–558. https://doi.org/10.1016/j.neuroscience.2004.10.007

Nikulin, V. V., Jönsson, E. G., & Brismar, T. (2012). Attenuation of long-range temporal correlations in the amplitude dynamics of alpha and beta neuronal oscillations in patients with schizophrenia. *NeuroImage*, *61*(1), 162–169. https://doi.org/10.1016/j.neuroimage.2012.03.008

Pal, D., Silverstein, B. H., Lee, H., & Mashour, G. A. (2016). Neural Correlates of Wakefulness, Sleep, and General Anesthesia: An Experimental Study in Rat. *Anesthesiology*, *125*(5), 929–942. https://doi.org/10.1097/ALN.0000000000001342

Palanca, B. J. A., Mitra, A., Larson-Prior, L., Snyder, A. Z., Avidan, M. S., & Raichle, M. E. (2015). Resting-state Functional Magnetic Resonance Imaging Correlates of Sevoflurane-induced Unconsciousness. *Anesthesiology*, *123*(2), 346–356. https://doi.org/10.1097/ALN.0000000000000731

Pavone, K. J., Su, L., Gao, L., Eromo, E., Vazquez, R., Rhee, J., Hobbs, L. E., Ibala, R., Demircioglu, G., Purdon, P. L., Brown, E. N., & Akeju, O. (2017). Lack of Responsiveness during the Onset and Offset of Sevoflurane Anesthesia Is Associated with Decreased Awake-Alpha Oscillation Power. *Frontiers in Systems Neuroscience*, *11*. https://doi.org/10.3389/fnsys.2017.00038

Peng, C. K., Havlin, S., Stanley, H. E., & Goldberger, A. L. (1995). Quantification of scaling exponents and crossover phenomena in nonstationary heartbeat time series. *Chaos (Woodbury, N.Y.)*, *5*(1), 82–87. https://doi.org/10.1063/1.166141

Poil, S.-S., Hardstone, R., Mansvelder, H. D., & Linkenkaer-Hansen, K. (2012). Critical-state dynamics of avalanches and oscillations jointly emerge from balanced excitation/inhibition in neuronal networks. *The Journal of Neuroscience: The Official Journal of the Society for Neuroscience*, *32*(29), 9817–9823. https://doi.org/10.1523/JNEUROSCI.5990-11.2012

Purdon, P. L., Pavone, K. J., Akeju, O., Smith, A. C., Sampson, A. L., Lee, J., Zhou, D. W., Solt, K., & Brown, E. N. (2015). The Ageing Brain: Age-dependent changes in the electroencephalogram during propofol and sevoflurane general anaesthesia. *British Journal of Anaesthesia*, *115 Suppl 1*, i46–i57. https://doi.org/10.1093/bja/aev213

Purdon, P. L., Pierce, E. T., Mukamel, E. A., Prerau, M. J., Walsh, J. L., Wong, K. F. K., Salazar-Gomez, A. F., Harrell, P. G., Sampson, A. L., Cimenser, A., Ching, S., Kopell, N. J., Tavares-Stoeckel, C., Habeeb, K., Merhar, R., & Brown, E. N. (2013). Electroencephalogram signatures of loss and recovery of consciousness from propofol. *Proceedings of the National Academy of Sciences of the United States of America*, *110*(12), E1142–E1151. https://doi.org/10.1073/pnas.1221180110

Ranft, A., Golkowski, D., Kiel, T., Riedl, V., Kohl, P., Rohrer, G., Pientka, J., Berger, S., Thul, A., Maurer, M., Preibisch, C., Zimmer, C., Mashour, G. A., Kochs, E. F., Jordan, D., & Ilg, R. (2016). Neural Correlates of Sevoflurane-induced Unconsciousness Identified by Simultaneous Functional Magnetic Resonance Imaging and Electroencephalography. *Anesthesiology*, *125*(5), 861–872. https://doi.org/10.1097/ALN.0000000000001322

Sanders, R. D., Tononi, G., Laureys, S., & Sleigh, J. W. (2012). Unresponsiveness ≠ unconsciousness. *Anesthesiology*, *116*(4), 946–959. https://doi.org/10.1097/ALN.0b013e318249d0a7

Sarasso, S., Boly, M., Napolitani, M., Gosseries, O., Charland-Verville, V., Casarotto, S., Rosanova, M., Casali, A. G., Brichant, J.-F., Boveroux, P., Rex, S., Tononi, G., Laureys, S., & Massimini, M. (2015). Consciousness and Complexity during Unresponsiveness Induced by Propofol, Xenon, and Ketamine. *Current Biology: CB*, *25*(23), 3099–3105. https://doi.org/10.1016/j.cub.2015.10.014

Shew, W. L., & Plenz, D. (2013). The functional benefits of criticality in the cortex. *The Neuroscientist: A Review Journal Bringing Neurobiology, Neurology and Psychiatry*, *19*(1), 88–100. https://doi.org/10.1177/1073858412445487

Shew, W. L., Yang, H., Petermann, T., Roy, R., & Plenz, D. (2009). Neuronal Avalanches Imply Maximum Dynamic Range in Cortical Networks at Criticality. *The Journal of Neuroscience*, *29*(49), 15595–15600. https://doi.org/10.1523/JNEUROSCI.3864-09.2009

Shew, W. L., Yang, H., Yu, S., Roy, R., & Plenz, D. (2011). Information capacity and transmission are maximized in balanced cortical networks with neuronal avalanches. *The Journal of Neuroscience: The Official Journal of the Society for Neuroscience*, *31*(1), 55–63. https://doi.org/10.1523/JNEUROSCI.4637-10.2011

Slezin, V. B., Korsakova, E. A., Dytjatkovsky, M. A., Schultz, E. A., Arystova, T. A., & Siivola, J. R. (2007). Multifractal analysis as an aid in the diagnostics of mental disorders. *Nordic Journal of Psychiatry*, *61*(5), 339–342. https://doi.org/10.1080/08039480701643175

Solovey, G., Alonso, L. M., Yanagawa, T., Fujii, N., Magnasco, M. O., Cecchi, G. A., & Proekt, A. (2015). Loss of Consciousness Is Associated with Stabilization of Cortical Activity. *The Journal of Neuroscience: The Official Journal of the Society for Neuroscience*, *35*(30), 10866–10877. https://doi.org/10.1523/JNEUROSCI.4895-14.2015

Suzuki, A., Katoh, T., & Ikeda, K. (1998). The effect of adenosine triphosphate on sevoflurane requirements for minimum alveolar anesthetic concentration and minimum alveolar anesthetic concentration-awake. *Anesthesia and Analgesia*, *86*(1), 179–183.

Theodoridis, S., & Koutroumbas, K. (2009). *Pattern recognition* (4. ed). Elsevier Acad. Press.

Tononi, G., Boly, M., Massimini, M., & Koch, C. (2016). Integrated information theory: From consciousness to its physical substrate. *Nature Reviews Neuroscience*, *17*(7), 450–461. https://doi.org/10.1038/nrn.2016.44

Tononi, G., & Koch, C. (2015). Consciousness: Here, there and everywhere? *Phil. Trans. R. Soc. B*, *370*(1668), 20140167. https://doi.org/10.1098/rstb.2014.0167

Tsuchiya, N., Wilke, M., Frässle, S., & Lamme, V. A. F. (2015). No-Report Paradigms: Extracting the True Neural Correlates of Consciousness. *Trends in Cognitive Sciences*, *19*(12), 757–770. https://doi.org/10.1016/j.tics.2015.10.002

Vijayan, S., Ching, S., Purdon, P. L., Brown, E. N., & Kopell, N. J. (2013). Thalamocortical mechanisms for the anteriorization of α rhythms during propofol-induced unconsciousness. *The Journal of Neuroscience: The Official Journal of the Society for Neuroscience*, *33*(27), 11070–11075. https://doi.org/10.1523/JNEUROSCI.5670-12.2013

Wang, J., Noh, G.-J., Choi, B.-M., Ku, S.-W., Joo, P., Jung, W.-S., Kim, S., & Lee, H. (2017). Suppressed neural complexity during ketamine- and propofol-induced unconsciousness. *Neuroscience Letters*, *653*, 320–325. https://doi.org/10.1016/j.neulet.2017.05.045

Ying, S.-W., Abbas, S. Y., Harrison, N. L., & Goldstein, P. A. (2006). Propofol block of Ih contributes to the suppression of neuronal excitability and rhythmic burst firing in thalamocortical neurons. *European Journal of Neuroscience*, *23*(2), 465–480. https://doi.org/10.1111/j.1460-9568.2005.04587.